212 SPRINGER TRACTS IN MODERN PHYSICS

Shang Yuan Ren

Electronic States in Crystals of Finite Size

Quantum Confinement of Bloch Waves

Springer

Springer Tracts in Modern Physics
Volume 212

Springer Tracts in Modern Physics

Springer Tracts in Modern Physics provides comprehensive and critical reviews of topics of current interest in physics. The following fields are emphasized: elementary particle physics, solid-state physics, complex systems, and fundamental astrophysics.
Suitable reviews of other fields can also be accepted. The editors encourage prospective authors to correspond with them in advance of submitting an article. For reviews of topics belonging to the above mentioned fields, they should address the responsible editor, otherwise the managing editor.
See also springeronline.com

Shang Yuan Ren

Electronic States in Crystals of Finite Size

Quantum Confinement of Bloch Waves

With 31 Figures

Springer

Shang Yuan Ren
Department of Physics
Peking University
Beijing 100871, P.R China
E-mail: syren@pku.edu.cn

Cover concept: eStudio Calamar Steinen

Physics and Astronomy Classification Scheme (PACS): 73.22.-f, 73.22. Dj, 73.20.-r, 73.20.At, 73.21. Fg, 73.21. Hb, 73.21. La, 71.15.-m

Library of Congress Control Number: 2005927517

ISBN-10: 0-387 -26303-9 e-ISBN 0-387-26304-7
ISBN-13: 978-0387-26303-8

Printed on acid-free paper.

Printed in the United States of America. (MVY)

9 8 7 6 5 4 3 2 1

springeronline.com

◆

To Mr. Jicheng Ren
and Ms. Shujuan Yang

◆

To Mr. Jicheng Ren and Ms. Shujuan Yang

Preface

The theory of electronic states in crystals is the very basis of modern solid state physics. In traditional solid state physics – based on the Bloch theorem – the theory of electronic states in crystals is essentially a theory of electronic states in crystals of infinite size. However, that any real crystal always has a finite size is a physical reality one has to face. The difference between the electronic structure of a real crystal of finite size and the electronic structure obtained based on the Bloch theorem becomes more significant as the crystal size decreases. A clear understanding of the properties of electronic states in real crystals of finite size has both theoretical and practical significance. Many years ago when the author was a student learning solid state physics at Peking University, he was bothered by a feeling that the general use of the periodic boundary conditions seemed unconvincing. At least the effects of such a significant simplification should be clearly understood. Afterward, he learned that many of his school mates had the same feeling. Among many solid state physics books, the author found that only in the classic book *Dynamic Theory of Crystal Lattices* by Born and Huang was there a more detailed discussion on the effects of such a simplification in an Appendix.

In the present book, a theory of electronic states in ideal crystals of finite size is developed by trying to understand the quantum confinement effects of Bloch waves. The lack of translational invariance had been a major obstacle in developing a general theory on the electronic states in crystals of finite size. In this book, it was found that on the basis of relevant theorems in the theory of second-order differential equations with periodic coefficients, this major obstacle or difficulty, actually, could be circumvented: Exact and general understanding on the electronic states in some simple and interesting ideal low-dimensional systems and finite crystals could be analytically obtained. Some of the results obtained in the book are quite different from what is traditionally believed in the solid state physics community.

This book consists of five parts. The first part gives a brief introduction to why a theory of electronic states in crystals of finite size is needed. The second part treats one-dimensional semi-infinite crystals and finite crystals; most results in this part can be rigorously proven. The third part treats low-dimensional systems or finite crystals in three-dimensional crystals. The basis is rigorous according to the author's understanding; however, much of

the reasoning in this part had to be based on physical intuition due to the lack of enough available mathematical understanding. The fourth part is devoted to concluding remarks. In the fifth part are two appendices. The contents of each chapter in Parts II and III are rather closely related; therefore, readers are expected to read these chapters in the given order. Without appropriate preparation from earlier chapters, readers may find the later chapters difficult to understand. Although the purpose of this book is to present a theory of electronic states in crystals of *finite size*, it is the clear understanding of the electronic states in *crystals with translational invariance* – as obtained in traditional solid state physics – that provided a basis for such a new theory.

One of the feelings the author had frequently while working on the problems in this book is that the mathematicians and the solid state physicists are rather unfamiliar with each other's problems and their respective results. The major mathematical basis of the work presented in this book, Eastham's *The Spectral Theory of Periodic Differential Equations*, was published more than 30 years ago; however, it seems that many of the important results obtained in his book are not yet well known in the solid state physics community. Although the Bloch function is the most fundamental function in the theory of electronic states in modern solid state physics, little is widely known in the community on the general properties of the function except that it can be expressed as the product of a plane wave function and a periodic function. For quite a long time, the author also knew only this about the Bloch function and had many hard working days on some problems without making substantial progress. By mere chance, he saw Eastham's book. He was discouraged by the seemingly difficult mathematics at the beginning but made an effort to understand the book and to apply the new mathematical results learned to relevant physics problems. The book presented here is essentially the result of such effort.

In addition to Eastham's book, the author has also greatly benefited from two classic books: Courant and Hilbert's *Methods of Mathematical Physics* and Titchmarsh's *Eigenfunction Expansions Associated with Second-Order Differential Equations*. The theorems presented in these two books are so powerful that some misconceptions on the electronic states in low-dimensional systems actually could have been clarified much earlier if some theorems in those books published many years ago were clearly and widely understood in the solid state physics community. Unfortunately, these excellent books are out of print now. The wide use of more and more powerful computer-based approaches has unquestionably made great contributions to our understanding of the low-dimensional systems. Nevertheless, the author hopes that the publishing of this book could stimulate more general interest in the use of analytical approaches in understanding these very interesting and challenging systems, which, at least, could be a substantial complement. After all, a really comprehensive and in-depth understanding of a physical problem can

usually be obtained from an analytical theory based on a simplified model correctly containing the most essential physics.

It is a pleasure of the author to take this opportunity to thank Professor Kun Huang for his many years of guidance, help, and discussions. It was he who led the author into the field of solid state physics. The author is very grateful to Ms. Avril Rhys (i.e., Mrs. Huang); her concern and help is one of the most appreciated experiences the author had in the process of writing the book. He also wishes to thank Professor Huan-Wu Peng for sharing his experience in the early stage of the solid state physics in the mid-1940s and many interesting discussions. The author was fortunate to have had opportunities to listen to Professor Huang' and Professor Peng's experiences when they worked with Max Born.

The author is grateful to Professors John D. Dow, Hanying Guo, Rushan Han, Walter A. Harrison, Zhongqi Ma, Shangfen Ren, Zhengxing Wang, Sicheng Wu, Shousheng Yan, Lo Yang, Shuxiang Yu, Jinyan Zeng, Ping Zhang, and Pingwen Zhang for their comments and/or discussions. He wishes to thank Miss Yulin Xuan and Miss Zhiling Ruan for much valuable help. He also wishes to thank Dr. Wei Cheng for his help in many computer-related problems.

Last but not least, the author is indebted to his family members, in particular his wife Weimin, his daughters Yujian and Yuhui, his sons-in-law Weidong and Jian, and his grandchildren Nana, Yangyang, and Weiwei. Their love and support not only gave him so much happiness in enjoying family life, but also brought him the strength and courage to fight the sufferings sometimes one had to experience, leading to the birth of this book.

Shang Yuan Ren
ZhongGuanYuan, Peking University, Beijing
March 2005

Contents

1 Introduction

Solid state physics is a field in modern physics in which one is mainly concerned with the physical properties of and physical processes in various solids. Besides its fundamental significance, a clear understanding of different physical properties of and physical processes in solids and their origin may provide insight for possible practical applications of relevant properties and physical processes. Since the middle of the twentieth century, many achievements in the field have made great contributions to modern science and technology, even resulting in revolutionary developments. We can expect that further achievements in this field will continually bring tremendous benefits to human beings and society.

A clear understanding of the electronic structure of a solid is always the basis for understanding the physical properties of the solid and the physical processes in the solid. In traditional solid state physics, the basic theory of electronic states in crystals has been established for more than 70 years. Most further theoretical developments afterward are mainly applications of the basic theory of electronic states to different physical problems and to calculations of detailed electronic structures of various solids. However, this traditional theory also has some fundamental difficulties. Those fundamental difficulties become more significant today, when one has to deal with crystals of much smaller size than before.

This chapter is organized as follows: In Sections 1.1–1.2, we briefly review some of the most basic understandings of the electronic structure of crystals in traditional solid state physics and how the theory of electronic states in crystals is the very basis for determining the physical properties of and the physical processes in the crystals, by using simple examples. In Section 1.3, we point out some fundamental difficulties of the theory of electronic states in traditional solid state physics. As consequences of these fundamental difficulties, the theory of electronic states in traditional solid state physics cannot treat the boundary effects and the size effects of crystals, which have substantial significance today when one has to deal with crystals in the submicron and nanometer size range – the low-dimensional systems. In Sections 1.4–1.5, we briefly review one of the most widely used approaches in theoretically investigating electronic states in low-dimensional systems – the effective mass

approximation approach – and some numerical results. In Section 1.6 is a brief introduction on the subject and the main findings of this book.

1.1 Electronic States Based on Translational Invariance

The very basis of the theory of electronic states in modern solid state physics – energy band theory – is the Bloch theorem [1]. It is based on the assumption that atoms in a crystal are periodically located – the potential in the crystal has a translational invariance [2–6].

The single-electron Schrödinger differential equation with a periodic potential can be written as

$$-\frac{\hbar^2}{2m}\nabla^2 y(\boldsymbol{x}) + [V(\boldsymbol{x}) - E]y(\boldsymbol{x}) = 0, \tag{1.1}$$

where $V(\boldsymbol{x})$ is the periodic potential:

$$V(\boldsymbol{x} + \boldsymbol{a}_1) = V(\boldsymbol{x} + \boldsymbol{a}_2) = V(\boldsymbol{x} + \boldsymbol{a}_3) = V(\boldsymbol{x}). \tag{1.2}$$

Here, $\boldsymbol{a}_1$, $\boldsymbol{a}_2$, and $\boldsymbol{a}_3$ are three primitive lattice vectors of the crystal.

Based on this assumption, the Bloch theorem states that the electronic states in the crystal have the property that

$$\phi(\boldsymbol{k}, \boldsymbol{x} + \boldsymbol{a}_i) = \mathrm{e}^{\mathrm{i}\boldsymbol{k}\cdot\boldsymbol{a}_i}\phi(\boldsymbol{k}, \boldsymbol{x}), \quad i = 1, 2, 3; \tag{1.3}$$

this can also be expressed as

$$\phi(\boldsymbol{k}, \boldsymbol{x}) = \mathrm{e}^{\mathrm{i}\boldsymbol{k}\cdot\boldsymbol{x}}u(\boldsymbol{k}, \boldsymbol{x}), \tag{1.4}$$

where $\boldsymbol{k}$ is a real wave vector in $\boldsymbol{k}$ space and $u(\boldsymbol{k}, \boldsymbol{x})$ is a function with the same period as the potential:

$$u(\boldsymbol{k}, \boldsymbol{x} + \boldsymbol{a}_1) = u(\boldsymbol{k}, \boldsymbol{x} + \boldsymbol{a}_2) = u(\boldsymbol{k}, \boldsymbol{x} + \boldsymbol{a}_3) = u(\boldsymbol{k}, \boldsymbol{x}). \tag{1.5}$$

The function $\phi(\boldsymbol{k}, \boldsymbol{x})$ in (1.3) and (1.4) is called the Bloch function or Bloch wave. This is the most fundamental function in modern solid state physics.

The range of the wave vector $\boldsymbol{k}$ in (1.3) or (1.4) can be limited to a specific region in the $\boldsymbol{k}$ space called the Brillouin zone [7], determined by three primitive vectors of the reciprocal lattice in $\boldsymbol{k}$ space $\boldsymbol{b}_1, \boldsymbol{b}_2$, and $\boldsymbol{b}_3$:

$$\boldsymbol{b}_1 = \frac{\boldsymbol{a}_2 \times \boldsymbol{a}_3}{\boldsymbol{a}_1 \cdot \boldsymbol{a}_2 \times \boldsymbol{a}_3}, \quad \boldsymbol{b}_2 = \frac{\boldsymbol{a}_3 \times \boldsymbol{a}_1}{\boldsymbol{a}_1 \cdot \boldsymbol{a}_2 \times \boldsymbol{a}_3}, \quad \boldsymbol{b}_3 = \frac{\boldsymbol{a}_1 \times \boldsymbol{a}_2}{\boldsymbol{a}_1 \cdot \boldsymbol{a}_2 \times \boldsymbol{a}_3} \tag{1.6}$$

and thus

$$\boldsymbol{a}_i \cdot \boldsymbol{b}_j = \delta_{i,j}; \tag{1.7}$$

here, $\delta_{i,j}$ is the Kronecker symbol.

As the wave vector $\boldsymbol{k}$ varies in the Brillouin zone, the permitted energy of each Bloch function $\phi(\boldsymbol{k}, \boldsymbol{x})$ – the eigenvalue E in (1.1) – also changes. These permitted energy ranges are called energy bands and can be written as $E_n(\boldsymbol{k})$; here, n is an energy band index. They can be ordered with increasing energy:

$$E_0(\boldsymbol{k}) \leq E_1(\boldsymbol{k}) \leq E_2(\boldsymbol{k}) \leq E_3(\boldsymbol{k}) \leq E_4(\boldsymbol{k}) \leq \cdots.$$

The corresponding eigenfunctions are denoted by $\phi_n(\boldsymbol{k}, x)$ and they can be written as

$$\phi_n(\boldsymbol{k}, \boldsymbol{x}) = \mathrm{e}^{\mathrm{i}\boldsymbol{k}\cdot\boldsymbol{x}} u_n(\boldsymbol{k}, \boldsymbol{x}), \tag{1.8}$$

where n is the energy band index, $\boldsymbol{k}$ is the wave vector, and $u_n(\boldsymbol{k}, \boldsymbol{x})$ is a function with the same period as the potential:

$$u_n(\boldsymbol{k}, \boldsymbol{x} + \boldsymbol{a}_1) = u_n(\boldsymbol{k}, \boldsymbol{x} + \boldsymbol{a}_2) = u_n(\boldsymbol{k}, \boldsymbol{x} + \boldsymbol{a}_3) = u_n(\boldsymbol{k}, \boldsymbol{x}).$$

The energy band structure formed by the valence electrons of a crystal plays a major role in determining the physical properties of the crystal and which physical processes may happen in the crystal. For example, if a crystal has a forbidden band gap between the highest occupied energy band(s) and the lowest unoccupied energy band(s), the crystal can have only very few conducting electrons at low temperature and the crystal is either a semiconductor or an insulator, depending on the details of the band structure, such as the size of the band gap. If a crystal does not have a forbidden band gap between the highest occupied energy band(s) and the lowest energy band(s) with unoccupied states, the crystal usually has net conducting electrons at low temperature and the crystal is a metal.

Any real crystal always has a finite size and does not have the hypothetical infinite size on which the translational invariance is based. To circumvent this difficulty, in traditional solid state physics for crystals of finite size the periodic boundary conditions are usually assumed: Suppose a crystal of parallelogram shape has three sides $N_1\boldsymbol{a}_1$, $N_2\boldsymbol{a}_2$, and $N_3\boldsymbol{a}_3$ meeting at a corner; the periodic boundary conditions require that the wave functions of the electronic states $\phi_n(\boldsymbol{k}, \boldsymbol{x})$ in the finite crystal have to satisfy [2–6]

$$\phi_n(\boldsymbol{k}, \boldsymbol{x} + N_1\boldsymbol{a}_1) = \phi_n(\boldsymbol{k}, \boldsymbol{x} + N_2\boldsymbol{a}_2) = \phi_n(\boldsymbol{k}, \boldsymbol{x} + N_3\boldsymbol{a}_3) = \phi_n(\boldsymbol{k}, \boldsymbol{x}). \tag{1.9}$$

The effect of (1.9) is to make the wave vector $\boldsymbol{k}$ assume discrete values:

$$\boldsymbol{k} = k_1\boldsymbol{b}_1 + k_2\boldsymbol{b}_2 + k_3\boldsymbol{b}_3, \tag{1.10}$$

where

$$k_i = \frac{j_i}{N_i} 2\pi, \quad j_i = 0, 1, 2, ..., N_i - 1, \quad i = 1, 2, 3. \tag{1.11}$$

Thus, in each energy band n, there are, in all,

$$N = N_1 N_2 N_3 \tag{1.12}$$

Bloch states $\phi_n(\boldsymbol{k}, \boldsymbol{x})$ for such a finite crystal.

1.2 Energy Band Structure of Several Typical Crystals

The energy band structure of any specific solid is usually described by its energy–wave vector dispersion relation $E_n(\boldsymbol{k})$. It was first clearly understood by Kramers [8] that the energy band structure of one-dimensional crystals generally has some especially simple characteristics (see Chapter 2). The energy band structure in three-dimensional crystals is usually more complicated [9].

Many different physical properties of a solid can be understood from its specific band structure. For semiconductors (and insulators), the energy bands occupied by valence electrons are called the valence bands and there is a band gap between the highest occupied valence bands and the lowest unoccupied energy bands called the conduction bands. For crystals with translational invariance, only the energies in permitted energy bands are allowed. No electronic state can have its energy in the band gap.

The most important physics processes in a semiconductor always happen near the band gap. Therefore, the details of the band structure near the band gap, such as the size of the energy band gap, the locations of the conduction band extreme(s) and the valence band extreme(s), the band structure behaviors near those extremes, and so forth, are almost always technically the most important and theoretically the most interesting features. It is these details that determine the physical properties of a semiconductor and its possible applications.

In the following are shown the band structure figures of the two most important cubic semiconductors: Si and GaAs. Si is the most important semi-

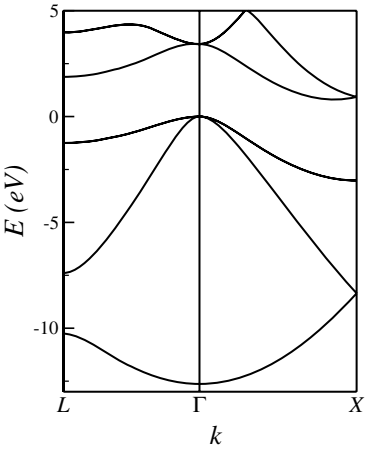

Fig. 1.1. Band structure of Si calculated by using the empirical pseudopotential method [10].

conductor material today due to the maturity of the processing technology for making devices with it and the abundant source of raw material. The band structure of Si is shown in Fig. 1.1. It has a band gap of about 1.2 eV and a valence band maximum (VBM) at the center of the Brillouin zone, with six conduction band minima located on the six equivalent [100] axes in the $\boldsymbol{k}$ space, near the boundary of the Brillouin zone. Despite its position as the number one semiconductor material in the electronic industry today, a significant shortcoming of Si is that it is an indirect semiconductor – the VBM and the conduction band minima are in different locations in the Brillouin zone, so that a direct optical transition between the VBM and any conduction band minimum is forbidden; thus, it is not easy to make optical devices with Si and to integrate optical processing devices with ordinary Si electronic integrated circuits.

After Si, GaAs is one of the most important semiconductor materials. The band structure of GaAs is shown in Fig. 1.2. It has a band gap of about 1.5 eV and both its VBM and its conduction band minimum are located at the center of the Brillouin zone. Therefore, GaAs is a direct-gap semiconductor – a direct optical transition between the VBM and the conduction band minimum is permitted and this makes GaAs one of the best semiconductor materials for making optical devices and optoelectronic integrated circuits.

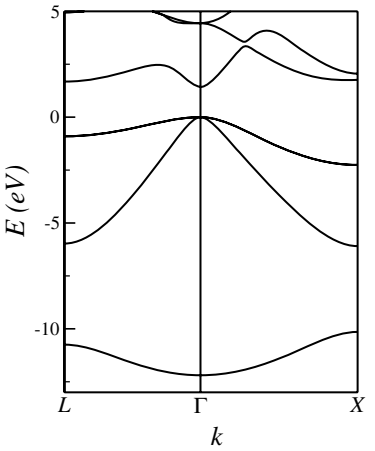

Fig. 1.2. Band structure of GaAs calculated by using the empirical pseudopotential method [10].

For metals, the most important physical processes happen near the Fermi surface; thus, the details of the band structure $E_n(\boldsymbol{k})$ near the Fermi surface are often of the greatest interest.

Modern solid state physics is essentially established on the basis of the theory of electronic states in crystals. Many theoretical methods have been developed to study various physical properties in different solids, most of them are based on general understandings such as the following: (i) The electronic states in crystals are Bloch waves and (ii) the physical properties of a specific solid are determined by its specific band structure. It has had great success – many of the electronic, electric, optical, magnetic, thermal, and mechanical properties of various solids of macroscopic size are well understood on the basis of this theory. Based on these understandings, many new electronic devices have been invented and developed; some of them – such as transistors and semiconductor integrated circuits – have brought revolutionary changes to modern science and technology.

1.3 Fundamental Difficulties of the Theory of the Electronic States in Traditional Solid State Physics

The theory of electronic states based on the translational invariance of the potential has been the basis of our current understanding of the electronic states in solids for more than 70 years and has achieved great success. Nevertheless, this traditional theory also has some fundamental difficulties. This is because the translational invariance of the potential can only exist in crystals of infinite size; thus, that the electronic states in crystals can be well described by Bloch waves (1.4) or (1.8) is correct only for crystals of infinite size. According to the Bloch theorem, Bloch waves (1.8) are progressive waves. In general, the flux density of Bloch waves is nonzero,

$$\phi_n^*(\boldsymbol{k},\boldsymbol{x})\nabla\phi_n(\boldsymbol{k},\boldsymbol{x}) - \phi_n(\boldsymbol{k},\boldsymbol{x})\nabla\phi_n^*(\boldsymbol{k},\boldsymbol{x}) \neq 0.$$

These progressive waves travel in all directions; only in the case of a crystal of infinite size will they always remain inside the crystal. Any real crystal has a finite size with a boundary. If the electronic states in a crystal of finite size are Bloch waves, these progressive waves can move beyond the boundary and the electrons in the crystal will flow away from the crystal, so that the crystal will continuously lose electrons. Consequently, the electronic states in a crystal of finite size cannot be progressive Bloch waves. To overcome this difficulty, the assumption of the periodic boundary conditions (1.9) actually implies that if an electron goes out from one boundary face of a crystal, it simultaneously comes back in from the opposite boundary face; obviously this is not true and not physically possible.

Any real crystal has a boundary. The existence of a boundary – the termination of the periodic potential – may introduce the existence of new types of electronic states. In 1932, Tamm [11] showed that in a one-dimensional Kronig–Penney [12] crystal, a termination of the periodic potential – a potential barrier outside the boundary of a semi-infinite crystal – can introduce

an additional type of electronic states existing in each band gap of the Bloch wave below the potential barrier. Electronic states of this new type – with energy inside the band gaps – are not permitted in crystals of infinite size or with periodic boundary conditions. They are called surface states because they are located near the surface of crystals. Since then, investigations on the surface states and relevant problems have become a rapidly developing and very productive field in solid state physics and chemistry [13,14]. It is now well understood that the existence and properties of the surface states can play a very significant role in affecting the physical properties of solids and physical processes in solids. The assumption of periodic boundary conditions (1.9) is a simplification that removes any possible boundary effects of the crystal; it does not correspond to the physical reality of any real crystal. For a finite crystal, it gives $N_1N_2N_3$ Bloch states for each energy band. Consequently, the traditional theory of electronic states in solids – based on translational invariance of the potential – cannot account for the existence of surface states. The very existence of the non-Bloch states has to be based on a separate and different theoretical consideration. This is another fundamental difficulty of the traditional theory of the electronic states in solids.

Since the theory on the electronic states in crystals in traditional solid state physics is essentially a theory of electronic states in crystals of infinite size, even some simple but also obviously fundamental problems, such as how many different types of electronic states there are in a simple finite crystal of orthorhombic shape such as shown in Fig. 1.3 and how these electronic states are different from each other, have not been well understood.

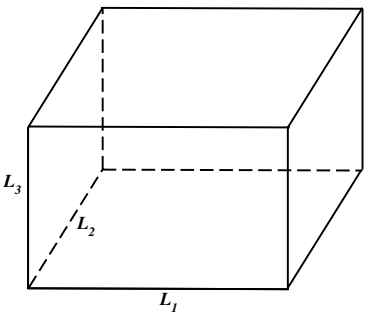

Fig. 1.3. An orthorhombic crystal with sides of length L_1, L_2, and L_3.

In traditional solid state physics, all electronic states are considered as Bloch waves. In the early days, when people mainly dealt with solids of macroscopic size in which the bulk properties of the solid were the main interest, this was acceptable because in crystals of macroscopic size, the number of bulk-like states is much larger than the number of surface-like states, side-like states, corner-like state, and so forth.

The difference between the electronic structure of a real crystal of finite size and the electronic structure obtained based on the translational invariance becomes more significant as the crystal size decreases. A clear understanding of the properties of electronic states in real crystals of finite size has both theoretical and practical significance. Since the early 1970s, investigations on the properties of low-dimensional systems such as quantum wells, wires, and dots in the submicron and nanometer size range has proceeded rapidly. It was found that in these low-dimensional systems, the properties of a semiconductor crystal change dramatically as the system size decreases: The measured optical bandgap increases as the system size decreases; some indirect semiconductors such as Si may become luminescent [e.g.,15], and direct semiconductors such as GaAs may develop into an indirect one [e.g.,16]. These very interesting size-dependent properties of semiconductors provide both a great potential for possible practical applications and a great theoretical challenge for a clear understanding of the fundamental physics, since the previous theory of electronic states in solids based on translational invariance can by no means account for these size-dependent effects.

Therefore, a clear understanding of the electronic states in low-dimensional systems and finite crystals can be both very interesting theoretically and very important practically. However, to develop a general analytical theory of the electronic states for low-dimensional systems or finite crystals with a boundary has been considered as a rather difficult problem: The lack of translational invariance in low-dimensional systems or finite crystals is a major obstacle. It is the use of the translational invariance – the Bloch theorem – that provides both a theoretical frame and a great mathematical simplification in solving the Schrödinger equation with a periodic potential. Without such a theoretical frame based on the Bloch theorem and the mathematical simplification, the corresponding problem for finite crystals with boundary seems to become rather difficult. Thus, most previous theoretical investigations on the electronic states in low-dimensional systems were based on approximate and/or numerical approaches and were usually on a specific material and/or on a specific model [e.g.,17–24]. One of the most widely used approximate methods or approaches is the effective mass approximation.

1.4 The Effective Mass Approximation

The effective mass approximation (EMA) is a widely used approximation in semiconductor physics. It has many different forms; nevertheless, basically the electrons in a semiconductor are treated as electrons with an "effective mass" instead of the free-electron mass. This is a very successful approach in investigating the behavior of electrons in a semiconductor under a weak and slowly varying external field – such as an applied electric and/or magnetic field or the field introduced by a shallow impurity [25].

The theory of electronic states in low-dimensional systems and finite crystals can also be considered as a theory on the quantum confinement of Bloch waves. The quantum confinement of plane waves – the simplest case is the well-known square potential problem – is a subject treated in almost all standard quantum mechanics textbooks and is well understood [26]. In the simplest case, when an electron in one dimension is completely confined in a square potential well of width L, the energy of the electron may only take discrete values:

$$E_j = \frac{j^2\hbar^2}{2mL^2}, \quad j = 1, 2, 3, ... \tag{1.13}$$

Here, m is the electron mass.[1] Therefore, the lowest possible energy $\hbar^2/2mL^2$ of the electron in the well increases as the well width L decreases. Equation (1.13) can be easily extended to the case where the confinement is in two or three directions. If the barrier heights outside the well are finite rather than infinite, the confinement will not be complete and, consequently, the energy levels inside the well will be somewhat lower. Therefore, the quantum confinement always raises the lowest possible energy level inside the well: The smaller the well width L and/or the higher the barrier outside the well, the higher the lowest possible energy level inside the well.

A well-known experimental fact is that the measured optical energy gap in a semiconductor low-dimensional system increases as the system size decreases. The well-understood concept of the quantum confinement effect of plane waves such as indicated in (1.13) was naturally borrowed to explain this notable fact [e.g.,28]. According to EMA, the "effective mass" of Bloch electrons should be used instead of the free-electron mass m in (1.13) or related formulas. In a semiconductor crystal, the Bloch electrons have a positive effective mass near the conduction band minimum and a negative effective mass near the VBM. Therefore, as the system size decreases, the consequence of EMA is that the lowest possible energy level in the conduction bands of a semiconductor crystal will go up and the highest possible energy level in the valence bands will go down, as shown in Fig. 1.4 – a consequence of the quantum confinement effect of plane waves.

Various forms of EMA have been very widely used in investigating the quantum confinement of Bloch electrons [e.g.,17–20,29]. It turns out that in comparison with the experimental results, the theoretical predictions from the various forms of EMA generally overestimate the gap increase as the system size decreases. These general overestimations were usually explained by some factors not included in the EMA, such as the nonparabolicity of the energy band structure and so forth. It is widely believed in the solid

[1] By including the relativistic effect, (1.13) can be further extended to

$$E_j^2 = m^2c^4 + j^2\hbar^2c^2\left(\frac{\pi}{L}\right)^2,$$

where c is the speed of light [27].

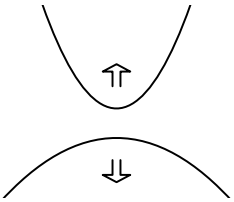

Fig. 1.4. According to EMA, the energy of the lowest unoccupied state will go up and the energy of the highest occupied state will go down as the size of the semiconductor crystal decreases.

state physics community that for quantum confinement of Bloch waves in semiconductor low-dimensional systems, a physics picture such as shown in Fig. 1.4 is conceptually and qualitatively correct although the EMA might not be able to give quantitatively accurate numerical results.

A natural comment on the use of various forms of EMA in investigating the quantum confinement of Bloch waves is that, originally, EMA was developed for treating the electronic states near band edges in the presence of a slowly varying and weak external perturbation, whereas in a quantum confinement problem, the perturbation is neither weak nor slowly varying at the confinement boundary, thus the conditions for justifying the use of EMA are completely violated. Much work has been done on this interesting puzzle, mainly using the envelope function approach [30].

1.5 Some Numerical Results

A very interesting work by Zhang and Zunger [31] on the energy spectrum of confined electrons in Si quantum films obtained results qualitatively different from what one would expect from EMA. In contrast to the prediction of the EMA, in their numerical investigation on Si (001) quantum films Zhang and Zunger [31] observed a band edge state whose energy was approximately equal to the energy of the VBM and hardly changes as the film thickness changes, as shown in Fig. 1.5. Such states have also been observed in numerical investigations on (110) free-standing Si and GaAs quantum film [31–33]. They were called "zero-confinement states." The very existence of such states is directly contradictory to the consequence of the EMA. The obvious failure of EMA for understanding the quantum confinement effect of these band edge states clearly indicates that the quantum confinement of Bloch waves might be fundamentally different from what one might expect from the well-known quantum confinement of plane waves. Without a clear understanding of the physical origin behind the existence of such states, the essential physics on the

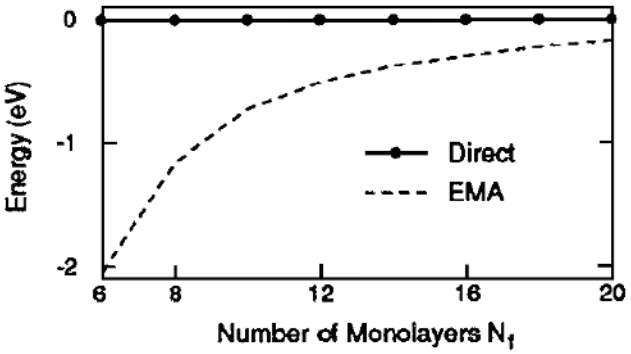

Fig. 1.5. Size dependence of the energy of the "zero-confinement" band edge state in Si (001) films. Reprinted with permission from S. B. Zhang and A. Zunger: Appl. Phys. Lett. **63**, 1399 (1993). Copyright by the American Institute of Physics.

quantum confinement of Bloch waves is not well understood. One may also naturally doubt whether EMA is suitable for describing the quantum confinement of Bloch waves even *conceptually* and one has to be careful when using EMA or EMA-derived ideas or approaches for treating the quantum confinement of Bloch waves, otherwise some important physics might be missed.

The "central observation" of the investigation of Zhang and Zunger in [31] is that the energy spectrum of confined electrons in Si (001) quantum films maps the energy band structure of Si approximately, as shown in Fig. 1.6.

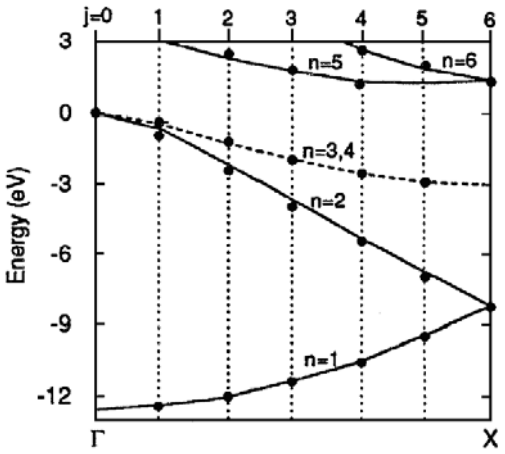

Fig. 1.6. A comparison between the energy bands $E_n(\boldsymbol{k})$ (lines) and the directly calculated eigenvalues in Si (001) film of 12 monolayers. Reprinted with permission from S. B. Zhang and A. Zunger: Appl. Phys. Lett. **63**, 1399 (1993). Copyright by the American Institute of Physics.

Similar maps of the energy spectra of confined electron states were observed in Si (110) and GaAs (110) quantum films [32]. Much previous work also indicates that the eigenvalues of confined Bloch states map *closely* the dispersion relations of the unconfined Bloch waves [e.g.,34].

All of these are *observations* obtained by numerical calculations. On the other hand, an analytical result by Pedersen and Hemmer [35] found that the energy spectrum of the majority of the confined electronic states in a finite one-dimensional Kronig–Penney crystal maps the energy bands exactly and does not depend on the boundary location. However, they were unable to treat either the quantum confinement of the bandedge states or the lowest energy band in their model.

A correct theory on the electronic states in low-dimensional systems and finite crystals should give clear explanations of the numerical results such as those shown in Figs. 1.5 and 1.6. It should give clear predictions on the properties of electronic states in low-dimensional systems, including giving an answer to the simple but fundamental problem on how many different types of electronic states there are in a simple finite crystal with an orthorhombic shape and how those electronic states are different from each other, as asked in Section 1.3. It should also clearly indicate the similarities and differences between the quantum confinement of Bloch waves and the well-known quantum confinement of plane waves.

1.6 Subject of the Book and Main Findings

In this book, we try to present a simple theory to obtain some of the most fundamental understandings of the electronic states in low-dimensional systems and finite crystals. We use the Born–Oppenheimer approximation; thus, we can consider the electronic states in a fixed atomic background. Further, we consider only a single-electron and nonspin theory.

Ideal low-dimensional systems and finite crystals are the simplest low-dimensional systems and finite crystals. By "ideal", it is assumed that (i) the potential $v(\boldsymbol{x})$ inside the low-dimensional system or finite crystal is the same as in a crystal with translational invariance and (ii) the electronic states are completely confined in the limited size of the low-dimensional system or finite crystal. These two simplifying assumptions facilitate the development of an analytical theory of the electronic states in ideal low-dimensional systems and finite crystals and allow us to try to explore and understand some of the most general physics related to the quantum confinement of Bloch waves and the electronic states in crystals of *finite* size.

Basically, we proceed by trying to understand two issues: (i) We try to understand the similarities and differences between the complete quantum confinement of plane waves and the complete quantum confinement of Bloch waves in one-dimensional space. It is now found that this problem can be

understood and it provides new and fundamental understanding on relevant physics problems. (ii) We try to understand the similarities and differences between the complete quantum confinement of Bloch waves in one-dimensional space and the complete quantum confinement of Bloch waves in three-dimensional space. This problem is more difficult and now we can only understand some simple cases.

An ideal low-dimensional system or finite crystal is a simplified model of a real low-dimensional system or finite crystal. A clear understanding of the electronic states in ideal low-dimensional systems and finite crystals is a first step and the basis for understanding electronic states – and relevant physical properties – of any real low-dimensional system or finite crystal. As Anderson pointed out in his Nobel Prize Lecture [36],

> Very often such a simplified model throws more light on the real workings of nature than any number of *ab initio* calculations of individual situations, which even where correct often contain so much details as to conceal rather than reveal reality. It can be a disadvantage rather than an advantage to be able to compute or to measure too accurately, since often what one measures or computes is irrelevant in terms of mechanism. After all, the perfect computation simply reproduces Nature, it does not explain her.

Real low-dimensional systems and finite crystals are more complicated than the ideal low-dimensional systems and finite crystals treated in this book. However, in comparison to crystals of infinite size, ideal low-dimensional systems and finite crystals are much closer to the physical reality of the real low-dimensional systems and finite crystals. We hope we have reason to expect that the understanding obtained for the ideal low-dimensional systems and finite crystals will be a significant step toward a clearer understanding of the electronic states in the real low-dimensional systems and finite crystals.

The book is organized as follows. In Part II, we treat one-dimensional semi-infinite crystals and finite crystals. These are the simplest systems that can manifest the effects of the existence of boundary and, in most cases, the relevant conclusions can be rigorously proven. We prepare some necessary mathematical basis on the theory of relevant ordinary differential equations in Chapter 2. In Chapter 3, we present a general analysis on the existence and properties of surface states in one-dimensional semi-finite crystals. It is found that, in general, the existence of a boundary does not always introduce a surface state in a specific band gap; only when the boundary of a semi-infinite crystal is located in some specific separated subintervals can a surface state exist in that specific band gap.

In Chapter 4, we present an analytical general theory of the electronic states in one-dimensional crystals of finite length. It is proven that in a one-dimensional finite crystal bounded at τ and $\tau + L$, where $L = Na$, a is the potential period, and N is a positive integer, there are two different types of electronic states: Corresponding to each energy band of the Bloch wave,

there are $N-1$ stationary Bloch states in the finite crystal whose energies are dependent on the crystal length L but not on the crystal boundary location τ and they map the energy band exactly. Corresponding to each band gap of the Bloch wave, there is always one and only one electronic state in the finite crystal whose energy is dependent on the boundary location τ but not on the crystal length L; this state can be either a surface state in the band gap or a band edge state. It is well known that if one-dimensional plane waves are completely confined, all of the permitted states are stationary waves. Therefore, the very existence of the boundary-dependent states is a fundamental distinction of the quantum confinement of Bloch waves.

A clear understanding of electronic states in one-dimensional crystals of finite length establishes a good basis and starting point for the further understanding of the electronic states in low-dimensional systems and three-dimensional crystals of finite size. Part III consists of three chapters devoted to these subjects.

There are similarities and differences between the quantum confinement of three-dimensional Bloch waves and one-dimensional Bloch waves. The problem on the electronic states in a free-standing quantum film can be considered as three-dimensional Bloch waves confined in one specific direction and is treated in Chapter 5. It is found in some simple and interesting cases where the electronic states in an ideal quantum film are bounded at $x_3 = \tau_3$ [2] and $x_3 = (\tau_3 + N_3)$ – here τ_3 defines the bottom boundary of the film and N_3 is a positive integer indicating the thickness in layers of the film – that there are two different types of electronic states: For each bulk energy band n and each wave vector $\hat{\boldsymbol{k}}$ in the film plane, there are $N_3 - 1$ stationary Bloch electronic states in the film whose energies are dependent on the film thickness N_3 but not on the film boundary τ_3 and one electronic state whose energy is dependent on τ_3 but not on N_3. The energies of these stationary Bloch electronic states map the energy band of the bulk exactly, whereas the energy of the τ_3-dependent state is usually above or occasionally equal to the highest energy in that energy band with that $\hat{\boldsymbol{k}}$. This τ_3-dependent state is usually a surface state, and, occasionally, it can be a single Bloch state. A significant difference of the quantum confinement of the three-dimensional Bloch waves is that, unlike the one-dimensional case discussed in Chapter 4, a surface state in such a film does not have to be in a band gap.

The electronic states in some simple quantum wires can be considered as merely two-dimensional Bloch waves in the quantum films further confined in one more direction. The electronic states in some simple finite crystals or quantum dots can be considered as one-dimensional Bloch waves in the quantum wires further confined in the third direction. By investigating the effects of the quantum confinement of the Bloch waves step by step, we can

[2] In this book, a position vector is usually written as $\boldsymbol{x} = x_1\boldsymbol{a}_1 + x_2\boldsymbol{a}_2 + x_3\boldsymbol{a}_3$. For quantum films, it is usually assumed that $\boldsymbol{a}_3$ is the only primitive lattice vector out of the film plane.

obtain a general understanding of the electronic states in some simple ideal low-dimensional systems and finite crystals.

The electronic states in a simple rectangular quantum wire having a thickness of N_3 layers and a boundary given by τ_3 in the $\boldsymbol{a}_3$ direction, and a width of N_2 layers and a boundary given by τ_2 in the $\boldsymbol{a}_2$ direction can be considered as having two-dimensional Bloch waves in the quantum film further confined in the $\boldsymbol{a}_2$ direction. This is the subject treated in Chapter 6. It is found in some simple and interesting cases that the electronic states in such an ideal rectangular quantum wire can be generally and exactly obtained. For such a quantum wire of crystals with a simple cubic, tetragonal, or orthorhombic Bravais lattice, for each bulk energy band n and each wave vector $\bar{\boldsymbol{k}}$ in the wire direction $\boldsymbol{a}_1$, there are $(N_2-1)(N_3-1)$ one-dimensional Bloch waves whose energies map the bulk energy band exactly and depend on N_2 and N_3 but not on τ_2 and τ_3, $(N_2-1)+(N_3-1)$ one-dimensional Bloch waves whose energies depend either on N_2 and τ_3 but not on τ_2 and N_3, or on N_3 and τ_2 but not on τ_3 and N_2, and one one-dimensional Bloch wave whose energy depends on τ_2 and τ_3 but not on N_2 and N_3. Correspondingly, those electronic states can be considered as bulk-like states, surface-like states, and side-like states in the quantum wire. For a rectangular quantum wire of crystals with a face-centered-cubic or body-centered-cubic Bravais lattice, the numbers of each type of electronic states are somewhat different. For the electronic states with the same bulk energy band index n and the same $\bar{\boldsymbol{k}}$, the following general relations exist:

The energy of the side-like state
$>$ The energy of every surface-like state
$>$ The energy of every relevant bulk-like state.

The electronic states in a simple orthorhombic finite crystal or quantum dot having a thickness of N_3 layers and a boundary given by τ_3 in the $\boldsymbol{a}_3$ direction, a width of N_2 layers and a boundary given by τ_2 in the $\boldsymbol{a}_2$ direction, and a length of N_1 layers and a boundary given by τ_1 in $\boldsymbol{a}_1$ direction can be considered as one-dimensional Bloch waves in a rectangular quantum wire further confined in the $\boldsymbol{a}_1$ direction. This is the subject treated in Chapter 7. It is found in some simple and interesting cases that the electronic states in such an ideal finite crystal or quantum dot can be generally and exactly obtained. For such a finite crystal or quantum dot of crystals with a simple cubic, tetragonal, or orthorhombic Bravais lattice, for each bulk energy band there are $(N_1-1)(N_2-1)(N_3-1)$ bulk-like states, $(N_1-1)(N_2-1)+(N_2-1)(N_3-1)+(N_3-1)(N_1-1)$ surface-like states, $(N_1-1)+(N_2-1)+(N_3-1)$ side-like states, and one corner-like state. For an orthorhombic finite crystal or quantum dot of crystals with a face-centered-cubic or body-centered-cubic Bravais lattice, the numbers of each type of electronic states are somewhat different. For electronic states with the same bulk energy band index n, the following general relations exist:

The energy of the corner-like state

> The energy of every side-like state
> > The energy of every relevant surface-like state
> > > The energy of every relevant bulk-like state.

Due to the existence of the boundary-dependent electronic states, the properties of electronic states in the low-dimensional systems and finite crystals may actually be substantially different from the properties of electronic states in crystals with translational invariance as understood in traditional solid state physics, they may also be substantially different from what is widely believed on the electronic states in low-dimensional systems in the solid state physics community, such as those originating from the EMA-derived ideas. For example, it is found that the real band gap in an ideal low-dimensional system of a cubic semiconductor is actually smaller than the band gap of the bulk semiconductor with translational invariance. It may even be possible that a low-dimensional system of a cubic semiconductor crystal could have the electrical conductivity of a metal.

Chapter 8 in Part IV is devoted to the concluding remarks. The understandings we have had actually are only the very beginning: For the little we have just understood, there is so much more we do not understand. In particular, a natural question is: Are those interesting results merely particular behaviors of this specific problem on the electronic states in low-dimensional systems or finite crystals, or might they actually be one of consequences of *a whole class* of more general relevant problems concerning the truncated translational invariance?

References

1. F. Bloch: Zeit. Phys. **52**, 555 (1928)
2. F. Seitz: *The Modern Theory of Solids* (McGraw-Hill, New York 1940)
3. H. Jones: *The Theory of Brillouin Zones and Electronic States in Crystals* (North-Holland, Amsterdam 1960)
4. W. A. Harrison: *Solid State Theory* (McGraw-Hill, New York 1970)
5. J. Callaway: *Quantum Theory of the Solid State*, 2nd ed. (Academic Press, London 1991)
6. C. Kittel: *Introduction to Solid State Physics*, 7th ed. (John Wiley & Sons, New York 1996)
7. L. Brillouin: J. Phys. Radium **1**, 377 (1930)
8. H. A. Kramers: Physica **2**, 483 (1935)
9. J. R. Chelikowsky and M. L. Cohen: *Electronic Structure and Optical Properties of Semiconductors*, 2nd ed. (Springer, Berlin Heidelberg 1989)
10. J. R. Chelikowsky and M. L. Cohen: Phys. Rev. **B14**, 556 (1976)
11. I. Tamm: Physik. Z. Sowj. **1**, 733 (1932)
12. R. L. Kronig and W. G. Penney: Proc. Roy. Soc. London. Ser. A **130**, 499 (1931)
13. S. G. Davison and M. Stęślicka: *Basic Theory of Surface States* (Clarendon Press, Oxford 1992)

14. M. -C. Desjonquéres and D. Spanjaard: *Concepts in Surface Physics* (Springer, Berlin Heidelberg 1993)
15. M. Nirmal and L. Brus: Acc. Chem. Res. **32**, 417 (1999); S. Ossicini, L. Pavesi, and F. Priolo: *Light Emitting Silicon for Microphotonics* (Springer, Berlin Heidelberg 2003) and the references therein
16. A. Franceschetti and A. Zunger: Phys. Rev. **B52**, 14664 (1995); A. Franceschetti and A. Zunger: J. Chem. Phys. **104**, 5572 (1996)
17. A. D. Yoffe: Adv. Phys. **42**, 173 (1993); A. D. Yoffe: Adv. Phys. **50**, 1 (2001); A. D. Yoffe: Adv. Phys. **51**, 799 (2002) and references therein
18. J. H. Davies: *The Physics of Low Dimensional Semiconductors* (Cambridge University Press, Cambridge 1998) and references therein
19. P. Harrison: *Quantum wells, wires and dots: Theoretical and Computational Physics* (John Wiley & Sons, New York 2000) and references therein
20. J. B. Xia: Phys. Rev. **B40**, 8500 (1989); T. Takagahara and K. Takeda: Phys. Rev. **B46**, 15578 (1992); T. Takagahara: Phys. Rev. **B47**, 4569 (1993); Al. L. Efros, M. Rosen, M. Kuno, M. Nirmal, D. J. Norris, and M. Bawendi: Phys. Rev. **B54**, 4843 (1996); Al. L. Efros and M. Rosen: Ann. Rev. Mat. Sci. **30**, 475 (2000); A. V. Rodina, Al. L. Efros, and A. Yu. Alekseev: Phys. Rev. **B67**, 155312 (2003); D. H. Feng, Z. Z. Xu, T. Q. Jia, X. X. Li, and S. Q. Gong: Phys. Rev. **B68**, 035334 (2003)
21. A. Di Carlo: Semicond. Sci. Tech. **18**, R1 (2003) and references therein
22. P. E. Lippens and M. Lannoo: Phys. Rev. **B39**, 10935 (1989); S. Y. Ren and J. D. Dow: Phys. Rev. **B45**, 6492 (1992); G. D. Sanders and Y. C. Chang: Phys. Rev. **B45**, 9202 (1992); G. Allan, C. Delurue, and M. Lannoo: Phys. Rev. Lett. **76**, 2961 (1996); S. Y. Ren: Phys. Rev. **B55**, 4665 (1997); S. Y. Ren: Solid State Commun. **102**, 479 (1997); Y. M. Niquet, G. Allan, C. Delurue, and M. Lannoo: Appl. Phys. Lett. **77**, 1182 (2000); Y. M. Niquet, C. Delurue, G. Allan, and M. Lannoo: Phys. Rev. **B62**, 5109 (2000); J. Sée, P. Dollfus, and S. Galdin: Phys. Rev. **B66**, 193307 (2002); S. Sapra and D. D. Sarma: Phys. Rev. **B69**, 125304 (2004); P. Chen and K. B. Whaley: Phys. Rev. **B70**, 045311 (2004); G. Allan and C. Delurue: Phys. Rev. **B70**, 245321 (2004)
23. L. W. Wang and A. Zunger: J. Chem. Phys. **100**, 2394 (1994); L. W. Wang and A. Zunger: J. Phys. Chem. **98**, 2158 (1994); L. W. Wang and A. Zunger: Phys. Rev. Lett. **73**, 1039 (1994); C. Y. Yeh, S. B. Zhang, and A. Zunger: Phys. Rev. **B50**, 14405 (1994); A. Tomasulo and M. V. Ramakrishna: J. Chem. Phys. **105**, 3612 (1996); L. W. Wang and A. Zunger: Phys. Rev. **B53**, 9579 (1996); H. X. Fu and A. Zunger: Phys. Rev. **B55**, 1642 (1997); H. X. Fu and A. Zunger: Phys. Rev. **B56**, 1496 (1997); L. W. Wang, J. N. Kim, and A. Zunger: Phys. Rev. **B59**, 5678 (1999); F. A. Reboredo, A. Franceschetti, and A. Zunger: Appl. Phys. Lett. **75**, 2972 (1999); A. Franceschetti, H. X. Fu, L. W. Wang, and A. Zunger: Phys. Rev. **B60**, 1919 (1999)
24. B. Delley and E. F. Steigmeier: Appl. Phys. Lett. **67**, 2370 (1995); S. Ogut, J. R. Chelikowsky, and S. G. Louie: Phys. Rev. Lett. **79**, 1770 (1997); C. S. Garoufalis, A. D. Zdetsis, and S. Grimme: Phys. Rev. Lett. **87**, 276402 (2001); H.-Ch. Weissker, J. Furthmüller, and F. Bechstedt: Phys. Rev. **B67**, 245304 (2003); A. S. Barnard, S. P. Russo, and I. K. Snook: Phys. Rev. **B68**, 235407 (2003); X. Zhao, C. M. Wei, L. Yang, and M. Y. Chou: Phys. Rev. Lett. **92**, 236805 (2004); R. Rurali and N. Lorenti: Phys. Rev. Lett. **94**, 026805 (2005); G. Nesher, L. Kronik, and J. R. Chelikowsky: Phys. Rev. **B71**, 035344 (2005)

25. J. M. Luttinger and W. Kohn: Phys. Rev. **97**, 869 (1957); W. Kohn: *Solid State Physics*, edited by F. Seitz and D. Turnbull (Academic Press, New York 1955), Vol. 5, pp. 257–320
26. L. I. Schiff: *Quantum Mechanics*, 3rd ed. (McGraw-Hill, New York 1968)
27. S. Y. Ren: Chin. Phys. Lett. **19**, 617 (2002)
28. Al. L. Efros and A. L. Efros: Sov. Phys. Semicon. **16**, 772 (1982); L. E. Brus: J. Phys. Chem. **80**, 4403 (1984); Y. Wang and N. Herron: J. Phys. Chem. **95**, 525 (1991)
29. M. J. Kelly: *Low-Dimensional Semiconductors: Materials, Physics, Technology, Devices*, 3rd ed. (Oxford University Press, Oxford 1995); B. K. Ridley: *Electrons and Phonons in Semiconductor Multilayers*, 3rd ed. (Cambridge University Press, Cambridge 1997); L. Bányai and S. W. Koch: *Semiconductor Quantum Dots* (World Scientific, Singapore 1993); C. Delerue and M. Lannoo: *Nanostructures: Theory and Modeling* (Springer, Berlin Heidelberg 2004); S. Glutch: *Excitons in Low-dimensional Semiconductors: Theory, Numerical Methods, Applications* (Springer, Berlin Heidelberg 2004)
30. M. G. Burt: J. Phys. Condens. Matter **4**, 6651 (1992) and references therein
31. S. B. Zhang and A. Zunger: Appl. Phys. Lett. **63**, 1399 (1993)
32. S. B. Zhang, C.-Y. Yeh, and A. Zunger: Phys. Rev. **B48**, 11204 (1993)
33. A. Franceschetti and A. Zunger: Appl. Phys. Lett. **68**, 3455 (1996)
34. Z. V. Popovic, M. Cardona, E. Richter, D. Strauch, L. Tapfer, and K. Ploog: Phys. Rev. **B40**, 1207 (1989); Z. V. Popovic, M. Cardona, E. Richter, D. Strauch, L. Tapfer, and K. Ploog: Phys. Rev. **B40**, 3040 (1989); Z. V. Popovic, M. Cardona, E. Richter, D. Strauch, L. Tapfer, and K. Ploog: Phys. Rev. **B41**, 5904 (1990)
35. F. B. Pedersen and P. C. Hemmer: Phys. Rev. **B50**, 7724 (1994)
36. P. W. Anderson: Rev. Mod. Phys. **50**, 191 (1978)

2 Mathematical Basis

One-dimensional crystals are the simplest crystals. Historically, much of our current fundamental understanding of the electronic structures of crystals were obtained through the analysis of one-dimensional crystals [1–3]. Among the most well-known examples are the Kronig–Penney model [4], Kramers' general analysis of the band structure of one-dimensional infinite crystals [5], Tamm's surface states [6], and so forth. In order to have a clear understanding of the electronic states in low-dimensional systems and finite crystals, the first step is to have a clear understanding of the electronic states in one-dimensional finite crystals. To prepare for this purpose, in this chapter we begin with a more general study on the properties of the solutions of the relevant differential equations – the second-order linear homogeneous ordinary differential equations with periodic coefficients. In the theory of boundary value problems for ordinary differential equations, the existence and locations of the zeros of the solutions of such equations are often of central importance. After reviewing some elementary knowledge on the theory of second-order linear ordinary differential equations, we introduce two basic theorems on the zeros of solutions of second-order linear homogeneous ordinary differential equations. In the major part of this chapter, we will learn some more advanced theory on the second-order linear homogeneous differential equations with periodic coefficients and the zeros of their solutions. Based on the mathematical theory and theorems learned in this chapter, the general results on the electronic states in ideal one-dimensional finite crystals can be rigorously proven. The majority of this part is essentially from Eastham's book [7]. However, the mathematicians usually are more interested in the generality and completeness of the theory for more general equations, whereas what we need as a mathematical basis in this book is the conclusions of the usually simpler and more specific equations we need to solve. Eastham's book [7] contains contents that are not really relevant to our purpose and might be more difficult to read for many nonmathematicians; therefore, the author has reorganized and rewritten much of the relevant materials to make them simpler, but still sufficient for our purpose. The author wishes that readers with some elementary background in the theory of differential equations can read this part without major difficulties. Readers who are interested in a more complete and general mathematical theory are recommended to read

Eastham's original book [7]. Readers who are not interested in the proofs of relevant theorems may skip those parts of this chapter.

2.1 Elementary Theory and Two Basic Theorems

We are interested in a class of very simple second-order linear ordinary differential equations[1]:

$$y'' + q(x)y = 0, \quad -\infty < x < +\infty. \tag{2.1}$$

Here, $q(x)$ is a piecewise continuous real function.

There are some very general results on the solutions of (2.1):

1. Two linearly independent solutions. Any nontrivial solution y of (2.1) can be written as a linear combination of two linearly independent solutions $y_1(x)$ and $y_2(x)$ of (2.1):

$$y = c_1 y_1(x) + c_2 y_2(x).$$

2. The Wronskian. The Wronskian of two functions y_1 and y_2 can be defined as

$$W(y_1, y_2) = y_1 y_2' - y_1' y_2. \tag{2.2}$$

If y_1 and y_2 are two linearly independent solutions of (2.1), the Wronskian $W(y_1, y_2)$ of y_1 and y_2 is nonzero. It is also easy to prove that $\frac{\mathrm{d}}{\mathrm{d}x} W(y_1, y_2) = 0$, thus $W(y_1, y_2)$ does not depend on x.

3. The variation of parameters formula. Let $y_1(x)$ and $y_2(x)$ be two linearly independent solutions of (2.1). The nonhomogeneous equation

$$z'' + q(x)z = F(x)$$

can be solved as

$$z = -\int^x \frac{F(t)y_2(t)}{W[y_1(t), y_2(t)]}\,\mathrm{d}t\; y_1(x) + \int^x \frac{F(t)y_1(t)}{W[y_1(t), y_2(t)]}\,\mathrm{d}t\; y_2(x). \tag{2.3}$$

These well-known results on the theory of second-order linear ordinary differential equations can be found in introductory textbooks on the theory of linear ordinary differential equations [e.g.,8-10].

Further, we need two very basic theorems on the zeros of solutions in the theory of second-order linear ordinary differential equations [e.g.,11,12] for our future work.

[1] In this book, a prime on a function denotes differentiation with respect to the variable of the function. If the function has two or more variables, a prime on the function denotes differentiation with respect to the variable x of the function.

Theorem 2.1 (Sturm Separation Theorem).
Let y_1 and y_2 be two linearly independent solutions of (2.1); then the zeros of y_1 are always separated from the zeros of y_2.

Proof. Suppose α and β are two consecutive zeros of y_1,

$$y_1(\alpha) = y_1(\beta) = 0; \tag{2.4}$$

then it can be proven that there is at least one zero of y_2 in (α, β).

We assume that this is not true — that there is no zero of y_2 in (α, β). Then we can write

$$\frac{\mathrm{d}}{\mathrm{d}x}\frac{y_1}{y_2} = -\frac{W(y_1, y_2)}{y_2^2} \tag{2.5}$$

in (α, β). Integrating (2.5) from α to β, we obtain that

$$\left[\frac{y_1}{y_2}\right]_\alpha^\beta = -\int_\alpha^\beta \frac{W(y_1, y_2)}{y_2^2}\,\mathrm{d}x. \tag{2.6}$$

The left side of (2.6) is zero due to (2.4); the right side of (2.6) is not zero since $W(y_1, y_2)$ is a nonzero constant if y_1 and y_2 are two linearly independent solutions of (2.1). The assumption leads to a self-contradictory result; hence, there is at least one zero of y_2 in (α, β).

However, if there are more than one zero of y_2 in (α, β), then according to what we have just proven, there is at least one extra zero of y_1 between two zeros of y_2 in (α, β); this is contradictory to the supposition that α and β are two consecutive zeros of y_1. Therefore, there is always one and only one zero of y_2 between two consecutive zeros of y_1. Similarly, there is always one and only one zero of y_1 between two consecutive zeros of y_2. The zeros of two linearly independent solutions y_1 and y_2 of (2.1) are distributed alternatively and thus are separated from each other. □

Theorem 2.2 (Sturm Comparison Theorem).
Suppose in two equations

$$y'' + q_1(x)y = 0, \quad z'' + q_2(x)z = 0, \tag{2.7}$$

that

$$q_2(x) \geq q_1(x) \tag{2.8}$$

is true; then there is at least one zero of any solution z of the second equation between two zeros (α, β) of any solution y of the first equation.

Proof. Suppose that this is not true — that z is not zero anywhere in (α, β). Without loss of generality we may assume that α and β are two consecutive zeros of y:

$$y(\alpha) = y(\beta) = 0, \tag{2.9}$$

$y > 0$ and $z > 0$ in (α, β). Then we have $y'(\alpha) > 0$ and $y'(\beta) < 0$.

From (2.7) we obtain that

$$\int_{\alpha}^{\beta} [zy'' - yz''] \, \mathrm{d}x = \int_{\alpha}^{\beta} [q_2(x) - q_1(x)]yz \, \mathrm{d}x. \tag{2.10}$$

However, the left side of (2.10) is

$$\int_{\alpha}^{\beta} [zy'' - yz''] \, \mathrm{d}x = \int_{\alpha}^{\beta} [zy' - yz']' \, \mathrm{d}x = [zy' - yz']_{\alpha}^{\beta} = [zy']_{\alpha}^{\beta} < 0.$$

However, the right side of (2.10) is

$$\int_{\alpha}^{\beta} [q_2(x) - q_1(x)]yz \, \mathrm{d}x \geq 0$$

due to the condition (2.8). Actually, this term is always larger than zero except that $q_2(x) = q_1(x)$ everywhere in (α, β). The supposition leads to two results contradictory to each other. Thus, the theorem is proven. □

These two theorems are very fundamental theorems in the theory of general second-order linear ordinary differential equations. In the following, we will meet some theorems on the theory of differential equations with periodic coefficients. In proving several theorems on the zeros of solutions of these equations, we will need to use the Sturm comparison theorem frequently. Both the Sturm separation theorem and the Sturm comparison theorem will be used in the later chapters.

2.2 Floquet Theory

Now, we consider a special case of (2.1) in which $q(x)$ is a periodic equation:

$$y'' + q(x)y = 0; \quad q(x + a) = q(x). \tag{2.11}$$

Here, a is a nonzero constant. Equation (2.11) is a simple form of the more general second-order linear ordinary differential equations with periodic coefficients – Hill's equation [13]:

$$[P(x)y'(x)]' + Q(x)y(x) = 0, \tag{2.12}$$

investigated by Hill in 1877. Here, $P(x)$ and $Q(x)$ are real functions[2] with period a. Hill's equation is a simple form of the more general second-order linear ordinary differential equations with periodic complex coefficients

$$a_0(x)y''(x) + a_1(x)y'(x) + a_2(x)y(x) = 0, \tag{2.13}$$

[2]It is assumed that $P(x)$ is continuous and nowhere zero and that $P'(x)$ and $Q(x)$ are piecewise continuous.

investigated by Floquet in 1883. In the following, we will introduce several theorems on (2.11), which are the simplified forms of theorems on (2.13) presented in [7]. Since (2.11) is simpler than (2.13), the proofs of the corresponding theorems are also somewhat simpler.

Theorem 2.3 (Theorem 1.1.1 in [7]).
There exist at least one nonzero constant ρ and one nontrivial solution $y(x)$ of (2.11) such that

$$y(x+a) = \rho\, y(x). \tag{2.14}$$

Proof. We can choose two linearly independent solutions $\eta_1(x)$ and $\eta_2(x)$ of (2.11) according to

$$\eta_1(0) = 1,\ \eta_1'(0) = 0;\quad \eta_2(0) = 0,\ \eta_2'(0) = 1. \tag{2.15}$$

These solutions are usually called normalized solutions of (2.11) [13].

Since the corresponding $\eta_1(x+a)$ and $\eta_2(x+a)$ are also two linearly independent nontrivial solutions of (2.11), we can write $\eta_1(x+a)$ and $\eta_2(x+a)$ as linearly combinations of $\eta_1(x)$ and $\eta_2(x)$:

$$\begin{aligned} \eta_1(x+a) &= A_{11}\eta_1(x) + A_{12}\eta_2(x), \\ \eta_2(x+a) &= A_{21}\eta_1(x) + A_{22}\eta_2(x), \end{aligned} \tag{2.16}$$

where A_{ij} $(1 \le i, j \le 2)$ are four constants. From (2.15) and (2.16), we obtain that

$$A_{11} = \eta_1(a),\ A_{21} = \eta_2(a),\ A_{12} = \eta_1'(a),\ A_{22} = \eta_2'(a).$$

Any nontrivial solution $y(x)$ of (2.11) can be written as

$$y(x) = c_1\eta_1(x) + c_2\eta_2(x),$$

where c_i are constants. If there is a nonzero ρ that makes

$$\begin{aligned} (A_{11} - \rho)c_1 + A_{21}c_2 &= 0, \\ A_{12}c_1 + (A_{22} - \rho)c_2 &= 0 \end{aligned} \tag{2.17}$$

true, then (2.11) has a nontrivial solution of the form (2.14). The requirement that c_i in (2.17) are not both zero leads to the condition

$$\rho^2 - [\eta_1(a) + \eta_2'(a)]\rho + 1 = 0. \tag{2.18}$$

Here, $\eta_1(a)\eta_2'(a) - \eta_1'(a)\eta_2(a) = \eta_1(0)\eta_2'(0) - \eta_1'(0)\eta_2(0) = 1$ has been used. The quadratic equation (2.18) is called the characteristic equation associate with (2.11) [13]. Equation (2.18) for ρ has at least one nonzero root since it has a nonzero constant term. □

We have proven that (2.11) has at least one nontrivial solution of the form (2.14). Actually, (2.11) may have two linearly independent nontrivial solutions of the form (2.14). Whether (2.11) can have two linearly independent

nontrivial solutions of the form (2.14) or only one such solution is determined by whether the matrix $A = (A_{ij})$ has two linearly independent eigenvectors or only one such eigenvector. If the characteristic equation (2.18) has two distinct roots ρ_1 and ρ_2, then the matrix $A = (A_{ij})$ always has two linearly independent eigenvectors and, thus, (2.11) has two linearly independent nontrivial solutions of the form (2.14). If the characteristic equation (2.18) has a repeated root, then the matrix $A = (A_{ij})$ may have either two linearly independent eigenvectors or only one independent eigenvector (see pp. 28-33). Correspondingly, (2.11) may have two linearly independent nontrivial solutions of the form (2.14) or only one such solution.

Theorem 2.4 (Theorem 1.1.2 in [7]).
There exist linearly independent solutions $y_1(x)$ and $y_2(x)$ of (2.11) such that either

$$(i) \quad y_1(x) = \mathrm{e}^{h_1 x} p_1(x), \quad y_2(x) = \mathrm{e}^{h_2 x} p_2(x),$$

where h_1 and h_2 are constants, not necessarily distinct, and $p_1(x)$ and $p_2(x)$ are periodic with period a, or

$$(ii) \quad y_1(x) = \mathrm{e}^{hx} p_1(x), \quad y_2(x) = \mathrm{e}^{hx}[x\ p_1(x) + p_2(x)],$$

where h is a constant and $p_1(x)$ and $p_2(x)$ are periodic with period a.

Proof. The characteristic equation (2.18) may have either two distinct roots or a repeated root.

1. If the characteristic equation (2.18) has two distinct roots ρ_1 and ρ_2, then there are two linearly independent nontrivial solutions of $y_1(x)$ and $y_2(x)$ of (2.11) such that

$$y_i(x + a) = \rho_i y_i(x), \ i = 1, 2.$$

We can define h_1 and h_2 so that

$$\mathrm{e}^{a h_i} = \rho_i \tag{2.19}$$

and then two functions $p_i(x)$ by

$$p_i(x) = \mathrm{e}^{-h_i x} y_i(x).$$

It is easy to see that $p_1(x)$ and $p_2(x)$ are periodic functions with period a:

$$p_i(x + a) = \mathrm{e}^{-h_i(x+a)} \rho_i y_i(x) = p_i(x).$$

Thus, (2.11) has two linearly independent non-trivial solutions:

$$y_1(x) = \mathrm{e}^{h_1 x} p_1(x); \quad y_2(x) = \mathrm{e}^{h_2 x} p_2(x). \tag{2.20}$$

2. Now, we consider the case that the characteristic equation (2.18) has a repeated root ρ. Define h by

$$\mathrm{e}^{ah} = \rho. \tag{2.21}$$

According to Theorem 2.3, (2.11) has a nontrivial solution of the form (2.14):

$$y_1(x+a) = \rho y_1(x).$$

Suppose $Y_2(x)$ is any solution of (2.11) that is linearly independent of $y_1(x)$. Since $Y_2(x+a)$ is also a nontrivial solution of (2.11), we can write

$$Y_2(x+a) = c_1 y_1(x) + c_2 Y_2(x) \tag{2.22}$$

and, here, c_1 and c_2 are constants. Since

$$W(y_1, Y_2)|_{x+a} = \rho c_2 W(y_1, Y_2)|_x$$

and $W(y_1, Y_2)|_x$ does not depend on x, therefore,

$$\rho c_2 = 1 = \rho^2,$$

the second equality is due to that the constant term in (2.18) is equal to 1. Thus,

$$c_2 = \rho.$$

Equation (2.22) can be written as

$$Y_2(x+a) = c_1 y_1(x) + \rho Y_2(x). \tag{2.23}$$

There could be two different cases:

2.1. $c_1 = 0$.

Equation (2.23) becomes

$$Y_2(x+a) = \rho Y_2(x).$$

We can choose $y_2(x) = Y_2(x)$. Thus, (2.11) has two linearly independent solutions $y_1(x)$ and $y_2(x)$ and

$$y_1(x+a) = \mathrm{e}^{ah} y_1(x), \qquad y_2(x+a) = \mathrm{e}^{ah} y_2(x).$$

The first part of the theorem is proven. This case corresponds to the case that the matrix $A = (A_{ij})$ has one repeated eigenvalue ρ but two linearly independent eigenvectors. Consequently, (2.11) may have two linearly independent nontrivial solutions of the form (2.14).

2.2. $c_1 \neq 0$.
Define

$$p_1(x) = \mathrm{e}^{-hx} y_1(x), \quad p_2(x) = (a\rho/c_1)\ \mathrm{e}^{-hx} Y_2(x) - x\ p_1(x);$$

then we have

$$p_1(x+a) = \mathrm{e}^{-h(x+a)} y_1(x+a) = p_1(x)$$

and

$$\begin{aligned} p_2(x+a) &= (a\rho/c_1)\ \mathrm{e}^{-h(x+a)} Y_2(x+a) - (x+a)p_1(x+a) \\ &= (a\rho/c_1)\ \mathrm{e}^{-h(x+a)}[c_1 y_1(x) + \rho Y_2(x)] - a p_1(x) - x\ p_1(x) \\ &= (a\rho/c_1)\ \mathrm{e}^{-hx} Y_2(x) - x\ p_1(x) = p_2(x). \end{aligned}$$

Thus, $p_1(x)$ and $p_2(x)$ are periodic functions. Since

$$y_1(x) = \mathrm{e}^{hx} p_1(x), \quad Y_2(x) = (c_1/a\rho)\ \mathrm{e}^{hx}[x\ p_1(x) + p_2(x)],$$

we may choose

$$y_2(x) = (a\rho/c_1)\ Y_2(x).$$

Thus,

$$y_2(x) = \mathrm{e}^{hx}[x\ p_1(x) + p_2(x)]$$

and part (ii) of the theorem is proven. This case corresponds to the cases in which the matrix $A = (A_{ij})$ has only one independent eigenvector. Correspondingly, (2.11) has only one independent nontrivial solution of the form (2.14).

□

Therefore, when (2.11) has two linearly independent nontrivial solutions of the form (2.14), part (i) of the theorem is true; when (2.11) has only one nontrivial solution of the form (2.14), part (ii) of the theorem is true. Whether (2.11) has two linearly independent nontrivial solutions of the form (2.14) or only one non-trivial solution of the form (2.14) is determined by whether the matrix $A = (A_{ij})$ has two linearly independent eigenvectors or only one such eigenvector.

2.3 Discriminant and Linearly Independent Solutions

From the last section, we see that the linearly independent solutions of (2.11) are determined by the roots ρ of the characteristic equation (2.18), which are determined by a real number:

$$D = \eta_1(a) + \eta_2'(a). \tag{2.24}$$

Thus, the real number D in (2.24) determines the linearly independent solutions of (2.11) in Theorem 2.4. This real number is called the discriminant of (2.11).

There can be five different cases.

A. $-2 < D < 2$.

The two roots ρ_1 and ρ_2 of the characteristic equation (2.18) are two distinct nonreal numbers. They are complex conjugates to each other and have moduli equal to unity. h_i in (2.19) can be chosen as imaginary numbers $\pm \mathrm{i}k$, where $0 < k < \pi/a$. Thus, there is a real number k for which $0 < ak < \pi$, giving

$$\mathrm{e}^{\mathrm{i}ak} = \rho_1; \quad \mathrm{e}^{-\mathrm{i}ak} = \rho_2. \tag{2.25}$$

Correspondingly, (2.11) has two linearly independent solutions,

$$y_1(x) = \mathrm{e}^{\mathrm{i}kx} p_1(x); \quad y_2(x) = \mathrm{e}^{-\mathrm{i}kx} p_2(x) \tag{2.26}$$

by (2.20). Here, $p_1(x)$ and $p_2(x)$ are periodic functions with period a.

B. $D = 2$.

The characteristic equation (2.18) has a repeated root $\rho = 1$. From (2.21), we obtain $h = 0$. There are two possible subcases:

B.1. $\eta_2(a)$ and $\eta_1'(a)$ are not both zero.

Now, not all elements in the matrix $(A - I\rho)$ are zero. The matrix $A = (A_{ij})$ has only one independent eigenvector.[3] Equation (2.11) can have only one solution of the form (2.14). Thus, part (ii) of Theorem 2.4 applies. Equation (2.11) can have two linearly independent nontrivial solutions as

$$y_1(x) = p_1(x); \quad y_2(x) = x\, p_1(x) + p_2(x). \tag{2.27}$$

B.2. $\eta_2(a) = \eta_1'(a) = 0$.

Since $W = \eta_1(a)\eta_2'(a) - \eta_1'(a)\eta_2(a) = 1$, we have

$$\eta_1(a)\eta_2'(a) = 1.$$

However,

$$\eta_1(a) + \eta_2'(a) = 2;$$

thus,

[3]Note that although (2.11) always has two linearly independent solutions, it does not mean that (2.17) can always have two independent solutions. Only when both of the two linearly independent solutions of (2.11) have the form (2.14) can (2.17) have two independent solutions and $A = (A_{ij})$ has two independent eigenvectors. If (2.17) has only one independent solution, then $A = (A_{ij})$ has only one independent eigenvector and only one solution of (2.11) has the form (2.14); the other linearly independent solution is given by $y_2(x)$ in part (ii) of Theorem 2.4.

$$\eta_1(a) = \eta_2'(a) = 1.$$

Now, in the matrix $(A - I\rho)$, all elements are zero and the matrix $A = (A_{ij})$ has two linearly independent eigenvectors. Equations (2.17) can have two independent solutions. Thus, (2.11) can have two linearly independent nontrivial solutions of the form (2.14) and part (i) of Theorem 2.4 applies:

$$y_1(x) = p_1(x); \quad y_2(x) = p_2(x). \tag{2.28}$$

C. $D > 2$.

The roots ρ_1 and ρ_2 of the characteristic equation (2.18) are two distinct positive real numbers that are not equal to unity. h_i in (2.19) can be chosen as real numbers $\pm\beta$. There is a real number $\beta > 0$ to make

$$\mathrm{e}^{a\beta} = \rho_1; \quad \mathrm{e}^{-a\beta} = \rho_2. \tag{2.29}$$

Correspondingly, (2.11) has two linearly independent solutions as

$$y_1(x) = \mathrm{e}^{\beta x} p_1(x); \quad y_2(x) = \mathrm{e}^{-\beta x} p_2(x) \tag{2.30}$$

by (2.20).

D. $D = -2$.

In this case, the characteristic equation (2.18) has repeated roots $\rho_1 = \rho_2 = -1$. h in (2.21) can be chosen as $\mathrm{i}\pi/a$. There are two possible subcases:

D.1. $\eta_2(a)$ and $\eta_1'(a)$ are not both zero.

Now, not all elements in the matrix $(A - I\rho)$ are zero. The matrix $A = (A_{ij})$ has only one independent eigenvector. Equation (2.11) can have only one solution of the form (2.14). Thus, part (ii) of Theorem 2.4 applies. Equation (2.11) can have two linearly independent nontrivial solutions as

$$y_1(x) = s_1(x); \quad y_2(x) = x\ s_1(x) + s_2(x). \tag{2.31}$$

Here, $s_i(x) = \mathrm{e}^{\mathrm{i}\frac{\pi}{a}\ x} p_i(x)$ and, thus, $s_i(x + a) = -s(x)$ are semi-periodic functions.

D.2. $\eta_2(a) = \eta_1'(a) = 0$.

Since $W = \eta_1(a)\eta_2'(a) - \eta_1'(a)\eta_2(a) = 1$, we have

$$\eta_1(a)\eta_2'(a) = 1.$$

However,

$$\eta_1(a) + \eta_2'(a) = -2;$$

thus,

$$\eta_1(a) = \eta_2'(a) = -1.$$

Now, in the matrix $(A - I\rho)$, all elements are zero and the matrix $A = (A_{ij})$ has two linearly independent eigenvectors. Equations (2.17) can have two independent solutions. Thus, (2.11) can have two linearly independent nontrivial solutions of the form (2.14) and part (i) of Theorem 2.4 applies. The two linearly independent nontrivial solutions of (2.11) can be chosen as

$$y_1(x) = s_1(x); \quad y_2(x) = s_2(x). \tag{2.32}$$

Here, $s_i(x)$ are semi-periodic functions $s_i(x + a) = -s_i(x)$.

E. $D < -2$.

The roots ρ_1 and ρ_2 of the characteristic equation (2.18) are two distinct negative real numbers and are not equal to -1. h_i in (2.19) can be chosen as complex numbers $\pm(\beta + \mathrm{i}\pi/a)$. Thus, there is a real number $\beta > 0$ to give

$$\mathrm{e}^{a(\beta+\mathrm{i}\frac{\pi}{a})} = \rho_1; \quad \mathrm{e}^{-a(\beta+\mathrm{i}\frac{\pi}{a})} = \rho_2. \tag{2.33}$$

Correspondingly, (2.11) can have two linearly independent solutions as

$$y_1(x) = \mathrm{e}^{\beta x} s_1(x); \quad y_2(x) = \mathrm{e}^{-\beta x} s_2(x). \tag{2.34}$$

Here, $s_i(x + a) = -s(x)$ are semi-periodic functions.

2.4 Basic Theory of the Schrödinger Equation in One-Dimensional Crystals

By introducing

$$v(x) = \frac{2m}{\hbar^2} V(x), \qquad \lambda = \frac{2m}{\hbar^2} E, \tag{2.35}$$

the Schrödinger equation in a one-dimensional crystal can be written as

$$-y'' + [v(x) - \lambda]y = 0; \tag{2.36}$$

here, $v(x+a) = v(x)$ is the reduced periodic potential. Hereafter, for brevity, we will call $v(x)$ the potential in the crystal and λ the energy. Equation (2.36) is a special form of (2.11). It is also a special form of the more general second-order linear ordinary differential equations with periodic coefficients,

$$[p(x)y'(x)]' + [\lambda s(x) - q(x)]y(x) = 0, \tag{2.37}$$

investigated by Eastham [7].[4] The normalized solutions of (2.36) are now defined as

[4] It is assumed that $p(x)$ is real-valued and continuous and nowhere zero and $p'(x)$ is piecewise continuous. $q(x)$ and $s(x)$ are real-valued and piecewise continuous. There is a constant $s > 0$ such that $s(x) \geq s$.

$$\eta_1(0,\lambda)=1,\ \eta_1'(0,\lambda)=0;\quad \eta_2(0,\lambda)=0,\ \eta_2'(0,\lambda)=1 \tag{2.38}$$

and the discriminant of (2.36) is now a function of λ:

$$D(\lambda)=\eta_1(a,\lambda)+\eta_2'(a,\lambda). \tag{2.39}$$

From what we learned in Section 2.3, we know that the two linearly independent solutions of the Schrödinger equation in a one-dimensional crystal (2.36) are determined by $D(\lambda)$ in (2.39). In order to understand the properties of solutions of (2.36), we need to know how $D(\lambda)$ changes as λ changes. For this purpose, we first give two definitions.

2.4.1 Two Different Eigenvalue Problems

We consider the solutions of (2.36) under the conditions

$$y(a)=y(0);\quad y'(a)=y'(0). \tag{2.40}$$

The corresponding eigenvalues are denoted by λ_n and can be ordered according to

$$\lambda_0\le\lambda_1\le\lambda_2\le\cdots$$

and the eigenfunctions can be chosen as to be real-valued and denoted as $\zeta_n(x)$. $\zeta_n(x)$ can be further required to form an orthonormal set over $[0,a]$:

$$\int_0^a \zeta_m(x)\zeta_n(x)\,\mathrm{d}x=\delta_{m,n}.$$

$\zeta_n(x)$ can be extended by (2.40) to the whole of $(-\infty,+\infty)$ as continuously differentiable functions with period a. Therefore, λ_n are the values of λ for which (2.36) has a nontrivial solution with period a.

Similarly, we can also consider the solutions of (2.36) under the conditions

$$y(a)=-y(0);\quad y'(a)=-y'(0). \tag{2.41}$$

The corresponding eigenvalues are denoted by μ_n and can be ordered according to

$$\mu_0\le\mu_1\le\mu_2\le\cdots.$$

The corresponding eigenfunctions can be chosen to be real-valued and denoted as $\xi_n(x)$. $\xi_n(x)$ can be further required to form an orthonormal set over $[0,a]$:

$$\int_0^a \xi_m(x)\xi_n(x)\,\mathrm{d}x=\delta_{m,n}.$$

$\xi_n(x)$ can be extended by (2.41) to the whole of $(-\infty,+\infty)$ as continuously differentiable functions with semi-period a. Therefore, μ_n are the values of λ for which (2.36) has a nontrivial solution with semi-period a.

2.4.2 The Function $D(\lambda)$

Regarding the eigenvalues λ_n and μ_n defined by the two eigenvalue problems in Section 2.4.1 and how $D(\lambda)$ changes as λ changes, there is the following theorem:

Theorem 2.5 (Theorem 2.3.1 in [7]).

(i) The numbers λ_n and μ_n occur in the order

$$\lambda_0 < \mu_0 \leq \mu_1 < \lambda_1 \leq \lambda_2 < \mu_2 \leq \mu_3 < \lambda_3 \leq \lambda_4 < \cdots. \tag{2.42}$$

As λ increases from $-\infty$ to $+\infty$, $D(\lambda)$ changes as given in the following, where $m = 0, 1, 2, \ldots$:

(ii) In the interval $(-\infty, \lambda_0)$, $D(\lambda) > 2$.
(iii) In the intervals $[\lambda_{2m}, \mu_{2m}]$, $D(\lambda)$ decreases from $+2$ to -2.
(iv) In the intervals (μ_{2m}, μ_{2m+1}), $D(\lambda) < -2$.
(v) In the intervals $[\mu_{2m+1}, \lambda_{2m+1}]$, $D(\lambda)$ increases from -2 to $+2$.
(vi) In the intervals $(\lambda_{2m+1}, \lambda_{2m+2})$, $D(\lambda) > 2$.

Proof. This theorem can be proven in several steps [5,7,14].

(1) *There exists a Λ such that for all $\lambda < \Lambda$, $D(\lambda) > 2$.* We can choose a Λ so that for all x in $(-\infty, +\infty)$,

$$v(x) - \Lambda > 0$$

is true.

Suppose $y(x)$ is *any* nontrivial solution of (2.36) for which $y(0) \geq 0$ and $y'(0) \geq 0$. Then there is always an interval $(0, \Delta)$ in which $y(x) > 0$. For all $\lambda \leq \Lambda$, in any interval $(0, X)$ for which $y(x) > 0$ we have

$$y''(x) = [v(x) - \lambda]y(x) > 0;$$

thus, in the interval $(0, X)$, we have $y'(x) > 0$ and $y(x)$ is increasing in $(0, X)$. Therefore, $y(x)$ has no zero $x = X$ in $(0, +\infty)$ and both $y(x)$ and $y'(x)$ are increasing in $(0, +\infty)$.

Since both $\eta_1(x, \lambda)$ and $\eta_2(x, \lambda)$ defined in (2.38) satisfy

$$\eta_1(0, \lambda) \geq 0,\ \eta_1'(0, \lambda) \geq 0;\quad \eta_2(0, \lambda) \geq 0,\ \eta_2'(0, \lambda) \geq 0,$$

both $\eta_1(x, \lambda)$ and $\eta_2(x, \lambda)$ and their derivatives are increasing in $(0, +\infty)$ for all $\lambda \leq \Lambda$. In particular, we have

$$\eta_1(a, \lambda) > \eta_1(0, \lambda) = 1;\quad \eta_2'(a, \lambda) > \eta_2'(0, \lambda) = 1.$$

Thus, for all $\lambda \leq \Lambda$, we have $D(\lambda) > 2$.

However, as λ increases, $y''(x)/y = v(x) - \lambda$ will become negative and, consequently, $D(\lambda)$ will decrease as λ increases.

(2) *For any λ such that $|D(\lambda)| < 2$, $D'(\lambda)$ is not zero.* Differentiating (2.36) with respect to λ with $y(x) = \eta_1(x, \lambda)$, we obtain

$$-\frac{\mathrm{d}^2}{\mathrm{d}x^2}\left[\frac{\partial \eta_1(x,\lambda)}{\partial \lambda}\right] + [v(x) - \lambda]\frac{\partial \eta_1(x,\lambda)}{\partial \lambda} = \eta_1(x, \lambda). \tag{2.43}$$

From the initial condition of $\eta_1(x, \lambda)$ in (2.38), we have

$$\frac{\partial \eta_1(0,\lambda)}{\partial \lambda} = \frac{\mathrm{d}}{\mathrm{d}x}\left[\frac{\partial \eta_1(0,\lambda)}{\partial \lambda}\right] = 0. \tag{2.44}$$

By using the variation of parameters formula (2.3), we solve $\partial \eta_1(x, \lambda)/\partial \lambda$ from (2.43) with the conditions (2.44) and obtain that

$$\frac{\partial \eta_1(x,\lambda)}{\partial \lambda} = \int_0^x [\eta_1(x,\lambda)\eta_2(t,\lambda) - \eta_2(x,\lambda)\eta_1(t,\lambda)]\eta_1(t,\lambda)\ \mathrm{d}t \tag{2.45}$$

by noting that $W[\eta_1(t, \lambda), \eta_2(t, \lambda)] = 1$. Similarly,

$$\frac{\partial \eta_2(x,\lambda)}{\partial \lambda} = \int_0^x [\eta_1(x,\lambda)\eta_2(t,\lambda) - \eta_2(x,\lambda)\eta_1(t,\lambda)]\eta_2(t,\lambda)\ \mathrm{d}t. \tag{2.46}$$

Differentiating (2.46) with respect to x, we obtain that

$$\frac{\partial \eta_2'(x,\lambda)}{\partial \lambda} = \int_0^x [\eta_1'(x,\lambda)\eta_2(t,\lambda) - \eta_2'(x,\lambda)\eta_1(t,\lambda)]\eta_2(t,\lambda)\ \mathrm{d}t.$$

Combining this equation and (2.45) and then putting $x = a$, we have that

$$D'(\lambda) = \int_0^a [\eta_1'\eta_2^2(t,\lambda) + (\eta_1 - \eta_2')\eta_1(t,\lambda)\eta_2(t,\lambda) - \eta_2\eta_1^2(t,\lambda)]\ \mathrm{d}t, \tag{2.47}$$

where we have written $\eta_i = \eta_i(a, \lambda)$ and $\eta_i' = \eta_i'(a, \lambda)$ for brevity. Since

$$\eta_1\eta_2' - \eta_1'\eta_2 = 1,$$

we have

$$D^2(\lambda) = 4 + (\eta_1 - \eta_2')^2 + 4\eta_1'\eta_2.$$

Thus, (2.47) can be written as[5]

$$\begin{aligned} 4\eta_2 D'(\lambda) = &- \int_0^a [2\eta_2\eta_1(t,\lambda) - (\eta_1 - \eta_2')\eta_2(t,\lambda)]^2\ \mathrm{d}t \\ &- [4 - D^2(\lambda)]\int_0^a \eta_2^2(t,\lambda)\ \mathrm{d}t. \end{aligned} \tag{2.48}$$

If $|D(\lambda)| < 2$, then from (2.48), we have $\eta_2 D'(\lambda) < 0$; thus, $D'(\lambda) \neq 0$. Therefore, only in the regions of λ in which $|D(\lambda)| \geq 2$ can $D'(\lambda) = 0$ be true.

[5] In the corresponding formula (2.3.9) on p. 28 in [7], the sign in front of $(\phi_1 - \phi_2')$ (corresponding to our $(\eta_1 - \eta_2')$) is positive. That is an error. In the corresponding formula (21.4.6) on p. 294 in [14], the corresponding sign is negative.

(3) *At a zero* λ_n *of* $D(\lambda) - 2 = 0$*, if and only if*

$$\eta_2(a, \lambda_n) = \eta_1'(a, \lambda_n) = 0, \tag{2.49}$$

$D'(\lambda_n) = 0$ *is true. Further, if* $D'(\lambda_n) = 0$*, then* $D''(\lambda_n) < 0$.

(3a) If (2.49) is true, $\eta_2(a, \lambda_n) = \eta_1'(a, \lambda_n) = 0$, as in **B.2** in Section 2.3, then

$$\eta_1(a, \lambda_n) = \eta_2'(a, \lambda_n) = 1 \tag{2.50}$$

must be true. Equation (2.47) gives that $D'(\lambda_n) = 0$. According to **B.2** in Section 2.3, this corresponds to the case that $D(\lambda) - 2$ has a double zero at $\lambda = \lambda_n$.

(3b) On the other hand, if $D'(\lambda_n) = 0$, then the first integrand on the right of (2.48) must be identically zero since $D(\lambda_n) = 2$. Since $\eta_1(t, \lambda)$ and $\eta_2(t, \lambda)$ are linearly independent, $\eta_2(a, \lambda_n) = 0$ and $\eta_1(a, \lambda_n) = \eta_2'(a, \lambda_n)$ must be true. From (2.47), we can obtain that $\eta_1'(a, \lambda_n) = 0$.

(3c) To further prove $D''(\lambda_n) < 0$ when $D'(\lambda_n) = 0$, we differentiate (2.43) with respect to λ and obtain

$$-\frac{\mathrm{d}^2}{\mathrm{d}x^2}\left[\frac{\partial^2 \eta_1(x, \lambda)}{\partial \lambda^2}\right] + [v(x) - \lambda]\frac{\partial^2 \eta_1(x, \lambda)}{\partial \lambda^2} = 2\frac{\partial}{\partial \lambda}\eta_1(x, \lambda). \tag{2.51}$$

From (2.38), we obtain that

$$\frac{\partial^2 \eta_1(0, \lambda)}{\partial \lambda^2} = \frac{\mathrm{d}}{\mathrm{d}x}\left[\frac{\partial^2 \eta_1(0, \lambda)}{\partial \lambda^2}\right] = 0. \tag{2.52}$$

Applying the variation of parameters formula (2.3) again to solve $\partial^2 \eta_1(x, \lambda)/\partial \lambda^2$ from (2.51) and using the conditions (2.52), we obtain

$$\frac{\partial^2 \eta_1(x, \lambda)}{\partial \lambda^2} = 2\int_0^x [\eta_1(x, \lambda)\eta_2(t, \lambda) - \eta_2(x, \lambda)\eta_1(t, \lambda)]\frac{\partial}{\partial \lambda}\eta_1(t, \lambda)\ \mathrm{d}t \tag{2.53}$$

by noting that $W[\eta_1(t, \lambda), \eta_2(t, \lambda)] = 1$.

Similarly,

$$\frac{\partial^2 \eta_2(x, \lambda)}{\partial \lambda^2} = 2\int_0^x [\eta_1(x, \lambda)\eta_2(t, \lambda) - \eta_2(x, \lambda)\eta_1(t, \lambda)]\frac{\partial}{\partial \lambda}\eta_2(t, \lambda)\ \mathrm{d}t$$

and, thus,

$$\frac{\partial^2 \eta_2'(x, \lambda)}{\partial \lambda^2} = 2\int_0^x [\eta_1'(x, \lambda)\eta_2(t, \lambda) - \eta_2'(x, \lambda)\eta_1(t, \lambda)]\frac{\partial}{\partial \lambda}\eta_2(t, \lambda)\ \mathrm{d}t. \tag{2.54}$$

Therefore, from (2.53) and (2.54) and noting that when $D'(\lambda_n) = 0$, (2.49) and (2.50) are true, we obtain that

$$D''(\lambda_n) = 2\int_0^a \left[\eta_2(t,\lambda_n)\frac{\partial\eta_1(t,\lambda_n)}{\partial\lambda} - \eta_1(t,\lambda_n)\frac{\partial\eta_2(t,\lambda_n)}{\partial\lambda}\right] \mathrm{d}t$$
$$= -2\int_0^a \mathrm{d}t \int_0^t [\eta_1(t,\lambda_n)\eta_2(\tau,\lambda_n) - \eta_2(t,\lambda_n)\eta_1(\tau,\lambda_n)]^2 \,\mathrm{d}\tau. \tag{2.55}$$

Equations (2.45) and (2.46) were used in obtaining the second equality. The right side of (2.55) is less than zero since the integrand in the double integral is positive.

(4) *It can be similarly proven that there is a corresponding result to (3) for the zeros* μ_n *of* $D(\lambda)+2$*: If and only if*

$$\eta_2(a,\mu_n) = \eta_1'(a,\mu_n) = 0, \tag{2.56}$$

$D'(\mu_n) = 0$ *is true. Further,* $D''(\mu_n) > 0$ *when* $D'(\mu_n) = 0$. This corresponds to that $D(\lambda)+2$ has a double zero at $\lambda = \mu_n$.

(5) Therefore, except cases in (3) or (4), only in the regions of λ in which $D(\lambda) < -2$ or $D(\lambda) > 2$ can $D'(\lambda) = 0$ be true. The $D(\lambda)$–λ curve can change direction only in such regions.

(6) From the results of (1)–(5), we can discuss when λ increases from $-\infty$ to $+\infty$ the behavior of $D(\lambda)$. When λ is a large negative real number, $D(\lambda) > 2$ by (1). As λ increases from $-\infty$, we have $D(\lambda) > 2$ until λ reaches the first zero λ_0 of $D(\lambda) - 2$. Since λ_0 is not a maximum of $D(\lambda)$, $D''(\lambda_0) \not< 0$; thus, $D'(\lambda_0) \neq 0$ by (3). The $D(\lambda)$–λ curve intersects the line $D = 2$ at $\lambda = \lambda_0$; thus, to the immediate right of λ_0, we have $D(\lambda) < 2$. Then by (2), as λ increases from λ_0, $D(\lambda)$ decreases until λ reaches the first zero μ_0 of $D(\lambda)+2$. Thus, in the interval $(-\infty, \lambda_0)$, $D(\lambda) > 2$, and in the interval $[\lambda_0, \mu_0]$, $D(\lambda)$ decreases from $+2$ to -2.

In general, μ_0 will be a simple zero of $D(\lambda)+2$, so the $D(\lambda)$–λ curve intersects the line $D = -2$ at $\lambda = \mu_0$, and to the immediate right of μ_0 $D(\lambda) < -2$. As λ increase, $D(\lambda) < -2$ will remain true until λ reaches the second zero μ_1 of $D(\lambda)+2$, since, by (5), the $D(\lambda)$–λ curve can change direction in a region where $D(\lambda) < -2$. Since μ_1 is not a minimum of $D(\lambda)$, μ_1 is a simple zero of $D(\lambda)+2$ and, thus, the $D(\lambda)$–λ curve intersects the line $D = -2$ again at $\lambda = \mu_1$, and to the immediate right of μ_1, we have $D(\lambda) > -2$; then according to (2), as λ increases from μ_1, $D(\lambda)$ increases until λ reaches the next zero λ_1 of $D(\lambda) - 2$. Thus, in the interval (μ_0, μ_1), $D(\lambda) < -2$, and in the interval $[\mu_1, \lambda_1]$, $D(\lambda)$ increases from -2 to $+2$.

In general, λ_1 will be a simple zero of $D(\lambda) - 2$, so the $D(\lambda)$–λ curve intersects the line $D = 2$ at $\lambda = \lambda_1$, and to the immediate right of λ_1, we have $D(\lambda) > 2$. As λ increase, $D(\lambda) > 2$ will remain to be true until λ reaches the third zero λ_2 of $D(\lambda) - 2$, since, by (5), the $D(\lambda)$–λ curve can change direction in a region where $D(\lambda) > 2$. The argument we used

starting from $\lambda = \lambda_0$ can be repeated starting from $\lambda = \lambda_2$ and can be repeated again and again as λ increases to $+\infty$.

Now all parts of the theorem have been proven except when $D(\lambda) \pm 2$ has double zeros. If, for example, $D(\lambda) - 2$ has a double zero at a specific $\lambda = \lambda_{2m+1}$ (i.e., $\lambda_{2m+2} = \lambda_{2m+1}$). From **B.2** in Section 2.3, this can happen only when $\eta_2(a, \lambda_{2m+1}) = \eta_1'(a, \lambda_{2m+1}) = 0$; therefore, $D'(\lambda_{2m+1}) = 0$ and $D''(\lambda_{2m+1}) < 0$ is true by (3). Consequently, to the immediate right of $\lambda = \lambda_{2m+1} = \lambda_{2m+2}$ we have $D(\lambda) < 2$. In such a case, the $D(\lambda)$–λ curve merely *touches* the line $D = 2$ at $\lambda = \lambda_{2m+1} = \lambda_{2m+2}$ rather than intersects the line $D = 2$ twice at $\lambda = \lambda_{2m+1}$ and at $\lambda = \lambda_{2m+2}$. The previous analysis of $D(\lambda)$ can repeatedly continue again. The cases where $D(\lambda) + 2$ has double zeros can be similarly analyzed by using (4). □

Therefore, in general, as λ changes, $D(\lambda)$ changes, as shown typically in Fig. 2.1 [1,5,15].

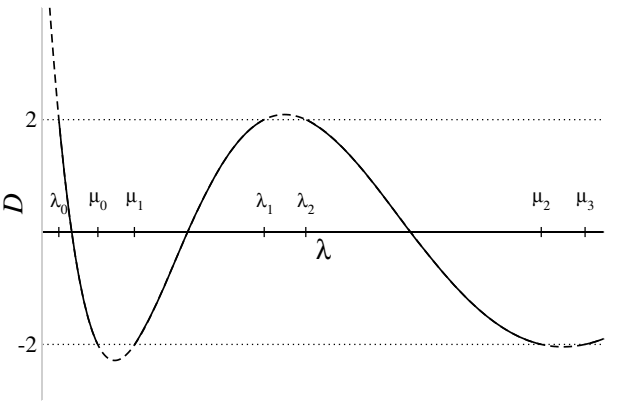

Fig. 2.1. A typical $D(\lambda)$–λ curve. The permitted energy bands in a one-dimensional crystal with translational invariance are in the ranges of λ for which $-2 \leq D(\lambda) \leq 2$ (solid lines). No electronic state exists in such a crystal in the ranges of λ for which $D(\lambda) > 2$ or $D(\lambda) < -2$ (dashed lines).

2.5 Energy Band Structure of One-Dimensional Crystals

As solutions of the one-dimensional Schrödinger differential equation with a periodic potential (2.36), the energy band structure of one-dimensional crystals with translational invariance has some especially simple and general properties [1,2,5]. This was first understood by Kramers [5].

We first point out that no electronic state exists in the range $(-\infty, \lambda_0)$. This is due to the fact that for any λ in $(-\infty, \lambda_0)$, $D(\lambda) > 2$, and according

to (2.30), the two linearly independent solutions of (2.36) are divergent in an infinite crystal. Therefore, only for λ in the range $[\lambda_0, +\infty)$ can electronic states exist in a crystal with translational invariance. There are five different cases:

A. λ in an interval (λ_{2m}, μ_{2m}) or $(\mu_{2m+1}, \lambda_{2m+1})$, $-2 < D(\lambda) < 2$.
According to (2.26), two linearly independent solutions of (2.36) can be chosen as

$$y_1(x,\lambda) = \mathrm{e}^{\mathrm{i}k(\lambda)x} p_1(x,\lambda), \quad y_2(x,\lambda) = \mathrm{e}^{-\mathrm{i}k(\lambda)x} p_2(x,\lambda), \tag{2.57}$$

where $0 < k(\lambda) < \pi/a$ and $p_i(x,\lambda)$ are periodic functions depending on λ. They are the two well-known one-dimensional Bloch states $\phi_n(k,x)$ and $\phi_n(-k,x)$ with wave vector k or $-k$. Their corresponding energies can be written as $\varepsilon_n(k)$ and $\varepsilon_n(-k)$, with $\varepsilon_n(-k) = \varepsilon_n(k)$. Therefore, the intervals (λ_{2m}, μ_{2m}) and $(\mu_{2m+1}, \lambda_{2m+1})$ correspond to the inside of permitted energy bands.

It has been shown that $\varepsilon_n(k)$ is always a monotonic function of k inside each permitted energy band [2]. Here we give another simple proof. Suppose this is not true, that there is an energy band in which $\varepsilon_n(k)$ is not a monotonic function of k. Then there must be at least one λ inside the energy band for which there are at least two distinct k_1 and k_2 in $(0, \frac{\pi}{a})$ for which $\varepsilon_n(k_1) = \varepsilon_n(k_2) = \lambda$. That means (2.36) has at least four linearly independent solutions for such a λ: two with $k = k_1$ and two with $k = k_2$ in (2.57). This is contradictory to the fact that a second-order linear homogeneous ordinary differential equation (2.36) can only have two linearly independent solutions.

B. At $\lambda = \lambda_n$, $D(\lambda) = 2$.

B.1. In most cases λ_n is a simple zero of $D(\lambda) - 2$. According to (2.27), (2.36) has two linearly independent solutions with forms as

$$y_1(x,\lambda) = p_1(x,\lambda_n), \quad y_2(x,\lambda) = x\ p_1(x,\lambda_n) + p_2(x,\lambda_n). \tag{2.58}$$

In crystals with translational invariance, only the periodic function solution y_1 is permitted. The permitted solution $y_1(x,\lambda)$ actually corresponds to a Bloch function $\phi_n(k,x)$ with a wave vector $k = 0$. It is the periodic function $\zeta_n(x)$ defined in Section 2.4.1 extended to $(-\infty, +\infty)$. λ_n corresponding to a band edge energy at $k = 0$, $\varepsilon_n(0)$. For $n > 0$, Case **B.1** corresponds to the cases where $\lambda_{2m+1} < \lambda_{2m+2}$; that is, $\varepsilon_{2m+1}(0) < \varepsilon_{2m+2}(0)$. There is a nonzero band gap between $\varepsilon_{2m+1}(0)$ and $\varepsilon_{2m+2}(0)$.

B.2. In some special cases, λ_n $(n > 0)$ is a double zero of $D(\lambda) - 2$: $\lambda_{2m+1} = \lambda_{2m+2}$. According to (2.28), (2.36) has two linearly independent solutions with forms as

$$y_1(x,\lambda) = p_1(x,\lambda_{2m+1}), \quad y_2(x,\lambda) = p_2(x,\lambda_{2m+1}). \tag{2.59}$$

Equation (2.59) gives two independent Bloch functions $\phi_{2m+1}(0,x)$ and $\phi_{2m+2}(0,x)$; their corresponding energies are $\varepsilon_{2m+1}(0) = \lambda_{2m+1}$ and $\varepsilon_{2m+2}(0) = \lambda_{2m+2}$. They both are periodic functions $\zeta_n(x)$ defined in Section 2.4.1 extended to $(-\infty, +\infty)$. Case **B.2** can be considered as having a zero band gap between $\varepsilon_{2m+1}(0)$ and $\varepsilon_{2m+2}(0)$.

C. λ in an interval $(\lambda_{2m+1}, \lambda_{2m+2})$, $D(\lambda) > 2$.
When $\lambda_{2m+1} \neq \lambda_{2m+2}$, $(\lambda_{2m+1}, \lambda_{2m+2})$ [i.e., $(\varepsilon_{2m+1}(0), \varepsilon_{2m+2}(0))$] corresponds to a nonzero band gap at $k = 0$. In the band gap, $D(\lambda) > 2$. According to (2.30), the two linearly independent solutions of (2.36) can be written as

$$y_1(x,\lambda) = \mathrm{e}^{\beta(\lambda)x} p_1(x,\lambda), \quad y_2(x,\lambda) = \mathrm{e}^{-\beta(\lambda)x} p_2(x,\lambda). \tag{2.60}$$

Here, $\beta(\lambda) > 0$ and $p_i(x,\lambda)$ are periodic functions. These solutions are not permitted in crystals with translational invariance. However, we will see that solutions such as those in (2.60) can play a significant role in electronic states in one-dimensional crystals of finite length.

D. At $\lambda = \mu_n$, $D(\lambda) = -2$.
D.1. In most cases, μ_n is a simple zero of $D(\lambda) + 2$. According to (2.31), (2.36) has two linearly independent solutions with forms as

$$y_1(x,\lambda) = s_1(x,\mu_n), \quad y_2(x,\lambda) = x\ s_1(x,\mu_n) + s_2(x,\mu_n). \tag{2.61}$$

In crystals of infinite size, only the semi-periodic function solution y_1 is permitted. The permitted solution $y_1(x,\lambda)$ actually corresponds to a Bloch function $\phi_n(k,x)$ with a wave vector $k = \frac{\pi}{a}$; it is the semi-periodic function $\xi_n(x)$ defined in Section 2.4.1 extended to $(-\infty, +\infty)$. μ_n corresponds to a band edge energy at $k = \frac{\pi}{a}$, $\varepsilon_n(\frac{\pi}{a})$. Case **D.1** corresponds to the cases where $\mu_{2m} < \mu_{2m+1}$, that is, $\varepsilon_{2m}(\frac{\pi}{a}) < \varepsilon_{2m+1}(\frac{\pi}{a})$. There is a nonzero band gap between $\varepsilon_{2m}(\frac{\pi}{a})$ and $\varepsilon_{2m+1}(\frac{\pi}{a})$.

D.2. In some special cases where μ_n is a double zero of $D(\lambda) + 2$: $\mu_{2m} = \mu_{2m+1}$. According to (2.32), (2.36) has two linearly independent solutions with forms as

$$y_1(x,\lambda) = s_1(x,\mu_{2m}), \quad y_2(x,\lambda) = s_2(x,\mu_{2m}). \tag{2.62}$$

Equation (2.62) gives two independent Bloch functions $\phi_{2m}(\frac{\pi}{a}, x)$ and $\phi_{2m+1}(\frac{\pi}{a}, x)$; their corresponding energies are $\varepsilon_{2m}(\frac{\pi}{a}) = \mu_{2m}$ and $\varepsilon_{2m+1}(\frac{\pi}{a}) = \mu_{2m+1}$. They both are semi-periodic functions $\xi_n(x)$ defined by (2.41) extended to $(-\infty, +\infty)$. Case **D.2** can be considered as having a zero band gap between $\varepsilon_{2m}(\frac{\pi}{a})$ and $\varepsilon_{2m+1}(\frac{\pi}{a})$.

E. λ in an interval (μ_{2m}, μ_{2m+1}), $D(\lambda) < -2$.
When $\mu_{2m} \neq \mu_{2m+1}$, (μ_{2m}, μ_{2m+1}) [i.e., $(\varepsilon_{2m}(\frac{\pi}{a}), \varepsilon_{2m+1}(\frac{\pi}{a}))$] corresponds to a nonzero band gap at $k = \frac{\pi}{a}$. In the band gap, $D(\lambda) < -2$. According

to (2.34), the two linearly independent solutions of (2.36) can be written as

$$y_1(x,\lambda) = \mathrm{e}^{\beta(\lambda)x} s_1(x,\lambda), \quad y_2(x,\lambda) = \mathrm{e}^{-\beta(\lambda)x} s_2(x,\lambda). \tag{2.63}$$

Here, $\beta(\lambda) > 0$ and $s_i(x,\lambda)$ are semi-periodic functions. These solutions are not permitted in crystals with translational invariance. However, we will see that solutions such as those in (2.63) can play a significant role in the electronic states in one-dimensional finite crystals.

Therefore, in cases **A, B**, and **D**, the permitted electronic state solutions can exist as solutions of the one-dimensional Schrödinger differential equation with a periodic potential (2.36). By combining our discussions in those three cases, we see that the wave vector k in $\varepsilon_n(k)$ and $\phi_n(k,x)$ is limited in the Brillouin zone,

$$-\frac{\pi}{a} < k \leq \frac{\pi}{a},$$

and that λ_n, μ_n and $\zeta(x)$, $\xi(x)$ defined in Section 2.4.1 are actually the bandedge energies and wave functions

$$\lambda_n = \varepsilon_n(0), \qquad \zeta_n(x) = \phi_n(0,x) \tag{2.64}$$

and

$$\mu_n = \varepsilon_n\left(\frac{\pi}{a}\right), \qquad \xi_n(x) = \phi_n\left(\frac{\pi}{a}, x\right). \tag{2.65}$$

Therefore, (2.42) can be rewritten as

$$\begin{aligned} \varepsilon_0(0) < \varepsilon_0\left(\frac{\pi}{a}\right) \leq \varepsilon_1\left(\frac{\pi}{a}\right) < \varepsilon_1(0) \leq \varepsilon_2(0) \\ < \varepsilon_2\left(\frac{\pi}{a}\right) \leq \varepsilon_3\left(\frac{\pi}{a}\right) < \varepsilon_3(0) \leq \varepsilon_4(0) < \cdots. \end{aligned} \tag{2.66}$$

We also understand that the energy band structure of one-dimensional crystals has some very simple and general properties:

1. Each energy band and each band gap occurs alternatively.
2. There is no energy band crossing or energy band overlap.
3. In each energy band, $\varepsilon_n(-k) = \varepsilon_n(k)$ and $\varepsilon_n(k)$ $(k > 0)$ is a monotonic function of k.
4. The minimum and the maximum of each energy band are always located either at $k = 0$ or at $k = \frac{\pi}{a}$.
5. The band gaps are between $\varepsilon_{2m}(\frac{\pi}{a})$ and $\varepsilon_{2m+1}(\frac{\pi}{a})$ or between $\varepsilon_{2m+1}(0)$ and $\varepsilon_{2m+2}(0)$.

A typical energy band structure of one-dimensional crystals is shown in Fig. 2.2.

The theory of second-order linear homogeneous ordinary differential equation with periodic coefficients discussed so far has provided a general understanding of the band structure of one-dimensional crystals with translational

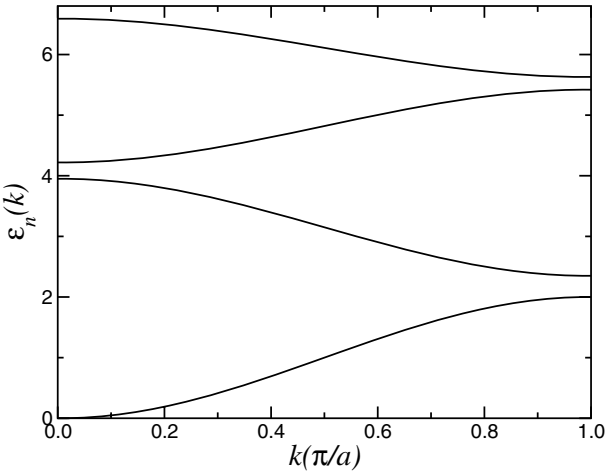

Fig. 2.2. A typical energy band structure of one-dimensional crystals.

invariance. In the next two chapters, we will develop a theory on the electronic states in ideal one-dimensional semi-infinite crystals and finite crystals, in which the translational invariance no longer exists. The following several theorems on the zeros of solutions of (2.36) play a significant role in helping us to understand the electronic states in those systems.

2.6 Zeros of Solutions

Now, we consider the solutions of (2.36) under the condition

$$y(a) = y(0) = 0. \tag{2.67}$$

The eigenvalues are denoted by Λ_n and the corresponding eigenfunctions are denoted by $\Psi_n(x)$.

Theorem 2.6 (Theorem 3.1.1 in [7]).
For $m = 0, 1, 2, ...,$ we have

$$\varepsilon_{2m}\left(\frac{\pi}{a}\right) \le \Lambda_{2m} \le \varepsilon_{2m+1}\left(\frac{\pi}{a}\right); \quad \varepsilon_{2m+1}(0) \le \Lambda_{2m+1} \le \varepsilon_{2m+2}(0). \tag{2.68}$$

Proof. Since $\Psi_n(x)$ is the eigenfunction corresponding to the n-th eigenvalue under the condition (2.67), it has exactly n zeros in $(0, a)$. According to (2.38), $\eta_2(0, \lambda) = 0$; thus, each Λ_n is the solution of the equation

$$\eta_2(a, \Lambda_n) = 0 \tag{2.69}$$

and the corresponding eigenfunction

$$\Psi_n(x) = \eta_2(x, \Lambda_n).$$

Therefore, $\eta_2(x, \Lambda_n)$ has exactly n zeros in the interval $(0, a)$. According to (2.38), $\eta_2'(0, \Lambda_n) > 0$; thus,

$$\eta_2'(a, \Lambda_n) < 0 \ (n = \text{even}); \quad \eta_2'(a, \Lambda_n) > 0 \ (n = \text{odd}). \tag{2.70}$$

Since

$$\eta_1(a, \Lambda_n)\eta_2'(a, \Lambda_n) - \eta_1'(a, \Lambda_n)\eta_2(a, \Lambda_n) = 1,$$

we have

$$\eta_1(a, \Lambda_n)\eta_2'(a, \Lambda_n) = 1,$$

by (2.69). Therefore,

$$D(\Lambda_n) = \eta_1(a, \Lambda_n) + \eta_2'(a, \Lambda_n) = [\eta_2'(a, \Lambda_n)]^{-1} + \eta_2'(a, \Lambda_n).$$

If $n =$ even, from (2.70), we have

$$-D(\Lambda_n) = [|\eta_2'(a, \Lambda_n)|^{-1/2} - |\eta_2'(a, \Lambda_n)|^{1/2}]^2 + 2 \geq 2;$$

that is,

$$D(\Lambda_{n=even}) \leq -2.$$

Similarly, we have

$$D(\Lambda_{n=odd}) \geq 2.$$

Therefore, Λ_n and Λ_{n+1} are always in different band gaps, if we consider the special cases in which $\varepsilon_{2m}(\frac{\pi}{a}) = \varepsilon_{2m+1}(\frac{\pi}{a})$ or $\varepsilon_{2m+1}(0) = \varepsilon_{2m+2}(0)$ as a band gap with the gap size being zero.

Now, we consider two consecutive zeros $\varepsilon_{2m+1}(0)$ and $\varepsilon_{2m+2}(0)$ of $D(\lambda) - 2$, with either $D(\lambda) > 2$ between them, or $D'(\lambda) = 0$ thus $D(\lambda) - 2$ has a double zero at $\lambda = \varepsilon_{2m+1}(0) = \varepsilon_{2m+2}(0)$ (see Fig. 2.1).

In the special cases where $D'(\varepsilon_{2m+1}(0)) = 0$, $D(\lambda) - 2$ has repeated solutions $\varepsilon_{2m+1}(0) = \varepsilon_{2m+2}(0)$; then by (2.49) we always have $\eta_2(a, \varepsilon_{2m+1}(0)) = 0$ and thus (2.69) has one solution $\Lambda_n = \varepsilon_{2m+1}(0)$.

In most cases, $D(\lambda) > 2$ in $(\varepsilon_{2m+1}(0), \varepsilon_{2m+2}(0))$. According to (2.48), we have $\eta_2(a, \lambda)D'(\lambda) \leq 0$ at both $\varepsilon_{2m+1}(0)$ and $\varepsilon_{2m+2}(0)$. Since $D'(\varepsilon_{2m+1}(0)) > 0$ and $D'(\varepsilon_{2m+2}(0)) < 0$, we have $\eta_2(a, \varepsilon_{2m+1}(0)) \leq 0$ and $\eta_2(a, \varepsilon_{2m+2}(0)) \geq 0$. Thus, $\eta_2(a, \lambda)$ has at least one zero in $[\varepsilon_{2m+1}(0), \varepsilon_{2m+2}(0)]$. Since Λ_n and Λ_{n+1} must be in different band gaps, there is no more than one Λ_n in $[\varepsilon_{2m+1}(0), \varepsilon_{2m+2}(0)]$. Thus, there is one Λ_n ($n =$ odd) in $[\varepsilon_{2m+1}(0), \varepsilon_{2m+2}(0)]$.

The cases of two consecutive zeros $\varepsilon_{2m}(\frac{\pi}{a})$ and $\varepsilon_{2m+1}(\frac{\pi}{a})$ of $D(\lambda) + 2$ can be similarly considered; we will obtain the conclusion that there is one and only one Λ_n ($n =$ even) in $[\varepsilon_{2m}(\frac{\pi}{a}), \varepsilon_{2m+1}(\frac{\pi}{a})]$.

Therefore, Λ_n starts occurring in $[\varepsilon_0(\frac{\pi}{a}), \varepsilon_1(\frac{\pi}{a})]$ and always occurs alternatively between $[\varepsilon_{2m}(\frac{\pi}{a}), \varepsilon_{2m+1}(\frac{\pi}{a})]$ or $[\varepsilon_{2m+1}(0), \varepsilon_{2m+2}(0)]$. □

Theorem 2.7 (Theorem 3.1.2 in [7]).
(i) $\phi_0(0,x)$ has no zero in $[0,a]$.
(ii) $\phi_{2m+1}(0,x)$ and $\phi_{2m+2}(0,x)$ have exactly $2m+2$ zeros in $[0,a)$.
(iii) $\phi_{2m}(\frac{\pi}{a},x)$ and $\phi_{2m+1}(\frac{\pi}{a},x)$ have exactly $2m+1$ zeros in $[0,a)$.

Proof. Since $\Psi_0(x)$ (i.e., $\eta_2(x,\Lambda_0)$) has no zero in $(0,a)$ and $\varepsilon_0(0) < \varepsilon_0(\frac{\pi}{a}) \le \Lambda_0$, from Theorem 2.2, $\phi_0(0,x)$ has at most one zero in $[0,a]$. Since it is a periodic function, $\phi_0(0,x)$ can only have an even numbers of zeros in $[0,a)$; thus, $\phi_0(0,x)$ has no zero in $[0,a)$ and no zero in $[0,a]$. Thus, part (i) of the theorem is proven.

Now, we consider $\phi_{2m+1}(0,x)$. As a periodic function, it can only have an even number of zeros in $[0,a)$. Since $\Lambda_{2m} < \varepsilon_{2m+1}(0) \le \Lambda_{2m+1}$ and in $(0,a)$ $\Psi_{2m}(x)$ has $2m$ zeros and $\Psi_{2m+1}(x)$ has $2m+1$ zeros respectively, from Theorem 2.2 we obtain that $\phi_{2m+1}(0,x)$ has at least $2m+1$ but no more than $2m+2$ zeros in $(0,a)$; thus, $\phi_{2m+1}(0,x)$ has exactly $2m+2$ zeros in $[0,a)$. By using $\Lambda_{2m+1} \le \varepsilon_{2m+2}(0) < \Lambda_{2m+2}$, it can be similarly proven that $\phi_{2m+2}(0,x)$ has exactly $2m+2$ zeros in $[0,a)$. Thus, part (ii) of the theorem is proven.

As semi-periodic functions, both $\phi_{2m}(\frac{\pi}{a},x)$ and $\phi_{2m+1}(\frac{\pi}{a},x)$ can only have an odd number of zeros in $[0,a)$. By using $\Lambda_{2m-1} < \varepsilon_{2m}(\frac{\pi}{a}) \le \Lambda_{2m}$ (when $m = 0$, the left inequality should be removed) and $\Lambda_{2m} \le \varepsilon_{2m+1}(\frac{\pi}{a}) < \Lambda_{2m+1}$, part (iii) of the theorem can be similarly proven. □

Now, we consider an eigenvalue problem of (2.36) in $[\tau,\tau+a]$ for a real number τ under the boundary condition

$$y(\tau) = y(\tau+a) = 0. \tag{2.71}$$

The corresponding eigenvalues can be written as $\Lambda_{\tau,n}$.

Theorem 2.8 (Theorem 3.1.3 in [7]).
As functions of τ, the ranges of $\Lambda_{\tau,2m}$ are $[\varepsilon_{2m}(\frac{\pi}{a}),\varepsilon_{2m+1}(\frac{\pi}{a})]$ and the ranges of $\Lambda_{\tau,2m+1}$ are $[\varepsilon_{2m+1}(0),\varepsilon_{2m+2}(0)]$.

Proof. Since $\varepsilon_n(0)$ are the values of λ for which the corresponding solutions $\phi_n(0,x)$ of (2.36) are periodic and $\varepsilon_n(\frac{\pi}{a})$ are the values of λ for which the corresponding solutions $\phi_n(\frac{\pi}{a},x)$ of (2.36) are semi-periodic, $\varepsilon_n(0)$ and $\varepsilon_n(\frac{\pi}{a})$ will remain unchanged if the basic interval in (2.40) and (2.41) is changed from $[0,a]$ to $[\tau,\tau+a]$. Consequently, the conclusions of Theorem 2.6 will remain unchanged if the basic interval is changed from $[0,a]$ to $[\tau,\tau+a]$. Therefore, from Theorem 2.6, we have

$$\varepsilon_{2m}\left(\frac{\pi}{a}\right) \le \Lambda_{\tau,2m} \le \varepsilon_{2m+1}\left(\frac{\pi}{a}\right), \quad \varepsilon_{2m+1}(0) \le \Lambda_{\tau,2m+1} \le \varepsilon_{2m+2}(0). \tag{2.72}$$

From part (iii) of Theorem 2.7, both $\phi_{2m}(\frac{\pi}{a},x)$ and $\phi_{2m+1}(\frac{\pi}{a},x)$ have exactly $2m+1$ zeros in $[0,a)$. Then according to Theorem 2.2, the zeros

of $\phi_{2m}(\frac{\pi}{a},x)$ and $\phi_{2m+1}(\frac{\pi}{a},x)$ must be distributed alternatively: There is always one and only one zero of $\phi_{2m+1}(\frac{\pi}{a},x)$ between two consecutive zeros of $\phi_{2m}(\frac{\pi}{a},x)$, and there is always one and only one zero of $\phi_{2m}(\frac{\pi}{a},x)$ between two consecutive zeros of $\phi_{2m+1}(\frac{\pi}{a},x)$.

Suppose x_0 is any zero of $\phi_{2m}(\frac{\pi}{a},x)$. Let $\tau = x_0$; then $\phi_{2m}(\frac{\pi}{a},x)$ satisfies (2.71):

$$\phi_{2m}\left(\frac{\pi}{a},\tau\right) = \phi_{2m}\left(\frac{\pi}{a},\tau+a\right) = 0.$$

Again, from part (iii) of Theorem 2.7, $\phi_{2m}(\frac{\pi}{a},x)$ has $2m$ zeros in the open interval (x_0, x_0+a); thus, $\phi_{2m}(\frac{\pi}{a},x)$ is an eigenfunction of (2.36) under the boundary condition (2.71) corresponding to the eigenvalue $\Lambda_{x_0,2m}$: $\Lambda_{x_0,2m} = \varepsilon_{2m}(\frac{\pi}{a})$. Similarly if x_1 is any zero of $\phi_{2m+1}(\frac{\pi}{a},x)$, then $\phi_{2m+1}(\frac{\pi}{a},x)$ is an eigenfunction of (2.36) under the boundary condition (2.71) corresponding to the eigenvalue $\Lambda_{x_1,2m}$: $\Lambda_{x_1,2m} = \varepsilon_{2m+1}(\frac{\pi}{a})$. Hence, as τ as a variable changes from $\tau = x_0$ to $\tau = x_1$, a zero of $\phi_{2m+1}(\frac{\pi}{a},x)$ next to x_0, as a function of τ, $\Lambda_{\tau,2m}$ correspondingly and continuously changes from $\varepsilon_{2m}(\frac{\pi}{a})$ to $\varepsilon_{2m+1}(\frac{\pi}{a})$. Similarly, as τ as a variable changes from $\tau = x_1$ to $\tau = x_2$, the other zero of $\phi_{2m}(\frac{\pi}{a},x)$ next to x_1, as a function of τ, $\Lambda_{\tau,2m}$ correspondingly and continuously changes back from $\varepsilon_{2m+1}(\frac{\pi}{a})$ to $\varepsilon_{2m}(\frac{\pi}{a})$. Therefore, as functions of τ, the ranges of $\Lambda_{\tau,2m}$ are $[\varepsilon_{2m}(\frac{\pi}{a}), \varepsilon_{2m+1}(\frac{\pi}{a})]$.

Similarly, we can obtain that as functions of τ, the ranges of $\Lambda_{\tau,2m+1}$ are $[\varepsilon_{2m+1}(0), \varepsilon_{2m+2}(0)]$. The theorem is proven. □

This theorem indicates that: *There is one and only one eigenvalue $\Lambda_{\tau,n}$ of (2.36) under the boundary condition (2.71) in each gap $[\varepsilon_{2m}(\frac{\pi}{a}), \varepsilon_{2m+1}(\frac{\pi}{a})]$ or $[\varepsilon_{2m+1}(0), \varepsilon_{2m+2}(0)]$ if $\varepsilon_{2m}(\frac{\pi}{a}) < \varepsilon_{2m+1}(\frac{\pi}{a})$ and $\varepsilon_{2m+1}(0) < \varepsilon_{2m+2}(0)$. In some special cases when $\varepsilon_{2m}(\frac{\pi}{a}) = \varepsilon_{2m+1}(\frac{\pi}{a})$ or $\varepsilon_{2m+1}(0) = \varepsilon_{2m+2}(0)$, then we have $\Lambda_{\tau,2m} = \varepsilon_{2m}(\frac{\pi}{a})$ or $\Lambda_{\tau,2m+1} = \varepsilon_{2m+1}(0)$.*

A direct consequence of Theorem 2.8 is that *in general a one-dimensional Bloch function $\phi_n(k,x)$ does not have a zero except $k = 0$ or $k = \frac{\pi}{a}$.* Since if $\phi_n(k,x)$ has a zero at $x = x_0$, $\phi_n(k,x_0) = 0$, then we must have $\phi_n(k, x_0+a) = 0$. According to Theorem 2.8, the corresponding eigenvalue $\Lambda_{\tau,n}$ must be in either $[\varepsilon_{2m}(\frac{\pi}{a}), \varepsilon_{2m+1}(\frac{\pi}{a})]$ or $[\varepsilon_{2m+1}(0), \varepsilon_{2m+2}(0)]$. Since $(\varepsilon_{2m}(\frac{\pi}{a}), \varepsilon_{2m+1}(\frac{\pi}{a}))$ and $(\varepsilon_{2m+1}(0), \varepsilon_{2m+2}(0))$ are band gaps, only the Bloch functions at a bandedge $\phi_{n\neq 0}(0,x)$ or $\phi_n(\frac{\pi}{a},x)$ may have a zero. This is probably quite different from what some people have thought to be the case [16].

Theorem 2.9 (Theorem 3.2.2 in [7]).
Any nontrivial solution of (2.36) with $\lambda \leq \varepsilon_0(0)$ has at most one zero in $-\infty \leq x \leq +\infty$.

Proof. : This theorem can be proven in two steps.

(1) From part (i) of Theorem 2.7, we know that $\phi_0(0,x)$, which is a nontrivial solution of (2.36) with $\lambda = \varepsilon_0(0)$, has no zero in $[0,a]$ and thus has no zero in $(-\infty, +\infty)$.

(2) If any nontrivial solution $y(x, \lambda)$ of (2.36) with $\lambda \leq \varepsilon_0(0)$ has more than one zero in $(-\infty, +\infty)$, then from Theorem 2.2, $\phi_0(0, x)$ would have at least one zero between the two zeros x_1 and x_2 of $y(x, \lambda)$. This is directly contradictory to (1). □

Theorems 2.7–2.9, especially Theorem 2.8, play a fundamental role in the theory of electronic states in ideal one-dimensional crystals of finite length.

References

1. F. Seitz: *The Modern Theory of Solids* (McGraw-Hill, New York 1940)
2. H. Jones: *The Theory of Brillouin Zones and Electronic States in Crystals* (North-Holland, Amsterdam 1960)
3. C. Kittel: *Introduction to Solid State Physics* 7th ed. (John Wiley & Sons, New York 1996)
4. R. L. Kronig and W. G. Penney: Proc. Roy. Soc. London. Ser. A. **130**, 499 (1931)
5. H. A. Kramers: Physica **2**, 483 (1935)
6. I. Tamm: Physik. Z. Sowj. **1**, 733 (1932)
7. M. S. P. Eastham: *The Spectral Theory of Periodic Differential Equations* (Scottish Academic Press, Edinburgh 1973) and references therein
8. A. L. Rabenstein: *Introduction to Ordinary Differential Equations*, 2nd ed. (Academic Press, New York 1972)
9. S. L. Ross: *Introduction to Ordinary Differential Equations*, 3rd ed. (John Wiley & Sons, New York 1980)
10. J. C. Robinson: *An Introduction to Ordinary Differential Equations* (Cambridge University Press, Cambridge 2004)
11. G. Birkhoff and G. Rota: *Ordinary Differential Equations* (John Wiley & Sons, New York 1969)
12. C. A. Swanson: *Comparison and Oscillation Theory of Linear Differential Equations* (Academic Press, New York 1968)
13. W. Magnus and S. Winkler: *Hill's Equation* (Interscience, New York 1966)
14. E. C. Titchmarsh: *Eigenfunction Expansions Associated with Second-Order Differential Equations* (Oxford University Press, Oxford 1958), Chapter XXI
15. W. Kohn: Phys. Rev. **115**, 809 (1959)
16. F. B. Pedersen and P. C. Hemmer: Phys. Rev. **B50**, 7724 (1994)

3 Surface States in One-Dimensional Semi-infinite Crystals

A one-dimensional semi-infinite crystal is the simplest periodic system with a boundary. Based on a Kronig–Penney model, Tamm was the first to find that the termination of the periodic potential due to the existence of a barrier at the boundary in a one-dimensional semi-infinite crystal can cause localized surface states to exist in band gaps below the barrier height [1]. Now after more than 70 years, the investigations of the properties of surface states and relevant physical and chemical processes have become an important field in solid state physics and chemistry [2–6]. Among the many surface states of different origins, the surface states caused purely by the termination of the crystal periodic potential are not only the simplest but also the most fundamental surface states. In this chapter, we present a general single-electron analysis on the existence and properties of surface states caused purely by the termination of the crystal periodic potential in one-dimensional semi-infinite crystals.

Basically, there are two different approaches for theoretical investigations of surface states: the potential approach and the atomic orbital or tight-binding approach [2,7]. The potential approach is mainly developed by physicists. The crystal potential models treated in the investigations of surface states in one-dimensional semi-infinite crystals include the Kronig–Penney model [1], the nearly-free electron model [8–10], the square potential model [10], the sinusoidal potential model [2,7,10,11], and so forth, and much significant progress has been made. In particular, by using a sinusoidal crystal potential model, Levine [11] systematically investigated the surface states caused by a step barrier of variable barrier height at a variable location and obtained many significant interesting results. In this chapter, we investigate the properties of surface states in general one-dimensional semi-infinite crystals without using a specific crystal potential model and try to obtain a more general understanding of the problem. This chapter is organized as follows: In Section 3.1, we present the problem in a general way. In Section 3.2, two general theorems on the properties of surface states in one-dimensional semi-infinite crystals are presented. In Section 3.3, we consider the simplest cases where the barrier height outside the crystal is infinite. In Section 3.4 we consider cases where the barrier height is finite. Section 3.5 is devoted to comparisons with previous work and includes discussions.

3.1 Basic Considerations

For a one-dimensional infinite crystal, the Schrödinger differential equation can be written as

$$-y''(x) + [v(x) - \lambda]y(x) = 0, \quad -\infty < x < +\infty, \tag{3.1}$$

where

$$v(x + a) = v(x)$$

is the periodic crystal potential. We assume (3.1) is solved and all solutions are known. The eigenvalues are energy bands $\varepsilon_n(k)$ and the corresponding eigenfunctions are Bloch functions $\phi_n(k, x)$, where $n = 0, 1, 2, ...$ and $-\frac{\pi}{a} < k \leq \frac{\pi}{a}$. We are mainly interested in cases where there is always a band gap between two consecutive energy bands. The band gaps of (3.1) are always located either at the center of the Brillouin zone $k = 0$ or at the boundary of the Brillouin zone $k = \frac{\pi}{a}$ and can be ordered: The band gap $n = 0$ is the lowest band gap at $k = \frac{\pi}{a}$, the band gap $n = 1$ is the lowest band gap at $k = 0$, and so on.

Up to now, most theoretical investigations of the basic physics of surface states were based on a semi-infinite crystal approach. It is usually assumed that the potential inside the crystal is the same as that in an infinite crystal. Based on this assumption, in general, a termination of the crystal periodic potential at the boundary of a semi-infinite one-dimensional crystal has two variables: the position of the termination τ and the potential outside the crystal $V_{out}(x)$.

For a one-dimensional semi-infinite crystal with a left boundary at τ, the potential can be written as

$$\begin{aligned} v(x, \tau) &= V_{out}(x) \quad \text{if } x \leq \tau \\ &= v(x) \qquad \text{if } x > \tau. \end{aligned} \tag{3.2}$$

We are only interested in cases where outside the semi-infinite crystal there is a barrier; that is, $V_{out}(x)$ is always above $v(x)$ and the energy of the surface state Λ. We call a semi-infinite crystal given by (3.2) a right semi-infinite crystal, whereas a left semi-infinite crystal is defined by a periodic potential in $(-\infty, \tau)$. The eigenvalues Λ and eigenfunctions $\psi(x)$ for a right semi-infinite crystal with a certain boundary condition at the boundary τ, determined by $V_{out}(x)$, can be obtained as solutions of the Schrödinger differential equation

$$-\psi''(x) + [v(x) - \Lambda]\psi(x) = 0, \quad \tau < x < +\infty. \tag{3.3}$$

A finite $V_{out}(x)$ will allow a small part of the electronic state to spill out of the semi-infinite crystal and thus make the boundary condition to become [12]

$$(\psi'/\psi)_{x=\tau} = \sigma, \tag{3.4}$$

where σ is a positive number depending on $V_{out}(x)$ for a right semi-infinite one-dimensional crystal given by (3.2). σ will decrease monotonically as $V_{out}(x)$ decreases. Although $V_{out}(x)$ may have different forms, the effect of different $V_{out}(x)$ on the problem treated here can be simplified to be given by the effect of σ.

In general, there may be two different types of solutions for (3.3) and (3.4).

For any τ and V_{out}, inside each energy band of the infinite crystal, that is, for any specific Λ in $(\varepsilon_{2m}(0), \varepsilon_{2m}(\frac{\pi}{a}))$ or $(\varepsilon_{2m+1}(\frac{\pi}{a}), \varepsilon_{2m+1}(0))$ where $m = 0, 1, 2, ...$, there is always a solution of (3.3) and (3.4) inside the semi-infinite crystal that is

$$\psi_{n,k}(x) = c_1\phi_n(k, x) + c_2\phi_n(-k, x), \tag{3.5}$$

where $0 < k < \frac{\pi}{a}$ can be uniquely determined by $\varepsilon_n(k) = \Lambda$. This is because both $\phi_n(k, x)$ and $\phi_n(-k, x)$ are two linearly independent nondivergent solutions of (3.3) and, thus, one of their linear combinations can always satisfy the boundary condition (3.4). In this chapter, we are not interested in those states.

However, for a specific Λ in an energy band gap of the infinite crystal $[\varepsilon_{2m}(\frac{\pi}{a}), \varepsilon_{2m+1}(\frac{\pi}{a})]$ or $[\varepsilon_{2m+1}(0), \varepsilon_{2m+2}(0)]$, there is only *one* nondivergent solution of (3.3) and this solution usually cannot also satisfy the boundary condition (3.4). Only when a nondivergent solution also satisfies (3.4) can we have a solution of both (3.3) and (3.4). If it exists, the energy Λ of such a solution is dependent on τ and V_{out}. The existence and properties of such a state are the main interest of this chapter.

In general, a solution of (3.3) and (3.4) with an energy Λ inside a band gap or at a band edge is different from (3.5) if it exists. Its wave function inside a right semi-infinite one-dimensional crystal always has the form[1]

$$\psi(x, \Lambda) = \mathrm{e}^{-\beta(\Lambda)x} f(x, \Lambda), \tag{3.6}$$

[1] Any solution $y(x)$ of (3.3) can always be expressed as a linear combination of two linearly independent solutions of (3.1):

$$y(x, \Lambda) = c_1 y_1(x, \Lambda) + c_2 y_2(x, \Lambda).$$

If Λ is *inside* a band gap at $k = 0$, the two linearly independent solutions y_1 and y_2 can be chosen as $y_1(x, \Lambda) = \mathrm{e}^{\beta(\Lambda)x} p_1(x, \Lambda)$ and $y_2(x, \Lambda) = \mathrm{e}^{-\beta(\Lambda)x} p_2(x, \Lambda)$, where $p_i(x, \Lambda)$ are periodic functions and $\beta(\Lambda)$ is a positive number, all depending on Λ. For a nondivergent solution in right semi-infinite crystals, $c_1 = 0$ has to be chosen.

If Λ is *at* a band edge at $k = 0$, the two linearly independent solutions y_1 and y_2 can be chosen as $y_1(x, \Lambda) = p_1(x, \Lambda)$ and $y_2(x, \Lambda) = x\, p_1(x, \Lambda) + p_2(x, \Lambda)$, where $p_i(x, \Lambda)$ are periodic functions depending on Λ. For a nondivergent solution in semi-infinite crystals, we have to choose $c_2 = 0$.

The combination of the two requirements leads to (3.6) for a band gap at $k = 0$. Similar arguments can be applied for a band gap at $k = \frac{\pi}{a}$ as well.

where $f(x, \Lambda)$ is a periodic function $f(x + a, \Lambda) = f(x, \Lambda)$ if the band gap is at the center of the Brillouin zone $k = 0$, or a semi-periodic function $f(x + a, \Lambda) = -f(x, \Lambda)$ if the band gap is at the boundary of the Brillouin zone $k = \frac{\pi}{a}$. $\beta(\Lambda)$ is a non-negative real number depending on Λ. A surface state located near the boundary has $\beta(\Lambda) > 0$. However, a state with $\beta(\Lambda) = 0$ can also be a solution of (3.3) and (3.4) for some specific τ and V_{out}, thus, should also be considered. It is easy to see that $\psi(x, \Lambda)$ in (3.6) can always be chosen as a real function.[2]

Correspondingly, inside a left semi-infinite one-dimensional crystal, such a state always has the form

$$\psi(x, \Lambda) = \mathrm{e}^{\beta(\Lambda)x} f(x, \Lambda). \tag{3.6a}$$

3.2 Two Relevant Theorems

If a specific boundary τ and a specific $V_{out}(x)$ cause a localized surface state to exist in a specific band gap in a right semi-infinite crystal, the following two relevant theorems concerning how the energy of the surface state depends on τ and V_{out} can be proven with the help of the Hellmann–Feynman theorem [13]:

Theorem 3.1.

For the energy Λ_n of a surface state in a specific n-th band gap,

$$\frac{\partial}{\partial \sigma} \Lambda_n > 0. \tag{3.7}$$

Proof. The theorem can be proven in two steps.

(1) In the simple cases where $V_{out}(x) = V_{out}$ is a step barrier. Define a new potential

$$\tilde{V}(x, \eta) = (1 - \eta) v_0(x, \tau) + \eta \; v_1(x, \tau),$$

where

$$\begin{aligned} v_i(x, \tau) &= V_i \qquad \text{if } x \le \tau \\ &= v(x) \quad \text{if } x > \tau; \end{aligned}$$

$V_1 = V_0 + \delta V$ and δV is an infinitesimal positive number. According to the Hellmann–Feynman theorem [13], for an eigenvalue $\tilde{\Lambda}_n(\eta)$ of a localized surface state $| \, \rangle_n$ of the Hamiltonian $\tilde{H} = T + \tilde{V}(x, \eta)$, where T is the kinetic energy operator, we have

$$\frac{\partial \tilde{\Lambda}_n(\eta)}{\partial \eta} = \left\langle \frac{\partial \tilde{H}(\eta)}{\partial \eta} \right\rangle_n = \left\langle \frac{\partial \tilde{V}(\eta)}{\partial \eta} \right\rangle_n = \langle v_1(x, \tau) - v_0(x, \tau) \rangle_n > 0.$$

[2] Since $\psi^*(x, \Lambda)$ must also be a solution of (3.3) and (3.4).

since $V_1 > V_0$. Thus, $\tilde{\Lambda}_n(\eta)$ is a monotonic increasing function of η. However, $\tilde{V}(x,0) = v_0(x,\tau)$; thus, $\tilde{\Lambda}_n(0) = \Lambda_n(\tau, V_{out} = V_0)$, whereas $\tilde{V}(x,1) = v_1(x,\tau)$ and thus $\tilde{\Lambda}_n(1) = \Lambda_n(\tau, V_{out} = V_1)$. Therefore, $\Lambda_n(\tau, V_{out} = V_1) > \Lambda_n(\tau, V_{out} = V_0)$; that is,

$$\frac{\partial \Lambda_n}{\partial V_{out}} > 0.$$

Obviously $\partial V_{out}/\partial\sigma > 0$ for a right semi-infinite crystal; consequently,

$$\frac{\partial \Lambda_n}{\partial \sigma} = \frac{\partial \Lambda_n}{\partial V_{out}} \frac{\partial V_{out}}{\partial \sigma} > 0$$

for those simple cases where $V_{out}(x)$ is a step barrier. This is a special case of (3.7).

(2) Since for a specific $v(x)$, Λ_n is a function of only τ and σ, (3.7) should also be true for more $V_{out}(x)$ in general. □

A similar discussion for a left semi-infinite crystal can lead to the statement that if a surface state solution of energy Λ_n exists in the same band gap in a left semi-infinite crystal with periodic potential in $(-\infty, \tau)$, then

$$\partial \Lambda_n/\partial\sigma < 0 \tag{3.7a}$$

is true, just the opposite of (3.7). This is due to the fact that for a left semi-infinite crystal, σ is a negative number depending on V_{out} and thus $\partial V_{out}/\partial\sigma < 0$.

Theorem 3.2.

The energy Λ_n of a surface state in a right semi-infinite crystal increases as τ increases, or

$$\frac{\partial}{\partial \tau}\Lambda_n > 0. \tag{3.8}$$

Proof. Suppose a surface state with an energy $\Lambda_n(\tau_0, V_{out})$ exists in the n-th band gap for a specific $\tau = \tau_0$ and V_{out}. Now, consider that $\tau_1 = \tau_0 + \delta\tau$, where $\delta\tau$ is an infinitesimal positive number. We can define a new potential

$$\tilde{V}(x,\eta) = (1-\eta)v(x,\tau_0) + \eta\, v(x,\tau_1),$$

where

$$\begin{aligned} v(x,\tau) &= V_{out} \quad \text{if } x \le \tau \\ &= v(x) \quad \text{if } x > \tau, \end{aligned}$$

and a new Hamiltonian $\tilde{H}(\eta) = T + \tilde{V}(x,\eta)$, where T is the kinetic energy operator. According to the Hellmann–Feynman theorem [13], for an eigenvalue $\tilde{\Lambda}_n(\eta)$ of a localized surface state $|\ \rangle_n$ of $\tilde{H}(\eta)$, we have

$$\frac{\partial \tilde{\Lambda}(\eta)}{\partial \eta} = \left\langle \frac{\partial \tilde{H}(\eta)}{\partial \eta} \right\rangle_n = \left\langle \frac{\partial \tilde{V}(\eta)}{\partial \eta} \right\rangle_n = \langle v(x,\tau_1) - v(x,\tau_0) \rangle_n > 0$$

since $V_{out} > v(x)$, thus $v(x,\tau_1) - v(x,\tau_0) > 0$. Hence, $\tilde{\Lambda}_n(\eta)$ is a monotonic increasing function of η. However, $\tilde{V}(x,0) = v(x,\tau_0)$, thus, $\tilde{\Lambda}_n(0) = \Lambda_n(\tau_0, V_{out})$, whereas $\tilde{V}(x,1) = v(x,\tau_1)$, thus, $\tilde{\Lambda}_n(1) = \Lambda_n(\tau_1, V_{out})$. Therefore, $\Lambda_n(\tau_1, V_{out}) > \Lambda_n(\tau_0, V_{out})$; that is $\partial\Lambda_n/\partial\tau > 0$. □

A similar discussion for a left semi-infinite crystal can lead to the interesting point that if a surface state solution of energy Λ_n exists in the same band gap in a left semi-infinite crystal with periodic potential in $(-\infty, \tau)$, then $\partial\Lambda_n/\partial(-\tau) > 0$ is true. In other words,

$$\frac{\partial}{\partial \tau}\Lambda_n < 0, \tag{3.8a}$$

just the opposite of (3.8).

These two theorems on the properties of the surface states in one-dimensional semi-infinite crystal should be true in general for any crystal potential $v(x)$, with the crystal boundary τ and the barrier potential outside the crystal $V_{out}(x)$.

3.3 Surface States in Ideal Semi-infinite Crystals

The significance of Theorem 3.2 and its consequence can be more clearly seen if we consider the ideal semi-infinite crystals where the potential outside the crystal is $V_{out}(x) = +\infty$ and thus (3.4) becomes

$$\psi(x,\Lambda)|_{x=\tau} = 0. \tag{3.9}$$

The solutions of (3.3) and (3.9) can be investigated with the help of the theorems in Chapter 2 regarding the *zeros* of solutions of one-dimensional Schrödinger differential equations with a periodic potential.

First, as a direct consequence of (3.9) and Theorem 2.8, there is *at most* one solution[3] of (3.3) and (3.9) in each band gap of (3.1).

Now, we consider a specific n-th band gap at $k = k_g$, where either $k_g = 0$ for $n = 1, 3, 5, ...$ or $k_g = \frac{\pi}{a}$ for $n = 0, 2, 4, ...$ According to Theorem 2.7, the two band edge wave functions $\phi_n(k_g, x)$ and $\phi_{n+1}(k_g, x)$ have exactly $n+1$ zeros for x in a potential period a. The locations of these zeros are determined

[3] A function (3.6) satisfying (3.9) must satisfy $\psi(\tau + a, \Lambda) = 0$ as well. According to Theorem 2.8, for any real τ there is always one and only one solution of (3.1) in each gap for which $y(\tau, \lambda) = y(\tau + a, \lambda) = 0$. However, such a solution may or may not have the form of (3.6): It may have the form of $y(x, \lambda) = \mathrm{e}^{-\beta(\lambda)x} f(x, \lambda)$. Only when such a solution has the form of (3.6) is it a solution of (3.3) and (3.9).

by the crystal potential $v(x)$. According to Theorem 2.2, the zeros of $\phi_n(k_g, x)$ and $\phi_{n+1}(k_g, x)$ must be distributed alternatively: There is always one and only one zero of $\phi_{n+1}(k_g, x)$ between two consecutive zeros of $\phi_n(k_g, x)$, and there is always one and only one zero of $\phi_n(k_g, x)$ between two consecutive zeros of $\phi_{n+1}(k_g, x)$.

If τ is at any one of these zeros, then a solution of (3.3) and (3.9) is simple: The corresponding bandedge wave function $\phi_n(k_g, x)$ or $\phi_{n+1}(k_g, x)$ satisfies both (3.3) and (3.9) and thus is a solution $\psi(x, \Lambda)$ of (3.3) and (3.9) in that band gap, with the eigenvalue $\Lambda_n(\tau)$ equal to the corresponding band edge energy $\varepsilon_n(k_g)$ or $\varepsilon_{n+1}(k_g)$. The semi-infinite semiconductor has a band edge state solution for this specific band gap n. We can use a label $M(n)$ to express the set of all zeros of $\phi_n(k_g, x)$ and $\phi_{n+1}(k_g, x)$. In the interval $[0, a)$ – where 0 can be chosen to be any specific zero of $\phi_n(k_g, x)$ – the set $M(n)$ contains $n + 1$ zeros of $\phi_n(k_g, x)$ and $n + 1$ zeros of $\phi_{n+1}(k_g, x)$.

If τ is not a zero of either $\phi_n(k_g, x)$ or $\phi_{n+1}(k_g, x)$, it must be between a zero of $\phi_n(k_g, x)$ and a zero of $\phi_{n+1}(k_g, x)$: Suppose $x_{l,n}$ and $x_{r,n}$ are two consecutive zeros of $\phi_n(k_g, x)$, on the left and the right of τ respectively, and suppose $x_{m,n+1}$ is the zero of $\phi_{n+1}(k_g, x)$ in the interval $(x_{l,n}, x_{r,n})$. Then τ must be either in the interval $(x_{l,n}, x_{m,n+1})$ or in the interval $(x_{m,n+1}, x_{r,n})$.

Because $\Lambda_n(x_{l,n}) = \Lambda_n(x_{r,n}) = \varepsilon_n(k_g)$ and $\Lambda_n(x_{m,n+1}) = \varepsilon_{n+1}(k_g)$, when τ increases from $x_{l,n}$ to $x_{m,n+1}$, $\Lambda_n(\tau)$ as a continuous function of τ goes up from $\varepsilon_n(k_g)$ to $\varepsilon_{n+1}(k_g)$. Therefore, when τ is in the interval $(x_{l,n}, x_{m,n+1})$, (3.8) is true and a surface state solution of (3.3) and (3.9) may exist in the right semi-infinite crystal. We can use a label $L(n)$ to express the set of all such points. In the interval $[0, a)$, the set $L(n)$ contains $n + 1$ sub-open-intervals, since from each of the $n + 1$ zeros of $\phi_n(k_g, x)$ in the interval $[0, a)$ one can obtain such an open interval in which (3.8) is true. As an example, in Fig. 3.1 is shown $\Lambda_1(\tau)$ (the energy of the surface state in the lowest band gap at $k = 0$) as a function of τ in an interval of length a for a right semi-infinite crystal.

We can also use a label $R(n)$ to express the set of all points in the interval $(x_{m,n+1}, x_{r,n})$. In the interval $[0, a)$, the set $R(n)$ also contains $n+1$ sub-open-intervals. It is easy to see that when τ is in any such interval $(x_{m,n+1}, x_{r,n})$, there is no solution for (3.3) and (3.9): If there were a solution, then $\Lambda_n(\tau)$ as a continuous function of τ would go down from $\varepsilon_{n+1}(k_g)$ to $\varepsilon_n(k_g)$ when τ goes from $x_{m,n+1}$ to $x_{r,n}$ and that means $\Lambda_n(\tau)$ would decrease as τ increases and this is contradictory to (3.8). However, when τ is in the interval $(x_{m,n+1}, x_{r,n})$, a surface state solution can exist in the left semi-infinite crystal $(-\infty, \tau)$ since then (3.8a) is true.[4] Figure 3.2 shows $\Lambda_1(\tau)$ as a function of τ in the interval $[0, a)$ for a left semi-infinite crystal. Note in both Fig. 3.1 and Fig. 3.2, there are regions in which there is no Λ_1 for a τ, indicating that no surface state solution exists in the right semi-infinite crystal or in the left semi-infinite

[4]Therefore, $\partial\Lambda_n/\partial\tau > 0$ when τ is in $L(n)$, $\partial\Lambda_n/\partial\tau < 0$ when τ is in $R(n)$, and $\partial\Lambda_n/\partial\tau = 0$ when τ is in $M(n)$.

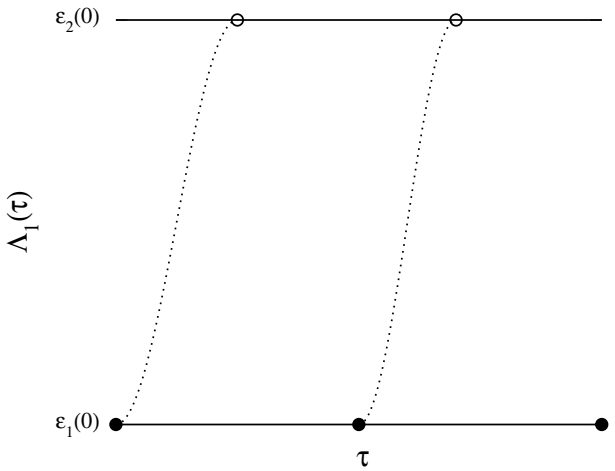

Fig. 3.1. $\Lambda_1(\tau)$ as a function of τ in the interval $[0, a]$ for a right semi-infinite crystal with periodic potential in $(\tau, +\infty)$. Zeros of $\phi_1(0, x)$ are shown as solid circles and zeros of $\phi_2(0, x)$ are shown as open circles. The dotted lines indicate that a surface state exists in the semi-infinite crystal if τ is in the corresponding regions.

crystal for that τ. Obviously, any τ in the interval $[0, a)$ must belong to one set of either $L(n)$, $M(n)$, or $R(n)$ for any specific band gap n. Therefore, for $V_{out} = +\infty$, it is not that a termination of the periodic potential at any τ in a potential period interval $[0, a)$ may cause a surface state existing in a specific band gap in the right semi-infinite one-dimensional crystal or in the left semi-infinite one-dimensional crystal.

Therefore, we have seen that there are two seemingly different types of solutions for (3.3) and (3.9) in a band gap: a band edge state or a surface state.[5] Essentially they are not very different: A band edge state can also be considered merely as a special surface-like state with its energy equal to a band edge energy and thus its decay factor in (3.6) is $\beta(\Lambda) = 0$.

[5] An interesting point is that due to (3.6), if τ is in either $L(n)$ or $M(n)$, a solution of (3.3) and (3.9) always has

$$\psi(x, \Lambda)|_{x=\tau+Na} = 0$$

if N is a positive integer; that is, a solution of the right semi-infinite crystal is also a solution of a finite crystal of length Na. Note that this equation is true for any integer N; therefore, the energy Λ of a such state is independent of the crystal length. Similarly, if τ is in $R(n)$ or $M(n)$, such a solution of the left semi-infinite crystal is also a solution for a finite crystal of length Na and its energy Λ is independent of the crystal length.

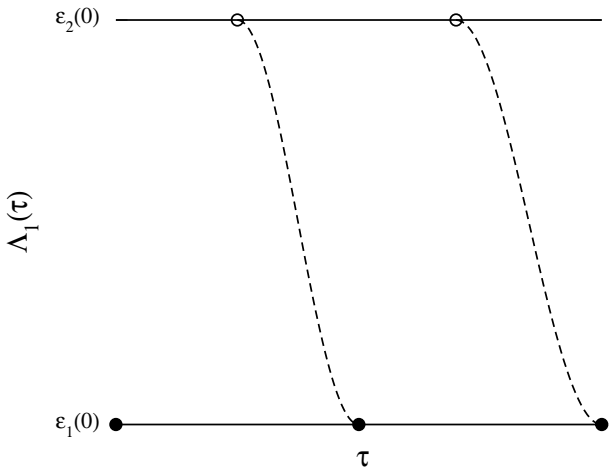

Fig. 3.2. $\Lambda_1(\tau)$ as a function of τ in the interval $[0, a]$ for a left semi-infinite crystal with periodic potential in $(-\infty, \tau)$. Zeros of $\phi_1(0, x)$ are shown as solid circles and zeros of $\phi_2(0, x)$ are shown as open circles. The dashed lines indicate that a surface state exists in the semi-infinite crystal if τ is in the corresponding regions.

3.4 Cases Where V_{out} Is Finite

Now, we consider cases where V_{out} is finite. For a finite V_{out}, the boundary condition (3.4) rather than (3.9) should be used for right semi-infinite one-dimensional crystals. Equation (3.9) corresponds to $\sigma = +\infty$ and σ will decrease monotonically as V_{out} decreases.

Since (3.6) is a general form of a solution of (3.3) and (3.4) in a band gap, from (3.4) and (3.6) we have

$$\left.\frac{f'(x, \Lambda)}{f(x, \Lambda)}\right|_{x=\tau} - \beta(\Lambda) = \sigma. \tag{3.10}$$

Unlike the simplest cases discussed in Section 3.3, now the intervals in which a termination boundary τ can cause a surface state in a band gap will depend on $V_{out}(x)$ and, consequently, the corresponding $\Lambda_n(\tau) - \tau$ curve in a right semi-infinite crystal such as shown in Fig. 3.1 will move to the right.

We still consider the lowest band gap at $k = 0$ as an example. For a solution of (3.3) and (3.4) with the energy at the lower band edge $\varepsilon_1(0)$, (3.10) becomes

$$\left.\frac{\phi_1'(0, x)}{\phi_1(0, x)}\right|_{x=\tau} = \sigma_{\varepsilon_1(0)} \tag{3.11}$$

by noting that $\beta(\Lambda) = 0$ in (3.6) for a state with an energy of a band edge and that σ depends on the energy of the state for a specific V_{out}. $\frac{\phi_1'(0,x)}{\phi_1(0,x)}$ is determined by the periodic potential $v(x)$. In Fig. 3.3 is shown a typical

$\frac{\phi_1'(0,x)}{\phi_1(0,x)}$ as a function of x. Given a specific finite V_{out} and thus a specific positive $\sigma_{\varepsilon_1(0)}$, on the right of a (any) zero $x_{a,1}$ (solid circle) of the lower band edge wave function $\phi_1(0,x)$, there is always a specific point $x_{a,1}+\delta_{a,1}$ where $\delta_{a,1}>0$, which makes

$$\frac{\phi_1'(0,x_{a,1}+\delta_{a,1})}{\phi_1(0,x_{a,1}+\delta_{a,1})}=\sigma_{\varepsilon_1(0)}$$

true, as is shown by the short-dashed lines in Fig. 3.3. The smaller V_{out} is, the smaller $\sigma_{\varepsilon_1(0)}$ is and the larger $\delta_{a,1}$ is, as can be clearly seen in Fig. 3.3.

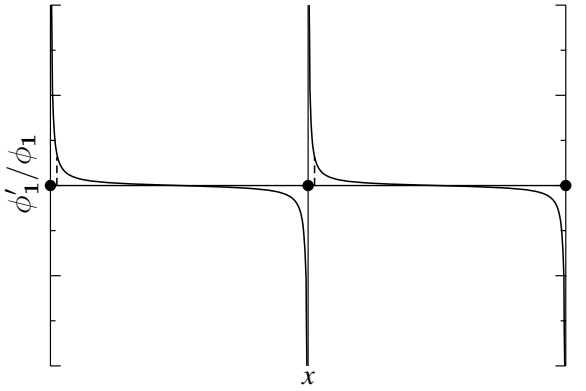

Fig. 3.3. $\frac{\phi_1'(0,x)}{\phi_1(0,x)}$ as function of x in the same interval $[0,a]$. Zeros of $\phi_1(0,x)$ are shown as solid circles. The two short lines indicate the two τ for which $\frac{\phi_1'(0,\tau)}{\phi_1(0,\tau)}=\sigma$ is satisfied. Note they are on the right of the zeros for a positive finite σ.

Depending on the crystal potential $v(x)$, the details of Fig. 3.3 might be more or less different, such as the shapes of $\frac{\phi_1'(0,x)}{\phi_1(0,x)}$ and the locations of the zeros of it. However, there is always at least one zero of $\phi_1'(0,x)$ and thus one zero of $\frac{\phi_1'(0,x)}{\phi_1(0,x)}$ between two consecutive zeros of $\phi_1(0,x)$; therefore, the analysis given here is generally valid for any $v(x)$: For a finite V_{out} and thus a finite $\sigma_{\varepsilon_1(0)}$, there is always a $x=x_{a,1}+\delta_{a,1}$ for which $\delta_{a,1}>0$, which makes (3.11) true. Thus, a right semi-infinite crystal with a boundary $\tau=x_{a,1}+\delta_{a,1}$ and a potential barrier V_{out} will have a solution of (3.3) and (3.4) with energy $\Lambda_1=\varepsilon_1(0)$; inside the semi-infinite crystal, the corresponding wave function obeys $\psi(x,\Lambda_1)=\phi_1(0,x)$.

A similar analysis can be applied to the corresponding upper band edge as well: When V_{out} decreases from $+\infty$ to a specific finite value, the boundary τ for a solution of (3.3) and (3.4) with $\Lambda_1=\varepsilon_2(0)$ (the upper band edge energy of the lowest band gap at $k=0$) will move to the right, from $\tau=x_{a,2}$ to a specific $\tau=x_{a,2}+\delta_{a,2}$, in which $\delta_{a,2}>0$. Similar analysis can also be applied

to each surface state in that band gap; thus, instead of the $\Lambda_1(\tau) - \tau$ curves in Fig. 3.1, we have $\Lambda_1(\tau) - \tau$ curves for a finite V_{out}, as shown in Fig. 3.4: The $\Lambda_1(\tau) - \tau$ curves in Fig. 3.4 are on the right of the $\Lambda_1(\tau) - \tau$ curves in

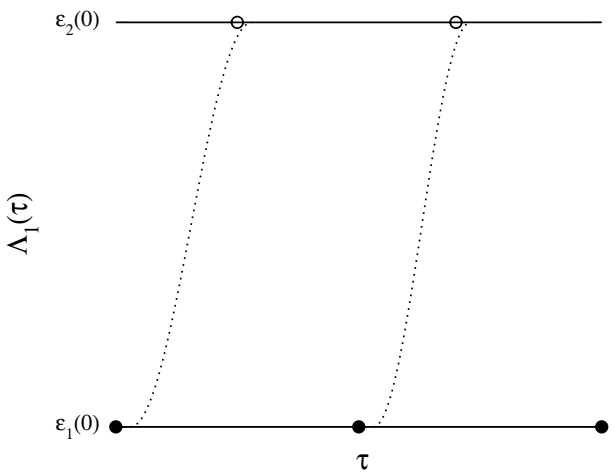

Fig. 3.4. $\Lambda_1(\tau)$ as a function of τ in the same interval $[0, a]$ for a finite $V_{out}(x)$ for a right semi-infinite crystal with periodic potential in $(\tau, +\infty)$. Zeros of $\phi_1(0, x)$ are shown as solid circles and zeros of $\phi_2(0, x)$ are shown as open circles. The dotted lines indicate that a surface state exists in the semi-infinite crystal if τ is in the corresponding regions. Note that no surface state exists when τ is in the near neighborhood of a solid circle.

Fig. 3.1; how far away it is depends on the barrier potential V_{out} (and the crystal potential $v(x)$).

Corresponding to Fig. 3.2, in Fig. 3.5 are shown the $\Lambda_1(\tau) - \tau$ curves in a left semi-infinite crystal with periodic potential in $(-\infty, \tau)$ for a finite V_{out}, for which $\frac{\psi'}{\psi} = \sigma < 0$ is the boundary condition. Thus, the curves in Fig. 3.5 are always on the left of the corresponding curves in Fig. 3.2.

Therefore, the effect of a finite V_{out} is to change the positions (and probably, the shapes) of the $\Lambda_1(\tau) - \tau$ curves. This can also be understood on the basis of the theorems in Section 3.2: Because for a surface state in the n-th gap, $\frac{\partial}{\partial \sigma}\Lambda_n > 0$ and $\frac{\partial}{\partial \tau}\Lambda_n > 0$ for a right semi-infinite crystal ($\frac{\partial}{\partial \sigma}\Lambda_n < 0$ and $\frac{\partial}{\partial \tau}\Lambda_n < 0$ for a left semi-infinite crystal), a τ increase in a right semi-infinite crystal (a τ decrease in a left semi-infinite crystal) is needed to compensate for the possible effect of a V_{out} decrease in order to keep a fixed Λ_1.

Again, in both Fig. 3.4 and Fig. 3.5, there are regions in which there is no Λ_1 for a τ, indicating that no surface state solution exists in a right semi-infinite crystal or in a left semi-infinite crystal for that τ. Therefore, for a specific finite V_{out}, again it is not that a termination of the periodic potential at any τ in a potential period interval $[0, a)$ may cause a surface state existing

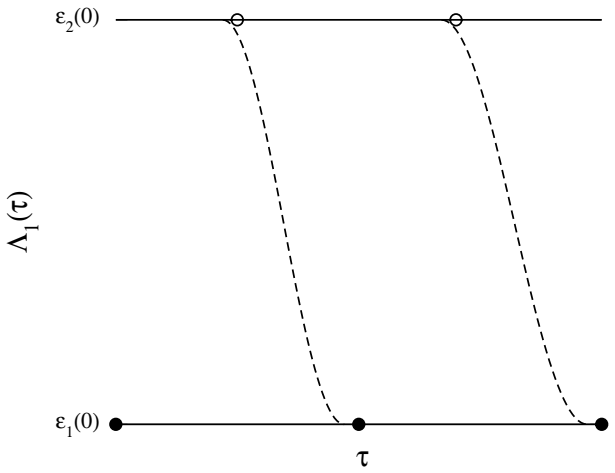

Fig. 3.5. $\Lambda_1(\tau)$ as a function of τ in the same interval $[0, a]$ for a finite $V_{out}(x)$ for a left semi-infinite crystal with periodic potential in $(-\infty, \tau)$. Zeros of $\phi_1(0, x)$ are shown as solid circles and zeros of $\phi_2(0, x)$ are shown as open circles. The dashed lines indicate that a surface state exists in the semi-infinite crystal if τ is in the corresponding regions. Note that no surface state exists when τ is in the near neighborhood of a solid circle.

in this band gap in the right semi-infinite one-dimensional crystal or in the left semi-infinite one-dimensional crystal. A consequence of the moving of $\Lambda_1(\tau) - \tau$ curves due to a finite V_{out} is that there is no longer a surface state or a band edge state possible for a τ in the near neighborhood of a zero of the *lower* band edge wave function, as can be clearly seen in Fig. 3.4 and Fig. 3.5.

The analysis presented here for the lowest band gap at $k = 0$ is valid for a general crystal potential $v(x)$ and outside potential V_{out}. A similar analysis can also be applied to other band gaps and results corresponding to Figs. 3.1–3.5 can be obtained.

The left side of (3.10) is determined by $v(x)$ and τ and the right side is determined by V_{out}. After $v(x)$ and V_{out} are given, $\Lambda_n(\tau)$ as a function of τ, such as shown in Fig. 3.4 and Fig. 3.5, is uniquely determined. Therefore, there is *at most* one state of type (3.6) or (3.6a) in each band gap in a semi-infinite one-dimensional crystal; that is, generally there is *at most* one surface state ($\beta > 0$) or band edge state ($\beta = 0$) in each band gap in a semi-infinite one-dimensional crystal under the assumption that the potential inside the crystal is the same as in an infinite crystal without a boundary.

3.5 Comparisons with Previous Work and Discussions

In this chapter, we have presented a general analysis of the surface states due to the termination of the crystal periodic potential in one-dimensional semi-infinite crystals. Although to the author's knowledge the two theorems in Section 3.2 and the general analysis given in this chapter have not been explicitly published before, many results presented here have been more or less given in previous theoretical investigations based on different specific potential models.

Many previous investigations of the conditions for the existence of surface states in one-dimensional semi-infinite crystals were based on a nearly free electron model and for the lowest band gap at $k = \frac{\pi}{a}$ [2]. By using a nearly free electron model, many authors [8–10] found that the termination of the periodic potential at a periodic potential minimum rather than at a potential maximum can cause a surface state in the lowest band gap at $k = \frac{\pi}{a}$; that is, only a "Tamm" type of surface state rather than a "Shockley" type of surface state could exist in that band gap. More generally, Goodwin [9] found that in a nearly free electron model, a surface state could appear in a specific band gap when the termination is at a minimum rather than at a maximum of the corresponding Fourier component of the crystal potential. All of these are consistent with our general result obtained in Section 3.4 that a surface state is not possible in a band gap for a τ equal to a zero of the *lower* band edge wave function: In a nearly free electron model, the zeros of the *lower* band edge wave function of a band gap are always at the maxima of the corresponding Fourier component of the crystal potential and the zeros of the *upper* band edge wave function are always at the minima of the corresponding component of the crystal potential. Our general results (Figs. 3.4 and 3.5) indicate that a surface state could not exist when τ is in the near neighborhood of the zeros of the *lower* band edge wave function. For the lowest band gap at $k = \frac{\pi}{a}$, this means that when τ is in the neighborhood of a maximum of the crystal potential, a surface state cannot exist. Therefore, only a "Tamm" type rather than a "Shockley" type of surface state can exist.

A particularly interesting work is a systematic investigation by Levine [11] on the existence of surface states in different band gaps in a sinusoidal crystal potential (Mathieu problem) for different boundary positions. By using some further approximations, Levine found that for the n-th band gap, a potential period $[0, a)$ can be separated into $2(n + 1)$ intervals, and only when the boundary is in one of the $n + 1$ specific intervals can there be a surface state in the band gap in the semi-infinite one-dimensional crystal. These $n+1$ surface-state-allowed intervals are separated by the $n+1$ surface-state-unallowed intervals. In each of the surface-state-allowed intervals, the energy of the surface state increases as the boundary goes inside the semi-infinite crystal. The results obtained in Section 3.4 are more general yet consistent with Levine's results. Since for a sinusoidal crystal potential the properties of two band edge wave functions $\phi_n(k_g, x)$ and $\phi_{n+1}(k_g, x)$ of a specific band

gap, including their zeros, $\frac{\phi_n'(k_g,x)}{\phi_n(k_g,x)}$, $\frac{\phi_{n+1}'(k_g,x)}{\phi_{n+1}(k_g,x)}$, and so forth, can be precisely known [e.g.,14], many results in [11] may be directly obtained from the general analysis in Sections 3.2–3.4 without the use of those further approximations.

Many people believed that a termination of the periodic potential in a one-dimensional semi-infinite crystal *always* causes a surface state to exist in each band gap below the potential barrier. From the analysis presented here, we have seen that this is in fact a misconception: The termination of the periodic potential $v(x)$ at the boundary of a semi-infinite one-dimensional crystal may or may not cause a state in a specific band gap. If it does cause a state for that specific band gap, this state may be either a surface state located near the boundary of the semi-infinite crystal or a band edge state with a decay factor $\beta = 0$; thus, it does not decay in the semi-infinite crystal at all.

It does not seem very easy to experimentally verify the behaviors of the electronic surface states as indicated by the two theorems given here. Nevertheless, although more work is needed to extend these theorems to describe the behavior of surface modes in photonic crystals, it is interesting to see that the behavior of the surface states has been observed experimentally or obtained in the numerical calculations of the surface modes in photonic crystals. For example, Robertson et al. [15] observed experimentally that the existence of surface modes in two-dimensional photonic crystals depends on the location of termination of the photonic crystal; Meade et al. [16] found that a "higher termination value" (corresponding to a "thicker" semi-infinite crystal) yields a lower value of the surface band frequency in their three-dimensional photonic crystal calculations; Ramos-Mendieta and Halevi [17] found in their calculation on two-dimensional semi-infinite photonic crystals that when the termination boundary goes inside, the frequency of the surface modes rises and the existence of the surface modes depends on the location of the termination of the photonic crystal. Yang et al. [18] in their investigations on the surface modes in two-dimensional photonic crystals obtained very similar results by calculations theoretically and observed them experimentally. Investigations by Vlasov et al. [19] also observed that the existence and the locations of surface modes in two-dimensional photonic crystals depends on the location of termination of the photonic crystal. All of these observations are consistent with the analysis on the electronic surface states made here.

References

1. I. Tamm: Physik. Z. Sowj. **1**, 733 (1932)
2. S. G. Davison and M. Stęślicka: *Basic Theory of Surface States* (Clarendon Press, Oxford 1992)
3. M. -C. Desjonquéres and D. Spanjaard: *Concepts in Surface Physics* (Springer, Berlin Heidelberg 1993)
4. A. Zangwill: *Physics at Surfaces* (Cambridge University Press, Cambridge 1988)

5. F. Bechstedt: *Principles of Surface Physics* (Springer, Berlin Heidelberg 2003)
6. A. Groß: *Theoretical Surface Science: A Microscopic Perspecpective* (Springer, Berlin Heidelberg 2003)
7. S. G. Davison and J. D. Levine: *Solid State Physics*, edited by H. Ehrenreich, F. Seitz, and D. Turnbull (Academic Press, New York 1970), Vol. 25, pp. 1–149
8. A. M. Maue: Z. Phy. **94**, 717 (1935); F. Forstmann: Z. Phy. **235**, 69 (1970); F. Forstmann: *Photoemission and the Electronic Properties of Surfaces*, edited by B. Feuerbacher, B. Fitten, and R. F. Willis (John Wiley & Sons, New York 1978), pp. 193–226; R. O. Jones: in *Surface Physics of Phosphors and Semiconductors*, edited by C. G. Scott and C. E. Reed (Academic Press, London 1975) pp. 95–142; J. B. Pendry and S. J. Gurman: Surf. Sci. **49**, 87 (1975)
9. E. T. Goodwin: Proc. Cambridge Phil. Soc. **35**, 205 (1939)
10. H. Statz: Z. Naturforsch. **5a**, 534 (1950)
11. J. D. Levine: Phys. Rev. **171**, 701 (1968)
12. W. Shockley: Phys. Rev. **56**, 317 (1939)
13. H. Hellmann: Acta Physicochimi. URSS I, **6**, 913 (1935); IV, **2**, 224 (1936); H. Hellmann: *Einführung in die Quantenchemie* (Deuticke, Leipzig 1937); R. P. Feynman: Phys. Rev. **56**, 340 (1939)
14. F. P. Mechel: *Mathieu Functions: Formulas, Generation, Use* (S. Hirzel Verlag, Stuttgart 1997)
15. W. M. Robertson, G. Arjavalinggam, R. D. Meade, K. D. Brommer, A. M. Rappe, and J. D. Joannopoulos: Opt. Lett. **18**, 528 (1993)
16. R. D. Meade, K. D. Brommer, A. M. Rappe, and J. D. Joannopoulos: Phys. Rev. **44**, 10961 (1991)
17. F. Ramos-Mendieta, and P. Halevi: Phys. Rev. **59**, 15112 (1999)
18. Jin-Kye Yang, Se-Heon Kim, Guk-Hyun Kim, Hong-Gyu Park, Yong-Hee Lee, and Sung-Bock Kim: Appl. Phys. Lett. **84**, 3016 (2004)
19. Y. A. Vlasov, N. Moll, and S. J. McNab: Opt. Lett. **29**, 2175 (2004)

4 Electronic States in Ideal One-Dimensional Crystals of Finite Length

In this chapter, we present a general investigation on the electronic states in ideal one-dimensional crystals of finite length $L = Na$, where a is the potential period and N is a positive integer.[1] On the basis of the theory of differential equations in Chapter 2, exact and general results on the electronic states in such an ideal finite crystal can be analytically obtained. We will see that in obtaining the results in this chapter, it is the understanding of the *zeros* of the solutions of a one-dimensional Schrödinger differential equation with a periodic potential that plays a fundamental role.

This chapter is organized as follows. After giving a basic consideration of the problem in Section 4.1, in Section 4.2 we prove the major results of this chapter: In contrast with the conception that all electronic states are Bloch waves in a one-dimensional infinite crystal, there are two different types of electronic states in an ideal one-dimensional finite crystal. In Section 4.3, we give more discussions on the boundary-dependent states, which are a basic distinction of the quantum confinement of Bloch waves. In Section 4.4, we treat one-dimensional symmetric finite crystals in which the energies of all electronic states can be obtained from the bulk energy band structure. In Sections 4.5–4.7 are comments on several relevant problems. In Section 4.8 is a simple summary.

4.1 Basic Considerations

We again write the Schrödinger differential equation (2.36) in a one-dimensional crystal with a periodic potential:

$$-y'' + [v(x) - \lambda]y = 0, \quad -\infty < x < +\infty, \tag{4.1}$$

where $v(x + a) = v(x)$ is the periodic crystal potential.

We assume that (4.1) is solved. The eigenvalues of (4.1) are energy bands $\varepsilon_n(k)$ and the corresponding eigenfunctions are Bloch functions $\phi_n(k, x)$, where $n = 0, 1, 2,$ ... and $-\frac{\pi}{a} < k \leq \frac{\pi}{a}$. We are mainly interested in the cases where there is always a band gap between two consecutive energy bands of (4.1). For these cases, the band edges $\varepsilon_n(0)$ and $\varepsilon_n(\frac{\pi}{a})$ occur in the order

[1] Part of the results in this chapter was published in [1, 2].

$$\varepsilon_0(0) < \varepsilon_0\left(\frac{\pi}{a}\right) < \varepsilon_1\left(\frac{\pi}{a}\right) < \varepsilon_1(0) < \varepsilon_2(0) < \varepsilon_2\left(\frac{\pi}{a}\right) < \varepsilon_3\left(\frac{\pi}{a}\right) < \varepsilon_3(0) < \varepsilon_4(0) < \cdots. \quad (4.2)$$

The band gaps are between $\varepsilon_{2m}(\frac{\pi}{a})$ and $\varepsilon_{2m+1}(\frac{\pi}{a})$ or between $\varepsilon_{2m+1}(0)$ and $\varepsilon_{2m+2}(0)$.

For an ideal one-dimensional crystal of finite length $L = Na$, we assume that the potential *inside* the crystal is still $v(x)$, as in (4.1). The two ends of the crystal are denoted as τ and $\tau + L$, where τ is a real number.

The eigenvalues Λ and eigenfunctions $\psi(x, \Lambda)$ of the electronic states in the finite crystal are solutions of the Schrödinger differential equation

$$-\psi''(x) + [v(x) - \Lambda]\psi(x) = 0, \quad \tau < x < \tau + L, \quad (4.3)$$

inside the crystal with certain boundary conditions at the two boundaries τ and $\tau + L$. For an ideal finite crystal, we have the boundary conditions

$$\psi(x) = 0, \quad x \le \tau \text{ or } x \ge \tau + L. \quad (4.4)$$

Our purpose is to find solutions of (4.3) under the boundary conditions (4.4).

Suppose $y_1(x, \lambda)$ and $y_2(x, \lambda)$ are two linearly independent solutions of (4.1). In general, a nontrivial solution of (4.3) and (4.4), if it exists, can be expressed as

$$\begin{aligned} \psi(x, \Lambda) &= y(x, \Lambda) \quad \text{if } \tau < x < \tau + L \\ &= 0 \qquad\quad \text{if } x \le \tau \text{ or } x \ge \tau + L. \end{aligned}$$

Here,

$$y(x, \lambda) = c_1 y_1(x, \lambda) + c_2 y_2(x, \lambda) \quad (4.5)$$

– in which c_1 and c_2 are not both zero – is a nontrivial solution of (4.1) and satisfies

$$y(\tau, \Lambda) = y(\tau + L, \Lambda) = 0. \quad (4.6)$$

The nontrivial solutions of (4.3) and (4.4) can be found through (4.5) and (4.6) based on the general properties of linearly independent solutions of (4.1) in different energy intervals, as discussed in Section 2.5.

4.2 Two Types of Electronic States

We have understood in Chapter 2 that the forms of linearly independent solutions $y_1(x, \lambda)$ and $y_2(x, \lambda)$ in (4.5) can be determined by the discriminant $D(\lambda)$ of (4.1). The existence and the properties of nontrivial solutions Λ and $y(x, \Lambda)$ in (4.6) can be straightforwardly obtained on this basis.

For a finite crystal, both the permitted and the forbidden energy ranges of the infinite crystal should be considered. In principle, we need to consider

solutions of (4.6) for λ in $(-\infty, +\infty)$. However, according to Theorem 2.9, any nontrivial solution of (4.1) with $\lambda \leq \varepsilon_0(0)$ can have only at most one zero for x in $(-\infty, +\infty)$; thus, it cannot satisfy (4.6). Consequently, there is not a nontrivial solution of (4.6) for λ in $(-\infty, \varepsilon_0(0)]$; we need only to consider λ in $(\varepsilon_0(0), +\infty)$. Similar to our discussions in Section 2.5, depending on λ, there are five different cases:

A. $|D(\lambda)| < 2$.

In this case, λ is inside an energy band of (4.1). According to (2.57), two linearly independent solutions of (4.1) can be chosen:

$$y_1(x, \lambda) = \mathrm{e}^{\mathrm{i}k(\lambda)x} p_1(x, \lambda), \quad y_2(x, \lambda) = \mathrm{e}^{-\mathrm{i}k(\lambda)x} p_2(x, \lambda),$$

where $k(\lambda)$ is a real number depending on λ and

$$0 < k(\lambda)a < \pi$$

and $p_1(x, \lambda)$ and $p_2(x, \lambda)$ have period a: $p_i(x + a, \lambda) = p_i(x, \lambda)$. All $k(\lambda)$ and $p_i(x, \lambda)$ are functions of λ. Simple mathematics leads to that the existence of nontrivial solutions of (4.5) and (4.6) requires [2]

$$\mathrm{e}^{\mathrm{i}k(\Lambda)L} - \mathrm{e}^{-\mathrm{i}k(\Lambda)L} = 0. \tag{A.1}$$

Note (A.1) does not contain τ. The nontrivial solutions can be obtained if

$$k(\Lambda)L = j\pi, \quad j = 1, 2, ..., N-1.$$

Thus in each energy band $\varepsilon_n(k)$, there are $N-1$ values of Λ_j, where $j = 1, 2, ..., N-1$, for which

$$k(\Lambda_j) = j\ \pi/L.$$

Correspondingly, for each energy band, there are $N-1$ electronic states whose energies are given by

$$\Lambda_{n,j} = \varepsilon_n \left(\frac{j\pi}{L} \right), \quad j = 1, 2, ..., N-1. \tag{4.7}$$

Each energy for this case is a function of L, the crystal length. However, all do not depend on the location of the crystal boundary τ or $\tau + L$. Correspondingly, there are $N-1$ eigenfunctions $y(x, \Lambda_j)$. These states are stationary Bloch states consisting of two Bloch waves with wave vectors $k = j\ \pi/L$ and $-k = -j\ \pi/L$ in the finite crystal, formed due to the multiple

[2] Otherwise

$$c_1 p_1(\tau, \Lambda) = 0, \quad \text{and} \quad c_2 p_2(\tau, \Lambda) = 0. \tag{A.2}$$

It was pointed out on p. 46 that in general a one-dimensional Bloch function $\phi_n(k, x)$ does not have a zero except $k = 0$ or $k = \frac{\pi}{a}$. Thus, neither $p_1(\tau, \Lambda)$ nor $p_2(\tau, \Lambda)$ in (A.2) can be zero. Therefore, (A.2) leads to $c_1 = c_2 = 0$ and no nontrivial solution of (A.2) exists.

reflection of Bloch waves at the two ends τ and $\tau + L$ of the finite crystal. For simplicity, we call these states L-dependent states; although only the eigenvalue of such a state is dependent only on L, the wave function of such a state is dependent on both τ and L.

The energies $\Lambda_{n,j}$ in (4.7) map the energy band structure $\varepsilon_n(k)$ of the infinite crystal exactly. By using a Kronig–Penney potential, Pedersen and Hemmer found that the energy spectrum of the confined Bloch waves maps the energy bands exactly [3]. The fact that the energy spectra of confined electrons in Si (001), (110) quantum films and in GaAs (110) quantum films approximately map the energy band structure of the bulk were observed in numerical calculations by Zhang and Zunger [4] and Zhang et al. [5]. Much previous work also finds that the eigenvalues of confined Bloch states map *closely* the dispersion relations of the unconfined Bloch waves [e.g.,6]. From (4.7), we see that this is in fact an exact correspondence for the electronic states in ideal one-dimensional crystals of finite length. Furthermore, this exact correspondence does not depend on τ, the location of the crystal boundary. These electronic states can be considered as bulk-like electronic states in a one-dimensional crystal of finite length.

B. $D(\lambda) = 2$.

In this case, λ is at a band edge at $k = 0$: $\lambda = \varepsilon_{2m+1}(0)$ or $\lambda = \varepsilon_{2m+2}(0)$.

According to (2.58), two linearly independent solutions of (4.1) for this case can be expressed as

$$y_1(x, \lambda) = p_1(x, \lambda), \quad y_2(x, \lambda) = x\ p_1(x, \lambda) + p_2(x, \lambda),$$

where $p_1(x, \lambda)$ and $p_2(x, \lambda)$ are periodic functions with period a.

Due to Theorem 2.1, the zeros of $p_1(x, \lambda)$ are separated from the zeros of $p_2(x, \lambda)$. From (4.5) and (4.6), simple mathematics shows that, in this case, the existence of a nontrivial solution (4.6) requires

$$p_1(\tau, \Lambda) = 0 \quad \text{and} \quad c_2 = 0. \tag{B.1}$$

(B.1) indicates that if a solution of (4.3) and (4.4) exists at a band edge at $k = 0$, the corresponding wave function $y(x, \Lambda)$ of the confined electronic state must be a periodic function, with a zero at the crystal boundary τ (and also $\tau + L$).

C. $D(\lambda) > 2$.

In this case, λ is *inside* a band gap at $k = 0$: $\varepsilon_{2m+1}(0) < \lambda < \varepsilon_{2m+2}(0)$. According to (2.60), two linearly independent solutions of (4.1) can be expressed as

$$y_1(x, \lambda) = \mathrm{e}^{\beta(\lambda)x} p_1(x, \lambda), \quad y_2(x, \lambda) = \mathrm{e}^{-\beta(\lambda)x} p_2(x, \lambda),$$

where $\beta(\lambda)$ is a positive real number depending on λ and $p_1(x, \lambda)$ and $p_2(x, \lambda)$ are periodic functions with a period a.

Again due to Theorem 2.1, the zeros of $p_1(x,\lambda)$ are separated from the zeros of $p_2(x,\lambda)$. If there is a nontrivial solution $y(x,\Lambda)$ in this case, simple mathematics from (4.5) and (4.6) gives that we must have either

$$p_1(\tau,\Lambda)=0 \ \text{ and } \ c_2=0 \tag{C.1}$$

or

$$p_2(\tau,\Lambda)=0 \ \text{ and } \ c_1=0. \tag{C.2}$$

(C.1) and (C.2) indicate that if a solution of (4.3) and (4.4) exists inside a band gap at $k=0$, the corresponding wave function $y(x,\Lambda)$ of the confined electronic state must be a product of an exponential function and a periodic function, with a zero at the crystal boundary τ (and also $\tau+L$). Note that (C.1) and (C.2) cannot be true simultaneously.

From the discussions on Case B and Case C, we can see that the existence of a nontrivial solution of (4.6) in a band gap $[\varepsilon_{2m+1}(0),\varepsilon_{2m+2}(0)]$ at $k=0$ requires that either one of (B.1), (C.1), or (C.2) must be true. Since all functions $p_i(x,\lambda)$ in (B.1), (C.1), and (C.2) are periodic functions, we always have $y(\tau+a,\Lambda)=0$ if we have $y(\tau,\Lambda)=0$. Therefore, the following equation is a necessary condition for having a solution Λ in (4.6) for a band gap at $k=0$:

$$y(\tau+a,\Lambda)=y(\tau,\Lambda)=0. \tag{4.8}$$

It is easy to see that (4.8) is also a sufficient condition for having a solution (4.6): From (4.8), one can obtain $y(\tau+\ell a,\Lambda)=0$, where $\ell=0,1,2,...,N$.

D. $D(\lambda)=-2$.

In this case, λ is at a band edge at $k=\frac{\pi}{a}:\lambda=\varepsilon_{2m}(\frac{\pi}{a})$ or $\lambda=\varepsilon_{2m+1}(\frac{\pi}{a})$.

According to (2.61), two linearly independent solutions of (4.1) can be expressed as

$$y_1(x,\lambda)=s_1(x,\lambda), \quad y_2(x,\lambda)=x\ s_1(x,\lambda)+s_2(x,\lambda),$$

where $s_1(x,\lambda)$ and $s_2(x,\lambda)$ are semi-periodic functions with semi-period a.

Due to Theorem 2.1, the zeros of $s_1(x,\lambda)$ are separated from the zeros of $s_2(x,\lambda)$. From (4.5) and (4.6), simple mathematics indicates that the existence of a nontrivial solution (4.6) in this case requires

$$s_1(\tau,\Lambda)=0 \ \text{ and } \ c_2=0. \tag{D.1}$$

(D.1) indicates that if a solution of (4.3) and (4.4) exists at a band edge at $k=\frac{\pi}{a}$, the corresponding wave function $y(x,\Lambda)$ of the confined electronic state must be a semi-periodic function with semi-period a, with a zero at the crystal boundary τ (and also $\tau+L$).

E. $D(\lambda)<-2$.

In this case, λ is *inside* a band gap at $k=\frac{\pi}{a}$: $\varepsilon_{2m}(\frac{\pi}{a})<\lambda<\varepsilon_{2m+1}(\frac{\pi}{a})$. According to (2.63), two linearly independent solutions of (4.1) can be expressed as

$$y_1(x,\lambda) = \mathrm{e}^{\beta(\lambda)x} s_1(x,\lambda), \quad y_2(x,\lambda) = \mathrm{e}^{-\beta(\lambda)x} s_2(x,\lambda),$$

where $\beta(\lambda)$ is a positive real number depending on λ and $s_1(x,\lambda)$ and $s_2(x,\lambda)$ are semi-periodic functions with semi-period a.

Again, due to Theorem 2.1, the zeros of $s_1(x,\lambda)$ are separated from the zeros of $s_2(x,\lambda)$. If there is a nontrivial solution $y(x,\Lambda)$ in this case, simple mathematics from (4.5) and (4.6) gives that we must have either

$$s_1(\tau,\Lambda) = 0 \ \text{ and } \ c_2 = 0 \tag{E.1}$$

or

$$s_2(\tau,\Lambda) = 0 \ \text{ and } \ c_1 = 0. \tag{E.2}$$

(E.1) and (E.2) indicate that if a solution of (4.3) and (4.4) exists inside a band gap at $k = \frac{\pi}{a}$, the corresponding wave function $y(x,\Lambda)$ of the confined electronic state must be a product of an exponential function and a semi-periodic function, with a zero at the crystal boundary τ (and also $\tau + L$). Note that (E.1) and (E.2) cannot be true simultaneously.

From the discussions of Case D and Case E, we can see that the existence of a nontrivial solution of (4.6) for a band gap $[\varepsilon_{2m}(\frac{\pi}{a}), \varepsilon_{2m+1}(\frac{\pi}{a})]$ at $k = \frac{\pi}{a}$ requires that either one of $(D.1), (E.1)$, or (E.2) must be true. Since all functions $s_i(x,\lambda)$ in $(D.1), (E.1)$, and (E.2) are semi-periodic functions with a semi-period a, we always have $y(\tau + a, \Lambda) = 0$ if we have $y(\tau,\Lambda) = 0$. We are led to the same equation (4.8) as a necessary and sufficient condition for having a solution (4.6) for a band gap at $k = \frac{\pi}{a}$. Therefore, (4.8) is a necessary and sufficient condition for having a solution of (4.6) corresponding to a band gap.

As pointed on p. 46, Theorem 2.8 indicates that for an arbitrary real number τ, there is always one and only one Λ for which (4.8) is true for each band gap $[\varepsilon_{2m}(\frac{\pi}{a}), \varepsilon_{2m+1}(\frac{\pi}{a})]$ or $[\varepsilon_{2m+1}(0), \varepsilon_{2m+2}(0)]$. Since no two linearly independent solutions of (4.1) with one Λ may have the same zeros (Theorem 2.1), such a Λ may only correspond to one $y(x,\Lambda)$; that is, there is one and only one solution $\psi(x,\Lambda)$ of (4.3) and (4.4) in each gap.

Equation (4.8) does not contain the crystal length L; thus, an eigenvalue Λ of (4.3) and (4.4) in a band gap is only dependent on τ, but not on L.

Therefore, *for any real number τ, there is always one and only one Λ and $\psi(x,\Lambda)$ as a solution of (4.3) and (4.4) in each band gap $[\varepsilon_{2m}(\frac{\pi}{a}), \varepsilon_{2m+1}(\frac{\pi}{a})]$ or $[\varepsilon_{2m+1}(0), \varepsilon_{2m+2}(0)]$. Such a Λ is dependent on τ but not on L.* For simplicity, we call these solutions τ-dependent states; although only the eigenvalue Λ of such a state is dependent on only τ, the wave function $\psi(x,\Lambda)$ of such a state is dependent on both τ and L.

The Λ's of these τ-dependent states are exactly the $\Lambda_{\tau,2m}$ or $\Lambda_{\tau,2m+1}$ defined by (2.71). According to Theorem 2.8, $\Lambda_{\tau,2m}$ is in $[\varepsilon_{2m}(\frac{\pi}{a}), \varepsilon_{2m+1}(\frac{\pi}{a})]$ and $\Lambda_{\tau,2m+1}$ is in $[\varepsilon_{2m+1}(0), \varepsilon_{2m+2}(0)]$.

As an example, in Fig. 4.1 is shown a comparison between the energy bands of (4.1) and the energies of the electronic states in a one-dimensional crystal (solutions of (4.3) and (4.4)) for a crystal length $L = 8a$.

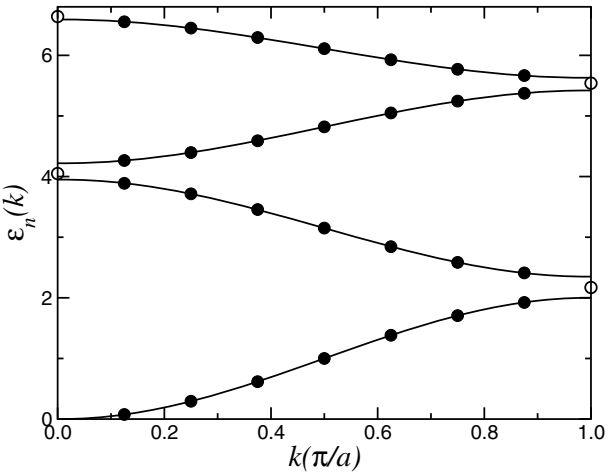

Fig. 4.1. A comparison between the energy bands $\varepsilon_n(k)$ of (4.1) (solid lines) and the energies Λ of the electronic states in a crystal of length $L = 8a$ (solid circles, L-dependent; open circles, τ-dependent). Note that the L-dependent energies map the energy bands exactly and satisfy (4.7); The τ-dependent energies satisfying (4.8) are in a band gap or at a band edge of (4.1). Reprinted with permission from S. Y. Ren: Ann. Phys.(NY) **301**, 22 (2002). Copyright by Elsevier.

The major results obtained in this section can be summarized as the following theorem:

Theorem 4.1. *There are two types of solutions of (4.3) and (4.4) if (4.2) is true. Corresponding to each energy band of (4.1), there are $N-1$ stationary Bloch state solutions of (4.3) and (4.4) whose energies are given by (4.7) thus are dependent on the crystal length L but not on the crystal boundary τ and map the energy band exactly. There is always one and only one solution of (4.3) and (4.4) corresponding to each band gap of (4.1), whose energy is dependent on the crystal boundary τ but not on the crystal length L.*

There could also exist the cases of zero band gap in which $\varepsilon_{2m}(\frac{\pi}{a}) = \varepsilon_{2m+1}(\frac{\pi}{a})$ or $\varepsilon_{2m+1}(0) = \varepsilon_{2m+2}(0)$, where (4.2) is not generally true. Suppose in a specific case that $\varepsilon_{2m}(\frac{\pi}{a}) = \varepsilon_{2m+1}(\frac{\pi}{a})$; then two linearly independent solutions of (4.1) can be chosen according to (2.62) as

$$y_1\left[x, \varepsilon_{2m}\left(\frac{\pi}{a}\right)\right] = s_1\left[x, \varepsilon_{2m}\left(\frac{\pi}{a}\right)\right], \quad y_2\left[x, \varepsilon_{2m}\left(\frac{\pi}{a}\right)\right] = s_2\left[x, \varepsilon_{2m}\left(\frac{\pi}{a}\right)\right],$$

and $s_1[x, \varepsilon_{2m}(\frac{\pi}{a})]$ and $s_2[x, \varepsilon_{2m}(\frac{\pi}{a})]$ are semi-periodic functions with semi-period a. It is easy to see that the function

$$\begin{aligned} y\left[x, \varepsilon_{2m}\left(\frac{\pi}{a}\right)\right] &= s_2\left[\tau, \varepsilon_{2m}\left(\frac{\pi}{a}\right)\right] s_1\left[x, \varepsilon_{2m}\left(\frac{\pi}{a}\right)\right] \\ &\quad - s_1\left[\tau, \varepsilon_{2m}\left(\frac{\pi}{a}\right)\right] s_2\left[x, \varepsilon_{2m}\left(\frac{\pi}{a}\right)\right] \end{aligned} \tag{4.9}$$

is a solution of (4.6). Since $s_1[\tau, \varepsilon_{2m}(\frac{\pi}{a})]$ and $s_2[\tau, \varepsilon_{2m}(\frac{\pi}{a})]$ are not both zero by Theorem 2.1, the function defined in (4.9) is a nontrivial solution of (4.3) and (4.4) and is a semi-periodic function whose energy $\Lambda = \varepsilon_{2m}(\frac{\pi}{a})$ does not depend on either L or τ. The cases where $\varepsilon_{2m+1}(0) = \varepsilon_{2m+2}(0)$ can be similarly discussed.

Therefore, in these cases, there is always a solution Λ of (4.3) and (4.4) that is dependent on neither L nor τ: $\Lambda = \varepsilon_{2m}(\frac{\pi}{a})$ or $\Lambda = \varepsilon_{2m+1}(0)$. $y(x, \Lambda)$ will be either a semi-periodic function (when $\varepsilon_{2m}(\frac{\pi}{a}) = \varepsilon_{2m+1}(\frac{\pi}{a})$) or a periodic function (when $\varepsilon_{2m+1}(0) = \varepsilon_{2m+2}(0)$).

A periodic potential $v(x + a) = v(x)$ obviously has the property that $v(x+2a) = v(x)$. If $\ell = 2a$ is chosen as the "new" potential period, the "new" Brillouin zone with boundaries at $\pm\pi/\ell$ is a half of the original Brillouin zone with boundaries at $\pm\frac{\pi}{a}$ and each energy band in the original Brillouin zone becomes two "new" energy bands in the "new" Brillouin zone (band-folding). Now, we consider a finite crystal of length $L = M\ell$, where M is a positive integer. According to the "new" description, it seems that there should be $(M-1)$ L-dependent states and one τ-dependent state for each "new" energy band and thus $2(M-1)$ L-dependent states and two τ-dependent states for each original energy band. From the original description, there are $2M-1$ L-dependent states and one τ-dependent state for each original energy band. This difference (one extra τ-dependent state and one less L-dependent state for each original energy band in the "new" description) comes from the fact that the "new" description ($\ell = 2a$ is the potential period) is not based on the whole symmetry of the system. Actually, in the "new" description, we always have $\varepsilon_{2m}(\pi/\ell) = \varepsilon_{2m+1}(\pi/\ell)$; that is, at the boundary π/ℓ of the "new" Brillouin zone, every band gap is a zero band gap. Therefore, in a finite crystal of length $L = M\ell$, there is always a state whose energy $\Lambda = \varepsilon_{2m}(\pi/\ell)$ depends neither on τ nor on L. Thus, the "extra" τ-dependent state in the "new" description actually is a L-dependent state with $j = M$ in the finite crystal of length $L = 2Ma$ in the original description. Its energy does not depend on τ since it is a L-dependent state. Its energy does not depend on L either, since for each band, the state $j = M$ always exists in a finite crystal of length $2Ma$. We mention this here since we will meet some relevant situations in Part III.

4.3 τ-Dependent States

It is well known that when one-dimensional plane waves are completely confined, all permitted states are stationary wave states. Thus, the very existence of the τ-dependent states in ideal one-dimensional finite crystals is a fundamental distinction of the quantum confinement of one-dimensional Bloch waves. In a one-dimensional finite crystal, such a τ-dependent state may have three different forms: a surface state localized near the left end τ of the crystal, a surface state localized near the right end $\tau + L$ of the crystal, or a band

edge state periodically distributed in the finite crystal – depending on the location of boundary τ.

We again take a band gap $[\varepsilon_{2m+1}(0), \varepsilon_{2m+2}(0)]$ at $k = 0$ as an example. In Section 2.6, we have seen how the τ-dependent eigenvalues $\Lambda_{\tau,n}$ change as τ changes. As τ goes to the right continuously from a (any) zero $x_{1,2m+1}$ of $\phi_{2m+1}(0, x)$ to $x_{1,2m+2}$, the zero of $\phi_{2m+2}(0, x)$ next to $x_{1,2m+1}$ and then to $x_{2,2m+1}$, the next zero of $\phi_{2m+1}(0, x)$,[3] the corresponding $\Lambda_{\tau,2m+1}$ will also go continuously from $\varepsilon_{2m+1}(0)$ up to $\varepsilon_{2m+2}(0)$ and then back to $\varepsilon_{2m+1}(0)$. We can consider such an up and down of $\Lambda_{\tau,2m+1}$ as a basic undulation. Corresponding to a basic undulation, in $[x_{1,2m+1}, x_{2,2m+1})$ the function $y(x, \Lambda)$ has different forms. Since for any solution of (4.3) and (4.4) in the band gap $[\varepsilon_{2m+1}(0), \varepsilon_{2m+2}(0)]$, one of $(B.1), (C.1)$, or $(C.2)$ in Sect. 4.2 must be true, we have three different cases:

1. When $\tau = x_{1,2m+1}$, $(B.1)$ is true and $\Lambda_{\tau,2m+1} = \varepsilon_{2m+1}(0)$, the corresponding solution $y(x, \Lambda)$ in (4.8) has the form

$$y[x, \varepsilon_{2m+1}(0)] = \phi_{2m+1}(0, x)$$

   and is a lower bandedge wave function of the band gap. Similarly, when $\tau = x_{1,2m+2}$, $(B.1)$ is true and $\Lambda_{\tau,2m+1} = \varepsilon_{2m+2}(0)$, the corresponding solution $y(x, \Lambda)$ in (4.8) has the form

$$y[x, \varepsilon_{2m+2}(0)] = \phi_{2m+2}(0, x)$$

   and is an upper bandedge wave function of the band gap. Either one of these two subcases corresponds to the fact that there is an electronic state in the finite crystal whose energy is the corresponding bandedge energy and does not depend on the crystal length L and whose wave function inside the crystal is the bandedge wave function: The τ-dependent state is a confined band edge state in the finite crystal.
2. In the section $(x_{1,2m+1}, x_{1,2m+2})$, $\frac{\partial}{\partial\tau}\Lambda_{\tau,2m+1} > 0$; thus, according to our discussion in Chapter 3, a surface state can exist in a right semi-infinite crystal with a left boundary at τ; correspondingly, $y(x, \Lambda_{\tau,2m+1})$ has the form $c_2 \mathrm{e}^{-\beta(\Lambda_{\tau,2m+1})x}\ p_2(x, \Lambda_{\tau,2m+1})$ with $p_2(\tau, \Lambda_{\tau,2m+1}) = 0$ $(C.2$ is true). A function with the form of $c_2 \mathrm{e}^{-\beta(\Lambda_{\tau,2m+1})x}\ p_2(x, \Lambda_{\tau,2m+1})$, in which $\beta(\Lambda_{\tau,2m+1}) > 0$ is mainly distributed near the left end τ of the finite crystal, due to the exponential factor. Thus, the τ-dependent state in this case is a surface state in the finite crystal introduced by the termination of the periodic potential.
3. In the other section $(x_{1,2m+2}, x_{2,2m+1})$, $\frac{\partial}{\partial\tau}\Lambda_{\tau,2m+1} < 0$; thus, according to our discussion in Chapter 3, a surface state can exist in a left semi-infinite crystal with a right boundary at τ; correspondingly, $y(x, \Lambda_{\tau,2m+1})$ has the form $c_1 \mathrm{e}^{\beta(\Lambda_{\tau,2m+1})x}\ p_1(x, \Lambda_{\tau,2m+1})$ with $p_1(\tau, \Lambda_{\tau,2m+1}) = 0$ $(C.1$

[3] Remember that the zeros of $\phi_{2m+1}(0, x)$ and $\phi_{2m+2}(0, x)$ are distributed alternatively.

is true). A function with the form of $c_1 e^{\beta(\Lambda_{\tau,2m+1})x}\ p_1(x, \Lambda_{\tau,2m+1})$, in which $\beta(\Lambda_{\tau,2m+1}) > 0$, is mainly distributed near the right end $\tau + L$ of the finite crystal, due to the exponential factor. Thus, the τ-dependent state in this case is also a surface state in the finite crystal introduced by the termination of the periodic potential.

Therefore, these three cases correspond to a wave function inside the crystal with a form $e^{\beta x} p(x, \Lambda)$, in which $\beta = 0$, $\beta < 0$ or $\beta > 0$. The latter two correspond to a surface state located near to either the left or the right end of the finite crystal. *Such a surface state is introduced into the band gap when the boundary τ is not a zero of either band edge wave function of the Bloch waves.* As an example, in Fig. 4.2 is shown $\Lambda_{\tau,1}$ as a function of τ in the interval $[x_{1,1}, x_{1,1} + a]$, where $x_{1,1}$ is a (any) zero of $\phi_1(0, x)$. In the figure, the two sections of a basic undulation are shown as a dotted line ($C.2$ is true) or a dashed line ($C.1$ is true), indicating two different locations of the surface state.

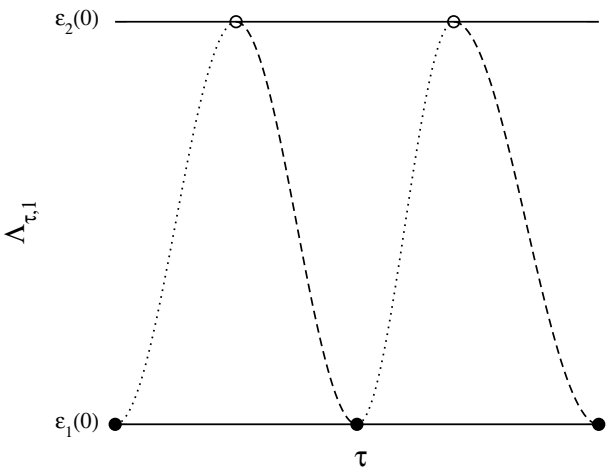

Fig. 4.2. $\Lambda_{\tau,1}$ as a function of τ in the interval $[x_{1,1}, x_{1,1} + a]$. The zeros of $\phi_1(0, x)$ are shown as solid circles and the zeros of $\phi_2(0, x)$ are shown as open circles. Note that $\Lambda_{\tau,1}$ completes two basic undulations in $[x_{1,1}, x_{1,1} + a)$. The dotted lines and dashed lines indicate that a surface state is located near either the left or the right end of the finite crystal.

Since according to Theorem 2.7, in the interval [0, a), both $\phi_{2m+1}(0, x)$ and $\phi_{2m+2}(0, x)$ have exactly $2m + 2$ zeros, then, in general, $\Lambda_{\tau,2m+1}$ as a function of τ always complete $2m + 2$ basic undulations in an interval of length a.

Of course, for the band gaps at $k = \frac{\pi}{a}$ $(\varepsilon_{2m}(\frac{\pi}{a}) < \Lambda_{\tau,2m} < \varepsilon_{2m+1}(\frac{\pi}{a}))$, a surface state has the form of either $c_1 e^{\beta(\Lambda_{\tau,2m})x}\ s_1(x, \Lambda_{\tau,2m})$ or $c_2 e^{-\beta(\Lambda_{\tau,2m})x}$

$s_2(x, \Lambda_{\tau,2m})$ inside the crystal, where $s_1(x, \Lambda_{\tau,2m})$ and $s_2(x, \Lambda_{\tau,2m})$ are semi-periodic functions. $\Lambda_{\tau,2m}$ as a function of τ will always complete $2m+1$ basic undulations in an interval of length a.

These discussions are closely related to the discussions we had in Section 3.3. The three possibilities of a τ-dependent state – a surface state located near the left end τ of the finite crystal, a surface state located near the right end $\tau + L$ of the finite crystal, or a confined band edge state – are actually determined by in which one of the three sets $L(n)$, $R(n)$, or $M(n)$, τ is. Naturally, a band edge state can also be considered as a special surface state with its energy equal to a band edge energy and its decay factor $\beta = 0$.

Many years ago, Tamm [7] showed that the termination of the periodic potential at the surface of a semi-infinite Kronig–Penney crystal can cause a surface state to exist in each band gap below the barrier height outside the crystal. More than 60 years later, Zhang and Zunger [4], Zhang et al. [5], and Franceschetti and Zunger [8] observed the existence of a "zero confinement state" in their numerical calculations. Now, we understand that in the one-dimensional case, a "zero confinement state" – a confined band edge state whose energy does not change as the crystal size changes – is simply a surface-like state with a decay factor $\beta = 0$. A surface state in the gap or a confined band edge state are different results of the termination of the periodic potential at the crystal boundary, depending on whether the boundary τ is a zero of a band edge wave function.

A slight change of the boundary location τ can change the properties of a τ-dependent state dramatically: It can change the τ-dependent state from a surface state located near one end of the crystal to a confined band edge state or to a surface state located near the other end. It can also change the energy of the surface state. This can be clearly seen in Fig. 4.2: If τ is in the region corresponding to a dotted line, the τ-dependent state is a surface state near the left end of the crystal. If τ is in the region corresponding to a dashed line, it is a surface state near the right end of the crystal. However, if τ is a zero of a band edge wave function (either a solid circle or an open circle in the figure), then $\tau + L$ is also a zero of the same band edge wave function and, consequently, the τ-dependent state is a confined band edge state. We can call these τ-dependent states surface-like states, in differentiation with the bulk-like states - the stationary Bloch states. The concept of surface-like states is an extended concept of the well-known surface states.

4.4 Electronic States in One-Dimensional Finite Symmetric Crystals

When a one-dimensional finite crystal is symmetric, the τ-dependent state for each gap is always a band edge state and the energies of all electronic states in the crystal can be obtained from the bulk band structure $\varepsilon_n(k)$.

A symmetric one-dimensional finite crystal means that (1) the crystal potential $v(x)$ has an inversion symmetry center and thus has an infinite number of inversion centers;[4] (2) the two ends of the crystal are also symmetric to one of these inversion centers and this inversion center can be chosen to be the origin: $v(-x) = v(x)$. Now, the two ends of the crystal are equivalent: one end $\tau = -L/2$ and the other end $\tau + L = L/2$. If this is the case, the energies of confined electronic states have an especially simple form.

Because $v(-x) = v(x)$, a noteworthy point is that $x = a/2$ is also an inversion center of the crystal potential $v(x)$ because $v(-x - a/2) = v(x + a/2) = v(x - a/2)$. Since the crystal length $L = Na$ and N is a positive integer, the two ends of the finite crystal $x = \tau = -L/2$ and $x = \tau + L = L/2$ must also be an inversion center of $v(x)$. Correspondingly, a band edge wave function will have a specific parity for an inversion relative to $x = L/2$ (and to $x = -L/2$), either an even parity or an odd parity. Furthermore, according to Theorem 2.7, the two band edge wave functions corresponding to a specific band gap have exactly the same number of zeros in $[0, a)$ and thus must have two different parities: One is even and the other is odd. The band edge wave function that has an odd parity for an inversion relative to $x = L/2$ (and to $x = -L/2$) will have a zero at the two ends of the finite crystal $x = L/2$ and $x = -L/2$; therefore, $\tau = -L/2$ is a zero of such a bandedge wave function. This corresponds to the case in Section 4.2 in which $(B.1)$ or $(D.1)$ is true. The band edge wave function satisfies both (4.3) and (4.6). Correspondingly, the energy of this band edge state will not change as the finite crystal length L changes. For a specific band gap, whether this is the upper band edge or the lower band edge depends on the crystal potential $v(x)$. For each band gap, there is always one band edge state whose energy does not change as the crystal length L changes. In Fig. 4.3 and Fig. 4.4 are shown the energies of two confined states near the two lowest band gap $[\varepsilon_0(\frac{\pi}{a}), \varepsilon_1(\frac{\pi}{a})]$ and $[\varepsilon_1(0), \varepsilon_2(0)]$ as functions of the crystal length L separately, obtained in [2].

Therefore, we can see that the existence of band edge states whose energies do not change as the crystal length changes and were observed in numerical calculations in [4,5,8] actually can quite often occur in one-dimensional finite symmetric crystals. Although such a state was called as "zero-confinement state" in [4,5,8], these states are really confined states. Nevertheless, the energy of these states does not change as L changes. We prefer to call these states confined band edge states. The fundamental reason for the existence of these confined band edge states in one-dimensional symmetric finite crystals is that due to the symmetry of the periodic potential, for each band gap there is always a band edge state that naturally has a zero at both ends of the finite crystal. Whether this is the upper band edge state or the lower band edge state depends on the specific form of $v(x)$ and the location of the band gap.

[4] Any point ℓa away from an inversion symmetry center of a periodic potential – here ℓ is an integer – is also an inversion symmetry center of the periodic potential.

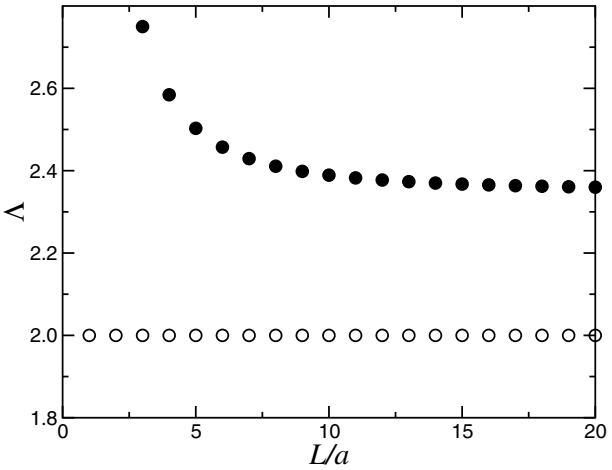

Fig. 4.3. The energies of two confined states near the lowest band gap as functions of the confinement length L. Note that the energy of the lower confined state is the band edge energy and is constant; only the energy of the higher confined state changes as L changes.

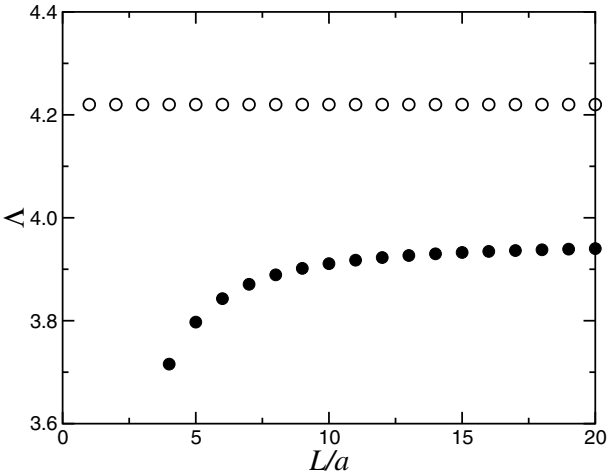

Fig. 4.4. The energies of two confined states near the second lowest band gap as functions of the crystal length L. Note that the energy of the higher confined state is the band edge energy and is constant; only the energy of the lower confined state changes as L changes.

Since the energy of each τ-dependent state in a one-dimensional symmetric finite crystal is always a band edge energy, the energies of all electronic states in such a finite crystal can be obtained from the band structure $\varepsilon_n(k)$ of the corresponding infinite crystal. Figure 4.5 shows a comparison between the energy bands $\varepsilon_n(k)$ as the solutions of (4.1) and the energy spectrum of $\Lambda_{n,j}$ and $\Lambda_{\tau,n}$ as solutions of (4.3) and (4.4) for a symmetric crystal of length $L = 8a$, obtained in [2].

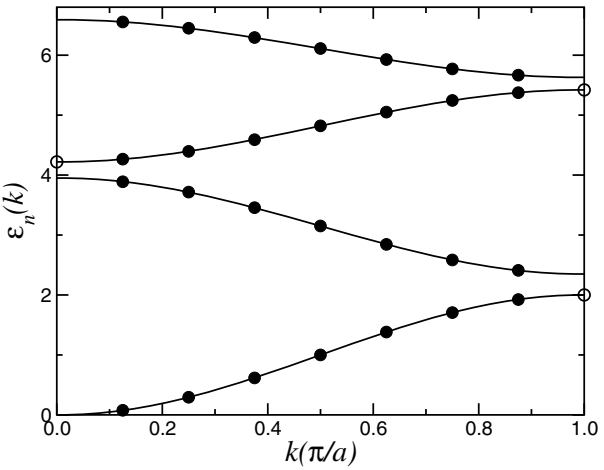

Fig. 4.5. A comparison between the energy spectrum of $\Lambda_{n,j}$ (solid circles) and $\Lambda_{\tau,n}$ (open circles) in a finite symmetric crystal of length $L = 8a$ and the energy bands $\varepsilon_n(k)$ (solid lines) for the lowest four bands. Note that (1) $\Lambda_{n,j}$ maps the energy bands exactly and (2) the existence of a confined band edge state in each band gap.

4.5 Comments on the Effective Mass Approximation

As we mentioned in Chapter 1, the effective mass approximation (EMA) has been widely used in investigating the quantum confinement of Bloch electrons. On the basis of a clearer understanding of the quantum confinement of one-dimensional Bloch waves, we can now make some comments on the use of EMA in the one-dimensional case.

(1) We have understood that the complete quantum confinement of one-dimensional Bloch waves produces two different types of electronic states. The very existence of the τ-dependent states is a fundamental distinction of the quantum confinement of Bloch waves. *EMA completely misses the very existence of the τ-dependent states and thus misses a fundamental distinction of the quantum confinement of Bloch waves.*

(2) *EMA can be a good approximation for the L-dependent states.*

From (4.7), we know that the energies of L-dependent electronic states can be written as

$$\Lambda_{n,j} = \varepsilon_n \left(\frac{j\pi}{L} \right), \quad j = 1, 2, ..., N-1.$$

Near a band edge, $\varepsilon_n(k)$ can be approximated. For example, near a band edge at $k = 0$, we may approximate $\varepsilon_n(k)$ as

$$\varepsilon_n(k) \approx \varepsilon_n(0) + \frac{1}{2} \left. \frac{\mathrm{d}^2 \varepsilon_n(k)}{\mathrm{d}k^2} \right|_{k=0} k^2. \tag{4.10}$$

Thus, for the L-dependent states near the band edge, we have

$$\Lambda_{n,j} \approx \varepsilon_n(0) + \frac{1}{2} \left. \frac{\mathrm{d}^2 \varepsilon_n(k)}{\mathrm{d}k^2} \right|_{k=0} \frac{j^2 \pi^2}{L^2}. \tag{4.11}$$

This is the EMA result for the complete quantum confinement of one-dimensional Bloch waves. Thus, for L-dependent states near a band edge at $k = 0$, as long as (4.10) is a good approximation, our exact results (4.7) approximately gives the results (4.11), the same as EMA. A corresponding expression of EMA can be easily obtained for the confined electronic states near a band gap at $k = \frac{\pi}{a}$.

Originally, the EMA was developed for treating the electronic states near band edges in the presence of slowly varying and weak perturbations, such as an external electric and/or magnetic field as well as the potential of shallow impurities [9]. Nevertheless, we have seen here that in treating the *L-dependent states* in one-dimensional finite crystals, the *only* requirement for the EMA to be used is that the energy band $\varepsilon_n(k)$ near the band edge can be approximated by a parabolic energy band such as in (4.10); even though in quantum confinement problems, the perturbation is neither weak nor slowly varying at the confinement boundaries, the original conditions for justifying the use of EMA are thus completely violated.[5] In Fig. 4.6 are shown the energies of three electronic states in crystals of different length near or in the lowest band gap of the Bloch waves as functions of the crystal length L, obtained in [1]. The two points we commented on here can be clearly seen.

4.6 Comments on the Surface States

The surface states in one-dimensional crystals are the simplest surface states. Some properties of surface states in one-dimensional crystals are usually easy

[5] This is true only for the cases where the interested band edge is located either at the center or at the boundary of the Brillouin zone. It may not be true in the low-dimensional systems or finite crystals investigated in Part III.

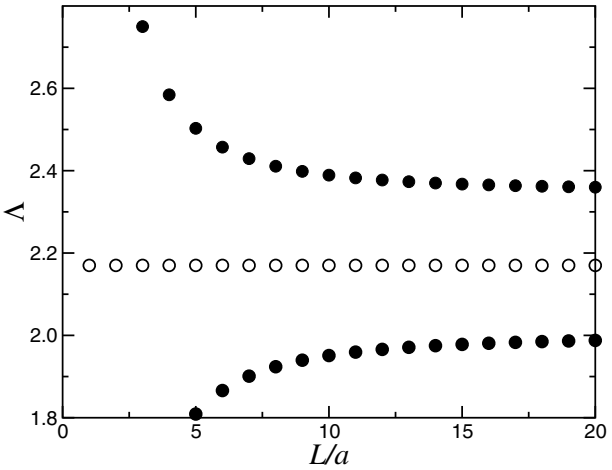

Fig. 4.6. The energies of three confined electronic states near or in the lowest band gap of (4.1) as functions of the crystal length L while τ is fixed. Note that the energy of the τ-dependent electronic state (open circles) in the gap is independent on L and the energies of the two L-dependent electronic states (solid circles) change as L changes. EMA completely neglects the existence of the τ-dependent state; however, it may give a good description for the behaviors of the two L-dependent states (see the text). Reprinted with permission from S. Y. Ren: Ann. Phys.(NY) **301**, 22 (2002). Copyright by Elsevier.

to analyze. On the basis of a clearer understanding of the electronic states in one-dimensional finite crystals, we can also make comments on several interesting problems on the surface states in one-dimensional crystals.

Although investigations of the surface states have made very significant progresses since Tamm's classical work [7] many years ago, it seems that some quite fundamental problems on surface states have not yet been very well understood. One of such problems is how many surface states are there in a simplest one-dimensional finite crystal with two ends. Fowler was the first to think [10] there are two surface states in each band gap in a one-dimensional finite crystal due to its two ends. Although he did not give a rigorous argument to prove his point, this idea seemed natural and was soon accepted [11]. A long-standing belief of many people in the solid state physics community is that there are two surface states in each gap of a one-dimensional finite crystal because it has two ends [12].

To the contrary, the general results on the electronic states in ideal one-dimensional finite crystals obtained here indicate that for each band gap there is always one and only one electronic state whose energy is dependent on the crystal boundary but not dependent on the crystal length. A surface state is one of the two possibilities of such a boundary-dependent state. Therefore, there is *at most* one surface state in each band gap in an ideal one-dimensional

finite crystal. This result is obviously different from that long-standing belief. The analytical results published in [1] were confirmed by recent numerical calculations [13,14].

Why can a finite one-dimensional crystal of *two ends* only have *at most one* surface state in each gap? This is due to the fact that (1) the two ends of a finite one-dimensional crystal in general are not equivalent and (2) as we analyzed in Chapter 3, a termination of the periodic potential $v(x)$ may or may not cause a state in a specific band gap.

Only in a symmetric one-dimensional finite crystal such as treated in Section 4.4 are the two ends of the crystal equivalent. We have understood that then there is always a confined band edge state rather than a surface state in each gap.

In most cases, the two ends of a finite one-dimensional crystal are generally not equivalent. The properties of the τ-dependent state for *each gap* will depend on the relation between the crystal boundary τ and the zeros of the two corresponding band edge wave functions. For a specific band gap, if τ is next to a zero of the upper band edge wave function *in the finite crystal*, then $\tau + L$ will be next to a zero of the lower band edge wave function *in the finite crystal*, and vice versa. Thus, the two ends of the finite crystals are not equivalent; it is possible that a surface state exists near only one of the two ends. From what we analyzed in Chapter 3, we can see that it is the end next to a zero of the upper band edge wave function $\phi_{2m+1}(\frac{\pi}{a}, x)$ or $\phi_{2m+2}(0, x)$ *in the finite crystal* that may have a surface state localized near it.

Figure 4.2 can also be considered as obtained by combining Fig. 3.1 with Fig. 3.2: If τ is in a dotted region of the Λ_1–τ curve (τ is next to an open circle *in the finite crystal*), there is a surface state located near the left end τ of the finite crystal; if τ is in a dashed region of the Λ_1–τ curve ($\tau + L$ will be next to an open circle *in the finite crystal*), there is a surface state located near the right end $\tau + L$ of the finite crystal; if τ is located at one of the circles, then there is a confined band edge state. Therefore, an ideal one-dimensional finite crystal bounded at τ and $\tau + L$ can have *at most* one surface state in each bandgap, even though it always has two ends.

More mathematically, this is due to the fact that for a finite one-dimensional crystal bounded at τ and $\tau + Na$, *both* the left end τ and the right end $\tau + Na$ actually always belong to the *same* one of the three sets $L(n)$, $M(n)$, and $R(n)$ in Section 3.3 and thus, correspondingly, only one of the three possibilities is possible: a surface state on the left of the finite crystal, a band edge state, or a surface state on the right of the finite crystal.

Having clearly understood the analysis presented here, we can see that the belief that a finite one-dimensional crystal always has two surface states in each gap is actually a misconception.[6]

[6] All of these discussions here are for ideal one-dimensional finite crystals defined by (4.3) and (4.4). An investigation on the electronic states in

In a tight-binding formalism, the number of permitted energy bands is determined by the number of states per unit cell. By using a nearest-neighbor tight-binding formalism, Hatsugai [15] proved that in a linear finite chain with q states per unit cell, there are a total of $q-1$ edge states, one in each of the $q-1$ gaps. The properties of those edge states in [15] are somewhat similar to the τ-dependent states in this chapter – they can either be located near either end of the chain or be a band edge state. It is well known that [e.g.,16] in a tight-binding formalism with a single state per unit cell, a linear finite chain does not have a surface state. The reason is quite simple – there is no band gap ($q = 1$) in the band structure in that formalism.

A surface electronic state is usually understood as a electronic state that is mainly distributed near a specific surface of the crystal. Now, we have a more extended concept of the surface-like states: The electronic states whose properties and energies are determined by the surface location, that is the τ-dependent states discussed in this chapter. A confined band edge state is merely a special case of a surface-like state with its decay factor β being zero – in ideal one-dimensional finite crystals, it happens when the surface location is a zero of a band edge wave function.

The spatial extension of a surface state is determined by its decay factor $\beta(\Lambda)$. $\beta(\lambda)$ as function of λ can be obtained from the discriminant $D(\lambda)$ of (4.1). In particular, for a surface state in a band gap at $k = 0$,[7]

$$\beta(\lambda)a = \ln\left[\frac{D(\lambda) + \sqrt{D^2(\lambda) - 4}}{2}\right]. \tag{4.12}$$

Therefore, the surface state with an energy Λ at which $D(\lambda)$ takes a maximum has the largest decay factor and thus the smallest spatial extension in such a band gap.

Similarly, for a surface states in a band gap at $k = \frac{\pi}{a}$, we have

$$\beta(\lambda)a = \ln\left[\frac{-D(\lambda) + \sqrt{D^2(\lambda) - 4}}{2}\right]. \tag{4.12a}$$

---

one-dimensional symmetric finite crystals with relaxed boundary conditions $(\psi'/\psi)_{x=\tau} = -(\psi'/\psi)_{x=L+\tau} = \sigma$ for finite σ can be found in Appendix A.

[7] Equation (4.12) can be obtained from (2.18), (2.24), and (2.29). Equation (4.12a) can be obtained from (2.18), (2.24), and (2.33). Similarly, one can also obtain that

$$\mathrm{e}^{\mathrm{i}k(\lambda)a} = \frac{D(\lambda) \pm \sqrt{D^2(\lambda) - 4}}{2}$$

for Bloch states in each energy band from (2.18), (2.24), and (2.25). Therefore, the complex energy band structure of any one-dimensional crystals can be completely and analytically obtained from the discriminant $D(\lambda)$ of its Schrödinger differential equation (4.1).

Thus, the surface state with an energy Λ at which $D(\lambda)$ takes a minimum has the largest decay factor and thus the smallest spatial extension in such a band gap.

From Fig. 2.1, we can see that roughly a surface state with its energy near the mid-gap has a larger decay factor β and thus a smaller spatial extension and a surface state with its energy near a band edge has a smaller decay factor β and thus a larger spatial extension. By considering the energy of a surface state as a function of the surface position τ such as shown in Fig. 4.2, we can obtain the following qualitative understandings: A surface position near a zero of the lower band edge wave function $\phi_{2m+1}(0, x)$ corresponds to a surface state with an energy near the lower band edge $\varepsilon_{2m+1}(0)$ and a smaller decay factor β and a larger spatial extension; a surface position near a zero of the upper band edge wave function $\phi_{2m+2}(0, x)$ corresponds to a surface state with an energy near the upper band edge $\varepsilon_{2m+2}(0)$ and also a smaller decay factor β and a larger spatial extension; a surface position near a mid-point between two consecutive zeros of two band edge wave functions corresponds to a surface state with an energy near the mid-gap and a larger decay factor β and a smaller spatial extension. A surface state in a band gap at $k = \frac{\pi}{a}$ can be similarly analyzed.

The value of the decay factor β of a surface state is determined by the corresponding $D(\lambda)$, according to (4.12) or (4.12a). Therefore, by a consideration either from a limit of wide energy bands and narrow band gap or from a limit of the contrary and by referring to Fig. 2.1, we can obtain such qualitative conclusions: For a specific band gap, the smaller the two relevant permitted band widths are and/or the larger the band gap is, the larger the largest decay factor β_{max} in the band gap can be.[8]

However, some conclusions obtained for surface states in one-dimensional crystals may not be true for surface states in three-dimensional crystals.

4.7 Two Other Comments

4.7.1 A Comment on the Formation of the Energy Bands

The electron states in an infinite crystal with translational invariance have an energy band structure; in each permitted energy band, the energy spectrum is a continuum. On the other hand, the electron states in a finite system always have a discrete energy spectrum. One interesting question is, How are those energy bands formed as the number of atoms increases gradually? From (4.7), we can see that, for the one-dimensional case, the mapping of

[8] A near-zero band gap makes the largest possible numerator in (4.12) or (4.12a) small; therefore, the largest decay factor β_{max} a surface state in the band gap may have is also small. On the contrary, a narrow permitted band width makes $|D'(\lambda)|$ at its band edge large and thus makes the largest possible numerator in (4.12) or (4.12a) large for the band gap, which leads to a large β_{max} in the band gap.

the energy bands by electronic states in finite crystals begins at $N = 2$ and linearly increases as N increases: A finite crystal of length $L = Na$ always has $N - 1$ stationary Bloch states in each energy band whose energies map the energy band exactly.

4.7.2 A Comment on the Boundary Locations

A consequence of the results obtained in this chapter is that the real boundary locations τ and $\tau + L$ of an ideal one-dimensional finite crystal discussed in this chapter are determined *only* by the τ-dependent electronic states. In our simplifying assumptions, the many body effects between the electrons are neglected; the total energy of the system is simply the summation of the energies of all occupied single-electronic states, including the L-dependent states and τ-dependent states. Therefore, the real boundary locations τ and $\tau + L$ of a finite crystal with a fixed length L in our simplified model are determined by the condition that the summation of the energies of all occupied τ-dependent states takes the minimum.

4.8 Summary

In summary, based on the mathematical results of the theory of ordinary differential equations with periodic coefficients – in particular, several theorems on the zeros of solutions of (4.1) – we have obtained exact and general results on the properties of all electronic states in the simplest finite crystals – the ideal one-dimensional crystals of finite length. For a one-dimensional crystal bounded at τ and $\tau + L$ where $L = Na$, there are two different types of electronic states: There are $N - 1$ Bloch stationary states corresponding to each energy band of (4.1). Their energies Λ are given by (4.7) and thus are dependent on the crystal length L but not on the crystal boundary location τ and map the energy band exactly. These stationary Bloch states can be considered as bulk-like states in the one-dimensional finite crystal. There is always one and only one electronic state corresponding to each band gap of (4.1); its eigenvalue Λ is dependent on the boundary location τ but not on the crystal length L. Such a τ-dependent state can be either a surface state in the band gap (if τ is not a zero of either band edge wave function of (4.1)) or a confined band edge state (if τ is a zero of a band edge wave function of (4.1)). A slight change of the crystal boundary location τ could change the properties and the energy of this τ-dependent state dramatically. These τ-dependent states can be considered as surface-like states in the finite crystal. A confined band edge state is a surface-like state with its decay factor $\beta = 0$.

The very existence of these τ-dependent surface-like states is a fundamental distinction of the quantum confinement of Bloch waves.

The exact and general results obtained indicate that the major difficulty or obstacle due to the lack of translational invariance in one-dimensional finite crystals in fact could be circumvented.

The general understandings obtained here provide a basis for further understanding of the quantum confinement of three-dimensional Bloch waves and the electronic states in low-dimensional systems and finite crystals in three-dimensional cases.

References

1. S. Y. Ren: Ann. Phys.(NY) **301**, 22 (2002)
2. S. Y. Ren: Phys. Rev. **B64**, 035322 (2001)
3. F. B. Pedersen and P. C. Hemmer: Phys. Rev. **B50**, 7724 (1994)
4. S. B. Zhang and A. Zunger: Appl. Phys. Lett. **63**, 1399 (1993)
5. S. B. Zhang, C-Y Yeh, and A. Zunger: Phys. Rev. **B48**, 11204 (1993)
6. Z. V. Popovic, M. Cardona, E. Richter, D. Strauch, L. Tapfer, and K. Ploog: Phys. Rev. **B40**, 1207 (1989); Z. V. Popovic, M. Cardona, E. Richter, D. Strauch, L. Tapfer, and K. Ploog: Phys. Rev. **B40**, 3040 (1989); Z. V. Popovic, M. Cardona, E. Richter, D. Strauch, L. Tapfer, and K. Ploog: Phys. Rev. **B41**, 5904 (1990)
7. I. Tamm: Physik. Z. Sowj. **1**, 733 (1932)
8. A. Franceschetti and A. Zunger: Appl. Phys. Lett. **68**, 3455 (1996)
9. J. M. Luttinger and W. Kohn: Phys. Rev. **97**, 869 (1957); W. Kohn: *Solid State Physics*, edited by F. Seitz and D. Turnbull (Academic Press, New York 1955), Vol. 5, pp. 257–320
10. R. H. Fowler: Proc. Roy. Soc. **141**, 56 (1933)
11. F. Seitz: *The Modern Theory of Solids* (McGraw-Hill, New York 1940)
12. S. G. Davison and M. Stęślicka: *Basic Theory of Surface States* (Clarendon Press, Oxford 1992)
13. Y. Zhang: private communications
14. Y. L. Xuan and P. W. Zhang: private communications
15. Y. Hatsugai: Phys. Rev. **B48**, 11851 (1993)
16. W. A. Harrison: Bull. Am. Phys. Soc. **47**, 367 (2002)

5 Electronic States in Ideal Quantum Films

Starting from this chapter, we extend our investigations in Part II to three-dimensional crystals. The major difference between the problems treated in this part and in Part II is that the corresponding Schrödinger equation for the electronic states in a three-dimensional crystal is a *partial* differential equation; therefore, now the problem is a more difficult one. This is due to the fact that relative to the solutions of ordinary differential equations, the properties of solutions of partial differential equations are much less understood mathematically [e.g.,1], not to mention solutions of partial differential equations with periodic coefficients [2]. The variety and complexity of the three-dimensional crystal structures and of the shapes of three-dimensional finite crystals further make the cases more variational and more complicated. Nevertheless, based on the results of extensions of a mathematical theorem in [3], we show that in many simple but interesting cases, the properties of electronic states in ideal low-dimensional systems and finite crystals can be understood, how the energies of these electronic states depend on the size and/or the shape of the system can be predicted, and the energies of many electronic states can be directly obtained from the energy band structure of the bulk. Again, the major obstacle due to the lack of translational invariance can be circumvented.[1]

The electronic states in a quantum film can be considered as the quantum confinement of three-dimensional Bloch waves in one specific direction. This is the simplest case of the quantum confinement of three-dimensional Bloch waves. Our purpose in this chapter is to try to understand the similarities and the differences between the effects of the quantum confinement of three-dimensional Bloch waves in one specific direction and the quantum confinement of one-dimensional Bloch waves treated in Chapter 4.

This chapter is organized as follows: In Section 5.1, we present a basic theorem that corresponds to Theorem 2.8 in the one-dimensional case and is the basis of the theory in this chapter. In Section 5.2, we briefly discuss some consequences of the theorem. In Sections 5.3–5.6, we obtain the electronic states in several ideal quantum films of different Bravais lattices based on this theorem, by considering the quantum confinement of three-dimensional Bloch waves in one direction. In Section 5.7, we compare our theory to pre-

[1] Part of the results in this chapter was published in [4].

viously published numerical results. In Section 5.8, we present some further discussions.

5.1 A Basic Theorem

The single-electron Schrödinger equation for a three-dimensional crystal can be written as

$$-\nabla^2 y(\boldsymbol{x}) + [v(\boldsymbol{x}) - \lambda]y(\boldsymbol{x}) = 0, \tag{5.1}$$

where $v(\boldsymbol{x})$ is a periodic potential:

$$v(\boldsymbol{x} + \boldsymbol{a}_1) = v(\boldsymbol{x} + \boldsymbol{a}_2) = v(\boldsymbol{x} + \boldsymbol{a}_3) = v(\boldsymbol{x}).$$

$\boldsymbol{a}_1$, $\boldsymbol{a}_2$, and $\boldsymbol{a}_3$ are three primitive lattice vectors of the crystal. The corresponding primitive lattice vectors in $\boldsymbol{k}$ space are denoted as $\boldsymbol{b}_1$, $\boldsymbol{b}_2$, and $\boldsymbol{b}_3$ and $\boldsymbol{a}_i \cdot \boldsymbol{b}_j = \delta_{i,j}$; here, $\delta_{i,j}$ is the Kronecker symbol. The position vector $\boldsymbol{x}$ can be written as $\boldsymbol{x} = x_1\boldsymbol{a}_1 + x_2\boldsymbol{a}_2 + x_3\boldsymbol{a}_3$ and the $\boldsymbol{k}$ vector as $\boldsymbol{k} = k_1\boldsymbol{b}_1 + k_2\boldsymbol{b}_2 + k_3\boldsymbol{b}_3$.

The eigenfunctions of (5.1) satisfying the condition

$$\phi(\boldsymbol{k}, \boldsymbol{x} + \boldsymbol{a}_i) = \mathrm{e}^{\mathrm{i}k_i}\phi(\boldsymbol{k}, \boldsymbol{x}), \quad -\pi < k_i \leq \pi, \quad i = 1, 2, 3, \tag{5.2}$$

are three-dimensional Bloch functions. As solutions of (5.1), the three-dimensional Bloch functions and the energy bands in this book are denoted as $\phi_n(\boldsymbol{k}, \boldsymbol{x})$ and $\varepsilon_n(\boldsymbol{k})$: $\varepsilon_0(\boldsymbol{k}) \leq \varepsilon_1(\boldsymbol{k}) \leq \varepsilon_2(\boldsymbol{k}) \leq \cdots$. The energy band structure in the Cartesian system is denoted as $\varepsilon_n(k_x, k_y, k_z)$.

For the quantum films investigated in this chapter, we choose the primitive vectors $\boldsymbol{a}_1$ and $\boldsymbol{a}_2$ in the film plane and use $\hat{\boldsymbol{k}}$ to express a wave vector in the film plane: $\hat{\boldsymbol{k}} = k_1\hat{\boldsymbol{b}}_1 + k_2\hat{\boldsymbol{b}}_2$. $\hat{\boldsymbol{b}}_1$ and $\hat{\boldsymbol{b}}_2$ are in the film plane and $\boldsymbol{a}_i \cdot \hat{\boldsymbol{b}}_j = \delta_{i,j}$ for $i, j = 1, 2$.

The major mathematical basis for understanding the electronic states in one-dimensional finite crystals is Theorem 2.8. Correspondingly, the mathematical basis for understanding the quantum confinement of three-dimensional Bloch waves in a specific direction $\boldsymbol{a}_3$ is the following eigenvalue problem (5.3) – which corresponds to the problem defined by (2.71) in the one-dimensional case – and a relevant theorem.

Suppose A is a parallelogram that has $\boldsymbol{a}_i$ forming the sides that meet at a corner and has the bottom face defined by $x_3 = \tau_3$ and thus the top face defined by $x_3 = (\tau_3 + 1)$ (See Fig. 5.1.).[2] The function set $\hat{\phi}(\hat{\boldsymbol{k}}, \boldsymbol{x}; \tau_3)$ is defined by the condition

[2]For a free-standing film with a boundary at $x_3 = \tau_3$, in general we have neither a reason to require that τ_3 to be a constant nor a reasonable way to assign $\tau_3(x_1, x_2)$ beforehand. However, since what we are interested in is mainly the quantum confinement effects, in this book it is assumed that the existence of the boundary τ_3 does not change the two-dimensional space group symmetry of the system, including but not limited to that $\tau_3 = \tau_3(x_1, x_2)$ must be a periodic function of x_1 and x_2: $\tau_3 = \tau_3(x_1, x_2) = \tau_3(x_1 + 1, x_2) = \tau_3(x_1, x_2 + 1)$.

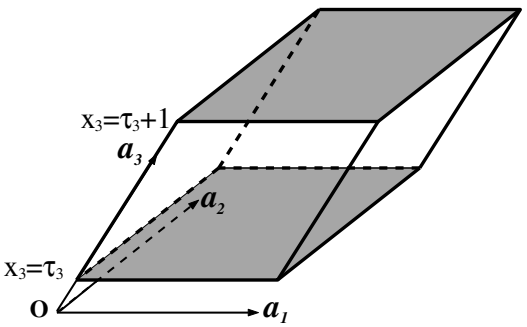

Fig. 5.1. The parallelogram A for the eigenvalue problem of (5.1) under the boundary condition (5.3). The two shadowed faces of ∂A_3 are defined by $x_3 = \tau_3$ and $x_3 = (\tau_3 + 1)$ and are the two faces on which the function $\hat{\phi}(\hat{\boldsymbol{k}}, \boldsymbol{x}; \tau_3)$ is zero.

$$\begin{aligned} \hat{\phi}(\hat{\boldsymbol{k}}, \boldsymbol{x} + \boldsymbol{a}_i; \tau_3) &= \mathrm{e}^{\mathrm{i}k_i}\hat{\phi}(\hat{\boldsymbol{k}}, \boldsymbol{x}; \tau_3), \quad -\pi < k_i \leq \pi, \quad i = 1, 2, \\ \hat{\phi}(\hat{\boldsymbol{k}}, \boldsymbol{x}; \tau_3) &= 0, \qquad\qquad\qquad\quad \text{if } \boldsymbol{x} \in \partial A_3, \end{aligned} \tag{5.3}$$

where ∂A_i means two opposite faces of the boundary ∂A of A determined by the beginning and the end of $\boldsymbol{a}_i$. The eigenvalues and eigenfunctions of (5.1) under the boundary condition (5.3) are denoted by $\hat{\lambda}_n(\hat{\boldsymbol{k}}; \tau_3)$ and $\hat{\phi}_n(\hat{\boldsymbol{k}}, \boldsymbol{x}; \tau_3)$ respectively, where $\hat{\boldsymbol{k}}$ is a wave vector in the film plane and $n = 0, 1, 2.....$

For the eigenvalues of (5.1) in two different eigenvalue problems defined by (5.2) or (5.3), the following theorem exists:

Theorem 5.1.

$$\hat{\lambda}_n(\hat{\boldsymbol{k}}; \tau_3) \geq \varepsilon_n(\boldsymbol{k}) \qquad \text{for } (\boldsymbol{k} - \hat{\boldsymbol{k}}) \cdot \boldsymbol{a}_i = 0, \quad i = 1, 2. \tag{5.4}$$

In (5.3) and (5.4), $\boldsymbol{k}$ is a three-dimensional wave vector defined in the whole Brillouin zone and $\hat{\boldsymbol{k}}$ is in the film plane. In (5.4), $\boldsymbol{k}$ and $\hat{\boldsymbol{k}}$ have the same components in the film plane.

Theorem 5.1 can be considered as an extension of Theorem 6.3.1 in [3] and the proof is similar, with some differences.

Proof. We choose $\phi_n(\boldsymbol{k}, \boldsymbol{x})$ to be normalized over A:
$\int_A \phi_n(\boldsymbol{k}; \boldsymbol{x})\phi_n^*(\boldsymbol{k}; \boldsymbol{x})\, \mathrm{d}\boldsymbol{x} = 1$.

We denote $\mathcal{F}$ as the set of all complex-valued functions $f(\boldsymbol{x})$ that are continuous in A and have piecewise continuous first-order partial derivatives in A. The Dirichlet integral $J(f, g)$ in three dimensions is defined by

$$J(f, g) = \int_A \{\nabla f(\boldsymbol{x}) \cdot \nabla g^*(\boldsymbol{x}) + v(\boldsymbol{x}) f(\boldsymbol{x}) g^*(\boldsymbol{x})\}\, \mathrm{d}\boldsymbol{x} \tag{5.5}$$

for $f(\boldsymbol{x})$ and $g(\boldsymbol{x})$ in $\mathcal{F}$. If in (5.5) $g(\boldsymbol{x})$ also has piecewise continuous second-order partial derivatives in A, from the Green's theorem we have

$$J(f,g)=\int_A f(\boldsymbol{x})\{-\nabla^2 g^*(\boldsymbol{x})+v(\boldsymbol{x})g^*(\boldsymbol{x})\}\,\mathrm{d}\boldsymbol{x}+\int_{\partial A} f\frac{\partial g^*}{\partial n}\,\mathrm{d}S, \tag{5.6}$$

where ∂A denotes the boundary of A, $\partial/\partial n$ denotes derivative along the outward normal to ∂A, and dS denotes an element of surface area of ∂A.

If $f(\boldsymbol{x})$ and $g(\boldsymbol{x})$ satisfy the conditions (5.2), the integral over ∂A in (5.6) is zero because the integrals over opposite faces of ∂A cancel out. In particular, when $g(\boldsymbol{x})=\phi_n(\boldsymbol{k},\boldsymbol{x})$, (5.6) gives

$$J(f,g)=\varepsilon_n(\boldsymbol{k})\int_A f(\boldsymbol{x})\phi_n^*(\boldsymbol{k},\boldsymbol{x})\,\mathrm{d}\boldsymbol{x}.$$

Thus, $J[\phi_m(\boldsymbol{k},\boldsymbol{x}),\phi_n(\boldsymbol{k},\boldsymbol{x})]=\varepsilon_n(\boldsymbol{k})$ if $m=n$, and $J[\phi_m(\boldsymbol{k},\boldsymbol{x}),\phi_n(\boldsymbol{k},\boldsymbol{x})]=0$ if $m\neq n$.

Now, we consider the function set $\hat{\phi}(\hat{\boldsymbol{k}},\boldsymbol{x};\tau_3)$, which satisfy the boundary conditions (5.3). We also choose $\hat{\phi}(\hat{\boldsymbol{k}},\boldsymbol{x};\tau_3)$ to be normalized over A:

$\int_A \hat{\phi}(\hat{\boldsymbol{k}},\boldsymbol{x};\tau_3)\hat{\phi}^*(\hat{\boldsymbol{k}},\boldsymbol{x};\tau_3)\,\mathrm{d}\boldsymbol{x}=1$.

Note that if $f(\boldsymbol{x})=\hat{\phi}(\hat{\boldsymbol{k}},\boldsymbol{x};\tau_3)$ and $g(\boldsymbol{x})=\phi_n(\boldsymbol{k},\boldsymbol{x})$, the integral over ∂A in (5.6) is also zero because the integral over two opposite faces of ∂A_1 and ∂A_2 cancel out since $(\boldsymbol{k}-\hat{\boldsymbol{k}})\cdot\boldsymbol{a}_i=0$ for $i=1,\ 2$ and the integral over each face of ∂A_3 is zero since $f(\boldsymbol{x})=0$ when $\boldsymbol{x}\in\partial A_3$.

Thus,

$$J[\hat{\phi}(\hat{\boldsymbol{k}},\boldsymbol{x};\tau_3),\phi_n(\boldsymbol{k},\boldsymbol{x})]=\varepsilon_n(\boldsymbol{k})f_n(\boldsymbol{k}),$$

where

$$f_n(\boldsymbol{k})=\int_A \hat{\phi}(\hat{\boldsymbol{k}},\boldsymbol{x};\tau_3)\phi_n^*(\boldsymbol{k},\boldsymbol{x})\,\mathrm{d}\boldsymbol{x},$$

and

$$\sum_{n=0}^{\infty}|f_n(\boldsymbol{k})|^2=1$$

by the Parseval formula [3,5]. An important property of the function $\hat{\phi}(\hat{\boldsymbol{k}},\boldsymbol{x};\tau_3)$ defined by (5.3) is

$$J[\hat{\phi}(\hat{\boldsymbol{k}},\boldsymbol{x};\tau_3),\hat{\phi}(\hat{\boldsymbol{k}},\boldsymbol{x};\tau_3)]\geq\sum_{n=0}^{\infty}\varepsilon_n(\boldsymbol{k})|f_n(\boldsymbol{k})|^2. \tag{5.7}$$

To prove (5.7), we assume $v(\boldsymbol{x})\geq 0$ first. Then $J(f,f)\geq 0$ from (5.5) for any f in $\mathcal{F}$. Thus, for any positive integer N, we have

$$J[\hat{\phi}(\hat{\boldsymbol{k}},\boldsymbol{x};\tau_3)-\sum_{n=0}^{N}f_n(\boldsymbol{k})\phi_n(\boldsymbol{k},\boldsymbol{x}),\hat{\phi}(\hat{\boldsymbol{k}},\boldsymbol{x};\tau_3)-\sum_{n=0}^{N}f_n(\boldsymbol{k})\phi_n(\boldsymbol{k},\boldsymbol{x})]\geq 0;$$

that is,

$$J[\hat{\phi}(\hat{\boldsymbol{k}},\boldsymbol{x};\tau_3),\hat{\phi}(\hat{\boldsymbol{k}},\boldsymbol{x};\tau_3)]\geq\sum_{n=0}^{N}\varepsilon_n(\boldsymbol{k})|f_n(\boldsymbol{k})|^2.$$

N can be as large as needed, therefore,

$$J[\hat{\phi}(\hat{\boldsymbol{k}}, \boldsymbol{x}; \tau_3), \hat{\phi}(\hat{\boldsymbol{k}}, \boldsymbol{x}; \tau_3)] \geq \sum_{n=0}^{\infty} \varepsilon_n(\boldsymbol{k}) |f_n(\boldsymbol{k})|^2 \quad \text{if } v(\boldsymbol{x}) \geq 0. \tag{5.8}$$

To prove (5.7) without the assumption that $v(\boldsymbol{x}) \geq 0$, let v_0 be a constant that is sufficiently large to make $v(\boldsymbol{x}) + v_0 \geq 0$ in A. Then (5.1) can be rewritten as

$$-\nabla^2 y(\boldsymbol{x}) + [V(\boldsymbol{x}) - \Lambda] y(\boldsymbol{x}) = 0, \tag{5.9}$$

where $V(\boldsymbol{x}) = v(\boldsymbol{x}) + v_0$ and $\Lambda = \lambda + v_0$. Since in (5.9), $V(\boldsymbol{x}) \geq 0$ in A, due to (5.8) we have

$$\int_A \{\nabla \hat{\phi}(\hat{\boldsymbol{k}}, \boldsymbol{x}; \tau_3) \cdot \nabla \hat{\phi}^*(\hat{\boldsymbol{k}}, \boldsymbol{x}; \tau_3) + [v(\boldsymbol{x}) + v_0] \hat{\phi}(\hat{\boldsymbol{k}}, \boldsymbol{x}; \tau_3) \hat{\phi}^*(\hat{\boldsymbol{k}}, \boldsymbol{x}; \tau_3)\} \, \mathrm{d}\boldsymbol{x}$$
$$\geq \sum_{n=0}^{\infty} [\varepsilon_n(\boldsymbol{k}) + v_0] |f_n(\boldsymbol{k})|^2;$$

that is,

$$\int_A [\nabla \hat{\phi}(\hat{\boldsymbol{k}}, \boldsymbol{x}; \tau_3) \cdot \nabla \hat{\phi}^*(\hat{\boldsymbol{k}}, \boldsymbol{x}; \tau_3) + v(\boldsymbol{x}) \hat{\phi}(\hat{\boldsymbol{k}}, \boldsymbol{x}; \tau_3) \hat{\phi}^*(\hat{\boldsymbol{k}}, \boldsymbol{x}; \tau_3)] \, \mathrm{d}\boldsymbol{x}$$
$$\geq \sum_{n=0}^{\infty} \varepsilon_n(\boldsymbol{k}) |f_n(\boldsymbol{k})|^2.$$

This is (5.7). On the basis of (5.7) we can prove (5.4).

We consider

$$\hat{\phi}(\hat{\boldsymbol{k}}, \boldsymbol{x}; \tau_3) = c_0 \hat{\phi}_0(\hat{\boldsymbol{k}}, \boldsymbol{x}; \tau_3) + c_1 \hat{\phi}_1(\hat{\boldsymbol{k}}, \boldsymbol{x}; \tau_3) + \cdots + c_n \hat{\phi}_n(\hat{\boldsymbol{k}}, \boldsymbol{x}; \tau_3)$$

and choose $n+1$ constants c_i to make

$$\sum_{i=0}^{n} |c_i|^2 = 1$$

and

$$f_i(\boldsymbol{k}) = \int_A \hat{\phi}(\hat{\boldsymbol{k}}, \boldsymbol{x}; \tau_3) \phi_i^*(\boldsymbol{k}, \boldsymbol{x}) \, \mathrm{d}\boldsymbol{x} = 0, \quad i = 0, 1, ..., n-1. \tag{5.10}$$

Equation (5.10) corresponds to n homogeneous algebraic equations for $n+1$ constants $c_0, c_1, ..., c_n$. A choice of such c_i's is always possible. Therefore,

$$\hat{\lambda}_n(\hat{\boldsymbol{k}}; \tau_3) \geq \sum_{i=0}^{n} |c_i|^2 \hat{\lambda}_i(\hat{\boldsymbol{k}}; \tau_3) = J[\hat{\phi}(\hat{\boldsymbol{k}}, \boldsymbol{x}; \tau_3), \hat{\phi}(\hat{\boldsymbol{k}}, \boldsymbol{x}; \tau_3)]$$
$$\geq \sum_{i=0}^{\infty} |f_i(\boldsymbol{k})|^2 \varepsilon_i(\boldsymbol{k}) = \sum_{i=n}^{\infty} |f_i(\boldsymbol{k})|^2 \varepsilon_i(\boldsymbol{k}) \geq \varepsilon_n(\boldsymbol{k}) \sum_{i=n}^{\infty} |f_i(\boldsymbol{k})|^2 = \varepsilon_n(\boldsymbol{k}).$$

This is (5.4). □

5.2 Consequences of the Theorem

Theorem 5.1 indicates that for each bulk energy band n and each $\hat{\boldsymbol{k}}$, for any specific τ_3 there is always one and only one $\hat{\lambda}_n(\hat{\boldsymbol{k}};\tau_3)$ and thus one $\hat{\phi}_n(\hat{\boldsymbol{k}},\boldsymbol{x};\tau_3)$.

Theorem 5.1 gives a relationship between two sets of eigenvalues $\varepsilon_n(\boldsymbol{k})$ and $\hat{\lambda}_n(\hat{\boldsymbol{k}};\tau_3)$. Actually, many consequences concerning the relationship between two sets of eigenfunctions $\phi_n(\boldsymbol{k},\boldsymbol{x})$ and $\hat{\phi}_n(\hat{\boldsymbol{k}},\boldsymbol{x};\tau_3)$ can be obtained from this theorem.

Theorem 5.1 gives a lower limit of $\hat{\lambda}_n(\hat{\boldsymbol{k}};\tau_3)$. As a direct consequence of this, only the *single* Bloch function $\phi_n(\boldsymbol{k},\boldsymbol{x})$ that corresponds to the energy maximum of $\varepsilon_n(\boldsymbol{k})$ for that $\hat{\boldsymbol{k}}$ *may have the possibility of being* $\hat{\phi}_n(\hat{\boldsymbol{k}},\boldsymbol{x};\tau_3)$ to make the equality in (5.4) to be true. If the equality in (5.4) is true, such a Bloch function $\phi_n(\boldsymbol{k},\boldsymbol{x})$ has a nodal surface (the surface on which the Bloch function is zero) at $x_3=\tau_3$.

Theorem 5.1 does not give an upper limit of $\hat{\lambda}_n(\hat{\boldsymbol{k}};\tau_3)$; the possibility that a Bloch function $\phi_{n'}(\boldsymbol{k},\boldsymbol{x})$ has a nodal surface at $x_3=\tau_3$ and thus be a $\hat{\phi}_n(\hat{\boldsymbol{k}},\boldsymbol{x};\tau_3)$ (in which $n<n'$) cannot be excluded; even $\varepsilon_{n'}(\boldsymbol{k})$ is not the energy maximum for that $\hat{\boldsymbol{k}}$.

In this chapter, we are mainly interested in the quantum films of crystals with a band structure $\varepsilon_n(\hat{\boldsymbol{k}}+k_3\boldsymbol{b}_3)=\varepsilon_n(\hat{\boldsymbol{k}}-k_3\boldsymbol{b}_3)$. In a case where $\hat{\phi}_n(\hat{\boldsymbol{k}},\boldsymbol{x};\tau_3)$ is a Bloch function $\phi_{n'}(\boldsymbol{k},\boldsymbol{x})$ in which $n\le n'$, the corresponding wave vector $\boldsymbol{k}$ must be either $\boldsymbol{k}=\hat{\boldsymbol{k}}$ or $\boldsymbol{k}=\hat{\boldsymbol{k}}+\pi\boldsymbol{b}_3$.[3] Therefore, only a Bloch function $\phi_{n'}(\boldsymbol{k},\boldsymbol{x})$ with such a wave vector $\boldsymbol{k}$ might have a nodal surface at $x_3=\tau_3$.[4] In particular, in the cases where $\hat{\boldsymbol{k}}=0$, only a Bloch function $\phi_{n'}(\boldsymbol{k}=0,\boldsymbol{x})$ or $\phi_{n'}(\boldsymbol{k}=\pi\boldsymbol{b}_3,\boldsymbol{x})$ might have a nodal surface at $x_3=\tau_3$.

These points can find similarities in the one-dimensional case.

However, even for a wave vector $\boldsymbol{k}=\hat{\boldsymbol{k}}$ or $\boldsymbol{k}=\hat{\boldsymbol{k}}+\pi\boldsymbol{b}_3$ and the corresponding $\varepsilon_n(\boldsymbol{k})$ is the energy maximum for that $\hat{\boldsymbol{k}}$; the corresponding Bloch function $\phi_n(\boldsymbol{k},\boldsymbol{x})$ might or might not have a nodal surface,[5] not to mention a specific nodal surface at $x_3=\tau_3$. Only when the specific $\varepsilon_n(\boldsymbol{k})$ is the energy maximum for that $\hat{\boldsymbol{k}}$ *and* the corresponding Bloch function $\phi_n(\boldsymbol{k},\boldsymbol{x})$ does have a nodal surface at $x_3=\tau_3$, can the equality in Theorem 5.1 be true and the Bloch function $\phi_n(\boldsymbol{k},\boldsymbol{x})$ be $\hat{\phi}_n(\hat{\boldsymbol{k}},\boldsymbol{x};\tau_3)$ for that specific τ_3.

Theorem 5.1 is not as strong as Theorem 2.8: No upper limit of $\hat{\lambda}_n(\hat{\boldsymbol{k}};\tau_3)$ is given except $\hat{\lambda}_n(\hat{\boldsymbol{k}};\tau_3)\le\hat{\lambda}_{n+1}(\hat{\boldsymbol{k}};\tau_3)$. It is this point that leads to a significant

---

[3] In such a case, $\hat{\lambda}_n(\hat{\boldsymbol{k}};\tau_3)=\varepsilon_{n'}(\hat{\boldsymbol{k}}+k_3\boldsymbol{b}_3)=\varepsilon_{n'}(\hat{\boldsymbol{k}}-k_3\boldsymbol{b}_3)$ is true. Only when either $k_3=0$ or $k_3=\pi$ is $\phi_{n'}(\hat{\boldsymbol{k}}\pm k_3\boldsymbol{b}_3,\boldsymbol{x})$ one single function and $\varepsilon_{n'}(\hat{\boldsymbol{k}}\pm k_3\boldsymbol{b}_3)$ one single eigenvalue.

[4] Note that we commented on the zeros of one-dimensional Bloch function $\phi_n(k,x)$ on p. 46, as a consequence of Theorem 2.8.

[5] In the one-dimensional case, it is Theorem 2.7 that warrants that a band-edge Bloch function at $k=0$ or $k=\frac{\pi}{a}$ always has zeros.

difference between the surface-like states in one-dimensional finite crystals and in ideal quantum films.[6]

More on these points and on the consequences of Theorem 5.1 will be seen later in this chapter. Essentially, it is the consequences of Theorem 5.1 that leads to the similarities and differences of the quantum confinement of three-dimensional Bloch waves in one specific direction in comparison with the results obtained in Chapter 4.

Since $v(\boldsymbol{x}+\boldsymbol{a}_3)=v(\boldsymbol{x})$, the function $\hat{\phi}_n(\hat{\boldsymbol{k}},\boldsymbol{x};\tau_3)$ has the form

$$\hat{\phi}_n(\hat{\boldsymbol{k}},\boldsymbol{x}+\boldsymbol{a}_3;\tau_3)=\mathrm{e}^{\mathrm{i}k_3}\hat{\phi}_n(\hat{\boldsymbol{k}},\boldsymbol{x};\tau_3). \tag{5.11}$$

Depending on n, $\hat{\boldsymbol{k}}$, and τ_3, k_3 in (5.11) can be complex or real. If in (5.11) k_3 is real, then $\hat{\phi}_n(\hat{\boldsymbol{k}},\boldsymbol{x};\tau_3)$ is a Bloch function. There exist such cases, but probably in more cases, $\hat{\phi}_n(\hat{\boldsymbol{k}},\boldsymbol{x};\tau_3)$ is not a Bloch function: Even though a specific Bloch function $\phi_{n'}(\boldsymbol{k},\boldsymbol{x})$ could have a nodal surface at a specific $x_3=\tau_3$ and thus is a $\hat{\phi}_n(\hat{\boldsymbol{k}},\boldsymbol{x};\tau_3)$, it seems unlikely that other Bloch functions with a different n' and/or $\hat{\boldsymbol{k}}$ will have a same nodal surface (see later in this chapter). Especially in our theory, τ_3 is treated as a general variable and k_3 in (5.11) can be real only in such special cases where $\hat{\phi}_n(\hat{\boldsymbol{k}},\boldsymbol{x};\tau_3)$ is a Bloch function for a specific τ_3; in most cases, k_3 is complex with a nonzero imaginary part.

Depending on n, $\hat{\boldsymbol{k}}$, and τ_3, the imaginary part of k_3 in (5.11) can be either positive or negative, corresponding to whether $\hat{\phi}_n(\hat{\boldsymbol{k}},\boldsymbol{x};\tau_3)$ decays in either the positive or the negative direction of $\boldsymbol{a}_3$. Such states $\hat{\phi}_n(\hat{\boldsymbol{k}},\boldsymbol{x};\tau_3)$ with a nonzero imaginary part of k_3 cannot exist in a bulk crystal with three-dimensional translational invariance since they are divergent in either the negative or the positive direction of $\boldsymbol{a}_3$. However, they can play a significant role in a quantum film of finite thickness.

5.3 Basic Considerations on the Electronic States in an Ideal Quantum Film

For the electronic states in an ideal low-dimensional system such as in an ideal quantum film, wire, dot, or finite crystal treated in this part, we assume that (i) the potential $v(\boldsymbol{x})$ *inside* the low-dimensional system is the same as in (5.1) and (ii) the electronic states are completely confined in the system.

The electronic states $\hat{\psi}(\hat{\boldsymbol{k}},\boldsymbol{x})$ in an ideal quantum film with N_3 layers in the $\boldsymbol{a}_3$ direction are solutions of the following two equations:

[6] Mathematically, it is the upper and lower limits in Theorem 2.8 that limits the energy range of any surface-like state in a one-dimensional finite crystal always in a band gap. This is further related to the fact that in a one-dimensional crystal, each permitted energy band and each band gap always exist alternatively as the energy increases.

$$-\nabla^2\hat{\psi}(\hat{\boldsymbol{k}},\boldsymbol{x})+[v(\boldsymbol{x})-\hat{\Lambda}]\hat{\psi}(\hat{\boldsymbol{k}},\boldsymbol{x})=0 \quad \text{if } \tau_3<x_3<\tau_3+N_3 \tag{5.12}$$

and

$$\hat{\psi}(\hat{\boldsymbol{k}},\boldsymbol{x})=0 \quad \text{if } x_3\le\tau_3 \ \text{ or } \ x_3\ge\tau_3+N_3, \tag{5.13}$$

where $x_3=\tau_3$ defines the bottom of the film and N_3 is a positive integer indicating the film thickness.[7] These electronic states $\hat{\psi}(\hat{\boldsymbol{k}},\boldsymbol{x})$ are two-dimensional Bloch waves in the film plane, with additional index(es) indicating the confinement in the $\boldsymbol{a}_3$ direction.

In the following, we try to find solutions of (5.12) and (5.13) in some simple cases. The main purpose is to understand the basic physics of the electronic states in low-dimensional systems in simple examples, rather than to explore more possibly treatable quantum films.

5.4 Stationary Bloch States

We can expect that one type of solutions of (5.12) and (5.13) should be linear combinations of three-dimensional Bloch functions: In the film, they are stationary Bloch states, formed due to multiple reflections of the Bloch waves $\phi_n(\boldsymbol{k},\boldsymbol{x})$ at the two boundary surfaces of the film, whereas they are two-dimensional Bloch waves in the film plane.

5.4.1 The Simplest Cases

The simplest cases are films of the crystals with a band structure having the following symmetry:

$$\varepsilon_n(k_1\boldsymbol{b}_1+k_2\boldsymbol{b}_2+k_3\boldsymbol{b}_3)=\varepsilon_n(k_1\boldsymbol{b}_1+k_2\boldsymbol{b}_2-k_3\boldsymbol{b}_3). \tag{5.14}$$

If (5.14) is true, we can expect that the stationary Bloch states in such a quantum film can be obtained from the linear combinations of $\phi_n(k_1\boldsymbol{b}_1+k_2\boldsymbol{b}_2+k_3\boldsymbol{b}_3,\boldsymbol{x})$ and $\phi_n(k_1\boldsymbol{b}_1+k_2\boldsymbol{b}_2-k_3\boldsymbol{b}_3,\boldsymbol{x})$, since, in general,

$$\begin{aligned} f_{n,k_1,k_2,k_3}(\boldsymbol{x}) &= c_+\phi_n(k_1\boldsymbol{b}_1+k_2\boldsymbol{b}_2+k_3\boldsymbol{b}_3,\boldsymbol{x}) \\ &\quad + c_-\phi_n(k_1\boldsymbol{b}_1+k_2\boldsymbol{b}_2-k_3\boldsymbol{b}_3,\boldsymbol{x}), \quad 0<k_3<\pi \end{aligned}$$

– where $c_\pm$ are nonzero constant coefficients – is a nontrivial solution of (5.1) due to (5.14). To be a solution of (5.12) and (5.13), the function $f_{n,k_1,k_2,k_3}(\boldsymbol{x};\tau_3)$ is required to be zero at the bottom of the film $x_3=\tau_3$ and at the top of the film $x_3=\tau_3+N_3$. By writing $\boldsymbol{x}=\hat{\boldsymbol{x}}+x_3\boldsymbol{a}_3$, where $\hat{\boldsymbol{x}}=x_1\boldsymbol{a}_1+x_2\boldsymbol{a}_2$, we should have

[7] In this book, such a film is usually called a film with N_3 layers in the $\boldsymbol{a}_3$ direction, despite the fact that the film may actually have more atomic layers.

$$\begin{aligned} &c_+\phi_n(k_1\boldsymbol{b}_1 + k_2\boldsymbol{b}_2 + k_3\boldsymbol{b}_3, \hat{\boldsymbol{x}} + \tau_3\boldsymbol{a}_3) \\ &\qquad + c_-\phi_n(k_1\boldsymbol{b}_1 + k_2\boldsymbol{b}_2 - k_3\boldsymbol{b}_3, \hat{\boldsymbol{x}} + \tau_3\boldsymbol{a}_3) = 0, \\ &c_+\phi_n[k_1\boldsymbol{b}_1 + k_2\boldsymbol{b}_2 + k_3\boldsymbol{b}_3, \hat{\boldsymbol{x}} + (\tau_3 + N_3)\boldsymbol{a}_3] \\ &\qquad + c_-\phi_n[k_1\boldsymbol{b}_1 + k_2\boldsymbol{b}_2 - k_3\boldsymbol{b}_3, \hat{\boldsymbol{x}} + (\tau_3 + N_3)\boldsymbol{a}_3] = 0. \end{aligned} \tag{5.15}$$

However, we have

$$\begin{aligned} &\phi_n[k_1\boldsymbol{b}_1 + k_2\boldsymbol{b}_2 + k_3\boldsymbol{b}_3, \hat{\boldsymbol{x}} + (\tau_3 + N_3)\boldsymbol{a}_3] \\ &\qquad = \mathrm{e}^{\mathrm{i}k_3N_3}\phi_n(k_1\boldsymbol{b}_1 + k_2\boldsymbol{b}_2 + k_3\boldsymbol{b}_3, \hat{\boldsymbol{x}} + \tau_3\boldsymbol{a}_3) \end{aligned}$$

and

$$\begin{aligned} &\phi_n[k_1\boldsymbol{b}_1 + k_2\boldsymbol{b}_2 - k_3\boldsymbol{b}_3, \hat{\boldsymbol{x}} + (\tau_3 + N_3)\boldsymbol{a}_3] \\ &\qquad = \mathrm{e}^{-\mathrm{i}k_3N_3}\phi_n(k_1\boldsymbol{b}_1 + k_2\boldsymbol{b}_2 - k_3\boldsymbol{b}_3, \hat{\boldsymbol{x}} + \tau_3\boldsymbol{a}_3). \end{aligned}$$

Therefore, for $c_\pm$ in (5.15) not both zero, $\mathrm{e}^{\mathrm{i}k_3N_3} - \mathrm{e}^{-\mathrm{i}k_3N_3} = 0$ has to be true for these stationary Bloch states, independent of τ_3.

Each stationary Bloch state solution of (5.12) and (5.13) has the form

$$\begin{aligned} \hat{\psi}_{n,j_3}(\hat{\boldsymbol{k}}, \boldsymbol{x}; \tau_3) &= f_{n,k_1,k_2,\kappa_3}(\boldsymbol{x}; \tau_3) \quad \text{if } \tau_3 < x_3 < \tau_3 + N_3 \\ &= 0 \qquad\qquad\qquad\quad \text{if } x_3 \le \tau_3 \text{ or } x_3 \ge \tau_3 + N_3, \end{aligned} \tag{5.16}$$

where

$$\begin{aligned} f_{n,k_1,k_2,k_3}(\boldsymbol{x}; \tau_3) &= c_{n,k_1,k_2,k_3;\tau_3}\phi_n(k_1\boldsymbol{b}_1 + k_2\boldsymbol{b}_2 + k_3\boldsymbol{b}_3, \boldsymbol{x}) \\ &\quad + c_{n,k_1,k_2,-k_3;\tau_3}\phi_n(k_1\boldsymbol{b}_1 + k_2\boldsymbol{b}_2 - k_3\boldsymbol{b}_3, \boldsymbol{x}), \end{aligned} \tag{5.17}$$

$c_{n,k_1,k_2,\pm k_3;\tau_3}$ depend on τ_3, $\hat{\boldsymbol{k}} = k_1\hat{\boldsymbol{b}}_1 + k_2\hat{\boldsymbol{b}}_2$, and

$$\kappa_3 = j_3\pi/N_3, \quad j_3 = 1, 2, ..., N_3 - 1, \tag{5.18}$$

independent of τ_3. Here, j_3 is a subband index. It is easy to see that $f_{n,k_1,k_2,k_3}(\boldsymbol{x}; \tau_3)$ defined in (5.17) is a two-dimensional Bloch wave with a wave vector $\hat{\boldsymbol{k}} = k_1\hat{\boldsymbol{b}}_1 + k_2\hat{\boldsymbol{b}}_2$ in the film plane:

$$f_{n,k_1,k_2,k_3}(\boldsymbol{x} + \boldsymbol{a}_i; \tau_3) = \mathrm{e}^{\mathrm{i}k_i}f_{n,k_1,k_2,k_3}(\boldsymbol{x}; \tau_3), \quad -\pi < k_i \le \pi, \ i = 1, 2. \tag{5.19}$$

The stationary Bloch state $\hat{\psi}_{n,j_3}(\hat{\boldsymbol{k}}, \boldsymbol{x}; \tau_3)$ has the energy

$$\hat{\Lambda}_{n,j_3}(\hat{\boldsymbol{k}}) = \varepsilon_n(k_1\boldsymbol{b}_1 + k_2\boldsymbol{b}_2 + \kappa_3\boldsymbol{b}_3). \tag{5.20}$$

Each energy $\hat{\Lambda}_{n,j_3}(\hat{\boldsymbol{k}})$ is a function of N_3, the film thickness.

The (001) quantum films of crystals with a simple cubic (sc), a tetragonal (tetr), or an orthorhombic (ortho) Bravais lattice have $\hat{\boldsymbol{b}}_1 = \boldsymbol{b}_1$ and $\hat{\boldsymbol{b}}_2 = \boldsymbol{b}_2$. Such quantum films with a bulk band structure having the symmetry (5.14) are the simplest cases to which the theory in this section can be applied. There are $N_3 - 1$ stationary Bloch state solutions $\hat{\psi}_{n,j_3}(\hat{\boldsymbol{k}}, \boldsymbol{x}; \tau_3)$ for each n and each $\hat{\boldsymbol{k}}$ in such a film of N_3 layers. They are two-dimensional Bloch waves with a wave vector $\hat{\boldsymbol{k}}$ in the film plane. Their energies $\hat{\Lambda}_{n,j_3}(\hat{\boldsymbol{k}})$ depend on the film thickness N_3 but not on the film boundary τ_3 and map the bulk energy band structure $\varepsilon_n(\boldsymbol{k})$ exactly. These states can be considered as bulk-like states in the quantum film.

5.4.2 More General Cases

For many crystals, in general (5.14) is not true; the arguments in 5.4.1 are not valid for general films. Nevertheless, it can be shown that if the band structure of a bulk crystal has the symmetry

$$\varepsilon_n(k_1\hat{\boldsymbol{b}}_1 + k_2\hat{\boldsymbol{b}}_2 + k_3\boldsymbol{b}_3) = \varepsilon_n(k_1\hat{\boldsymbol{b}}_1 + k_2\hat{\boldsymbol{b}}_2 - k_3\boldsymbol{b}_3) \tag{5.21}$$

in a film of N_3 layers, there are $N_3 - 1$ stationary Bloch states for each n and each $\hat{\boldsymbol{k}} = k_1\hat{\boldsymbol{b}}_1 + k_2\hat{\boldsymbol{b}}_2$, similar to the cases in Section 5.4.1. The energies of these stationary Bloch states can be similarly obtained.

We can write that $\hat{\boldsymbol{b}}_i = \boldsymbol{b}_i + \alpha_i\boldsymbol{b}_3$ $(i = 1, 2)$; thus,

$$k_1\hat{\boldsymbol{b}}_1 + k_2\hat{\boldsymbol{b}}_2 + k_3\boldsymbol{b}_3 = k_1\boldsymbol{b}_1 + k_2\boldsymbol{b}_2 + (\alpha_1k_1 + \alpha_2k_2 + k_3)\boldsymbol{b}_3.$$

Actually, there are many different ways to choose the primitive lattice vectors. For example, we can choose a new primitive lattice vector system as $\boldsymbol{a}'_1 = \boldsymbol{a}_1$, $\boldsymbol{a}'_2 = \boldsymbol{a}_2$, and $\boldsymbol{a}'_3 = m_1\boldsymbol{a}_1 + m_2\boldsymbol{a}_2 + \boldsymbol{a}_3$, where m_1 and m_2 are two integers. The new primitive lattice vectors in $\boldsymbol{k}$ space are $\boldsymbol{b}'_1 = \boldsymbol{b}_1 - m_1\boldsymbol{b}_3$, $\boldsymbol{b}'_2 = \boldsymbol{b}_2 - m_2\boldsymbol{b}_3$, and $\boldsymbol{b}'_3 = \boldsymbol{b}_3$. In describing a quantum film, the primitive lattice vector systems given by $\boldsymbol{a}_i$ and $\boldsymbol{a}'_i$ are essentially equivalent. A position vector $\boldsymbol{x}$ can be expressed as either $\boldsymbol{x} = x_1\boldsymbol{a}_1 + x_2\boldsymbol{a}_2 + x_3\boldsymbol{a}_3$ or $\boldsymbol{x} = x'_1\boldsymbol{a}'_1 + x'_2\boldsymbol{a}'_2 + x'_3\boldsymbol{a}'_3$, and $x_1 = x'_1 + m_1x'_3$, $x_2 = x'_2 + m_2x'_3$, and $x_3 = x'_3$. Correspondingly, a wave vector $\boldsymbol{k}$ can be expressed as either $\boldsymbol{k} = k_1\boldsymbol{b}_1 + k_2\boldsymbol{b}_2 + k_3\boldsymbol{b}_3$ or $\boldsymbol{k} = k'_1\boldsymbol{b}'_1 + k'_2\boldsymbol{b}'_2 + k'_3\boldsymbol{b}'_3$, and $k_1 = k'_1$, $k_2 = k'_2$, and $k_3 = -m_1k'_1 - m_2k'_2 + k'_3$. Thus,

$$\begin{aligned} k_1\hat{\boldsymbol{b}}_1 + k_2\hat{\boldsymbol{b}}_2 + k_3\boldsymbol{b}_3 = {} & k_1\boldsymbol{b}'_1 + k_2\boldsymbol{b}'_2 \\ & + [(m_1k_1 + \alpha_1k_1 + m_2k_2 + \alpha_2k_2) + k_3]\boldsymbol{b}'_3. \end{aligned}$$

If for a pair k_1, k_2, we can find two integers m_1 and m_2 to make

$$(m_1 + \alpha_1)k_1 + (m_2 + \alpha_2)k_2 = 0; \tag{5.22}$$

then for such a pair k_1, k_2, in the primitive lattice vector system specified by $\boldsymbol{a}'_3 = m_1\boldsymbol{a}_1 + m_2\boldsymbol{a}_2 + \boldsymbol{a}_3$, (5.21) and (5.22) lead to

$$\varepsilon_n(k_1\boldsymbol{b}'_1 + k_2\boldsymbol{b}'_2 + k_3\boldsymbol{b}'_3) = \varepsilon_n(k_1\boldsymbol{b}'_1 + k_2\boldsymbol{b}'_2 - k_3\boldsymbol{b}'_3).$$

By comparison with (5.14), we can see that in the primitive lattice vector system specifyied by $\boldsymbol{a}'_i$, the theory in Section 5.4.1 can be applied for such a pair k_1, k_2:

$$\begin{aligned} f_{n,k_1,k_2,k_3}(\boldsymbol{x}) = {} & c_+\ \phi_n(k_1\boldsymbol{b}'_1 + k_2\boldsymbol{b}'_2 + k_3\boldsymbol{b}'_3, \boldsymbol{x}) \\ & + c_-\ \phi_n(k_1\boldsymbol{b}'_1 + k_2\boldsymbol{b}'_2 - k_3\boldsymbol{b}'_3, \boldsymbol{x}), \quad 0 < k_3 < \pi, \end{aligned} \tag{5.23}$$

can be used to construct stationary Bloch states between the $x'_3 = \tau_3$ surface and the $x'_3 = \tau_3 + N_3$ surface, that is, between the $x_3 = \tau_3$ surface and the $x_3 = \tau_3 + N_3$ surface, since $x_3 = x'_3$.

It is easy to see that $f_{n,k_1,k_2,k_3}(\boldsymbol{x})$ defined in (5.23) is a two-dimensional Bloch wave with a wave vector $\hat{\boldsymbol{k}} = k_1\hat{\boldsymbol{b}}_1 + k_2\hat{\boldsymbol{b}}_2$ in the film plane:

$$\begin{aligned} f_{n,k_1,k_2,k_3}(\boldsymbol{x}+\boldsymbol{a}_i) &= f_{n,k_1,k_2,k_3}(\boldsymbol{x}+\boldsymbol{a}'_i) \\ &= \mathrm{e}^{\mathrm{i}k_i} f_{n,k_1,k_2,k_3}(\boldsymbol{x}), \quad -\pi < k_i \le \pi, \quad i = 1,2. \end{aligned}$$

Since

$$\phi_n(k_1\boldsymbol{b}'_1 + k_2\boldsymbol{b}'_2 + k_3\boldsymbol{b}'_3, \boldsymbol{x}+\boldsymbol{a}'_3) = \mathrm{e}^{\mathrm{i}k_3}\phi_n(k_1\boldsymbol{b}'_1 + k_2\boldsymbol{b}'_2 + k_3\boldsymbol{b}'_3, \boldsymbol{x})$$

and

$$\phi_n(k_1\boldsymbol{b}'_1 + k_2\boldsymbol{b}'_2 - k_3\boldsymbol{b}'_3, \boldsymbol{x}+\boldsymbol{a}'_3) = \mathrm{e}^{-\mathrm{i}k_3}\phi_n(k_1\boldsymbol{b}'_1 + k_2\boldsymbol{b}'_2 - k_3\boldsymbol{b}'_3, \boldsymbol{x}),$$

the stationary Bloch states $\hat{\psi}_{n,j_3}(\hat{\boldsymbol{k}}, \boldsymbol{x}; \tau_3)$ should have the form

$$\begin{aligned} \hat{\psi}_{n,j_3}(\hat{\boldsymbol{k}}, \boldsymbol{x}; \tau_3) &= f_{n,k_1,k_2,\kappa_3}(\boldsymbol{x}; \tau_3) \quad \text{if } \tau_3 < x'_3 < \tau_3 + N_3 \\ &= 0 \qquad\qquad\qquad\quad \text{if } x'_3 \le \tau_3 \text{ or } x'_3 \ge \tau_3 + N_3, \end{aligned} \tag{5.24}$$

where

$$\begin{aligned} f_{n,k_1,k_2,k_3}(\boldsymbol{x}; \tau_3) &= c_{n,k_1,k_2,k_3;\tau_3}\phi_n(k_1\boldsymbol{b}'_1 + k_2\boldsymbol{b}'_2 + k_3\boldsymbol{b}'_3, \boldsymbol{x}) \\ &\quad + c_{n,k_1,k_2,-k_3;\tau_3}\phi_n(k_1\boldsymbol{b}'_1 + k_2\boldsymbol{b}'_2 - k_3\boldsymbol{b}'_3, \boldsymbol{x}), \end{aligned} \tag{5.25}$$

$c_{n,k_1,k_2,\pm k_3;\tau_3}$ depend on τ_3, and

$$\kappa_3 = j_3\pi/N_3, \quad j_3 = 1, 2, ..., N_3 - 1,$$

as in (5.18). This is the results of Section 5.4.1 applied to such a pair k_1, k_2. The expressions (5.24) and (5.25) of the stationary Bloch states are based on the specific primitive lattice vectors system $\boldsymbol{a}'_i$. However, we have

$$\begin{aligned} \phi_n(k_1\boldsymbol{b}'_1 + k_2\boldsymbol{b}'_2 + k_3\boldsymbol{b}'_3, \boldsymbol{x}) &= \phi_n[k_1(\boldsymbol{b}_1 - m_1\boldsymbol{b}_3) + k_2(\boldsymbol{b}_2 - m_2\boldsymbol{b}_3) + k_3\boldsymbol{b}_3, \boldsymbol{x}] \\ &= \phi_n\{k_1[\hat{\boldsymbol{b}}_1 - (\alpha_1 + m_1)\boldsymbol{b}_3] \\ &\qquad + k_2[\hat{\boldsymbol{b}}_2 - (\alpha_2 + m_2)\boldsymbol{b}_3] + k_3\boldsymbol{b}_3, \boldsymbol{x}\} \\ &= \phi_n(k_1\hat{\boldsymbol{b}}_1 + k_2\hat{\boldsymbol{b}}_2 + k_3\boldsymbol{b}_3, \boldsymbol{x}) \end{aligned} \tag{5.26}$$

due to (5.22), and, similarly,

$$\phi_n(k_1\boldsymbol{b}'_1 + k_2\boldsymbol{b}'_2 - k_3\boldsymbol{b}'_3, \boldsymbol{x}) = \phi_n(k_1\hat{\boldsymbol{b}}_1 + k_2\hat{\boldsymbol{b}}_2 - k_3\boldsymbol{b}_3, \boldsymbol{x}). \tag{5.27}$$

By using (5.26) and (5.27), (5.24) and (5.25) can be rewritten as

$$\begin{aligned} \hat{\psi}_{n,j_3}(\hat{\boldsymbol{k}}, \boldsymbol{x}; \tau_3) &= f_{n,k_1,k_2,\kappa_3}(\boldsymbol{x}; \tau_3) \quad \text{if } \tau_3 < x_3 < \tau_3 + N_3 \\ &= 0 \qquad\qquad\qquad\quad \text{if } x_3 \le \tau_3 \text{ or } x_3 \ge \tau_3 + N_3, \end{aligned} \tag{5.28}$$

where

$$f_{n,k_1,k_2,k_3}(\boldsymbol{x};\tau_3) = c_{n,k_1,k_2,k_3;\tau_3}\phi_n(k_1\hat{\boldsymbol{b}}_1 + k_2\hat{\boldsymbol{b}}_2 + k_3\boldsymbol{b}_3, \boldsymbol{x}) + c_{n,k_1,k_2,-k_3;\tau_3}\phi_n(k_1\hat{\boldsymbol{b}}_1 + k_2\hat{\boldsymbol{b}}_2 - k_3\boldsymbol{b}_3, \boldsymbol{x}), \tag{5.29}$$

$c_{n,k_1,k_2,\pm k_3;\tau_3}$ depend on τ_3, and

$$\kappa_3 = j_3\pi/N_3, \quad j_3 = 1, 2, ..., N_3 - 1, \tag{5.30}$$

as in (5.18). Equations (5.28)–(5.30) do not depend on m_1 or m_2 thus are not based on the specific $\boldsymbol{a}_i'$ any more: the states in the film are made of $\phi_n(\hat{\mathbf{k}} \pm \kappa_3\boldsymbol{b}_3)$.

Therefore, for a quantum film for which (5.21) is true, for *any* pair of k_1, k_2 for which two integers m_1 and m_2 can be found to make (5.22) true, there are $N_3 - 1$ solutions of (5.12) and (5.13) in a film of N_3 layers for each bulk energy band n. Each solution $\hat{\psi}_{n,j_3}(\hat{\boldsymbol{k}}, \boldsymbol{x}; \tau_3)$ in (5.28)–(5.30) is a stationary Bloch state in the normal direction $\boldsymbol{b}_3$ of the film, whereas it is a two-dimensional Bloch wave with a wave vector $\hat{\boldsymbol{k}} = k_1\hat{\boldsymbol{b}}_1 + k_2\hat{\boldsymbol{b}}_2$ in the film plane:

$$\hat{\psi}_{n,j_3}(\hat{\boldsymbol{k}}, \boldsymbol{x} + \boldsymbol{a}_i; \tau_3) = \mathrm{e}^{\mathrm{i}k_i}\hat{\psi}_{n,j_3}(\hat{\boldsymbol{k}}, \boldsymbol{x}; \tau_3), \quad -\pi < k_i \le \pi, \quad i = 1, 2 \tag{5.31}$$

due to (5.29). The corresponding energy for each such state is

$$\hat{\Lambda}_{n,j_3}(\hat{\boldsymbol{k}}) = \varepsilon_n(\hat{\boldsymbol{k}} + \kappa_3\boldsymbol{b}_3). \tag{5.32}$$

There are many pairs (k_1, k_2) for which the condition (5.22) cannot be true. Nevertheless, in a small circle centered in any specific pair (k_1, k_2) in the k_1, k_2 plane, there are always an infinite number of pairs ($k_{1,c}$, $k_{2,c}$), which can be as close to (k_1, k_2) as needed: For each pair ($k_{1,c}$, $k_{2,c}$), two integers m_1 and m_2 can be found to make $(m_1 + \alpha_1)k_{1,c} + (m_2 + \alpha_2)k_{2,c} = 0$. Thus, (5.28)–(5.32) will be true for each such pair ($k_{1,c}$, $k_{2,c}$). Since both $\hat{\psi}_{n,j_3}(\hat{\boldsymbol{k}}, \boldsymbol{x}; \tau_3)$ and $\phi_n(k_1\hat{\boldsymbol{b}}_1 + k_2\hat{\boldsymbol{b}}_2 \pm \kappa_3\boldsymbol{b}_3, \boldsymbol{x})$ (both $\hat{\Lambda}_{n,j_3}(\hat{\boldsymbol{k}})$ and $\varepsilon_n(\hat{\boldsymbol{k}} + \kappa_3\boldsymbol{b}_3)$ too) are continuous functions of k_1 and k_2, (5.28)–(5.32) must be true for any k_1 and k_2.

For example, for a pair $(k_1, k_2) = (\pi/\sqrt{2}, 0)$, (5.22) could not be true. If $\alpha_1 = \alpha_2 = 1/2$, for a pair $(k_{1,c}, k_{2,c}) = (2.221, 0.001)$ close to (k_1, k_2), one can find $m_1 = -1$ and $m_2 = 1110$ to make $(m_1 + \alpha_1)k_{1,c} + (m_2 + \alpha_2)k_{2,c} = 0$. For a pair $(k_{1,c}, k_{2,c}) = (2.221441, 0.000001)$ closer to (k_1, k_2), one can find $m_1 = -1$ and $m_2 = 1110720$ to make $(m_1 + \alpha_1)k_{1,c} + (m_2 + \alpha_2)k_{2,c} = 0$.

For another pair $(k_1, k_2) = (\pi/3, -\sqrt{7})$, (5.22) could not be true either. If $\alpha_1 = \alpha_2 = 1/2$, for a pair $(k_{1,c}, k_{2,c}) = (1.047, -2.645)$ close to (k_1, k_2), one can find $m_1 = 1322$ and $m_2 = 523$ to make $(m_1 + \alpha_1)k_{1,c} + (m_2 + \alpha_2)k_{2,c} = 0$. For a pair $(k_{1,c}, k_{2,c}) = (1.047197, -2.645751)$ closer to (k_1, k_2), one can find $m_1 = 1322875$ and $m_2 = 523598$ to make $(m_1 + \alpha_1)k_{1,c} + (m_2 + \alpha_2)k_{2,c} = 0$.

A (001) quantum film of a crystal with a sc, tetr, or ortho Bravais lattice and with a bulk band structure (5.14) can also be considered as a special

simple case of the more general cases discussed in this subsection. For such a film $\alpha_1 = \alpha_2 = 0$ and $m_1 = m_2 = 0$ for any k_1 and k_2.

Equation (5.28)–(5.32) are similar to that there are $N-1$ bulk-like states in each band in a one-dimensional finite crystal of length $L = Na$, as indicated by (4.7). The electronic states $\hat{\psi}_{n,j_3}(\hat{\boldsymbol{k}}, \boldsymbol{x}; \tau_3)$ in (5.28)–(5.30) can be considered as bulk-like electronic states in the quantum film and each $\hat{\Lambda}_{n,j_3}(\hat{\boldsymbol{k}})$ can be considered as a bulk-like subband: $\hat{\Lambda}_{n,j_3}(\hat{\boldsymbol{k}})$ maps the bulk energy band $\varepsilon_n(\boldsymbol{k})$ exactly by (5.32) and depends on the film thickness N_3, but not on the film boundary τ_3.

5.5 τ_3-Dependent States

It is expected that for each n and each $\hat{\boldsymbol{k}}$, there are N_3 electronic states for an ideal quantum film of N_3 layers. For films in which (5.21) is true, $N_3 - 1$ states were obtained in (5.28)–(5.30); the other type of nontrivial solutions of (5.12) and (5.13) can be obtained from (5.11) by assigning

$$\begin{aligned} \hat{\psi}_n(\hat{\boldsymbol{k}}, \boldsymbol{x}; \tau_3) &= c_{N_3} \hat{\phi}_n(\hat{\boldsymbol{k}}, \boldsymbol{x}; \tau_3) \quad \text{if } \tau_3 < x_3 < \tau_3 + N_3 \\ &= 0 \qquad\qquad\qquad\quad \text{if } x_3 \le \tau_3 \text{ or } x_3 \ge \tau_3 + N_3, \end{aligned} \tag{5.33}$$

where c_{N_3} is a normalization constant. Correspondingly, the energy of such a state is given by

$$\hat{\Lambda}_n(\hat{\boldsymbol{k}}; \tau_3) = \hat{\lambda}_n(\hat{\boldsymbol{k}}; \tau_3). \tag{5.34}$$

There is one solution (5.33) of (5.12) and (5.13) for each energy band n and each $\hat{\boldsymbol{k}}$. Each $\hat{\psi}_n(\hat{\boldsymbol{k}}, \boldsymbol{x}; \tau_3)$ defined in (5.33) is an electronic state in the film whose energy $\hat{\Lambda}_n(\hat{\boldsymbol{k}}; \tau_3)$ (5.34) depends on the film boundary τ_3 but not on the film thickness N_3. By Theorem 5.1, $\hat{\Lambda}_n(\hat{\boldsymbol{k}}; \tau_3)$ is either above or, occasionally, at the energy maximum of $\varepsilon_n(\boldsymbol{k})$ with that n and that $\hat{\boldsymbol{k}}$.

In the special cases where $\hat{\phi}_n(\hat{\boldsymbol{k}}, \boldsymbol{x}; \tau_3)$ in (5.33) is a Bloch function,

$$\hat{\phi}_n(\hat{\boldsymbol{k}}, \boldsymbol{x}; \tau_3) = \phi_{n'}(\boldsymbol{k}, \boldsymbol{x}), \quad n \le n', \tag{5.35}$$

the corresponding Bloch function $\phi_{n'}(\boldsymbol{k}, \boldsymbol{x})$ has a nodal surface at $x_3 = \tau_3$ and thus has nodal surfaces at $x_3 = \tau_3 + \ell$, where $\ell = 1, 2, ..., N_3$. As we pointed out in Section 5.2, the wave vector has to be either $\boldsymbol{k} = \hat{\boldsymbol{k}}$ or $\boldsymbol{k} = \hat{\boldsymbol{k}} + \pi \boldsymbol{b}_3$. If $n = n'$, $\varepsilon_n(\boldsymbol{k})$ has to be the energy maximum for that n and that $\hat{\boldsymbol{k}}$.

In most cases, $\hat{\phi}_n(\hat{\boldsymbol{k}}, \boldsymbol{x}; \tau_3)$ in (5.33) is not a Bloch function. Consequently, in these cases there is a nonzero imaginary part of k_3 in (5.11), indicating that $\hat{\psi}_n(\hat{\boldsymbol{k}}, \boldsymbol{x}; \tau_3)$ now is a surface state located near either the top or the bottom of the film. Correspondingly, the energy of such a state

$$\hat{\Lambda}_n(\hat{\boldsymbol{k}}; \tau_3) > \varepsilon_n(\boldsymbol{k}) \quad \text{for } (\boldsymbol{k} - \hat{\boldsymbol{k}}) \cdot \boldsymbol{a}_i = 0, \quad i = 1, 2, \tag{5.36}$$

is true by Theorem 5.1. However, there is no reason to expect that $\hat{\Lambda}_n(\hat{\boldsymbol{k}};\tau_3)$ has to be in a band gap, as Theorem 2.8 requires of $\Lambda_{\tau,n}$ in the one-dimensional case.

Each $\hat{\psi}_n(\hat{\boldsymbol{k}},\boldsymbol{x};\tau_3)$ can be considered as a surface-like state in the film, in differentiation with the bulk-like states $\hat{\psi}_{n,j_3}(\hat{\boldsymbol{k}},\boldsymbol{x};\tau_3)$. Therefore, for an ideal quantum film bounded at $x_3=\tau_3$ and $x_3=(\tau_3+N_3)$ in which (5.21) is true, for each bulk energy band n there are N_3-1 bulk-like subbands $\hat{\Lambda}_{n,j_3}(\hat{\boldsymbol{k}})$ in (5.32) and one surface-like subband $\hat{\Lambda}_n(\hat{\boldsymbol{k}};\tau_3)$ in (5.34) in the quantum film.

Because of (5.4), (5.32), and (5.34), in the ideal quantum film discussed here, for each bulk energy band n the corresponding surface-like subband $\hat{\Lambda}_n(\hat{\boldsymbol{k}};\tau_3)$ is *always above* the bulk-like subbands $\hat{\Lambda}_{n,j_3}(\hat{\boldsymbol{k}})$:[8]

$$\hat{\Lambda}_n(\hat{\boldsymbol{k}};\tau_3) > \hat{\Lambda}_{n,j_3}(\hat{\boldsymbol{k}}). \tag{5.37}$$

The electronic states in each subband are two-dimensional Bloch waves in the film plane.

These results should be correct for (001) films of crystals with a sc, a tetr, or an ortho Bravais lattice for which (5.14) is true. More generally, they should also be correct for films of crystals for which (5.21) is true. In particular, they should be correct for ideal (001) or (110) quantum films of crystals with a face-centered-cubic (fcc) or a body-centered-cubic (bcc) Bravais lattice for which (5.21) is true.

5.6 Several Practically More Interesting Films

All cubic semiconductors and many metals have a fcc Bravais lattice. All alkali metals (Li, Na, K, Rb, Cs, Fr) and many other metals have a bcc Bravais lattice. Therefore, the quantum films of crystals with a fcc Bravais lattice or a bcc Bravais lattice often are practically more interesting.

5.6.1 (001) Films with a fcc Bravais Lattice

For the fcc (001) films, the primitive lattice vectors can be chosen as

$$\boldsymbol{a}_1=a/2(1,-1,0),\quad \boldsymbol{a}_2=a/2(1,1,0),\quad \boldsymbol{a}_3=a/2(1,0,1); \tag{5.38}$$

thus, $\boldsymbol{b}_1=1/a(1,-1,-1)$, $\boldsymbol{b}_2=1/a(1,1,-1)$, and $\boldsymbol{b}_3=1/a(0,0,2)$. Correspondingly, $\hat{\boldsymbol{b}}_1=1/a(1,-1,0)$ and $\hat{\boldsymbol{b}}_2=1/a(1,1,0)$. Here, a is the lattice constant. This corresponds to $\alpha_1=\alpha_2=1/2$ in Section 5.4.2.

In general, the band structure of a cubic semiconductor or a fcc metal has the symmetry

[8] $\hat{\Lambda}_{n,j_3}(\hat{\boldsymbol{k}})$ can never be equal to $\hat{\Lambda}_n(\hat{\boldsymbol{k}};\tau_3)$: $\hat{\boldsymbol{k}}+\kappa_3\boldsymbol{b}_3$ is neither $\hat{\boldsymbol{k}}$ nor $\hat{\boldsymbol{k}}+\pi\boldsymbol{b}_3$. The equality in (5.4) can be excluded in (5.37).

$$\varepsilon_n(k_x, k_y, k_z) = \varepsilon_n(k_x, k_y, -k_z);$$

thus, for such a (001) film, (5.21) is true. Therefore, the results in Sections 5.4.2 and 5.5 can be applied to these films: For a film of N_3 layers, there are $N_3 - 1$ bulk-like subbands and one surface-like subband in the film for each bulk energy band. Equation (5.32) for (001) films can be written as

$$\hat{\Lambda}_{n,j_3}(\hat{\boldsymbol{k}}) = \varepsilon_n \left[k_1 \hat{\boldsymbol{b}}_1 + k_2 \hat{\boldsymbol{b}}_2 + \frac{j_3 \pi}{N_3 a}(0, 0, 2) \right] \tag{5.39}$$

for any $\hat{\boldsymbol{k}} = k_1 \hat{\boldsymbol{b}}_1 + k_2 \hat{\boldsymbol{b}}_2$, where $j_3 = 1, 2, ..., N_3 - 1$, given by (5.30).

Now, τ_3 can be written as τ_{001}. By (5.37), each surface-like subband $\hat{\Lambda}_n(\hat{\boldsymbol{k}}; \tau_{001})$ is always above each relevant bulk-like subband $\hat{\Lambda}_{n,j_3}(\hat{\boldsymbol{k}})$. If a $\hat{\psi}_n(\hat{\boldsymbol{k}} = 0, \boldsymbol{x}; \tau_{001})$ inside the film is a Bloch function $\phi_n(\boldsymbol{k}, \boldsymbol{x})$, either $\boldsymbol{k} = 0$ or $\boldsymbol{k} = \frac{2\pi}{a}(0, 0, 1)$ must be true and the corresponding energy is the energy maximum of $\varepsilon_n(0, 0, \frac{2k_3}{a})$. It is assumed that the existence of boundary faces of the film does not change the two-dimensional space group symmetry of the system (Footnote 2 on page 90). For each surface-like subband $\hat{\Lambda}_n(\hat{\boldsymbol{k}}; \tau_{001})$, it is expected that $\hat{\Lambda}_n(k_1 \hat{\boldsymbol{b}}_1 + k_2 \hat{\boldsymbol{b}}_2; \tau_{001}) = \hat{\Lambda}_n(k_1 \hat{\boldsymbol{b}}_1 - k_2 \hat{\boldsymbol{b}}_2; \tau_{001})$ is true.

A "new" way of choosing the primitive lattice vectors is

$$\boldsymbol{a}_1 = a/2(1, -1, 0), \quad \boldsymbol{a}_2 = a/2(1, 1, 0), \quad \boldsymbol{a}_3 = a(0, 0, 1), \tag{5.38a}$$

and thus $\boldsymbol{b}_1 = \hat{\boldsymbol{b}}_1 = 1/a(1, -1, 0)$, $\boldsymbol{b}_2 = \hat{\boldsymbol{b}}_2 = 1/a(1, 1, 0)$, and $\boldsymbol{b}_3 = 1/a(0, 0, 1)$.

In this "new" way of choosing the primitive lattice vectors, the "new" Brillouin zone with two boundaries at $(0, 0, \pm 1)\frac{\pi}{a}$ is half of the original Brillouin zone with two boundaries at $(0, 0, \pm 2)\frac{\pi}{a}$ and each original bulk energy band now becomes two "new" energy bands in the "new" Brillouin zone (band-folding). For a (001) film of thickness $N_{001}a$, where N_{001} is a positive integer, according to the "new" description it seems that there should be $(N_{001} - 1)$ bulk-like subbands and one surface-like subband for each "new" energy band and thus $2(N_{001} - 1)$ bulk-like subbands and two surface-like subbands for each original energy band. From the original description, since $N_3 = 2N_{001}$, there are $2N_{001} - 1$ bulk-like subbands and one surface-like subband for each original energy band. This difference (one extra surface-like subband and one less bulk-like subband for each original bulk energy band in the "new" description) comes from the fact that the "new" description (5.38a) is only based on half of the whole symmetry of the film in the [001] direction. Thus, the "extra" surface-like subband in the "new" description actually is a bulk-like subband in the original primitive lattice vector system (5.38) where the full symmetry of the film in the [001] direction is used. We mention this point here since we will meet some relevant situations later.

5.6.2 (110) Films with a fcc Bravais Lattice

For the fcc (110) films, the primitive lattice vectors can be chosen as

$$\boldsymbol{a}_1 = a/2(1,-1,0), \quad \boldsymbol{a}_2 = a(0,0,-1), \quad \boldsymbol{a}_3 = a/2(0,1,1); \tag{5.40}$$

thus, $\boldsymbol{b}_1 = 1/a(2,0,0)$, $\boldsymbol{b}_2 = 1/a(1,1,-1)$, and $\boldsymbol{b}_3 = 1/a(2,2,0)$. Correspondingly, $\hat{\boldsymbol{b}}_1 = 1/a(1,-1,0)$ and $\hat{\boldsymbol{b}}_2 = 1/a(0,0,-1)$. This corresponds to $\alpha_1 = \alpha_2 = -1/2$ in Section 5.4.2.

In general, the band structure of a cubic semiconductor or a fcc metals has the symmetry

$$\varepsilon_n(k_x, k_y, k_z) = \varepsilon_n(k_y, k_x, k_z);$$

thus, for such a (110) film, (5.21) is true. Therefore, the results in Sections 5.4.2 and 5.5 can be applied to these films: For a film of N_3 layers, there are $N_3 - 1$ bulk-like subbands and one surface-like subband in the film for each bulk energy band. Equation (5.32) can also be written as

$$\hat{\Lambda}_{n,j_3}(\hat{\boldsymbol{k}}) = \varepsilon_n \left[k_1\hat{\boldsymbol{b}}_1 + k_2\hat{\boldsymbol{b}}_2 + \frac{j_3\pi}{N_3 a}(2,2,0) \right] \tag{5.41}$$

for any $\hat{\boldsymbol{k}} = k_1\hat{\boldsymbol{b}}_1 + k_2\hat{\boldsymbol{b}}_2$, where $j_3 = 1, 2, ..., N_3 - 1$, given by (5.30).

Now, τ_3 can be written as τ_{110}. Because of (5.37), each surface-like subband $\hat{\Lambda}_n(\hat{\boldsymbol{k}}; \tau_{110})$ is always above each relevant bulk-like subband $\hat{\Lambda}_{n,j_3}(\hat{\boldsymbol{k}})$. If a $\hat{\psi}_n(\hat{\boldsymbol{k}} = 0, \boldsymbol{x}; \tau_{110})$ inside the film is a Bloch function $\phi_n(\boldsymbol{k}, \boldsymbol{x})$, either $\boldsymbol{k} = 0$ or $\boldsymbol{k} = \frac{\pi}{a}(2,2,0)$ must be true and the corresponding energy is the energy maximum of $\varepsilon_n[\frac{k_3}{a}(2,2,0)]$. It is assumed that the existence of boundary faces of the film does not change the two-dimensional space group symmetry of the system (Footnote 2 on page 90). For each surface-like subband $\hat{\Lambda}_n(\hat{\boldsymbol{k}}; \tau_{110})$, it is expected that $\hat{\Lambda}_n(k_1\hat{\boldsymbol{b}}_1 + k_2\hat{\boldsymbol{b}}_2; \tau_{110}) = \hat{\Lambda}_n(k_1\hat{\boldsymbol{b}}_1 - k_2\hat{\boldsymbol{b}}_2; \tau_{110})$ is true.

Similar to Section 5.6.1, there is a "new" way of choosing the primitive lattice vectors as

$$\boldsymbol{a}_1 = a/2(1,-1,0), \quad \boldsymbol{a}_2 = a(0,0,-1), \quad \boldsymbol{a}_3 = a/2(1,1,0) \tag{5.40a}$$

and, thus, $\boldsymbol{b}_1 = \hat{\boldsymbol{b}}_1 = 1/a(1,-1,0)$, $\boldsymbol{b}_2 = \hat{\boldsymbol{b}}_2 = 1/a(0,0,-1)$, and $\boldsymbol{b}_3 = 1/a\ (1,1,0)$.

In this "new" way of choosing the primitive lattice vectors, the "new" Brillouin zone with two boundaries at $\pm(1,1,0)\frac{\pi}{a}$ is half of the original Brillouin zone with two boundaries at $\pm(2,2,0)\frac{\pi}{a}$ and each orginal energy band now becomes two "new" energy bands in the "new" Brillouin zone (band-folding). For a (110) film of thickness $N_{110}\sqrt{2}a/2$, where N_{110} is a positive integer, according to the "new" description, it seems that there should be $(N_{110} - 1)$ bulk-like subbands and one surface-like subband for each "new" energy band and thus $2(N_{110} - 1)$ bulk-like subbands and two surface-like subbands for each original bulk energy band. From the original description since $N_3 = 2N_{110}$ there are $2N_{110} - 1$ bulk-like subbands and one surface-like subband for each original bulk energy band. This difference (one extra surface-like subband and one less bulk-like subband for each original bulk energy band in the "new" description) comes from the fact that the "new"

description (5.40a) is only based on half of the whole symmetry of the film in the [110] direction. Thus, the "extra" surface-like subband in the "new" description actually is a bulk-like subband in the original primitive lattice vector system (5.40), where the full symmetry of the film in the [110] direction is used. We mention this point here since we will meet some relevant situations later.

5.6.3 (001) Films with a bcc Bravais Lattice

For the bcc (001) films, the primitive lattice vectors can be chosen as $\boldsymbol{a}_1 = a(1,0,0)$, $\boldsymbol{a}_2 = a(0,1,0)$, and $\boldsymbol{a}_3 = a/2(1,1,1)$; thus, $\boldsymbol{b}_1 = 1/a(1,0,-1)$, $\boldsymbol{b}_2 = 1/a(0,1,-1)$, and $\boldsymbol{b}_3 = 1/a(0,0,2)$. Correspondingly, $\hat{\boldsymbol{b}}_1 = 1/a(1,0,0)$, $\hat{\boldsymbol{b}}_2 = 1/a(0,1,0)$. This corresponds to $\alpha_1 = \alpha_2 = 1/2$ in Section 5.4.2. In general, the band structure of a bcc metal has the symmetry $\varepsilon_n(k_x,k_y,k_z) = \varepsilon_n(k_x,k_y,-k_z)$; thus, for such (001) films, (5.21) is true. Therefore, the results in Sections 5.4.2 and 5.5 can be applied to these films: For a film of N_3 layers, there are N_3-1 bulk-like subbands and one surface-like subband in the film for each bulk energy band. In the Cartesian system, (5.32) for bcc (001) films can be written as

$$\hat{\Lambda}_{n,j_3}(k_x,k_y) = \varepsilon_n(k_x,k_y,2\kappa_3/a) \tag{5.42}$$

for any k_x and k_y, where κ_3 is given by (5.30).

Because of (5.37), each surface-like subband $\hat{\Lambda}_n(\hat{\boldsymbol{k}};\tau_3)$ is always above each relevant bulk-like subband $\hat{\Lambda}_{n,j_3}(\hat{\boldsymbol{k}})$.

5.6.4 (110) Films with a bcc Bravais Lattice

For the bcc (110) films, the primitive lattice vectors can be chosen as $\boldsymbol{a}_1 = a/2(1,-1,1)$, $\boldsymbol{a}_2 = a/2(1,-1,-1)$, and $\boldsymbol{a}_3 = a/2(1,1,1)$; thus $\boldsymbol{b}_1 = 1/a(0,-1,1)$, $\boldsymbol{b}_2 = 1/a(1,0,-1)$, and $\boldsymbol{b}_3 = 1/a(1,1,0)$. Correspondingly, $\hat{\boldsymbol{b}}_1 = 1/a(1/2,-1/2,1)$ and $\hat{\boldsymbol{b}}_2 = 1/a(1/2,-1/2,-1)$. This corresponds to $\alpha_1 = -\alpha_2 = 1/2$ in Section 5.4.2. In general, the band structure of a bcc metal has the symmetry $\varepsilon_n(k_x,k_y,k_z) = \varepsilon_n(k_y,k_x,k_z)$; thus, for such (110) films, (5.21) is true. Therefore, the results in Sections 5.4.2 and 5.5 can be applied to these films: For a film of N_3 layers, there are N_3-1 bulk-like subbands and one surface-like subband in the film for each bulk energy band. Equation (5.32) can also be written as

$$\hat{\Lambda}_{n,j_3}(k_1\hat{\boldsymbol{b}}_1+k_2\hat{\boldsymbol{b}}_2) = \varepsilon_n[(\kappa_3+k_1/2+k_2/2)/a,(\kappa_3-k_1/2-k_2/2)/a,(k_1-k_2)/a] \tag{5.43}$$

for any k_1 and k_2, where κ_3 is given by (5.30).

Because of (5.37), each surface-like subband $\hat{\Lambda}_n(\hat{\boldsymbol{k}};\tau_3)$ is always above each relevant bulk-like subband $\hat{\Lambda}_{n,j_3}(\hat{\boldsymbol{k}})$.

5.7 Comparisons with Previous Numerical Results

There are some previously published numerical results [6–9] to which our results obtained in this chapter can be compared.

5.7.1 Si (001) Films

Equations (5.32) and (5.39) can be used for Si (001) films. Zhang and Zunger [6] and Zhang et al. [7] calculated the electronic structure of thin Si (001) films using a pseudopotential method. Their results for even numbers N_f of monolayers can be directly compared with (5.39): The N_3 in (5.39) is equal to their $N_f/2$. Their "central observation" in [6] is that the energy spectrum of electronic states in a Si (001) quantum film ($N_f = 12$) maps the energy band structure of Si approximately, as shown in Fig. 1.6 and Fig. 5.2. Equation (9) in [6], which Zhang and Zunger obtained from their numerical results, is a special case of (5.39) with $k_1 = k_2 = 0$. Therefore, (5.39) is a more general prediction.

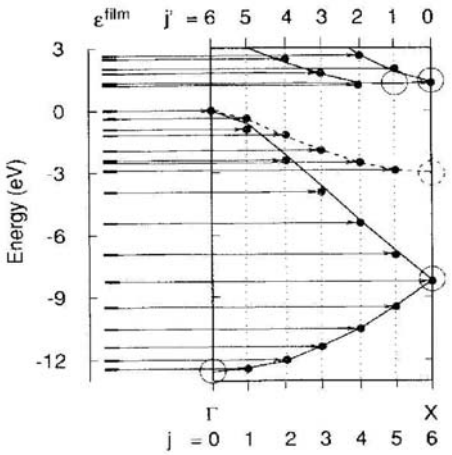

Fig. 5.2. Mapping of the directly calculated film energy levels in Si (001) film of 12 monolayers at the center of the two-dimensional Brillouin zone by Zhang et al. (solid dots) onto the energy bands of the bulk Si. A solid (dashed) open circle indicates that one (two) state(s) does not exist in the film. Reprinted with permission from S. B. Zhang, C-Y Yeh, and A. Zunger: Phys. Rev. **B48**, 11204 (1993). Copyright by the American Physical Society.

One of the triply-degenerated VBM states and one of the doubly-degenerated X_{1v} states in the valence bands may have a (001) nodal surface; thus, for these Bloch states, (5.35) can be true. This can be observed in the results in [6, 7] for Si (001) films such as in Fig. 1.5, Fig. 1.6, and Fig. 5.2. Note that

these Bloch states (X_{1v} or VBM) have the highest energy for that energy band ($n = 0$ or $n = 1$) and that $\hat{\boldsymbol{k}} = 0$, corresponding to that, (5.35) is true for these two cases: $n = n' = 0$ for one of doubly-degenerated states X_{1v}, and $n = n' = 1$ for one of triply-degenerated states VBM.

Although the VBM in Si (Γ'_{25}) is triply-degenerated, only one of the triply-degenerated VBM states may have a nodal surface in (001) plane to make (5.35) true; thus, there is only one VBM band edge state in (001) films whose energy does not depend on the film thickness, as observed in [6,7] and shown in those figures.

Each one of the other two VBM states has the highest energy for that energy band ($n = 2$ or $n = 3$) and that $\hat{\boldsymbol{k}} = 0$ and each has a nodal surface, but not in the (001) plane. Consequently, $\hat{\Lambda}_{n=2,3}(\hat{\boldsymbol{k}} = 0; \tau_3) > \varepsilon_n(k_3\boldsymbol{b}_3)$ ((5.36) for $\hat{\boldsymbol{k}} = 0$) is true for any k_3; thus, there must be two occupied surface-like states in the (001) films whose energies $\hat{\Lambda}_{n=2,3}(\hat{\boldsymbol{k}} = 0; \tau_3)$ are *above* the VBM and do not depend on the film thickness. This is the reason that two occupied surface bands were observed in a Si quantum (001) film, such as a Si (001) film of 12 monolayers (corresponding $N_3 = 6$ in our notations) investigated in [6,7].[9] Therefore, the VBM state shown in Fig. 1.5, Fig. 1.6, or Fig. 5.2 is an occupied VBM state but actually is *not* the highest occupied state in the quantum films.

Although our theory is a theory for ideal quantum films and the numerical calculations in [6,7] used a more realistic potential outside the film, those rather good agreements indicate that the simplified model we used may have given correctly the most essential physics of the electronic states in quantum films.

An interesting tight-binding calculation on Si (001) films by Gavrilenko and Koch [8] found that there are three different groups of electronic states in the films: (i) bulk-related states whose energies depend strongly on the thickness of the film; (ii) surface-like states whose energies do not strongly depend on the film thickness; (iii) electronic states whose energies do not strongly depend on the film thickness and whose wave functions are not localized near the boundary faces of the film. This is also consistent with the results obtained in this chapter: The energies $\hat{\Lambda}_{n,j_3}(\hat{\boldsymbol{k}})$ of bulk-like states depend on the film thickness N_3, whereas the energies $\hat{\Lambda}_n(\hat{\boldsymbol{k}}; \tau_3)$ of surface-like states do not depend on the film thickness N_3. The corresponding wave functions $\hat{\psi}_n(\hat{\boldsymbol{k}}, \boldsymbol{x}; \tau_3)$ of the surface-like states may be either localized near one boundary surface of the film (the imaginary part of k_3 in (5.11) is not zero) or delocalized (the imaginary part of k_3 in (5.11) is zero).

[9] Therefore, the existence of two occupied surface bands above the VBM are due to the fact that (5.36) is true for two valence bands, rather than due to the fact that the film has two surfaces.

5.7.2 Si (110) Films and GaAs (110) Films

In cases where $k_1 = k_2 = 0$, (5.41) gives

$$\hat{\Lambda}_{n,j_3}(0) = \varepsilon_n \left(\frac{2j_3\pi}{N_3 a}, \frac{2j_3\pi}{N_3 a}, 0 \right).$$

This is what was observed in the numerical calculations on a Si (110) film in [6] and on a six-layer Si (110) film and a six-layer GaAs (110) film in [7], as shown in Fig. 5.3. Again, (5.41) is a more general prediction for fcc (110) films.

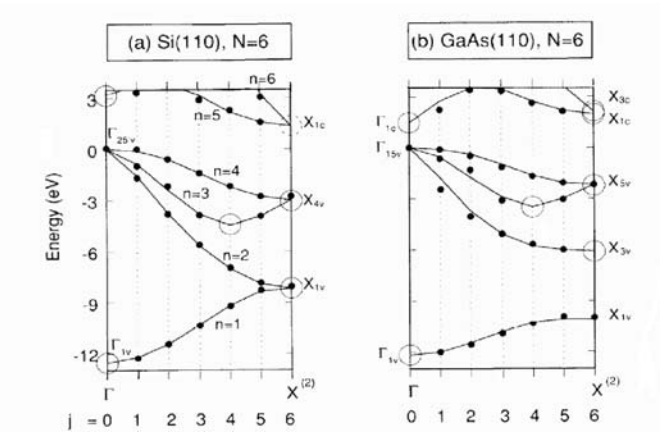

Fig. 5.3. Mapping of the directly calculated film energy levels in [7] (solid dots) at the center of the two-dimensional Brillouin zone on to the energy bands of the bulk for (a) six-layer Si (110) film and (b) a six-layer GaAs film. The legends are the same as in Fig. 5.2. Reprinted with permission from S. B. Zhang, C-Y Yeh, and A. Zunger: Phys. Rev. **B48**, 11204 (1993). Copyright by the American Physical Society.

One of the triply-degenerated VBM states (Γ'_{25} or Γ_{15}) in Si or GaAs may have a nodal surface in the (110) plane; therefore, there may be one VBM state in free-standing Si (110) or GaAs (110) films whose energy does not depend on the film thickness, as observed in [7] and [9].

Each one of the other two VBM states does have a nodal surface, but not in the (110) plane. Correspondingly, $\hat{\Lambda}_{n=2,3}(\hat{\boldsymbol{k}} = 0; \tau_3) > \varepsilon_n(k_3 \boldsymbol{b}_3)$ ((5.36) for $\hat{\boldsymbol{k}} = 0$) is true for any k_3; thus, there are also two occupied surface-like states in the (110) films whose energies $\hat{\Lambda}_n(\hat{\boldsymbol{k}} = 0; \tau_3)$ are above the VBM and do not depend on the film thickness. Therefore, the VBM states shown in Fig. 5.3 (and also in Fig. 5.4) are actually not the highest occupied state in these quantum films either.

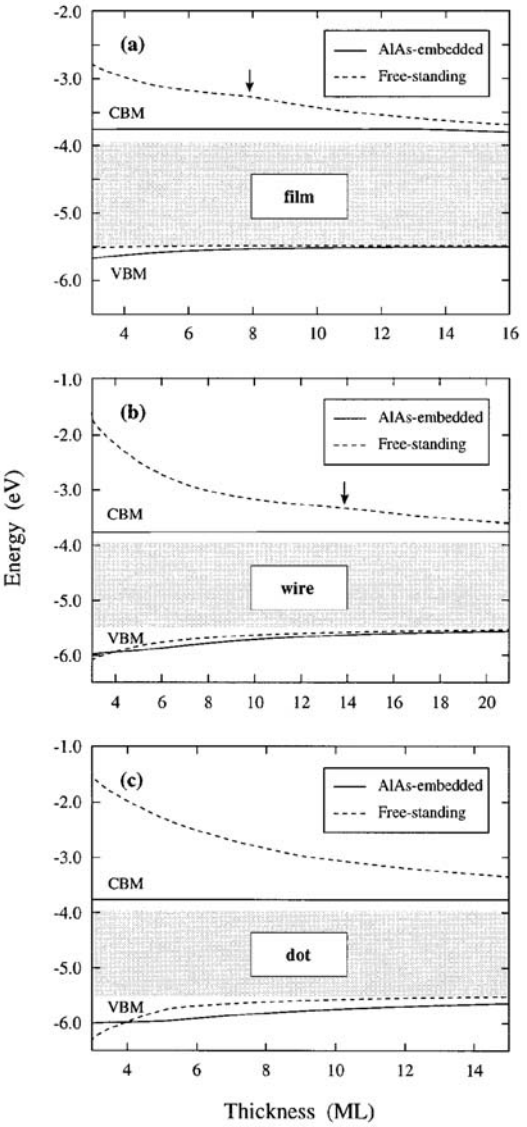

Fig. 5.4. Bandedge energies of AlAs-embeded (solid lines) and free-standing (dashed lines) GaAs films (a), wires (b), and dots (c) from numerical calculations in [9]. The shaded areas denote the GaAs bulk band gap. The arrows indicate the critical size for the direct/indirect transition in free-standing quantum films and wires. Reprinted with permission from A. Franceschetti and A. Zunger: Appl. Phys. Lett. **68**, 3455 (1996). Copyright by American Institute of Physics.

Franceschetti and Zunger [9] investigated the bandedge energies in free-standing and AlAs-embedded GaAs films, quantum wires, and quantum dots, as shown in Fig. 5.4.

Note that in the numerical results on the electronic states in free-standing GaAs (110) films and AlAs-embedded GaAs (110) films shown in Fig. 5.4(a), the bandedge energy of free-standing GaAs (110) films stays almost unchanged, but the bandedge energy of AlAs-embedded GaAs (110) films is always below the bandedge energy of free-standing GaAs (110) films of the same thickness as the film thickness decreases. If one thinks in an EMA way, the figure shows a stronger quantum confinement effect in AlAs-embedded GaAs (110) films than in free-standing GaAs (110) films since the effective mass at the VBM is negative. However, the free-standing GaAs (110) films have a much stronger confinement potential. This leads to a real puzzle for EMA: A weaker confinement potential leads to a stronger quantum confinement effect. This is another example indicating that EMA might be qualitatively incorrect in some cases. However, this is a natural consequence in our theory: Higher confinement potential in free-standing GaAs (110) films makes the corresponding energy in these films higher.

5.8 Further Discussions

We have seen that in ideal (001) or (110) quantum films of cubic semiconductors, the existence of a VBM state whose energy does not change as the film thickness changes, as shown in Figs. 1.5, 1.6, 5.2, 5.3, and 5.4, is simply due to the fact that there is always one VBM state that may have a nodal surface in the (001) plane or in the (110) plane. However, for the quantum confinement of the three-dimensional Bloch waves in quantum films, an even more interesting point is the existence of the other two higher occupied surface-like bands – simply due to the fact that the other two states of the triply-degenerated VBM may not have the same nodal surface in the (001) or in the (110) plane. In contrast with an EMA picture such as shown in Fig. 1.4, the highest occupied electronic states in ideal (001) and (110) quantum films of cubic semiconductors – the maximum of the surface-like subbands $\hat{\Lambda}_n(\hat{\boldsymbol{k}};\tau_3)$ for $n = 2, 3$ – actually are *above* the VBM, the highest occupied states in the bulk without quantum confinement.

It is the energies of the highest occupied bulk-like states that are always below the VBM and decrease as the film thickness decreases. The well-known fact that the band gap increases as the film thickness decreases actually is true only for the bulk-like electronic states in semiconductor quantum films. If the surface-like occupied subbands $\hat{\Lambda}_n(\hat{\boldsymbol{k}};\tau_3)$ for $n = 2, 3$ are also considered, the real band gap in a semiconductor quantum film may actually be *smaller* than the band gap of the bulk. It may even be possible that for some $\hat{\boldsymbol{k}}$,

$$\hat{\Lambda}_{n=2,3}(\hat{\boldsymbol{k}};\tau_3) > \hat{\Lambda}_{4,j_3}(\hat{\boldsymbol{k}}) \tag{5.44}$$

is true; that is, for some $\hat{\boldsymbol{k}}$ the two surface-like subbands originating from two valence bands ($n = 2, 3$) may be higher than the bulk-like subbands originating from the lowest conduction band ($n = 4$). If this happens, a film of a semiconductor crystal may actually become a film with the electrical conductivity of a metal: The equivalence of the Fermi level in the film will force electrons to move from the surface-like subbands $\hat{\Lambda}_{n=2,3}(\hat{\boldsymbol{k}}; \tau_3)$ into the bulk-like subbands $\hat{\Lambda}_{4,j_3}(\hat{\boldsymbol{k}})$, possibly to make the film an electrical conductor. These predictions are based on Theorem 5.1 and the properties of the VBM of cubic semiconductors. The thinner the film is, the more significant are the contributions from those surface-like states to the physical properties of the film. In the numerical calculations on a Si (001) quantum film in [7], the surface-like states were found at 1.2–1.6 eV above the VBM, indicating that the condition (5.44) is realistic.

Carefully designed experimental investigations to explore these possible physics phenomena will be very interesting.

Although our predictions for ideal (001) and (110) films with a fcc Bravais lattice are more general, many of them are consistent with numerical calculations for Si (001) films, Si (110) films, and GaAs (110) films in [6,7,9], there are also some differences.

Since the VBM of a cubic semiconductor are triply-degenerated and there is only one band (the lowest valence band $n = 0$ in our notation) below the three upper valence bands, as a consequence of Theorem 5.1, we have

$$\hat{\Lambda}_1(\hat{\boldsymbol{k}} = 0; \tau_3) \geq \text{VBM}$$

in these films; that is, only one $\hat{\Lambda}_{n=0}(\hat{\boldsymbol{k}} = 0; \tau_3)$ can exist below the VBM. In particular for the cases investigated in [6, 7], there could be only one $\hat{\Lambda}_{n=0}(\hat{\boldsymbol{k}} = 0; \tau_3)$ with an energy below the VBM at the boundary of the Brillouin zone in those films. This is what was observed in the numerical results on Si (001) films in [6, 7]: Only one of the doubly-degenerated X_{1v} states exists in Si (001) films, as shown in Figs. 1.6 and 5.2. However, in the numerical results on a six-layer Si(110) film and a six-layer GaAs (110) film in [7], two such states were presented in both films: X_{1v} and X_{4v} in the Si (110) film and X_{1v} and X_{5v} in the GaAs (110) film, as shown in Figs. 5.3(a) and 5.3(b). In the ideal films treated by our theory, the very existence of two such states is contradictory to Theorem 5.1.[10]

Another difference is that, according to our theory, in an ideal quantum film of N_3 layers for each energy band n and each $\hat{\boldsymbol{k}}$, there are $N_3 - 1$ bulk-like stationary Bloch states $\hat{\psi}_{n,j_3}(\hat{\boldsymbol{k}}, \boldsymbol{x}; \tau_3)$ where $j_3 = 1, 2, ..., N_3 - 1$. In the

[10]Neither any one of the doubly-degenerated X_{1v} states in Si nor the X_{1v} state in GaAs could have a nodal (110) plane and, thus, the X_{1v} state in an ideal Si (110) film and the X_{1v} state in an ideal GaAs (110) film cannot exist. Therefore, we can only have $\hat{\Lambda}_0(\hat{\boldsymbol{k}} = 0; \tau_3) = X_{4v}$ for an ideal Si (110) film and $\hat{\Lambda}_0(\hat{\boldsymbol{k}} = 0; \tau_3) = X_{5v}$ for an ideal GaAs (110) film. These are two examples of the special cases mentioned on p. 94 and on p. 101 in which $n = 0$ while $n' = 2$.

numerical calculations in [6, 7], the results are somewhat different: The $n = 5, j = 5$ (corresponding to our $n = 4, j_3 = 5$) state in Fig. 1.6 and Fig. 5.2 and the $n = 3, j = 4$ (corresponding to our $n = 2, j_3 = 4$)[11] state in Figs. 5.3(a) and 5.3(b) are missing.

A clear understanding of the origin of these differences will be interesting.

Although, in an ideal quantum film, each surface state with a specific n and a specific $\hat{\boldsymbol{k}}$ is located near either the top or the bottom of the film, since there is not a clear understanding of the properties of solutions of the second-order partial differential equations with periodic coefficients, there is no reason to expect that all surface states in one surface-like subband have to be located near the same surface of the film. Depending on τ_3 and $\hat{\boldsymbol{k}}$, some of them may be located near the top surface of the film and the others may be located near the bottom surface of the film, even though they all belong to the same surface-like subband in the film. This is significantly different from the surface-like states in one-dimensional finite crystals, where a surface state in a specific band gap can only be located near one end of the finite crystal.

As mentioned in Sections 5.2 and 5.5, another significant difference from one-dimensional cases is that a surface-like state in a quantum film does not have to be in a band gap. Essentially, the fundamental reason is that Theorem 5.1 does not give an upper limit for $\hat{\lambda}_n(\hat{\boldsymbol{k}}; \tau_3)$, unlike Theorem 2.8 in the one-dimensional case. Therefore, a surface-like state in a film may have an energy in the range of permitted energy bands of the bulk and it still can decay in either the positive or the negative direction of $\boldsymbol{a}_3$: Only in the one-dimensional case must such a decaying state be in a band gap.[12]

Since in the ideal quantum films discussed here, for each bulk energy band $\varepsilon_n(\boldsymbol{k})$ there are one surface-like subband $\hat{\Lambda}_n(\hat{\boldsymbol{k}}; \tau_3)$ and $N_3 - 1$ bulk-like subbands $\hat{\Lambda}_{n,j_3}(\hat{\boldsymbol{k}})$ in a film of N_3 layers, the physical origin of a surface-like subband is essentially related to a bulk energy band rather than to a bulk band gap. Such an understanding is not easy to obtain either in a one-dimensional analysis or in an ordinary semi-infinite crystal analysis: Many previous theoretical investigations on surface electronic states, including an investigation by the author [10], consider that the surface-like states are related to the band gap(s).

In particular, the tight-binding approach mentioned in Section 4.6 has such a problem; it leads to the result that in a tight-binding formalism a linear finite chain with a single state per unit cell does not have a surface state. According to the understanding we have obtained here, any ideal finite one-dimensional crystal always has a surface-like state for each bulk energy

[11] Note that in our notations the lowest energy band index $n = 0$.

[12] Mathematically, this is due to the fact that only for ordinary differential equations with periodic coefficients can it be proven that a solution with a factor $\mathrm{e}^{\beta x}$ or $\mathrm{e}^{-\beta x}$ in which β is a nonzero real number can only exist in a band gap. A surface state with an energy in the range of permitted energy bands is usually called a surface resonance state.

band. Furthermore, it is in the one-dimensional case that such a surface-like state must be in a band gap. It is a consequence of the *tight-binding approximation* that a crystal with a single state per unit cell has no band gap and, thus, such a linear finite chain has no surface state.

The general relationship between the surface-like subband $\hat{\Lambda}_n(\hat{\boldsymbol{k}};\tau_3)$ and the bulk-like subbands $\hat{\Lambda}_{n,j_3}(\hat{\boldsymbol{k}})$ in a quantum film (5.37) will lead to some other interesting consequences.

Since, as a consequence of Theorem 5.1, there is one surface subband $\hat{\Lambda}_n(\hat{\boldsymbol{k}};\tau_3)$ for each bulk energy band $\varepsilon_n(\boldsymbol{k})$, an ideal (001) or (110) film of a cubic compound semiconductor can have *at most one* surface-like subband $\hat{\Lambda}_0(\hat{\boldsymbol{k}};\tau_3)$ in the minor band gap between the lowest valence band $n=0$ and the upper valence bands, even though a film always has *two* surfaces.

Since the surface-like subbands $\hat{\Lambda}_n(\hat{\boldsymbol{k}};\tau_3)$ near the bulk band gap for an ideal semiconductor quantum film originate from the valence bands, in an everywhere neutral semiconductor film these surface-like subbands should be occupied. Unoccupied states in these surface-like subbands cause the surfaces to be positively charged.

A similar effect probably might be more notable in (001) and (110) films of alkali metals since the conduction band is not fully occupied; the Fermi surface of an alkali metal is usually inside the conduction band. All alkali metals (Li, Na, K, Rb, Cs, Fr) have a bcc Bravais lattice. Corresponding to the conduction band in which the conducting electrons are occupied, there is a surface-like subband in a (001) or (110) quantum film. This surface-like subband in the film is, by (5.37), generally higher in energy than the corresponding bulk-like subbands. In an everywhere neutral alkali metal film, the surface-like subband should be equally occupied by electrons as the corresponding bulk-like subbands. However, the equivalence of the Fermi energy in the film must force some electrons to flow from the surface-like subband into the bulk-like subbands inside the film and, thus, the surfaces of the film should be positively charged.

This prediction seems to be supported by the positive surface-atom core-level shift in alkali metal (110) films, as reported by Riffe et al.(RWBC), [e.g.,11]. Although the surface-atom core-level shifts in most other metals (transition metals and noble metals) were explained by a small charge flow between the surface and the inside of the metal [12], no reason for such a charge flow between the surface and the inside of alkali metals was known previously. The authors in [11] used the spill-out of the conducting electrons to explain the fact that the surfaces of these alkali metals are positively charged. However, the theory in this chapter provided a clear reason for why the electrons in alkali (110) films could flow from the surfaces into the film and thus make the surfaces of the film positive charged, thus giving an alternative possible explanation for the positive surface-atom core-level shift observed in alkali metal (110) films. If this explanation is correct, then the surface-atom

core-level shift in metals can be understood on the same basis, as a charge flow between the surface and the inside of the metal.

In the RWBC model, the conducting electrons spill *outside* into the vacuum, whereas in the theory of this chapter, conducting electrons mainly flow *inside*. Therefore, the surface-atom top layer relaxation [13, 14] in an alkali metal is more likely to be an expansion if the RWBC model dominates. On the other hand, if conducting electrons flowing inside dominates, the surface-atom top layer relaxation in an alkali metal is more likely to be a contraction. Experimental investigations to explore this will be interesting.

There are also surface-like subbands corresponding to the bulk conduction bands in semiconductor films. Those surface-like subbands will be even higher in energy than the bulk conduction bands and, thus, will usually not be occupied. It seems unlikely that those surface-like subbands will have a significant effect on the properties of a semiconductor quantum film.

Similar to being stated in the comments in Section 4.5, the very existence of the boundary-dependent states in quantum films is neglected in the EMA. Furthermore, if the concerned energy extreme is not located at the center of the Brillouin zone or at the boundary of the Brillouin zone, such as the conduction band minima in Si or Ge, the use of EMA is not justified, even for the bulk-like electronic states in ideal quantum films.

In summary, by considering the effects of quantum confinement of three-dimensional Bloch waves in a specific direction, exact and general results on the properties of the electronic states in interesting quantum films – such as in ideal (001) films of crystals with a sc, tetr, or ortho Bravais lattice for which (5.14) is true or in ideal (001) or (110) films of crystals with a fcc Bravais lattice or a bcc Bravais lattice for which (5.21) is true – can be predicted: For a film bounded at $x_3 = \tau_3$ and $x_3 = (\tau_3 + N_3)$, for each bulk energy band and each wave vector $\hat{\boldsymbol{k}}$ in the film plane, there are $N_3 - 1$ bulk-like electronic states $\hat{\psi}_{n,j_3}(\hat{\boldsymbol{k}}, \boldsymbol{x}; \tau_3)$ by (5.28), whose energies $\hat{\Lambda}_{n,j_3}(\hat{\boldsymbol{k}})$ by (5.32) are dependent on the film thickness N_3 but not on the film boundary τ_3, and there is one surface-like electronic state $\hat{\psi}_n(\hat{\boldsymbol{k}}, \boldsymbol{x}; \tau_3)$ by (5.33) in the film whose energy $\hat{\Lambda}_n(\hat{\boldsymbol{k}}; \tau_3)$ by (5.34) is dependent on the film boundary τ_3 but not on the film thickness N_3 and is always above bulk-like subbands $\hat{\Lambda}_{n,j_3}(\hat{\boldsymbol{k}})$, by (5.37). The energies $\hat{\Lambda}_{n,j_3}(\hat{\boldsymbol{k}})$ of bulk-like states map the bulk energy band $\varepsilon_n(\boldsymbol{k})$ exactly. These are similar to the properties of the electronic states in a one-dimensional finite crystal. However, the surface-like states in an ideal quantum film may have some different interesting properties due to the differences between Theorem 5.1 and Theorem 2.8. The differences between Theorem 5.1 and Theorem 2.8 are actually further related to the fact that the solutions of the second-order partial differential equation with periodic coefficients (5.1) do not have the simple and general properties of the solutions of the second-order ordinary differential equation with periodic coefficients (2.36) described in Chapter 2.

Therefore, in the ideal quantum films considered in this chapter, the effect of the lack of translational invariance in one specific direction is that there is always one and only one boundary-dependent surface-like subband $\hat{\Lambda}_n(\hat{\boldsymbol{k}};\tau_3)$ for each bulk energy band $\varepsilon_n(\boldsymbol{k})$; the energies of all other bulk-like subbands $\hat{\Lambda}_{n,j_3}(\hat{\boldsymbol{k}})$ can be directly obtained from the energy band structure $\varepsilon_n(\boldsymbol{k})$ of the corresponding bulk crystal, by (5.32).

The approach used in this chapter can be naturally extended to investigate the effects of the further confinement of two-dimensional Bloch waves $\hat{\psi}_{n,j_3}(\hat{\boldsymbol{k}},\boldsymbol{x};\tau_3)$ and $\hat{\psi}_n(\hat{\boldsymbol{k}},\boldsymbol{x};\tau_3)$ in an ideal quantum wire.

References

1. D. Gilbarg and N. S. Trudinger: *Elliptic Partial Differential Equations of Second Order* (Springer, Berlin Heidelberg 1998)
2. For some of the most recent mathematical results on the spectral theory of partial differential equations with periodic coefficients, see, for example, P. A. Kuchment: Russ. Math. Surveys, **37**, No. 4, 1 (1982); I. M. Krichever: Russ. Math. Surveys, **44**, No. 2, 145 (1984) and references therein
3. M. S. P. Eastham: *The Spectral Theory of Periodic Differential Equations* (Scottish Academic Press, Edinburgh 1973) and references therein
4. S. Y. Ren: Europhys. Lett. **64**, 783 (2003)
5. E. C. Titchmarsh: *Eigenfunction Expansions Associated with Second-Order Differential Equations* (Oxford University Press, Oxford 1958), Part II
6. S. B. Zhang and A. Zunger: Appl. Phys. Lett. **63**, 1399 (1993)
7. S. B. Zhang, C-Y Yeh, and A. Zunger: Phys. Rev. **B48**, 11204 (1993)
8. V. I. Gavrilenko and F. Koch: J. Appl. Phys. **77**, 3284 (1995)
9. A. Franceschetti and A. Zunger: Appl. Phys. Lett. **68**, 3455 (1996)
10. S. Y. Ren: Ann. Phys.(NY) **301**, 22 (2002)
11. D. M. Riffe, G. K. Wertheim, D. N. E. Buchanan, and P. H. Citrin: Phys. Rev. **B45**, 6216 (1992) and references therein
12. P. H. Citrin, G. K. Wertheim, and Y. Baer: Phys. Rev. **B27**, 3160 (1983); P. H. Citrin, and G. K. Wertheim: Phys. Rev. **B27**, 3176 (1983)
13. F. Bechstedt: *Principles of Surface Physics* (Springer, Berlin Heidelberg 2003)
14. A. Groß: *Theoretical Surface Science: A Microscopic Perspecpective* (Springer, Berlin Heidelberg 2003)

6 Electronic States in Ideal Quantum Wires

In this chapter, we investigate the electronic states in ideal quantum wires. We are interested in the electronic states in rectangular quantum wires, which can be considered as the electronic states in a quantum film discussed in Chapter 5 further confined in one more direction. In particular, we are interested in those simple cases where the two primitive lattice vectors $\boldsymbol{a}_1$ and $\boldsymbol{a}_2$ in the film plane are perpendicular to each other. By using an approach similar to that used in Chapter 5, we try to understand the further quantum confinement effects in a quantum wire of two-dimensional Bloch waves $\hat{\psi}_{n,j_3}(\hat{\boldsymbol{k}}, \boldsymbol{x}; \tau_3)$ in (5.28) and $\hat{\psi}_n(\hat{\boldsymbol{k}}, \boldsymbol{x}; \tau_3)$ in (5.33) in a quantum film that were obtained in Chapter 5. It is found that each type of two-dimensional Bloch waves will produce two different types of one-dimensional Bloch waves in the quantum wire.

A rectangular quantum wire always has four boundary faces: two faces in the $(h_2k_2l_2)$ plane and two faces in the $(h_3k_3l_3)$ plane. The electronic states in such a quantum wire can be considered either as the electronic states in a quantum film with two boundary faces in the $(h_3k_3l_3)$ plane further confined by two boundary faces in the $(h_2k_2l_2)$ plane, or, equivalently, as the electronic states in a quantum film with two boundary faces in the $(h_2k_2l_2)$ plane further confined by two boundary faces in the $(h_3k_3l_3)$ plane. The results obtained in these two different confinement orders are equally valid and are complementary to each other. By combining the results obtained from the two different confinement orders, we can obtain a more comprehensive understanding of the electronic states in the quantum wire.

The simplest cases are the electronic states in an ideal rectangular quantum wire of crystals with a sc, tetr, or an ortho Bravais lattice. In these crystals, the three primitive lattice vectors $\boldsymbol{a}_1$, $\boldsymbol{a}_2$, and $\boldsymbol{a}_3$ are perpendicular to each other and are equivalent. Exact and general results on the electronic states in such a quantum wire in the direction of one specific primitive lattice vector $\boldsymbol{a}_1$ and with four faces in the (010) or in the (001) plane can be obtained by considering the electronic states in a quantum film with two boundary faces in the (001) plane further confined by the two boundary faces in the (010) plane, or, equivalently, as the electronic states in a quantum film with two boundary faces in (010) plane further confined by the two boundary faces in the (001) plane.

Based on the understanding of the further quantum confinement of two-dimensional Bloch waves $\hat{\psi}_{n,j_3}(\hat{\boldsymbol{k}}, \boldsymbol{x}; \tau_3)$ and $\hat{\psi}_n(\hat{\boldsymbol{k}}, \boldsymbol{x}; \tau_3)$ and by considering two different confinement orders, we can also obtain predictions on the electronic states in some practically more interesting ideal rectangular quantum wires of crystals with a fcc or a bcc Bravais lattice. Electronic states in such a quantum wire can be considered as the two-dimensional Bloch waves in a quantum film discussed in Section 5.6 further confined in one more direction.

This chapter is organized as follows. After giving basic considerations of the problem in Section 6.1, in Sections 6.2 to 6.3 we investigate the effects produced when the two types of two-dimensional Bloch waves obtained in Chapter 5 are further confined in one more specific direction. In Sections 6.4 to 6.7, we obtain predictions on the electronic states in ideal quantum wires of crystals with several different Bravais lattices by applying the results obtained in Sections 6.1 to 6.3 and by considering two different confinement orders. In Section 6.8 are a summary and some discussions on the results obtained.

6.1 Basic Considerations

In an ideal quantum film discussed in Chapter 5, there are two different types of electronic states: surface-like states $\hat{\psi}_n(\hat{\boldsymbol{k}}, \boldsymbol{x}; \tau_3)$ in (5.33) and bulk-like states $\hat{\psi}_{n,j_3}(\hat{\boldsymbol{k}}, \boldsymbol{x}; \tau_3)$ in (5.28). Both are two-dimensional Bloch waves in the film plane. Similar to the problem we treated in Chapter 5, in a quantum wire, each type of these two-dimensional Bloch waves will be further confined in one more direction.

We choose the primitive vector $\boldsymbol{a}_1$ in the wire direction. Such a rectangular quantum wire can be defined by a bottom face $x_3 = \tau_3$, a top face $x_3 = \tau_3 + N_3$, a front face perpendicularly intersecting the $\boldsymbol{a}_2$ axis at $\tau_2\boldsymbol{a}_2$, and a rear face perpendicularly intersecting the $\boldsymbol{a}_2$ axis at $(\tau_2 + N_2)\boldsymbol{a}_2$, where τ_2 and τ_3 define the boundary face locations of the wire and N_2 and N_3 are two positive integers indicating the wire size and shape. We use $\bar{\boldsymbol{k}}$ to express a wave vector in the wire direction: $\bar{\boldsymbol{k}} = k_1\bar{\boldsymbol{b}}_1$, $\boldsymbol{a}_1 \cdot \bar{\boldsymbol{b}}_1 = 1$. Since in this chapter we are only interested in the cases where $\boldsymbol{a}_1 \cdot \boldsymbol{a}_2 = 0$, we have $\bar{\boldsymbol{b}}_1 = \hat{\boldsymbol{b}}_1$.

For the further confinement of two-dimensional Bloch waves $\hat{\psi}_n(\hat{\boldsymbol{k}}, \boldsymbol{x}; \tau_3)$ and $\hat{\psi}_{n,j_3}(\hat{\boldsymbol{k}}, \boldsymbol{x}; \tau_3)$, we look for the eigenvalues $\bar{\Lambda}$ and eigenfunctions $\bar{\psi}(\bar{\boldsymbol{k}}, \boldsymbol{x})$ of the following two equations:

$$-\nabla^2\bar{\psi}(\bar{\boldsymbol{k}}, \boldsymbol{x}) + [v(\boldsymbol{x}) - \bar{\Lambda}]\bar{\psi}(\bar{\boldsymbol{k}}, \boldsymbol{x}) = 0 \quad \text{if } \boldsymbol{x} \in \text{ the wire} \tag{6.1}$$

and

$$\bar{\psi}(\bar{\boldsymbol{k}}, \boldsymbol{x}) = 0 \quad \text{if } \boldsymbol{x} \notin \text{ the wire.} \tag{6.2}$$

The solutions $\bar{\psi}(\bar{\boldsymbol{k}}, \boldsymbol{x})$ of (6.1) and (6.2) are one-dimensional Bloch waves with a wave vector $\bar{\boldsymbol{k}}$ in the wire direction $\boldsymbol{a}_1$.

The further quantum confinement of each type of two-dimensional Bloch waves $\hat{\psi}_n(\hat{\boldsymbol{k}}, \boldsymbol{x}; \tau_3)$ or $\hat{\psi}_{n,j_3}(\hat{\boldsymbol{k}}, \boldsymbol{x}; \tau_3)$ will have a new eigenvalue problem and a corresponding theorem and will give two different types of electronic states in the quantum wire. Correspondingly, we will obtain four different sets of one-dimensional Bloch waves in the quantum wire.

6.2 Further Quantum Confinement of $\hat{\psi}_n(\hat{k}, x; \tau_3)$

For the quantum confinement of two-dimensional Bloch waves $\hat{\psi}_n(\hat{\boldsymbol{k}}, \boldsymbol{x}; \tau_3)$, we consider an orthorhombic parallelogram B as shown in Fig. 6.1 with surfaces oriented in the $\boldsymbol{a}_1$, $\boldsymbol{a}_2$, or the film surface direction[1] and having a rectangular bottom face at $x_3 = \tau_3$, a rectangular top face at $x_3 = \tau_3 + 1$, a front face intersecting the $\boldsymbol{a}_2$ axis at $\tau_2 \boldsymbol{a}_2$ [2] and a rear face intersecting it at $(\tau_2 + 1)\boldsymbol{a}_2$, and a left face and a right face separated by $\boldsymbol{a}_1$ and perpendicular to the $\boldsymbol{a}_1$ axis. Since each $\hat{\psi}_n(\hat{\boldsymbol{k}}, \boldsymbol{x}; \tau_3)$ is zero on the film bottom surface

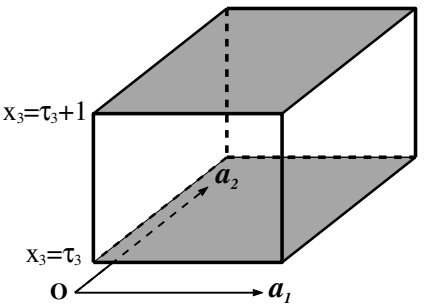

Fig. 6.1. The orthorhombic parallelogram B for the eigenvalue problem of (5.1) under the boundary condition (6.3). The two shadowed faces of ∂B_3 are the two faces on which each $\hat{\psi}_n(\hat{\boldsymbol{k}}, \boldsymbol{x}; \tau_3)$ is zero (thus the specific direction of $\boldsymbol{a}_3$ no longer matters). The two thick-lined faces of ∂B_2 are the two faces on which each function $\bar{\phi}(\bar{\boldsymbol{k}}, \boldsymbol{x}; \tau_2, \tau_3)$ is further required to be zero.

$x_3 = \tau_3$ and on the surface $x_3 = \tau_3 + 1$ and is a two-dimensional Bloch wave in the film plane, the function set $\bar{\phi}(\bar{\boldsymbol{k}}, \boldsymbol{x}; \tau_2, \tau_3)$ is defined by the condition

$$\begin{aligned} \bar{\phi}(\bar{\boldsymbol{k}}, \boldsymbol{x} + \boldsymbol{a}_1; \tau_2, \tau_3) &= \mathrm{e}^{\mathrm{i}k_1} \bar{\phi}(\bar{\boldsymbol{k}}, \boldsymbol{x}; \tau_2, \tau_3) \quad -\pi < k_1 \leq \pi \\ \bar{\phi}(\bar{\boldsymbol{k}}, \boldsymbol{x}; \tau_2, \tau_3) &= 0 \qquad\qquad\qquad\quad \text{if } \boldsymbol{x} \in \partial B_2 \text{ or } \boldsymbol{x} \in \partial B_3, \end{aligned} \tag{6.3}$$

[1] That is, in the $\hat{\boldsymbol{b}}_1$, $\hat{\boldsymbol{b}}_2$, or $\boldsymbol{b}_3$ direction.

[2] For the further quantum confinement of these two-dimensional Bloch waves, it is assumed that in Sections 6.2 and 6.3, the existence of boundary τ_2 does not change the one-dimensional translational symmetry in the $\boldsymbol{a}_1$ direction.

where ∂B_3 means two opposite faces of the boundary ∂B of B determined by $x_3 = \tau_3$ and $x_3 = \tau_3 + 1$ and ∂B_2 means two opposite faces of the boundary ∂B of B in the $\boldsymbol{a}_2$ direction. The eigenvalues and eigenfunctions of (5.1) under the condition (6.3) are denoted by $\bar{\lambda}_n(\bar{\boldsymbol{k}}; \tau_2, \tau_3)$ and $\bar{\phi}_n(\bar{\boldsymbol{k}}, \boldsymbol{x}; \tau_2, \tau_3)$, where $n = 0, 1, 2, ...$

For each eigenvalue $\bar{\lambda}_n(\bar{\boldsymbol{k}}; \tau_2, \tau_3)$ defined by (5.1) and the boundary condition (6.3), we have the following theorem connecting $\bar{\lambda}_n(\bar{\boldsymbol{k}}; \tau_2, \tau_3)$ with the eigenvalues $\hat{\Lambda}_n(\hat{\boldsymbol{k}}; \tau_3)$ of $\hat{\psi}_n(\hat{\boldsymbol{k}}, \boldsymbol{x}; \tau_3)$ given in (5.34).

Theorem 6.1.

$$\bar{\lambda}_n(\bar{\boldsymbol{k}}; \tau_2, \tau_3) \geq \hat{\Lambda}_n(\hat{\boldsymbol{k}}; \tau_3) \quad \text{for } (\bar{\boldsymbol{k}} - \hat{\boldsymbol{k}}) \cdot \boldsymbol{a}_1 = 0. \tag{6.4}$$

Note that in (6.3) and (6.4), $\bar{\boldsymbol{k}}$ is a wave vector in the wire direction and $\hat{\boldsymbol{k}}$ is a wave vector in the film plane. In (6.4), $\bar{\boldsymbol{k}}$ and $\hat{\boldsymbol{k}}$ have the same component in the wire direction $\boldsymbol{a}_1$.

Since the two-dimensional Bloch wave $\hat{\psi}_n(\hat{\boldsymbol{k}}, \boldsymbol{x}; \tau_3)$ satisfies

$$\begin{aligned} \hat{\psi}(\hat{\boldsymbol{k}}, \boldsymbol{x} + \boldsymbol{a}_i; \tau_3) &= \mathrm{e}^{\mathrm{i}k_i} \hat{\psi}(\hat{\boldsymbol{k}}, \boldsymbol{x}; \tau_3) \qquad -\pi < k_i \leq \pi, \quad i = 1, 2 \\ \hat{\psi}(\hat{\boldsymbol{k}}, \boldsymbol{x}; \tau_3) &= 0 \qquad\qquad \text{if } \boldsymbol{x} \in \partial B_3, \end{aligned} \tag{6.5}$$

Theorem 6.1 can be proved similar to Theorem 5.1 of Chapter 5. The major difference is in the Dirichlet integral

$$\begin{aligned} J(f, g) &= \int_B \{\nabla f(\boldsymbol{x}) \cdot \nabla g^*(\boldsymbol{x}) + v(\boldsymbol{x}) f(\boldsymbol{x}) g^*(\boldsymbol{x})\} \, \mathrm{d}\boldsymbol{x} \\ &= \int_B f(\boldsymbol{x}) \{-\nabla^2 g^*(\boldsymbol{x}) + v(\boldsymbol{x}) g^*(\boldsymbol{x})\} \, \mathrm{d}\boldsymbol{x} + \int_{\partial B} f \frac{\partial g^*}{\partial n} \, \mathrm{d}S; \end{aligned} \tag{6.6}$$

if both $f(\boldsymbol{x})$ and $g(\boldsymbol{x})$ satisfy the conditions (6.5), the integral over ∂B in (6.6) is zero due to the fact that the integrals over two opposite faces of ∂B_1 and ∂B_2 cancel out and $\hat{\psi}(\hat{\boldsymbol{k}}, \boldsymbol{x}; \tau_3) = 0$ when $\boldsymbol{x} \in \partial B_3$. If $f(\boldsymbol{x}) = \bar{\phi}(\bar{\boldsymbol{k}}, \boldsymbol{x}; \tau_2, \tau_3)$ and $g(\boldsymbol{x}) = \hat{\psi}(\hat{\boldsymbol{k}}, \boldsymbol{x}; \tau_3)$, the integral over ∂B in (6.6) is also zero because the integrals over two opposite faces of ∂B_1 cancel out since $(\bar{\boldsymbol{k}} - \hat{\boldsymbol{k}}) \cdot \boldsymbol{a}_1 = 0$ and the integral over each face of ∂B_2 and ∂B_3 is zero since $f(\boldsymbol{x}) = 0$ when $\boldsymbol{x} \in \partial B_2$ or $\boldsymbol{x} \in \partial B_3$.

Theorem 6.1 is similar to Theorem 5.1; the consequences of the quantum confinement of three-dimensional Bloch waves $\phi_n(\boldsymbol{k}, \boldsymbol{x})$ in the $\boldsymbol{a}_3$ direction due to Theorem 5.1 can be similarly applied to the quantum confinement of two-dimensional Bloch waves $\hat{\psi}_n(\hat{\boldsymbol{k}}, \boldsymbol{x}; \tau_3)$ in the $\boldsymbol{a}_2$ direction.

For each bulk energy band n and each $\bar{\boldsymbol{k}}$, there is one $\bar{\phi}_n(\bar{\boldsymbol{k}}, \boldsymbol{x}; \tau_2, \tau_3)$.

Because $v(\boldsymbol{x} + \boldsymbol{a}_2) = v(\boldsymbol{x})$, the function $\bar{\phi}_n(\bar{\boldsymbol{k}}, \boldsymbol{x}; \tau_2, \tau_3)$ has the form

$$\bar{\phi}_n(\bar{\boldsymbol{k}}, \boldsymbol{x} + \boldsymbol{a}_2; \tau_2, \tau_3) = \mathrm{e}^{\mathrm{i}k_2} \bar{\phi}_n(\bar{\boldsymbol{k}}, \boldsymbol{x}; \tau_2, \tau_3) \tag{6.7}$$

and, here, k_2 can be complex. If in (6.7) k_2 is real, then $\bar{\phi}_n(\bar{\boldsymbol{k}}, \boldsymbol{x}; \tau_2, \tau_3)$ is a $\hat{\psi}_{n'}(\hat{\boldsymbol{k}}, \boldsymbol{x}; \tau_3)$. According to Theorem 6.1, a $\hat{\psi}_{n'}(\hat{\boldsymbol{k}}, \boldsymbol{x}; \tau_3)$ cannot be a

$\bar{\phi}_n(\bar{\boldsymbol{k}}, \boldsymbol{x}; \tau_2, \tau_3)$ except in some special cases when $\hat{\psi}_{n'}(\hat{\boldsymbol{k}}, \boldsymbol{x}; \tau_3)$ has a nodal surface perpendicularly intersecting the $\boldsymbol{a}_2$ axis at $\tau_2 \boldsymbol{a}_2$. Therefore, k_2 in (6.7) can be real only in such special cases; in most cases, k_2 in (6.7) is complex with a nonzero imaginary part.

Depending on τ_2 (and also τ_3), n, and $\bar{\boldsymbol{k}}$, the imaginary part of k_2 in (6.7) can be either positive or negative, corresponding to whether $\bar{\phi}_n(\bar{\boldsymbol{k}}, \boldsymbol{x}; \tau_2, \tau_3)$ decays in either the positive or the negative direction of $\boldsymbol{a}_2$. Such states $\bar{\phi}_n(\bar{\boldsymbol{k}}, \boldsymbol{x}; \tau_2, \tau_3)$ with a nonzero imaginary part of k_2 in (6.7) cannot exist in a film with two-dimensional translational invariance because they are divergent in either the negative or the positive direction of $\boldsymbol{a}_2$. However, they can play a significant role in a quantum wire with a finite size in the $\boldsymbol{a}_2$ direction.

The further quantum confinement of the two-dimensional Bloch waves $\hat{\psi}_n(\hat{\boldsymbol{k}}, \boldsymbol{x}; \tau_3)$ in the $\boldsymbol{a}_2$ direction will produce two different types of electronic states in the quantum wire.

One type of nontrivial solutions of (6.1) and (6.2) from the quantum confinement of $\hat{\psi}_n(\hat{\boldsymbol{k}}, \boldsymbol{x}; \tau_3)$ can be obtained from (6.7) by assigning

$$\begin{aligned} \bar{\psi}_n(\bar{\boldsymbol{k}}, \boldsymbol{x}; \tau_2, \tau_3) &= c_{N_2,N_3} \bar{\phi}_n(\bar{\boldsymbol{k}}, \boldsymbol{x}; \tau_2, \tau_3), \quad \text{if } \boldsymbol{x} \in \text{ the wire} \\ &= 0 \qquad\qquad\qquad\qquad\quad \text{if } \boldsymbol{x} \notin \text{ the wire}, \end{aligned} \tag{6.8}$$

where c_{N_2,N_3} is a normalization constant. The corresponding eigenvalue

$$\bar{\Lambda}_n(\bar{\boldsymbol{k}}; \tau_2, \tau_3) = \bar{\lambda}_n(\bar{\boldsymbol{k}}; \tau_2, \tau_3) \tag{6.9}$$

is dependent on τ_2 and τ_3 but not on N_2 and N_3.

Therefore, for each bulk energy band n and each wave vector $\bar{\boldsymbol{k}}$, there is one electronic state $\bar{\psi}_n(\bar{\boldsymbol{k}}, \boldsymbol{x}; \tau_2, \tau_3)$ that is $\bar{\phi}_n(\bar{\boldsymbol{k}}, \boldsymbol{x}; \tau_2, \tau_3)$ inside the wire but is zero otherwise, whose energy $\bar{\Lambda}_n(\bar{\boldsymbol{k}}; \tau_2, \tau_3)$ depends on τ_2 and τ_3 but not on N_2 and N_3. This is a side-like state because $\bar{\phi}_n(\bar{\boldsymbol{k}}, \boldsymbol{x}; \tau_2, \tau_3)$ decays in either the positive or the negative direction of $\boldsymbol{a}_2$ and $\boldsymbol{a}_3$ in most cases.

Now, we try to find other solutions of (6.1) and (6.2) from the quantum confinement of $\hat{\psi}_n(\hat{\boldsymbol{k}}, \boldsymbol{x}; \tau_3)$. We can expect that there are stationary Bloch states in the $\boldsymbol{a}_2$ direction, formed due to the multiple reflections of $\hat{\psi}_n(\hat{\boldsymbol{k}}, \boldsymbol{x}; \tau_3)$ between two confinement boundary surfaces that perpendicularly intersect the $\boldsymbol{a}_2$ axis at τ_2 and $(\tau_2 + N_2)$.

Since it is assumed that the existence of the boundary τ_3 does not change the two-dimensional space group symmetry of the system, in many quantum films discussed in Chapter 5

$$\hat{\Lambda}_n(k_1 \bar{\boldsymbol{b}}_1 + k_2 \hat{\boldsymbol{b}}_2; \tau_3) = \hat{\Lambda}_n(k_1 \bar{\boldsymbol{b}}_1 - k_2 \hat{\boldsymbol{b}}_2; \tau_3) \tag{6.10}$$

in (5.34) is true; thus, in general,

$$\begin{aligned} f_{n,k_1,k_2}(\boldsymbol{x}; \tau_3) &= c_+ \hat{\psi}_n(k_1 \bar{\boldsymbol{b}}_1 + k_2 \hat{\boldsymbol{b}}_2, \boldsymbol{x}; \tau_3) \\ &\quad + c_- \hat{\psi}_n(k_1 \bar{\boldsymbol{b}}_1 - k_2 \hat{\boldsymbol{b}}_2, \boldsymbol{x}; \tau_3), \quad 0 < k_2 < \pi, \end{aligned}$$

where $c_\pm$ are not zero, is a nontrivial solution of (6.1) due to (6.10). It is easy to see that $f_{n,k_1,k_2}(\boldsymbol{x};\tau_3)$ is a one-dimensional Bloch wave with a wave vector $\bar{\boldsymbol{k}} = k_1\bar{\boldsymbol{b}}_1$ in the wire direction:

$$f_{n,k_1,k_2}(\boldsymbol{x}+\boldsymbol{a}_1;\tau_3) = \mathrm{e}^{\mathrm{i}k_1} f_{n,k_1,k_2}(\boldsymbol{x};\tau_3), \quad -\pi < k_1 \le \pi,$$

due to (6.5). To be a solution of (6.1) and (6.2), the function $f_{n,k_1,k_2}(\boldsymbol{x};\tau_3)$ is required to be zero at the front face and the rear face of the wire. By writing the front face equation of the wire as $x_2 = x_{2,f}(x_1,x_3)$ and the rear face equation of the wire as $x_2 = x_{2,r}(x_1,x_3)$, we should have

$$\begin{aligned} c_+\hat{\psi}_n[k_1\bar{\boldsymbol{b}}_1 + k_2\hat{\boldsymbol{b}}_2, \boldsymbol{x} \in x_{2,f}(x_1,x_3);\tau_3] \\ + c_-\hat{\psi}_n[k_1\bar{\boldsymbol{b}}_1 - k_2\hat{\boldsymbol{b}}_2, \boldsymbol{x} \in x_{2,f}(x_1,x_3);\tau_3] = 0, \\ c_+\hat{\psi}_n[k_1\hat{\boldsymbol{b}}_1 + k_2\hat{\boldsymbol{b}}_2, \boldsymbol{x} \in x_{2,r}(x_1,x_3);\tau_3] \\ + c_-\hat{\psi}_n[k_1\bar{\boldsymbol{b}}_1 - k_2\hat{\boldsymbol{b}}_2, \boldsymbol{x} \in x_{2,r}(x_1,x_3);\tau_3] = 0. \end{aligned} \tag{6.11}$$

Since $x_{2,r}(x_1,x_3) = x_{2,f}(x_1,x_3) + N_2$, we have

$$\begin{aligned} \hat{\psi}_n[k_1\bar{\boldsymbol{b}}_1 + k_2\hat{\boldsymbol{b}}_2, \boldsymbol{x} \in x_{2,r}(x_1,x_3);\tau_3] \\ = \mathrm{e}^{\mathrm{i}k_2N_2}\hat{\psi}_n[k_1\bar{\boldsymbol{b}}_1 + k_2\hat{\boldsymbol{b}}_2, \boldsymbol{x} \in x_{2,f}(x_1,x_3);\tau_3] \end{aligned}$$

and

$$\begin{aligned} \hat{\psi}_n[k_1\bar{\boldsymbol{b}}_1 - k_2\hat{\boldsymbol{b}}_2, \boldsymbol{x} \in x_{2,r}(x_1,x_3);\tau_3] \\ = \mathrm{e}^{-\mathrm{i}k_2N_2}\hat{\psi}_n[k_1\bar{\boldsymbol{b}}_1 - k_2\hat{\boldsymbol{b}}_2, \boldsymbol{x} \in x_{2,f}(x_1,x_3);\tau_3] \end{aligned}$$

due to (6.5). Therefore, for $c_\pm$ in (6.11) are not both zero, $\mathrm{e}^{\mathrm{i}k_2N_2} - \mathrm{e}^{-\mathrm{i}k_2N_2} = 0$ has to be true for these stationary Bloch states, independent of τ_2.

The stationary Bloch state solutions of (6.1) and (6.2) obtained from the further quantum confinement of $\hat{\psi}_n(\hat{\boldsymbol{k}},\boldsymbol{x};\tau_3)$ should have the form

$$\begin{aligned} \bar{\psi}_{n,j_2}(\bar{\boldsymbol{k}},\boldsymbol{x};\tau_2,\tau_3) &= f_{n,k_1,\kappa_2}(\boldsymbol{x};\tau_2,\tau_3) \quad \text{if } \boldsymbol{x} \in \text{ the wire} \\ &= 0 \qquad\qquad\qquad\quad \text{if } \boldsymbol{x} \notin \text{ the wire,} \end{aligned} \tag{6.12}$$

where $\bar{\boldsymbol{k}} = k_1\bar{\boldsymbol{b}}_1$ and

$$\begin{aligned} f_{n,k_1,k_2}(\boldsymbol{x};\tau_2,\tau_3) = c_{n,k_1,k_2;\tau_2}\hat{\psi}_n(k_1\bar{\boldsymbol{b}}_1 + k_2\hat{\boldsymbol{b}}_2, \boldsymbol{x};\tau_3) \\ + c_{n,k_1,-k_2;\tau_2}\hat{\psi}_n(k_1\bar{\boldsymbol{b}}_1 - k_2\hat{\boldsymbol{b}}_2, \boldsymbol{x};\tau_3), \end{aligned}$$

$c_{n,k_1,\pm k_2;\tau_2}$ are dependent on τ_2, and

$$\kappa_2 = j_2\ \pi/N_2, \quad j_2 = 1,2,...,N_2-1; \tag{6.13}$$

here, j_2 is a subband index. The energies $\bar{\Lambda}$ of these stationary Bloch states are given by

$$\bar{\Lambda}_{n,j_2}(\bar{\boldsymbol{k}};\tau_3) = \hat{\Lambda}_n(\bar{\boldsymbol{k}} + \kappa_2\hat{\boldsymbol{b}}_2;\tau_3). \tag{6.14}$$

Each eigenvalue $\bar{\Lambda}_{n,j_2}(\bar{\boldsymbol{k}}; \tau_3)$ is dependent on N_2 and τ_3 but not on τ_2 and N_3. These states are surface-like states since $\hat{\psi}_n(\hat{\boldsymbol{k}}, \boldsymbol{x}; \tau_3)$ are surface-like states in the quantum film.

Similar to (5.37), due to (6.4), (6.9), and (6.14) in general in an ideal quantum wire, the energy of a side-like state is above the energy of a relevant surface-like state:

$$\bar{\Lambda}_n(\bar{\boldsymbol{k}}; \tau_2, \tau_3) > \bar{\Lambda}_{n,j_2}(\bar{\boldsymbol{k}}; \tau_3). \tag{6.15}$$

6.3 Further Quantum Confinement of $\hat{\psi}_{n,j_3}(\hat{\boldsymbol{k}}, x; \tau_3)$

The further confinement of two-dimensional Bloch waves $\hat{\psi}_{n,j_3}(\hat{\boldsymbol{k}}, \boldsymbol{x}; \tau_3)$ in the $\boldsymbol{a}_2$ direction can be similarly discussed. Each one of $\hat{\psi}_{n,j_3}(\hat{\boldsymbol{k}}, \boldsymbol{x}; \tau_3)$ with different j_3 will be confined in the $\boldsymbol{a}_2$ direction independently.

Suppose B' is an orthorhombic parallelogram with surfaces oriented in the $\boldsymbol{a}_1$, $\boldsymbol{a}_2$, or the film surface direction[3] and having a rectangular bottom face at $x_3 = \tau_3$, a rectangular top face at $x_3 = \tau_3 + N_3$, a front face perpendicularly intersecting the $\boldsymbol{a}_2$ axis at $\tau_2 \boldsymbol{a}_2$ and a rear face perpendicularly intersecting it at $(\tau_2 + 1)\boldsymbol{a}_2$, and a left face and a right face separated by $\boldsymbol{a}_1$ and perpendicular to the $\boldsymbol{a}_1$ axis, as shown in Fig. 6.2. The function set $\bar{\phi}_{j_3}(\bar{\boldsymbol{k}}, \boldsymbol{x}; \tau_2, \tau_3)$ is defined by the condition that each function is zero at the bottom face and top face of B' and behaves as a Bloch stationary state with a wave number $j_3/N_3\ \pi|\boldsymbol{b}_3|$ in the $\boldsymbol{b}_3$ direction as $\hat{\psi}_{j_3}(\hat{\boldsymbol{k}}, \boldsymbol{x}; \tau_3)$,[4] is zero at the front face and the rear face of B', and $\bar{\phi}_{j_3}(\bar{\boldsymbol{k}}, \boldsymbol{x} + \boldsymbol{a}_1; \tau_2, \tau_3) = \mathrm{e}^{\mathrm{i}k_1} \bar{\phi}_{j_3}(\bar{\boldsymbol{k}}, \boldsymbol{x}; \tau_2, \tau_3)$, where $-\pi < k_1 \leq \pi$. The eigenvalues and eigenfunctions of (5.1) under this condition are denoted by $\bar{\lambda}_{n,j_3}(\bar{\boldsymbol{k}}; \tau_2)$ and $\bar{\phi}_{n,j_3}(\bar{\boldsymbol{k}}, \boldsymbol{x}; \tau_2, \tau_3)$, where $n = 0, 1, 2....$

For each eigenvalue $\bar{\lambda}_{n,j_3}(\bar{\boldsymbol{k}}; \tau_2)$ defined by (5.1) and this condition, similar to Theorem 6.1 we have the following theorem connecting $\bar{\lambda}_{n,j_3}(\bar{\boldsymbol{k}}; \tau_2)$ with the eigenvalues $\hat{\Lambda}_{n,j_3}(\hat{\boldsymbol{k}})$ in (5.32) of $\hat{\psi}_{n,j_3}(\hat{\boldsymbol{k}}, \boldsymbol{x}; \tau_3)$.

Theorem 6.2.

$$\bar{\lambda}_{n,j_3}(\bar{\boldsymbol{k}}; \tau_2) \geq \hat{\Lambda}_{n,j_3}(\hat{\boldsymbol{k}}) \quad \text{for } (\bar{\boldsymbol{k}} - \hat{\boldsymbol{k}}) \cdot \boldsymbol{a}_1 = 0. \tag{6.16}$$

As in (6.4), in (6.16) $\bar{\boldsymbol{k}}$ is a wave vector in the wire direction and $\hat{\boldsymbol{k}}$ is a wave vector in the film plane. In (6.16), $\bar{\boldsymbol{k}}$ and $\hat{\boldsymbol{k}}$ have the same component in the wire direction $\boldsymbol{a}_1$. Theorem 6.2 can be proved very similar to Theorem 6.1, since $\hat{\psi}_{n,j_3}(\hat{\boldsymbol{k}}, \boldsymbol{x}; \tau_3)$ with different j_3 are orthogonal to each other, thus each one of $\hat{\psi}_{n,j_3}(\hat{\boldsymbol{k}}, \boldsymbol{x}; \tau_3)$ will be confined in the $\boldsymbol{a}_2$ direction independently.

Theorem 6.2 is similar to Theorem 6.1; the consequences of the quantum confinement of two-dimensional Bloch waves $\hat{\psi}_n(\hat{\boldsymbol{k}}, \boldsymbol{x}; \tau_3)$ in the $\boldsymbol{a}_2$ direction

[3] That is, in the $\hat{\boldsymbol{b}}_1$, $\hat{\boldsymbol{b}}_2$, or $\boldsymbol{b}_3$ direction.

[4] $\hat{\psi}_{j_3}(\hat{\boldsymbol{k}}, \boldsymbol{x}; \tau_3)$ generally can be a (any) linear combination of $\hat{\psi}_{n,j_3}(\hat{\boldsymbol{k}}, \boldsymbol{x}; \tau_3)$ of different n.

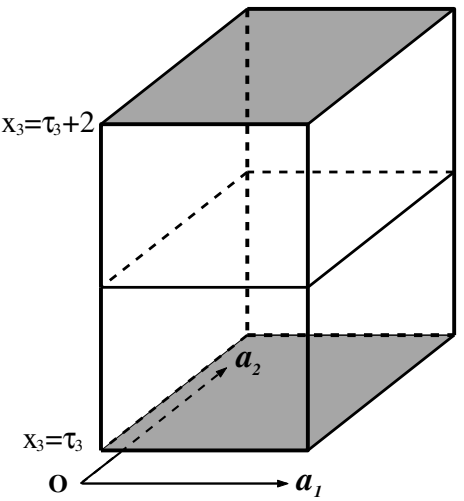

Fig. 6.2. The parallelogram B' for the quantum confinement of $\hat{\psi}_{n,j_3}(\hat{\boldsymbol{k}}, \boldsymbol{x}; \tau_3)$. The two shadowed faces of $\partial B_3'$ determined by $x_3 = \tau_3$ and $x_3 = (\tau_3 + N_3)$ (in the figure is shown the case $N_3 = 2$) are the two faces on which each $\hat{\psi}_{n,j_3}(\hat{\boldsymbol{k}}, \boldsymbol{x}; \tau_3)$ is zero (thus, the specific direction of $\boldsymbol{a}_3$ no longer matters). The two thick-lined faces of $\partial B_2'$ perpendicularly intersecting the $\boldsymbol{a}_2$ axis at $\tau_2 \boldsymbol{a}_2$ and $(\tau_2 + 1)\boldsymbol{a}_2$ are the two faces on which each function $\bar{\phi}_{j_3}(\bar{\boldsymbol{k}}, \boldsymbol{x}; \tau_2, \tau_3)$ is further required to be zero.

due to Theorem 6.1 can be similarly applied to the quantum confinement of two-dimensional Bloch waves $\hat{\psi}_{n,j_3}(\hat{\boldsymbol{k}}, \boldsymbol{x}; \tau_3)$ in the $\boldsymbol{a}_2$ direction.

Because $v(\boldsymbol{x} + \boldsymbol{a}_2) = v(\boldsymbol{x})$, the function $\bar{\phi}_{n,j_3}(\bar{\boldsymbol{k}}, \boldsymbol{x}; \tau_2, \tau_3)$ has the form

$$\bar{\phi}_{n,j_3}(\bar{\boldsymbol{k}}, \boldsymbol{x} + \boldsymbol{a}_2; \tau_2, \tau_3) = \mathrm{e}^{\mathrm{i}k_2} \bar{\phi}_{n,j_3}(\bar{\boldsymbol{k}}, \boldsymbol{x}; \tau_2, \tau_3) \tag{6.17}$$

and k_2 is either complex with a nonzero imaginary part or a real number.

If k_2 is real in (6.17), $\bar{\phi}_{n,j_3}(\bar{\boldsymbol{k}}, \boldsymbol{x}; \tau_2, \tau_3)$ is a $\hat{\psi}_{n',j_3}(\hat{\boldsymbol{k}}, \boldsymbol{x}; \tau_3)$. According to Theorem 6.2, a $\hat{\psi}_{n',j_3}(\hat{\boldsymbol{k}}, \boldsymbol{x}; \tau_3)$ cannot be a $\bar{\phi}_{n,j_3}(\bar{\boldsymbol{k}}, \boldsymbol{x}; \tau_2, \tau_3)$ except in some special cases when $\hat{\psi}_{n',j_3}(\hat{\boldsymbol{k}}, \boldsymbol{x}; \tau_3)$ has a nodal surface intersecting the $\boldsymbol{a}_2$ axis at $\tau_2 \boldsymbol{a}_2$. Therefore, k_2 in (6.17) can be real only in such special cases; in most cases, k_2 in (6.17) is complex with a nonzero imaginary part.

The imaginary part of k_2 in (6.17) can be either positive or negative; this corresponds to that $\bar{\phi}_{n,j_3}(\bar{\boldsymbol{k}}, \boldsymbol{x}; \tau_2, \tau_3)$ decays in either the positive or the negative direction of $\boldsymbol{a}_2$. Such states $\bar{\phi}_{n,j_3}(\bar{\boldsymbol{k}}, \boldsymbol{x}; \tau_2, \tau_3)$ with a nonzero imaginary part of k_2 cannot exist in a film with two-dimensional translational invariance since they are divergent in either the negative or the positive direction of $\boldsymbol{a}_2$. However, they can play a significant role in a quantum wire with a finite size in the $\boldsymbol{a}_2$ direction.

The quantum confinement of two-dimensional Bloch waves $\hat{\psi}_{n,j_3}(\hat{\boldsymbol{k}}, \boldsymbol{x}; \tau_3)$ in the $\boldsymbol{a}_2$ direction will produce two different types of solutions of (6.1) and (6.2) in the quantum wire.

One type of nontrivial solutions can be obtained from (6.17) by assigning

$$\begin{aligned} \bar{\psi}_{n,j_3}(\bar{\boldsymbol{k}}, \boldsymbol{x}; \tau_2, \tau_3) &= c_{N_2,N_3} \bar{\phi}_{n,j_3}(\bar{\boldsymbol{k}}, \boldsymbol{x}; \tau_2, \tau_3) \quad \text{if } \boldsymbol{x} \in \text{ the wire} \\ &= 0 \qquad\qquad\qquad\qquad\qquad\quad \text{if } \boldsymbol{x} \notin \text{ the wire,} \end{aligned} \tag{6.18}$$

where c_{N_2,N_3} is a normalization constant. The corresponding eigenvalue

$$\bar{\Lambda}_{n,j_3}(\bar{\boldsymbol{k}}; \tau_2) = \bar{\lambda}_{n,j_3}(\bar{\boldsymbol{k}}; \tau_2) \tag{6.19}$$

is dependent on τ_2 and N_3 but not on N_2 and τ_3. A consequence of Theorem 6.2 is that for each bulk energy band n, each j_3, and each wave vector $\bar{\boldsymbol{k}}$, there is one such solution (6.18) of (6.1) and (6.2). This is a surface-like state since $\bar{\phi}_{n,j_3}(\bar{\boldsymbol{k}}, \boldsymbol{x}; \tau_2, \tau_3)$ decays in either the positive or negative direction of $\boldsymbol{a}_2$ in most cases.

Now, we try to find other solutions of (6.1) and (6.2) from the further quantum confinement of $\hat{\psi}_{n,j_3}(\hat{\boldsymbol{k}}, \boldsymbol{x}; \tau_3)$. We can expect that there are stationary Bloch states in the $\boldsymbol{a}_2$ direction, formed due to the multiple reflections of $\hat{\psi}_{n,j_3}(\hat{\boldsymbol{k}}, \boldsymbol{x}; \tau_3)$ between two boundary surfaces of the wire perpendicular to the $\boldsymbol{a}_2$ axis.

In the many quantum films we discussed in Chapter 5 in (5.32)

$$\hat{\Lambda}_{n,j_3}(k_1\bar{\boldsymbol{b}}_1 + k_2\hat{\boldsymbol{b}}_2) = \hat{\Lambda}_{n,j_3}(k_1\bar{\boldsymbol{b}}_1 - k_2\hat{\boldsymbol{b}}_2) \tag{6.20}$$

is true; thus, in general,

$$\begin{aligned} f_{n,k_1,k_2,j_3}(\boldsymbol{x}; \tau_3) &= c_+ \hat{\psi}_{n,j_3}(k_1\bar{\boldsymbol{b}}_1 + k_2\hat{\boldsymbol{b}}_2, \boldsymbol{x}; \tau_3) \\ &\quad + c_- \hat{\psi}_{n,j_3}(k_1\bar{\boldsymbol{b}}_1 - k_2\hat{\boldsymbol{b}}_2, \boldsymbol{x}; \tau_3), \quad 0 < k_2 < \pi, \end{aligned}$$

where the $c_\pm$ are not zero, is a non-trivial solution of (6.1) due to (6.20). It is easy to see that $f_{n,k_1,k_2,j_3}(\boldsymbol{x}; \tau_3)$ is a one-dimensional Bloch wave with a wave vector $\bar{\boldsymbol{k}} = k_1\bar{\boldsymbol{b}}_1$ in the wire direction:

$$f_{n,k_1,k_2,j_3}(\boldsymbol{x} + \boldsymbol{a}_1; \tau_3) = \mathrm{e}^{\mathrm{i}k_1} f_{n,k_1,k_2,j_3}(\boldsymbol{x}; \tau_3), \quad -\pi < k_1 \le \pi,$$

due to (5.31). To be a solution of (6.1) and (6.2), the function $f_{n,k_1,k_2,j_3}(\boldsymbol{x}; \tau_3)$ is required to be zero at the front face and the rear face of the wire. By writing the front face equation of the wire as $x_2 = x_{2,f}(x_1, x_3)$ and the rear face equation of the wire as $x_2 = x_{2,r}(x_1, x_3)$, we should have

$$\begin{aligned} &c_+ \hat{\psi}_{n,j_3}[k_1\bar{\boldsymbol{b}}_1 + k_2\hat{\boldsymbol{b}}_2, \boldsymbol{x} \in x_{2,f}(x_1, x_3); \tau_3] \\ &\qquad + c_- \hat{\psi}_{n,j_3}[k_1\bar{\boldsymbol{b}}_1 - k_2\hat{\boldsymbol{b}}_2, \boldsymbol{x} \in x_{2,f}(x_1, x_3); \tau_3] = 0, \\ &c_+ \hat{\psi}_{n,j_3}[k_1\bar{\boldsymbol{b}}_1 + k_2\hat{\boldsymbol{b}}_2, \boldsymbol{x} \in x_{2,r}(x_1, x_3); \tau_3] \\ &\qquad + c_- \hat{\psi}_{n,j_3}[k_1\bar{\boldsymbol{b}}_1 - k_2\hat{\boldsymbol{b}}_2, \boldsymbol{x} \in x_{2,r}(x_1, x_3); \tau_3] = 0. \end{aligned}$$

Since $x_{2,r}(x_1, x_3) = x_{2,f}(x_1, x_3) + N_2$, we have

$$\hat{\psi}_{n,j_3}[k_1\bar{\boldsymbol{b}}_1 + k_2\hat{\boldsymbol{b}}_2, \boldsymbol{x} \in x_{2,r}(x_1, x_3); \tau_3] \\ = \mathrm{e}^{\mathrm{i}k_2 N_2}\hat{\psi}_{n,j_3}[k_1\bar{\boldsymbol{b}}_1 + k_2\hat{\boldsymbol{b}}_2, \boldsymbol{x} \in x_{2,f}(x_1, x_3); \tau_3]$$

and

$$\hat{\psi}_{n,j_3}[k_1\bar{\boldsymbol{b}}_1 - k_2\hat{\boldsymbol{b}}_2, \boldsymbol{x} \in x_{2,r}(x_1, x_3); \tau_3] \\ = \mathrm{e}^{-\mathrm{i}k_2 N_2}\hat{\psi}_{n,j_3}[k_1\bar{\boldsymbol{b}}_1 - k_2\hat{\boldsymbol{b}}_2, \boldsymbol{x} \in x_{2,f}(x_1, x_3); \tau_3]$$

due to (5.31). Therefore, for $c_\pm$ not both zero, $\mathrm{e}^{\mathrm{i}k_2 N_2} - \mathrm{e}^{-\mathrm{i}k_2 N_2} = 0$ has to be true for these stationary Bloch states, independent of τ_2.

Therefore, the stationary Bloch state solutions of (6.1) and (6.2) from the quantum confinement of $\hat{\psi}_{n,j_3}(\hat{\boldsymbol{k}}, \boldsymbol{x}; \tau_3)$ should have the form

$$\bar{\psi}_{n,j_2,j_3}(\bar{\boldsymbol{k}}, \boldsymbol{x}; \tau_2, \tau_3) = f_{n,k_1,\kappa_2,j_3}(\boldsymbol{x}; \tau_2, \tau_3) \quad \text{if } \boldsymbol{x} \in \text{ the wire} \\ = 0 \qquad\qquad\qquad\qquad\quad \text{if } \boldsymbol{x} \notin \text{ the wire}, \tag{6.21}$$

where

$$f_{n,k_1,k_2,j_3}(\boldsymbol{x}; \tau_2, \tau_3) = c_{n,k_1,k_2,j_3;\tau_2}\hat{\psi}_{n,j_3}(k_1\bar{\boldsymbol{b}}_1 + k_2\hat{\boldsymbol{b}}_2, \boldsymbol{x}; \tau_3) \\ + c_{n,k_1,-k_2,j_3;\tau_2}\hat{\psi}_{n,j_3}(k_1\bar{\boldsymbol{b}}_1 - k_2\hat{\boldsymbol{b}}_2, \boldsymbol{x}; \tau_3),$$

$c_{n,k_1,\pm k_2,j_3;\tau_2}$ are dependent on τ_2, and

$$\kappa_2 = j_2\ \pi/N_2, \quad j_2\ = 1, 2, ..., N_2 - 1;$$

here, j_2 is a subband index, as in (6.13). The stationary Bloch states $\bar{\psi}_{n,j_2,j_3}(\bar{\boldsymbol{k}}, \boldsymbol{x}; \tau_2, \tau_3)$ satisfying (6.1) and (6.2) have the energies

$$\bar{\Lambda}_{n,j_2,j_3}(\bar{\boldsymbol{k}}) = \hat{\Lambda}_{n,j_3}(\bar{\boldsymbol{k}} + \kappa_2\hat{\boldsymbol{b}}_2). \tag{6.22}$$

Each energy $\bar{\Lambda}_{n,j_2,j_3}(\bar{\boldsymbol{k}})$ for this case is dependent on N_2 and N_3, the wire size, but independent of the wire boundaries τ_2 and τ_3. There are $(N_2-1)(N_3-1)$ such stationary Bloch states for each n and $\bar{\boldsymbol{k}}$ in the quantum wire. Their energies map the $\hat{\Lambda}_{n,j_3}(\hat{\boldsymbol{k}})$ exactly and thus also map the corresponding bulk energy band $\varepsilon_n(\boldsymbol{k})$ exactly by (5.32): $\bar{\Lambda}_{n,j_2,j_3}(\bar{\boldsymbol{k}}) = \hat{\Lambda}_{n,j_3}(\bar{\boldsymbol{k}} + \kappa_2\hat{\boldsymbol{b}}_2) = \varepsilon_n(\bar{\boldsymbol{k}} + \kappa_2\hat{\boldsymbol{b}}_2 + \kappa_3\boldsymbol{b}_3)$. Therefore, $\bar{\psi}_{n,j_2,j_3}(\bar{\boldsymbol{k}}, \boldsymbol{x}; \tau_2, \tau_3)$ can be considered as bulk-like states in the quantum wire.

Similar to (6.15), due to (6.16), (6.19), and (6.22) in general in an ideal quantum wire,

$$\bar{\Lambda}_{n,j_3}(\bar{\boldsymbol{k}}; \tau_2) > \bar{\Lambda}_{n,j_2,j_3}(\bar{\boldsymbol{k}}) \tag{6.23}$$

is true between the energies of a surface-like state and a relevant bulk-like state obtained from the quantum confinement of $\hat{\psi}_{n,j_3}(\hat{\boldsymbol{k}}, \boldsymbol{x}; \tau_3)$.

We have seen that for the further quantum confinement of two-dimensional Bloch waves $\hat{\psi}_n(\hat{\boldsymbol{k}}, \boldsymbol{x}; \tau_3)$ or $\hat{\psi}_{n,j_3}(\hat{\boldsymbol{k}}, \boldsymbol{x}; \tau_3)$, each one will produce two different types of one-dimensional Bloch waves in an ideal quantum wire. For an

ideal rectangular quantum wire obtained from a quantum film of N_3 layers in the $\boldsymbol{a}_3$ direction and with the bottom face defined by $\tau_3\boldsymbol{a}_3$ being further confined by two boundary faces in the $\boldsymbol{a}_2$ direction defined by τ_2 and $N_2\boldsymbol{a}_2$ apart from each other, there are four sets of electronic states in the quantum wire:

The energy $\bar{\Lambda}_{n,j_2,j_3}(\bar{\boldsymbol{k}})$ [(6.22)] of each electronic state $\bar{\psi}_{n,j_2,j_3}(\bar{\boldsymbol{k}},\boldsymbol{x};\tau_2,\tau_3)$ in (6.21) depends on N_2 and N_3 but not on τ_2 and τ_3. The energies of these states map the energy band of the bulk $\varepsilon_n(\boldsymbol{k})$ exactly. These states are bulk-like states and there are $(N_2-1)(N_3-1)$ such states in the quantum wire for each bulk energy band n and each $\bar{\boldsymbol{k}}$.

The energy $\bar{\Lambda}_{n,j_2}(\bar{\boldsymbol{k}};\tau_3)$ [(6.14)] of each electronic state $\bar{\psi}_{n,j_2}(\bar{\boldsymbol{k}},\boldsymbol{x};\tau_2,\tau_3)$ in (6.12) depends on N_2 and τ_3 but not on τ_2 and N_3. The energies of these states map the surface-like energy subband $\hat{\Lambda}_n(\hat{\boldsymbol{k}};\tau_3)$ in the film exactly. These states are surface-like states and there are (N_2-1) such states in the quantum wire for each bulk energy band n and each $\bar{\boldsymbol{k}}$.

The energy $\bar{\Lambda}_{n,j_3}(\bar{\boldsymbol{k}};\tau_2)$ [(6.19)] of each state $\bar{\psi}_{n,j_3}(\bar{\boldsymbol{k}},\boldsymbol{x};\tau_2,\tau_3)$ in (6.18) depends on N_3 and τ_2 but not on τ_3 and N_2. These are also surface-like states and there are (N_3-1) such states in the quantum wire for each bulk energy band n and each $\bar{\boldsymbol{k}}$.

The energy $\bar{\Lambda}_n(\bar{\boldsymbol{k}};\tau_2,\tau_3)$ [(6.9)] of each electronic state $\bar{\psi}_n(\bar{\boldsymbol{k}},\boldsymbol{x};\tau_2,\tau_3)$ in (6.8) depends on τ_2 and τ_3 but not on N_2 and N_3. These are side-like states. Although a rectangular quantum wire always has *four* sides, there is only one such side-like state for each bulk energy band n and each $\bar{\boldsymbol{k}}$.

We have seen again that the effect of the quantum confinement in one more direction actually is to *always have one and only one* boundary-dependent sub-subband for each subband of the electronic states in the film obtained in Chapter 5; the energies of all other states can be directly obtained either from the $\hat{\Lambda}_{n,j_3}(\hat{\boldsymbol{k}})$ (which originally is determined by the energy band structure $\varepsilon_n(\boldsymbol{k})$ of the bulk crystal by (5.32)) by (6.22) or from the surface-like band structure, such as $\hat{\Lambda}_n(\hat{\boldsymbol{k}};\tau_3)$ by (6.14). In general, a boundary-dependent state always has a higher energy than the relevant size-dependent states.

The results in Sections 6.2 and 6.3 were obtained by a specific quantum confinement order. In order to obtain a more comprehensive understanding on the electronic states in an ideal quantum wire, we need to consider the results obtained in two different confinement orders.

6.4 Quantum Wires of Crystals with a sc, tetr, or ortho Bravais Lattice

We expect that the simplest cases where the theory in this chapter is applicable are the rectangular quantum wires of crystals with a sc, tetr, or ortho Bravais lattice in which (5.14), (6.10), and (6.20) are true. In these crystals, the three primitive lattice vectors $\boldsymbol{a}_1$, $\boldsymbol{a}_2$, and $\boldsymbol{a}_3$ are perpendicular to each

other and equivalent; consequently, the three primitive lattice vectors in k space, $\boldsymbol{b}_1$, $\boldsymbol{b}_2$, and $\boldsymbol{b}_3$ are also perpendicular to each other and equivalent. Such a quantum wire in the direction of $\boldsymbol{a}_1$ can be considered as a film with the film plane defined by $\boldsymbol{a}_1$ and $\boldsymbol{a}_2$ being further confined in the $\boldsymbol{a}_2$ direction as we have done so far. Equivalently, it can also be considered as a film with the film plane defined by $\boldsymbol{a}_1$ and $\boldsymbol{a}_3$ being further confined in the $\boldsymbol{a}_3$ direction. If we consider the electronic states in the quantum wire in the latter way, we will obtain that

$$\begin{aligned} \bar{\psi}_{n,j_3}(\bar{\boldsymbol{k}}, \boldsymbol{x}; \tau_2, \tau_3) &= f_{n,k_1,\kappa_3}(\boldsymbol{x}; \tau_2, \tau_3) \quad \text{if } \boldsymbol{x} \in \text{ the wire} \\ &= 0 \qquad\qquad\qquad\quad \text{if } \boldsymbol{x} \notin \text{ the wire} \end{aligned} \tag{6.24}$$

instead of (6.18), where $\bar{\boldsymbol{k}} = k_1 \bar{\boldsymbol{b}}_1$ and

$$\begin{aligned} f_{n,k_1,k_3}(\boldsymbol{x}; \tau_2, \tau_3) = {} & c_{n,k_1,k_3;\tau_3} \hat{\psi}_n(k_1 \bar{\boldsymbol{b}}_1 + k_3 \boldsymbol{b}_3, \boldsymbol{x}; \tau_2) \\ & + c_{n,k_1,-k_3;\tau_3} \hat{\psi}_n(k_1 \bar{\boldsymbol{b}}_1 - k_3 \boldsymbol{b}_3, \boldsymbol{x}; \tau_2), \end{aligned}$$

$c_{n,k_1,\pm k_3;\tau_3}$ are dependent on τ_3 and κ_3 and j_3 are given by (5.30). Equation (6.24) gives a more specific relationship between the surface-like states $\bar{\psi}_{n,j_3}(\bar{\boldsymbol{k}}, \boldsymbol{x}; \tau_2, \tau_3)$ in the quantum wire and the surface-like states $\hat{\psi}_n(\hat{\boldsymbol{k}}, \boldsymbol{x}; \tau_2)$ in the quantum film with a film plane defined by $\boldsymbol{a}_1$ and $\boldsymbol{a}_3$. Correspondingly,

$$\bar{\Lambda}_{n,j_3}(\bar{\boldsymbol{k}}; \tau_2) = \hat{\Lambda}_n(\bar{\boldsymbol{k}} + \kappa_3 \boldsymbol{b}_3; \tau_2) \tag{6.25}$$

can be obtained instead of (6.19). Equation (6.25) gives a more specific relationship between the surface-like subbands $\bar{\Lambda}_{n,j_3}(\bar{\boldsymbol{k}}; \tau_2)$ in the quantum wire and the surface-like subband $\hat{\Lambda}_n(\hat{\boldsymbol{k}}; \tau_2)$ in the quantum film with a film plane defined by $\boldsymbol{a}_1$ and $\boldsymbol{a}_3$.

Similar to (6.15) and (6.23), we can obtain that

$$\bar{\Lambda}_n(\bar{\boldsymbol{k}}; \tau_2, \tau_3) > \bar{\Lambda}_{n,j_3}(\bar{\boldsymbol{k}}; \tau_2) \tag{6.26}$$

and

$$\bar{\Lambda}_{n,j_2}(\bar{\boldsymbol{k}}; \tau_3) > \bar{\Lambda}_{n,j_2,j_3}(\bar{\boldsymbol{k}}). \tag{6.27}$$

Therefore, for an ideal rectangular quantum wire of crystals with a sc, tetr, or ortho Bravais lattice, if its two boundary faces in the $\boldsymbol{a}_2$ direction are defined by τ_2 and are $N_2 \boldsymbol{a}_2$ apart from each other, the two other boundary faces in the $\boldsymbol{a}_3$ direction are defined by τ_3 and are $N_3 \boldsymbol{a}_3$ apart from each other, for each bulk energy band n, there are the following:
$(N_2 - 1)(N_3 - 1)$ bulk-like subbands with energies

$$\bar{\Lambda}_{n,j_2,j_3}(\bar{\boldsymbol{k}}) = \varepsilon_n \left(\bar{\boldsymbol{k}} + \frac{j_2 \pi}{N_2} \boldsymbol{b}_2 + \frac{j_3 \pi}{N_3} \boldsymbol{b}_3 \right) \tag{6.28}$$

from (6.22) and (5.32);
$(N_3 - 1)$ surface-like subbands with energies

$$\bar{\Lambda}_{n,j_3}(\bar{\boldsymbol{k}};\tau_2) = \hat{\Lambda}_n\left(\bar{\boldsymbol{k}} + \frac{j_3\pi}{N_3}\boldsymbol{b}_3;\tau_2\right) \tag{6.29}$$

from (6.25) and (5.30);
$(N_2 - 1)$ surface-like subbands with energies

$$\bar{\Lambda}_{n,j_2}(\bar{\boldsymbol{k}};\tau_3) = \hat{\Lambda}_n\left(\bar{\boldsymbol{k}} + \frac{j_2\pi}{N_2}\boldsymbol{b}_2;\tau_3\right) \tag{6.30}$$

from (6.14) and (6.13);
one side-like subband with energy

$$\bar{\Lambda}_n(\bar{\boldsymbol{k}};\tau_2,\tau_3) = \bar{\lambda}_n(\bar{\boldsymbol{k}};\tau_2,\tau_3) \tag{6.31}$$

from (6.9). Here, $j_2 = 1, 2, ..., N_2 - 1$ and $j_3 = 1, 2, ..., N_3 - 1$. $\bar{\boldsymbol{k}}$ is a wave vector in the wire direction and $\hat{\Lambda}_n(\hat{\boldsymbol{k}};\tau_3)$ is the surface-like band structure of a quantum film with the film plane oriented in the $\boldsymbol{a}_3$ direction with a wave vector $\hat{\boldsymbol{k}}$ in the film plane. $\hat{\Lambda}_n(\hat{\boldsymbol{k}};\tau_2)$ is the surface-like band structure of a quantum film with the film plane oriented in the $\boldsymbol{a}_2$ direction with a wave vector $\hat{\boldsymbol{k}}$ in the film plane.

Between energies of the electronic states with the same bulk energy band index n and with the same wave vector $\bar{\boldsymbol{k}}$ in the quantum wire, the following general relations exist:

$$\begin{aligned}
\bar{\Lambda}_n(\bar{\boldsymbol{k}};\tau_2,\tau_3) &> \bar{\Lambda}_{n,j_2}(\bar{\boldsymbol{k}};\tau_3),\\
\bar{\Lambda}_n(\bar{\boldsymbol{k}};\tau_2,\tau_3) &> \bar{\Lambda}_{n,j_3}(\bar{\boldsymbol{k}};\tau_2),\\
\bar{\Lambda}_{n,j_3}(\bar{\boldsymbol{k}};\tau_2) &> \bar{\Lambda}_{n,j_2,j_3}(\bar{\boldsymbol{k}}),\\
\bar{\Lambda}_{n,j_2}(\bar{\boldsymbol{k}};\tau_3) &> \bar{\Lambda}_{n,j_2,j_3}(\bar{\boldsymbol{k}}),
\end{aligned}$$

from (6.15), (6.26), (6.23), and (6.27) respectively.

However, probably the practically more interesting cases are quantum wires of crystals with a fcc or bcc Bravais lattice in which (5.21), (6.10), and (6.20) are true. For these crystals, the choice of primitive lattice vectors for films depends on the film direction, as we have seen in Section 5.6. In the following, we try to obtain predictions on the electronic states in several such quantum wires, based on the results obtained in Sections 6.1 to 6.3.

6.5 fcc Quantum Wires with (110) and (001) Surfaces

We consider a fcc $[1\bar{1}0]$ quantum wire with (110) and (001) surfaces and having a rectangular cross section $N_{110}a/\sqrt{2} \times N_{001}a$, where N_{110} and N_{001} are two positive integers. The electronic states in such a quantum wire can be considered as the electronic states in a (001) fcc quantum film of thickness $N_{001}a$ discussed in Section 5.6.1 further confined by two (110) boundary surfaces. They can also equivalently be considered as the electronic states in a (110) fcc quantum film of thickness $N_{110}a/\sqrt{2}$, discussed in Section 5.6.2, further confined by two (001) boundary surfaces.

6.5.1 fcc Quantum Wires Obtained from (001) Films Further Confined by Two (110) Surfaces

For a fcc quantum wire obtained from a (001) film further confined by two (110) surfaces, we begin with a fcc (001) film of thickness $N_{001}a$ and choose the primitive lattice vectors as in (5.38): $\boldsymbol{a}_1 = a/2(1,-1,0)$ and $\boldsymbol{a}_2 = a/2(1,1,0)$, $\boldsymbol{a}_3 = a/2(1,0,1)$ and thus $\boldsymbol{b}_1 = 1/a(1,-1,-1)$, $\boldsymbol{b}_2 = 1/a(1,1,-1)$, and $\boldsymbol{b}_3 = 1/a(0,0,2)$. Correspondingly, $\hat{\boldsymbol{b}}_1 = 1/a(1,-1,0)$ and $\hat{\boldsymbol{b}}_2 = 1/a(1,1,0)$. Here, a is the lattice constant.

Now, we have a (001) film with $N_3 = 2N_{001}$. From the results obtained in Section 5.6.1, in such a film for each bulk energy band there are $2N_{001}-1$ bulk-like subbands with energies

$$\hat{\Lambda}_{n,j_3}(k_1\hat{\boldsymbol{b}}_1 + k_2\hat{\boldsymbol{b}}_2) = \varepsilon_n\left[k_1\hat{\boldsymbol{b}}_1 + k_2\hat{\boldsymbol{b}}_2 + \frac{j_3\pi}{N_{001}a}(0,0,1)\right]$$

by (5.39), where

$$j_3 = 1, 2, ..., 2N_{001} - 1,$$

and one surface-like subband whose energy

$$\hat{\Lambda}_n(k_1\hat{\boldsymbol{b}}_1 + k_2\hat{\boldsymbol{b}}_2; \tau_{001}) = \hat{\lambda}_n(k_1\hat{\boldsymbol{b}}_1 + k_2\hat{\boldsymbol{b}}_2; \tau_{001})$$

by (5.34) since now $\tau_3 = \tau_{001}$. $\hat{\boldsymbol{k}} = k_1\hat{\boldsymbol{b}}_1 + k_2\hat{\boldsymbol{b}}_2$ is a wave vector in the (001) plane.

Then we consider the (001) fcc quantum film further confined by two (110) boundary surfaces which are $N_{110}a/\sqrt{2}$ apart. The energies $\hat{\Lambda}_{n,j_3}(\hat{\boldsymbol{k}})$ of bulk-like states $\hat{\psi}_{n,j_3}(\hat{\boldsymbol{k}}, \boldsymbol{x}; \tau_3)$ in the (001) quantum film satisfy (6.20): $\hat{\Lambda}_{n,j_3}(k_1\bar{\boldsymbol{b}}_1 + k_2\hat{\boldsymbol{b}}_2) = \hat{\Lambda}_{n,j_3}(k_1\bar{\boldsymbol{b}}_1 - k_2\hat{\boldsymbol{b}}_2)$. We also expect that the energies $\hat{\Lambda}_n(\hat{\boldsymbol{k}}; \tau_{001})$ of surface-like states $\hat{\psi}_n(\hat{\boldsymbol{k}}, \boldsymbol{x}; \tau_{001})$ in the fcc (001) film satisfy (6.10): $\hat{\Lambda}_n(k_1\bar{\boldsymbol{b}}_1 + k_2\hat{\boldsymbol{b}}_2; \tau_{001}) = \hat{\Lambda}_n(k_1\bar{\boldsymbol{b}}_1 - k_2\hat{\boldsymbol{b}}_2; \tau_{001})$ (see Section 5.6.1). Therefore, the results obtained in Sections 6.2 and 6.3 can be applied. We now have $N_2 = N_{110}$ and $\tau_2 = \tau_{110}$; thus, for each bulk energy band, there are four different sets of one-dimensional Bloch waves in the quantum wire.

From (6.22), there are $(N_{110}-1)(2N_{001}-1)$ bulk-like subbands for each bulk energy band n in the quantum wire; each subband has the energy

$$\bar{\Lambda}_{n,j_{110},j_3}(\bar{\boldsymbol{k}}) = \varepsilon_n\left[\bar{\boldsymbol{k}} + \frac{j_{110}\pi}{N_{110}a}\,(1,1,0) + \frac{j_3\pi}{N_{001}a}\,(0,0,1)\right], \tag{6.32}$$

where $\bar{\boldsymbol{k}}$ is a wave vector in the wire direction $\boldsymbol{a}_1$,

$$j_3 = 1, 2, ..., 2N_{001} - 1$$

and

$$j_{110} = 1, 2, ..., N_{110} - 1. \tag{6.33}$$

By defining

$$\begin{aligned} j_{001} &= j_3 \qquad\qquad \text{if } j_3 < N_{001} \\ &= 2N_{001} - j_3 \quad \text{if } j_3 > N_{001}, \end{aligned} \tag{6.34}$$

where

$$j_{001} = 1, 2, ..., N_{001} - 1; \tag{6.35}$$

those $(N_{110}-1)(2N_{001}-1)$ bulk-like subbands in (6.32) in the quantum wire can be separated to three subsets according to (6.34). They are as follows:
$(N_{110}-1)(N_{001}-1)$ bulk-like subbands in the quantum wire with energies

$$\bar{\Lambda}^{bk,a}_{n,j_{110},j_{001}}(\bar{\boldsymbol{k}}) = \varepsilon_n \left[\bar{\boldsymbol{k}} + \frac{j_{110}\pi}{N_{110}a}\,(1,1,0) + \frac{j_{001}\pi}{N_{001}a}\,(0,0,1) \right], \tag{6.32a}$$

$(N_{110}-1)$ bulk-like subbands in the quantum wire with energies

$$\bar{\Lambda}^{bk,b}_{n,j_{110}}(\bar{\boldsymbol{k}}) = \varepsilon_n \left[\bar{\boldsymbol{k}} + \frac{j_{110}\pi}{N_{110}a}\,(1,1,0) + \frac{\pi}{a}\,(0,0,1) \right], \tag{6.32b}$$

$(N_{110}-1)(N_{001}-1)$ bulk-like subbands in the quantum wire with energies[5]

$$\begin{aligned} \bar{\Lambda}^{bk,c}_{n,j_{110},j_{001}}(\bar{\boldsymbol{k}}) &= \varepsilon_n \left[\bar{\boldsymbol{k}} + \frac{j_{110}\pi}{N_{110}a}\,(1,1,0) - \frac{j_{001}\pi}{N_{001}a}\,(0,0,1) + \frac{2\pi}{a}\,(0,0,1) \right] \\ &= \varepsilon_n \left[\bar{\boldsymbol{k}} + \frac{j_{110}\pi}{N_{110}a}\,(1,1,0) + \frac{j_{001}\pi}{N_{001}a}\,(0,0,1) + \frac{2\pi}{a}\,(0,0,1) \right]. \end{aligned} \tag{6.32c}$$

From (6.19), for each bulk energy band n, there are $2N_{001}-1$ surface-like subbands in the quantum wire due to the existence of (110) boundary surfaces with the energies

$$\bar{\Lambda}_{n,j_3}(\bar{\boldsymbol{k}};\tau_{110}) = \bar{\lambda}_{n,j_3}(\bar{\boldsymbol{k}};\tau_{110}). \tag{6.36}$$

By (6.34), these $2N_{001}-1$ surface-like bands in (6.36) can be separated in to three subsets. They are as follows:
$N_{001}-1$ surface-like subbands in the quantum wire with energies

$$\bar{\Lambda}^{sf,1}_{n,j_{001}}(\bar{\boldsymbol{k}};\tau_{110}) = \bar{\lambda}_{n,j_{001}}(\bar{\boldsymbol{k}};\tau_{110}), \tag{6.36a}$$

one surface-like subband in the quantum wire with energy

$$\bar{\Lambda}^{sf,2}_{n,N_{001}}(\bar{\boldsymbol{k}};\tau_{110}) = \bar{\lambda}_{n,N_{001}}(\bar{\boldsymbol{k}};\tau_{110}), \tag{6.36b}$$

[5]Since for cubic semiconductors and fcc metals, in general, $\varepsilon_n(k_x,k_y,k_z) = \varepsilon_n(k_x,k_y,-k_z)$ and $1/a(0,0,2)$ is a reciprocal lattice vector for crystals with a fcc Bravais lattice.

$N_{001}-1$ surface-like subbands in the quantum wire with energies

$$\bar{\Lambda}^{sf,3}_{n,j_{001}}(\bar{\boldsymbol{k}};\tau_{110})=\bar{\lambda}_{n,2N_{001}-j_{001}}(\bar{\boldsymbol{k}};\tau_{110}). \tag{6.36c}$$

From (6.14), due to the existence of (001) boundary surfaces for each bulk energy band n, there are $N_{110}-1$ surface-like subbands in the quantum wire with energies

$$\bar{\Lambda}^{sf,a}_{n,j_{110}}(\bar{\boldsymbol{k}};\tau_{001})=\hat{\Lambda}_n\left[\bar{\boldsymbol{k}}+\frac{j_{110}\pi}{N_{110}a}\,(1,1,0);\tau_{001}\right]. \tag{6.37}$$

From (6.9), for each bulk energy band n, there is one side-like subband in the quantum wire with energy

$$\bar{\Lambda}^{sd}_{n}(\bar{\boldsymbol{k}};\tau_{110},\tau_{001})=\bar{\lambda}_n(\bar{\boldsymbol{k}};\tau_{110},\tau_{001}). \tag{6.38}$$

6.5.2 fcc Quantum Wires Obtained from (110) Films Further Confined by Two (001) Surfaces

For a fcc quantum wire obtained from a (110) film further confined by two (001) surfaces, we begin with a (110) film and the primitive lattice vectors can be chosen as in (5.40): $\boldsymbol{a}_1=a/2(1,-1,0)$, $\boldsymbol{a}_2=a(0,0,-1)$, and $\boldsymbol{a}_3=a/2(0,1,1)$ and, thus, $\boldsymbol{b}_1=1/a(2,0,0)$, $\boldsymbol{b}_2=1/a(1,1,-1)$, and $\boldsymbol{b}_3=1/a(2,2,0)$. Correspondingly, $\hat{\boldsymbol{b}}_1=1/a(1,-1,0)$ and $\hat{\boldsymbol{b}}_2=1/a(0,0,-1)$.

For a fcc quantum wire with a rectangular cross section $N_{110}a/\sqrt{2}\times N_{001}a$, we now have $N_3=2N_{110}$, $\tau_3=\tau_{110}$, and $N_2=N_{001}$, $\tau_2=\tau_{001}$. The energies $\hat{\Lambda}_{n,j_3}(\hat{\boldsymbol{k}})$ of bulk-like states $\hat{\psi}_{n,j_3}(\hat{\boldsymbol{k}},\boldsymbol{x};\tau_{110})$ in the (110) quantum film satisfy (6.20): $\hat{\Lambda}_{n,j_3}(k_1\bar{\boldsymbol{b}}_1+k_2\hat{\boldsymbol{b}}_2)=\hat{\Lambda}_{n,j_3}(k_1\bar{\boldsymbol{b}}_1-k_2\hat{\boldsymbol{b}}_2)$. We also expect that the energies $\hat{\Lambda}_n(\hat{\boldsymbol{k}};\tau_{110})$ of surface-like states $\hat{\psi}_n(\hat{\boldsymbol{k}},\boldsymbol{x};\tau_{110})$ in the fcc (110) film satisfy (6.10): $\hat{\Lambda}_n(k_1\bar{\boldsymbol{b}}_1+k_2\hat{\boldsymbol{b}}_2;\tau_{110})=\hat{\Lambda}_n(k_1\bar{\boldsymbol{b}}_1-k_2\hat{\boldsymbol{b}}_2;\tau_{110})$ (see Section 5.6.2). Therefore, the results obtained in Sections 6.2 and 6.3 can be applied. Similar to the results obtained in Section 6.5.1, for each bulk energy band n we have four different sets of one-dimensional Bloch waves in the quantum wire.

From (6.22), for each bulk energy band n there are $(N_{001}-1)(2N_{110}-1)$ bulk-like subbands in the quantum wire; each subband has the energy

$$\bar{\Lambda}_{n,j_{001},j_3}(\bar{\boldsymbol{k}})=\varepsilon_n\left[\bar{\boldsymbol{k}}+\frac{j_{001}\pi}{N_{001}a}\,(0,0,1)+\frac{j_3\pi}{N_{110}a}\,(1,1,0)\right], \tag{6.39}$$

where $\bar{\boldsymbol{k}}$ is a wave vector in the wire direction $\boldsymbol{a}_1$,

$$j_{001}=1,2,...,N_{001}-1, \tag{6.40}$$

and

$$j_3=1,2,...,2N_{110}-1.$$

By defining

$$\begin{aligned} j_{110} &= j_3 \qquad\qquad \text{if } j_3 < N_{110} \\ &= 2N_{110} - j_3 \quad \text{if } j_3 > N_{110}, \end{aligned} \tag{6.41}$$

where

$$j_{110} = 1, 2, ..., N_{110} - 1; \tag{6.42}$$

those $(N_{001}-1)(2N_{110}-1)$ bulk-like subbands in (6.39) in the quantum wire can be separated into three subsets according to (6.41) and (6.42). They are as follows:
$(N_{001}-1)(N_{110}-1)$ bulk-like subbands in the quantum wire with energies

$$\bar{\Lambda}^{bk,a}_{n,j_{001},j_{110}}(\bar{\boldsymbol{k}}) = \varepsilon_n \left[\bar{\boldsymbol{k}} + \frac{j_{001}\pi}{N_{001}a}\,(0,0,1) + \frac{j_{110}\pi}{N_{110}a}\,(1,1,0) \right], \tag{6.39a}$$

$(N_{001}-1)$ bulk-like subbands in the quantum wire with energies

$$\bar{\Lambda}^{bk,b}_{n,j_{001}}(\bar{\boldsymbol{k}}) = \varepsilon_n \left[\bar{\boldsymbol{k}} + \frac{j_{001}\pi}{N_{001}a}\,(0,0,1) + \frac{\pi}{a}\,(1,1,0) \right], \tag{6.39b}$$

$(N_{001}-1)(N_{110}-1)$ bulk-like subbands in the quantum wire with energies[6]

$$\begin{aligned} \bar{\Lambda}^{bk,c}_{n,j_{001},j_{110}}(\bar{\boldsymbol{k}}) &= \varepsilon_n \left[\bar{\boldsymbol{k}} + \frac{j_{001}\pi}{N_{001}a}\,(0,0,1) - \frac{j_{110}\pi}{N_{110}a}\,(1,1,0) + \frac{2\pi}{a}\,(1,1,0) \right] \\ &= \varepsilon_n \left[\bar{\boldsymbol{k}} + \frac{j_{001}\pi}{N_{001}a}\,(0,0,1) + \frac{j_{110}\pi}{N_{110}a}\,(1,1,0) + \frac{2\pi}{a}\,(1,1,0) \right]. \end{aligned} \tag{6.39c}$$

From (6.19), for each bulk energy band n there are $2N_{110}-1$ surface-like subbands in the quantum wire due to the existence of two boundary surfaces in the (001) plane with energies

$$\bar{\Lambda}_{n,j_3}(\bar{\boldsymbol{k}};\tau_{001}) = \bar{\lambda}_{n,j_3}(\bar{\boldsymbol{k}};\tau_{001}). \tag{6.43}$$

By (6.41), these $2N_{110}-1$ subbands in (6.43) can be separated into three subsets. They are as follows:
$N_{110}-1$ surface-like subbands in the quantum wire with energies

$$\bar{\Lambda}^{sf,1}_{n,j_{110}}(\bar{\boldsymbol{k}};\tau_{001}) = \bar{\lambda}_{n,j_{110}}(\bar{\boldsymbol{k}};\tau_{001}). \tag{6.43a}$$

one surface-like subband in the quantum wire with energy

$$\bar{\Lambda}^{sf,2}_{n}(\bar{\boldsymbol{k}};\tau_{001}) = \bar{\lambda}_{n,N_{110}}(\bar{\boldsymbol{k}};\tau_{001}), \tag{6.43b}$$

[6]Since for cubic semiconductors and fcc metals, in general, $\varepsilon_n(k_x,k_y,k_z) = \varepsilon_n(k_y,k_x,k_z)$ and $1/a(2,2,0)$ is a reciprocal lattice vector for crystals with a fcc Bravais lattice.

$N_{110}-1$ surface-like subbands in the quantum wire with energies

$$\bar{\Lambda}^{sf,3}_{n,j_{110}}(\bar{\boldsymbol{k}};\tau_{001})=\bar{\lambda}_{n,2N_{110}-j_{110}}(\bar{\boldsymbol{k}};\tau_{001}). \tag{6.43c}$$

From (6.14), due to the existence of (110) boundary surfaces, for each bulk energy band n there are $N_{001}-1$ surface-like subbands in the quantum wire with energies

$$\bar{\Lambda}^{sf,a}_{n,j_{001}}(\bar{\boldsymbol{k}};\tau_{110})=\hat{\Lambda}_n\left[\bar{\boldsymbol{k}}+\frac{j_{001}\pi}{N_{001}a}\,(0,0,1);\tau_{110}\right]. \tag{6.44}$$

From (6.9), for each bulk energy band n there is one side-like subband in the quantum wire with energy

$$\bar{\Lambda}^{sd}_{n}(\bar{\boldsymbol{k}};\tau_{001},\tau_{110})=\bar{\lambda}_n(\bar{\boldsymbol{k}};\tau_{001},\tau_{110}). \tag{6.45}$$

6.5.3 Results Obtained by Combining Sections 6.5.1 and 6.5.2

For a fcc quantum wire with (001) surfaces and (110) surfaces and with a rectangular cross section $N_{110}a/\sqrt{2}\times N_{001}a$, the electronic states are one-dimensional Bloch waves with a wave vector $\bar{\boldsymbol{k}}$ in the $[1\bar{1}0]$ direction. We can consider it either from the method in Section 6.5.1 or from that in Section 6.5.2. However, in each method the whole symmetry of the system has not been considered, since each specific way of choosing the primary lattice vectors does not contain the full symmetry of the system: In Section 6.5.1, the symmetry of the system in the (110) direction is not fully used; there is a band-folding at $\frac{\pi}{a}(1,1,0)$. In Section 6.5.2, the symmetry of the system in the (001) direction is not fully used; there is a band-folding at $\frac{\pi}{a}(0,0,-1)$. Nevertheless, by combining the results obtained in those two different methods, a more complete and comprehensive understanding on the electronic states in the quantum wire can be obtained.

We can easily see that some equations for the energies of the electronic states in the wire in Sections 6.5.1 or 6.5.2 are the same, such as (6.32a) and (6.39a). Some are actually the same, such as (6.32c) and (6.39c).[7] Some of them seem not the same: In Section 6.5.1, there are $2N_{001}$ subbands whose energies depend on τ_{110} ($2N_{001}-1$ subbands in (6.36) and one subband in (6.38)) whereas in Section 6.5.2, there are N_{001} subbands whose energies depend on τ_{110} ($N_{001}-1$ subbands in (6.44) and one subband in (6.45)). From the discussions in Section 5.6.2, we see that this is due to the fact that in Section 6.5.1, the symmetry of the system in the (110) direction is not fully used; there is a band-folding at $\frac{\pi}{a}(1,1,0)$; In Section 6.5.2, there are $2N_{110}$ subbands whose energies depend on τ_{001} ($2N_{110}-1$ subbands in (6.43) and one subband in (6.45)), whereas in Section 6.5.1, there are N_{110} subbands

[7] Since $1/a(1,1,-1)$ is a reciprocal lattice vector for crystals with a fcc Bravais lattice.

whose energies depend on τ_{001} ($N_{110}-1$ subbands in (6.37) and one subband in (6.38)). From the discussions in Section 5.6.1, we see that this is due to the fact that in Section 6.5.2, the symmetry of the system in the (001) direction is not fully used; there is a band-folding at $\frac{\pi}{a}(0,0,-1)$.

By considering these points, we can predict that the electronic states in such an ideal quantum wire should be as follows:

For each bulk energy band n there are $2(N_{001}-1)(N_{110}-1)+(N_{001}-1)+(N_{110}-1)+1$ bulk-like subbands. They include the following:
$(N_{001}-1)(N_{110}-1)$ subbands with energies

$$\bar{\Lambda}^{bk,a}_{n,j_{001},j_{110}}(\bar{\boldsymbol{k}}) = \varepsilon_n\left[\bar{\boldsymbol{k}} + \frac{j_{001}\pi}{N_{001}a}(0,0,1) + \frac{j_{110}\pi}{N_{110}a}(1,1,0)\right] \tag{6.46}$$

from either (6.32a) or (6.39a),
$(N_{001}-1)(N_{110}-1)$ subbands with energies

$$\bar{\Lambda}^{bk,c}_{n,j_{001},j_{110}}(\bar{\boldsymbol{k}}) = \varepsilon_n\left[\bar{\boldsymbol{k}} + \frac{j_{001}\pi}{N_{001}a}(0,0,1) + \frac{j_{110}\pi}{N_{110}a}(1,1,0) + \frac{2\pi}{a}(1,1,0)\right] \tag{6.47}$$

from either (6.32c) or (6.39c),
$(N_{001}-1)$ subbands with energies

$$\bar{\Lambda}^{bk,b_1}_{n,j_{001}}(\bar{\boldsymbol{k}}) = \varepsilon_n\left[\bar{\boldsymbol{k}} + \frac{j_{001}\pi}{N_{001}a}(0,0,1) + \frac{\pi}{a}(1,1,0)\right] \tag{6.48}$$

from (6.39b),
$(N_{110}-1)$ subbands with energies

$$\bar{\Lambda}^{bk,b_2}_{n,j_{110}}(\bar{\boldsymbol{k}}) = \varepsilon_n\left[\bar{\boldsymbol{k}} + \frac{j_{110}\pi}{N_{110}a}(1,1,0) + \frac{\pi}{a}(0,0,1)\right] \tag{6.49}$$

from (6.32b).
Here the range of j_{001} or j_{110} is given by (6.35) or (6.33).

In addition to those bulk-like subbands, for each bulk energy band n there is one bulk-like subband in the wire with energy given by

$$\bar{\Lambda}^{bk,d}_{n}(\bar{\boldsymbol{k}}) = \varepsilon_n\left[\bar{\boldsymbol{k}} + \frac{\pi}{a}(0,0,1) + \frac{\pi}{a}(1,1,0)\right]. \tag{6.50}$$

This is obtained from (6.36b) and (6.43b): By (6.36b), each state in this subband is a stationary Bloch state with a $\kappa_{001}=\pi/2$ in [001] direction; thus, its energy does not depend on τ_{001}; By (6.43b), each state in this subband is a stationary Bloch state with a $\kappa_{110}=\pi/2$ in [110] direction; thus, its energy does not depend on τ_{110}.

For each bulk energy band n, there are $(N_{001}-1)+(N_{110}-1)$ surface-like subbands. They are $(N_{001}-1)$ subbands with energies

$$\bar{\Lambda}^{sf,a_1}_{n,j_{001}}(\bar{\boldsymbol{k}};\tau_{110}) = \hat{\Lambda}_n\left[\bar{\boldsymbol{k}} + \frac{j_{001}\pi}{N_{001}a}(0,0,1);\tau_{110}\right] \tag{6.51}$$

from (6.44) and $(N_{110}-1)$ subbands with energies

$$\bar{\Lambda}^{sf,a_2}_{n,j_{110}}(\bar{\boldsymbol{k}};\tau_{001}) = \hat{\Lambda}_n\left[\bar{\boldsymbol{k}} + \frac{j_{110}\pi}{N_{110}a}(1,1,0);\tau_{001}\right] \tag{6.52}$$

from (6.37).

For each bulk energy band n, there is one side band in the wire with energy given by (6.38) (i.e., (6.45)).

Therefore, among $2N_{001}-1$ subbands $\bar{\Lambda}_{n,j_3}(\bar{\boldsymbol{k}};\tau_{110})$ in (6.36) in Section 6.5.1, actually there are $N_{001}-1$ bulk-like subbands $\bar{\Lambda}^{bk,b_1}_{n,j_{001}}(\bar{\boldsymbol{k}})$ in (6.48), one bulk-like subband $\bar{\Lambda}^{bk,d}_{n}(\bar{\boldsymbol{k}})$ in (6.50), and $N_{001}-1$ surface-like subbands $\bar{\Lambda}^{sf,a_1}_{n,j_{001}}(\bar{\boldsymbol{k}};\tau_{110})$ in (6.51). Thus, there are a total of N_{001} subbands in the quantum wire whose energies are dependent on τ_{110}: $N_{001}-1$ surface-like subbands $\bar{\Lambda}^{sf,a_1}_{n,j_{001}}(\bar{\boldsymbol{k}};\tau_{110})$ in (6.51) plus one side-like subband $\bar{\Lambda}^{sd}_{n}(\bar{\boldsymbol{k}};\tau_{110},\tau_{001})$ in (6.38). We should also have

$$\bar{\Lambda}^{sf,a_1}_{n,j_{001}}(\bar{\boldsymbol{k}};\tau_{110}) > \bar{\Lambda}^{bk,b_1}_{n,j_{001}}(\bar{\boldsymbol{k}}) \tag{6.53}$$

and

$$\bar{\Lambda}^{sd}_{n}(\bar{\boldsymbol{k}};\tau_{110},\tau_{001}) > \bar{\Lambda}^{bk,d}_{n}(\bar{\boldsymbol{k}}), \tag{6.54}$$

since in our discussions on the two different ways of choosing the primitive lattice vectors in Section 5.6.2, the true surface-like subband has a higher energy by (5.37).

Similarly, among $2N_{110}-1$ subbands $\bar{\Lambda}_{n,j_3}(\bar{\boldsymbol{k}};\tau_{001})$ in (6.43) in Section 6.5.2, actually there are $N_{110}-1$ bulk-like subbands $\bar{\Lambda}^{bk,b_2}_{n,j_{110}}(\bar{\boldsymbol{k}})$ in (6.49), one bulk-like subband $\bar{\Lambda}^{bk,d}_{n}(\bar{\boldsymbol{k}})$ in (6.50), and $N_{110}-1$ surface-like subbands $\bar{\Lambda}^{sf,a_2}_{n,j_{110}}(\bar{\boldsymbol{k}};\tau_{001})$ in (6.52). There are a total of N_{110} subbands in the quantum wire whose energies are dependent on τ_{001}: $N_{110}-1$ surface-like subbands $\bar{\Lambda}^{sf,a_2}_{n,j_{110}}(\bar{\boldsymbol{k}};\tau_{001})$ in (6.52) plus one side-like subband $\bar{\Lambda}^{sd}_{n}(\bar{\boldsymbol{k}};\tau_{110},\tau_{001})$ in (6.45). We should also have

$$\bar{\Lambda}^{sf,a_2}_{n,j_{110}}(\bar{\boldsymbol{k}};\tau_{001}) > \bar{\Lambda}^{bk,b_2}_{n,j_{110}}(\bar{\boldsymbol{k}}) \tag{6.55}$$

and $\bar{\Lambda}^{sd}_{n}(\bar{\boldsymbol{k}};\tau_{110},\tau_{001}) > \bar{\Lambda}^{bk,d}_{n}(\bar{\boldsymbol{k}})$ as in (6.54).

Since one of the triply-degenerated VBM states in a cubic semiconductor can have one nodal surface either in (001) plane or in (110) plane, there can be one such state in Si (001) films and (110) films and in GaAs (110) films whose energy is the energy of the VBM and does not change as the film thickness changes, as observed in [1–3]. However, one VBM state in either Si or GaAs cannot have *two* nodal surfaces in both (001) plane and (110) plane simultaneously; therefore, there is not an electronic state in an ideal rectangular quantum wire of a cubic semiconductor discussed here whose energy is the energy of the VBM and does not change as the wire size changes. Consequently, it is predicted that there must be at least *three side-like states*

in such a quantum wire with surfaces oriented in the (110) or the (001) direction whose energies $\bar{\Lambda}_n^{sd}(\bar{\boldsymbol{k}} = 0; \tau_{001}, \tau_{110})$ for $n = 1, 2, 3$ are *above* the VBM and do not depend on the wire size and/or shape.

6.6 fcc Quantum Wires with (110) and (1$\bar{1}$0) Surfaces

The electronic states in an ideal quantum wire of fcc crystals with (110) and (1$\bar{1}$0) surfaces are one-dimensional Bloch waves with a wave vector $\bar{\boldsymbol{k}}$ in the [001] direction. Such a quantum wire has a rectangular cross section $N_{110}a/\sqrt{2} \times N_{1\bar{1}0}a/\sqrt{2}$, where N_{110} and $N_{1\bar{1}0}$ are positive integers. By using an approach similar to that used in Section 6.5, the properties of electronic states in such a quantum wire can be predicted.

For each bulk energy band n, there are $2(N_{1\bar{1}0} - 1)(N_{110} - 1) + (N_{1\bar{1}0} - 1) + (N_{110} - 1) + 1$ bulk-like subbands in the quantum wire. They include $(N_{1\bar{1}0} - 1)(N_{110} - 1)$ subbands with energies

$$\bar{\Lambda}^{bk,a}_{n,j_{1\bar{1}0},j_{110}}(\bar{\boldsymbol{k}}) = \varepsilon_n \left[\bar{\boldsymbol{k}} + \frac{j_{1\bar{1}0}\pi}{N_{1\bar{1}0}a}(1,-1,0) + \frac{j_{110}\pi}{N_{110}a}(1,1,0)\right], \tag{6.56}$$

$(N_{1\bar{1}0} - 1)(N_{110} - 1)$ subbands with energies

$$\bar{\Lambda}^{bk,c}_{n,j_{1\bar{1}0},j_{110}}(\bar{\boldsymbol{k}}) = \varepsilon_n \left[\bar{\boldsymbol{k}} + \frac{j_{1\bar{1}0}\pi}{N_{1\bar{1}0}a}(1,-1,0) + \frac{j_{110}\pi}{N_{110}a}(1,1,0) + \frac{2\pi}{a}(1,1,0)\,\right], \tag{6.57}$$

$(N_{1\bar{1}0} - 1)$ subbands with energies

$$\bar{\Lambda}^{bk,b_1}_{n,j_{1\bar{1}0}}(\bar{\boldsymbol{k}}) = \varepsilon_n \left[\bar{\boldsymbol{k}} + \frac{j_{1\bar{1}0}\pi}{N_{1\bar{1}0}a}(1,-1,0) + \frac{\pi}{a}(1,1,0)\right], \tag{6.58}$$

and $(N_{110} - 1)$ subbands with energies

$$\bar{\Lambda}^{bk,b_2}_{n,j_{110}}(\bar{\boldsymbol{k}}) = \varepsilon_n \left[\bar{\boldsymbol{k}} + \frac{j_{110}\pi}{N_{110}a}(1,1,0) + \frac{\pi}{a}(1,-1,0)\right]. \tag{6.59}$$

Here, $j_{1\bar{1}0} = 1, 2, ..., N_{1\bar{1}0} - 1$ and $j_{110} = 1, 2, ..., N_{110} - 1$.

For each bulk energy band n, there is one bulk-like subband in the wire with energy

$$\bar{\Lambda}^{bk,d}_{n}(\bar{\boldsymbol{k}}) = \varepsilon_n \left[\bar{\boldsymbol{k}} + \frac{\pi}{a}(1,1,0) + \frac{\pi}{a}(1,-1,0)\right]. \tag{6.60}$$

For each bulk energy band n, there are $(N_{1\bar{1}0} - 1) + (N_{110} - 1)$ surface-like subbands in the quantum wire. They are $(N_{1\bar{1}0} - 1)$ subbands with energies

$$\bar{\Lambda}^{sf,a_1}_{n,j_{1\bar{1}0}}(\bar{\boldsymbol{k}}; \tau_{110}) = \hat{\Lambda}_n \left[\bar{\boldsymbol{k}} + \frac{j_{1\bar{1}0}\pi}{N_{1\bar{1}0}a}(1,-1,0); \tau_{110}\right] \tag{6.61}$$

and $(N_{110}-1)$ subbands with energies

$$\bar{\Lambda}^{sf,a_2}_{n,j_{110}}(\bar{\boldsymbol{k}};\tau_{1\bar{1}0}) = \hat{\Lambda}_n\left[\bar{\boldsymbol{k}} + \frac{j_{110}\pi}{N_{110}a}(1,1,0);\tau_{1\bar{1}0}\right]. \tag{6.62}$$

Here, τ_{110} and $\tau_{1\bar{1}0}$ define the boundary faces of the quantum wire in the [110] and $[1\bar{1}0]$ directions.

For each bulk energy band n, there is one side-like subband in the quantum wire with energy

$$\bar{\Lambda}^{sd}_{n}(\bar{\boldsymbol{k}};\tau_{110},\tau_{1\bar{1}0}) = \bar{\lambda}_n(\bar{\boldsymbol{k}};\tau_{110},\tau_{1\bar{1}0}). \tag{6.63}$$

Since none of the triply-degenerated VBM states in a cubic semiconductor can have *two* nodal surfaces in both (110) plane and $(1\bar{1}0)$ plane simultaneously, there is not an electronic state in an ideal quantum wire of a cubic semiconductor with surfaces oriented in the (110) or the $(1\bar{1}0)$ direction whose energy is the energy of the VBM and does not change as the wire size and/or shape changes. This is a fact observed in the numerical calculations of Franceschetti and Zunger [3] on GaAs free-standing quantum wires, as shown in Fig. 5.4(b). Consequently, it is also predicted that there must be at least *three side states* in such a rectangular quantum wire whose energies $\bar{\Lambda}^{sd}_{n}(\bar{\boldsymbol{k}}=0;\tau_{110},\tau_{1\bar{1}0})$ for $n=1,2,3$ are *above* the VBM and do not depend on the wire size and/or shape.

6.7 bcc Quantum Wires with (001) and (010) Surfaces

For a bcc quantum wire with (010) and (001) surfaces and having a rectangular cross section $N_{010}a \times N_{001}a$, where N_{010} and N_{001} are positive integers, the electronic states are one-dimensional Bloch waves with a wave vector $\bar{\boldsymbol{k}}$ in the [100] direction. They can be similarly obtained as in Section 6.5.

For each bulk energy band n, there are $2(N_{010}-1)(N_{001}-1)+(N_{010}-1)+(N_{001}-1)+1$ bulk-like subbands in the quantum wire. They include $(N_{010}-1)(N_{001}-1)$ subbands with energies

$$\bar{\Lambda}^{bk,a}_{n,j_{010},j_{001}}(\bar{\boldsymbol{k}}) = \varepsilon_n\left[\bar{\boldsymbol{k}} + \frac{j_{010}\pi}{N_{010}a}(0,1,0) + \frac{j_{001}\pi}{N_{001}a}(0,0,1)\right], \tag{6.64}$$

$(N_{001}-1)(N_{010}-1)$ subbands with energies

$$\bar{\Lambda}^{bk,c}_{n,j_{010},j_{001}}(\bar{\boldsymbol{k}}) = \varepsilon_n\left[\bar{\boldsymbol{k}} + \frac{j_{010}\pi}{N_{010}a}(0,1,0) + \frac{j_{001}\pi}{N_{001}a}(0,0,1) + \frac{2\pi}{a}(0,1,0)\right], \tag{6.65}$$

$(N_{001}-1)$ subbands with energies

$$\bar{\Lambda}^{bk,b_1}_{n,j_{001}}(\bar{\boldsymbol{k}}) = \varepsilon_n\left[\bar{\boldsymbol{k}} + \frac{j_{001}\pi}{N_{001}a}(0,0,1) + \frac{\pi}{a}(0,1,0)\right], \tag{6.66}$$

and $(N_{010}-1)$ subbands with energies

$$\bar{\Lambda}^{bk,b_2}_{n,j_{010}}(\bar{\boldsymbol{k}}) = \varepsilon_n\left[\bar{\boldsymbol{k}} + \frac{j_{010}\pi}{N_{010}a}(0,1,0) + \frac{\pi}{a}(0,0,1)\right]. \tag{6.67}$$

Here $j_{001} = 1, 2, ..., N_{001}-1$ and $j_{010} = 1, 2, ..., N_{010}-1$.

For each bulk energy band n, there is one bulk-like subband with energy

$$\bar{\Lambda}^{bk,d}_{n}(\bar{\boldsymbol{k}}) = \varepsilon_n\left[\bar{\boldsymbol{k}} + \frac{\pi}{a}(0,1,0) + \frac{\pi}{a}(0,0,1)\right]. \tag{6.68}$$

For each bulk energy band n, there are $(N_{001}-1)+(N_{010}-1)$ surface-like subbands in the quantum wire. They are $(N_{001}-1)$ subbands with energies

$$\bar{\Lambda}^{sf,a_1}_{n,j_{001}}(\bar{\boldsymbol{k}};\tau_{010}) = \hat{\Lambda}_n\left[\bar{\boldsymbol{k}} + \frac{j_{001}\pi}{N_{001}a}(0,0,1);\tau_{010}\right] \tag{6.69}$$

and $(N_{010}-1)$ subbands with energies

$$\bar{\Lambda}^{sf,a_2}_{n,j_{010}}(\bar{\boldsymbol{k}};\tau_{001}) = \hat{\Lambda}_n\left[\bar{\boldsymbol{k}} + \frac{j_{010}\pi}{N_{010}a}(0,1,0);\tau_{001}\right]. \tag{6.70}$$

Here, τ_{010} and τ_{001} define the boundary faces of the quantum wire in the [010] and [001] directions.

For each bulk energy band n, there is one side-like subband in the quantum wire with energy

$$\bar{\Lambda}^{sd}_{n}(\bar{\boldsymbol{k}};\tau_{001},\tau_{010}) = \bar{\lambda}_n(\bar{\boldsymbol{k}};\tau_{001},\tau_{010}). \tag{6.71}$$

6.8 Summary and Discussions

Therefore, from the understanding of the further quantum confinement of two-dimensional Bloch waves $\hat{\psi}_n(\hat{\boldsymbol{k}},\boldsymbol{x};\tau_3)$ and $\hat{\psi}_{n,j_3}(\hat{\boldsymbol{k}},\boldsymbol{x};\tau_3)$ in one more direction obtained in Sections 6.1–6.3 and by considering two different confinement orders, the properties of electronic states in ideal quantum wires discussed in Sections 6.4–6.7 can be generally and analytically understood. There are three different types of electronic states in an ideal quantum wire: bulk-like states, surface-like states, and side-like states.

Similar to a surface-like subband, the physics origin of a side-like subband is also related to a bulk energy band. Just as a surface-like electronic state is better understood as an electronic state whose properties and energy are determined by the surface location, a side-like electronic state in a quantum wire is better understood as an electronic state whose properties and energy are determined by the side location, rather than that the state is located near a specific side. Only when a Bloch function has two different nodal surfaces which are the surfaces of the quantum wire, might the side state be a Bloch

state. It seems that such cases rarely happen in most quantum wires of cubic semiconductors of general interest.

Because of the crystal structure difference of fcc crystals or bcc crystals, the numbers of each type of electronic states in the quantum wires discussed in Sections 6.5–6.7 are somewhat different from the numbers of each type of electronic states in the quantum wires of crystals with a sc, tetr, or ortho Bravais lattice discussed in Section 6.4.

However, since the results in Sections 6.5–6.7 were also obtained from an understanding of the further quantum confinement effects of $\hat{\psi}_n(\hat{\boldsymbol{k}}, \boldsymbol{x}; \tau_3)$ and $\hat{\psi}_{n,j_3}(\hat{\boldsymbol{k}}, \boldsymbol{x}; \tau_3)$ investigated in Sections 6.1–6.3, there are similar relationships between the three different types of electronic states. For example, for an ideal fcc quantum wire with (110) and (001) surfaces, we should have

$$\bar{\Lambda}_n^{sd}(\bar{\boldsymbol{k}}; \tau_{001}, \tau_{110}) > \bar{\Lambda}_{n,j_{001}}^{sf,a_1}(\bar{\boldsymbol{k}}; \tau_{110}) \tag{6.72}$$

and

$$\bar{\Lambda}_n^{sd}(\bar{\boldsymbol{k}}; \tau_{001}, \tau_{110}) > \bar{\Lambda}_{n,j_{110}}^{sf,a_2}(\bar{\boldsymbol{k}}; \tau_{001}) \tag{6.73}$$

between the energy of a side-like state in (6.38) or (6.45) and the energies of relevant surface-like states in (6.51) and in (6.52). These two equations are obtained from the relationship (6.15) between (6.38) and (6.37) (i.e., (6.52)) or from the relationship (6.15) between (6.45) and (6.44) (i.e., (6.51)). We also have

$$\bar{\Lambda}_n^{sd}(\bar{\boldsymbol{k}}; \tau_{001}, \tau_{110}) > \bar{\Lambda}_n^{bk,d}(\bar{\boldsymbol{k}}) \tag{6.74}$$

between the energy of a side-like state in (6.38) or (6.45) and the energy of a relevant bulk-like state in (6.50). This is from the relationship (6.54) between (6.38) and (6.50).

We have

$$\bar{\Lambda}_{n,j_{001}}^{sf,a_1}(\bar{\boldsymbol{k}}; \tau_{110}) > \bar{\Lambda}_{n,j_{001}}^{bk,b_1}(\bar{\boldsymbol{k}}), \tag{6.75}$$

$$\bar{\Lambda}_{n,j_{001}}^{sf,a_1}(\bar{\boldsymbol{k}}; \tau_{110}) > \bar{\Lambda}_{n,j_{001},j_{110}}^{bk,a}(\bar{\boldsymbol{k}}), \tag{6.76}$$

and

$$\bar{\Lambda}_{n,j_{001}}^{sf,a_1}(\bar{\boldsymbol{k}}; \tau_{110}) > \bar{\Lambda}_{n,j_{001},j_{110}}^{bk,c}(\bar{\boldsymbol{k}}) \tag{6.77}$$

between the energy of a surface-like state in (6.51) and the energies of relevant bulk-like states in (6.48), in (6.46), and in (6.47). These three equations are obtained from the relationship (6.23) between (6.36) and (6.32) and/or from (6.53). Similarly, we have

$$\bar{\Lambda}_{n,j_{110}}^{sf,a_2}(\bar{\boldsymbol{k}}; \tau_{001}) > \bar{\Lambda}_{n,j_{110}}^{bk,b_2}(\bar{\boldsymbol{k}}), \tag{6.78}$$

$$\bar{\Lambda}_{n,j_{110}}^{sf,a_2}(\bar{\boldsymbol{k}}; \tau_{001}) > \bar{\Lambda}_{n,j_{001},j_{110}}^{bk,a}(\bar{\boldsymbol{k}}), \tag{6.79}$$

and

$$\bar{\Lambda}^{sf,a_2}_{n,j_{110}}(\bar{\boldsymbol{k}};\tau_{001}) > \bar{\Lambda}^{bk,c}_{n,j_{001},j_{110}}(\bar{\boldsymbol{k}}) \tag{6.80}$$

between the energy of a surface-like state in (6.52) and the energies of relevant bulk-like states in (6.49), in (6.46), and in (6.47). These three equations are obtained from the relationship (6.23) between (6.43) and (6.39) and/or from (6.55).

Corresponding relationships for the electronic states in an ideal fcc quantum wire with (110) and $(1\bar{1}0)$ surfaces or in an ideal bcc quantum wire with (001) and (010) surfaces can be similarly obtained.

Therefore, in an ideal quantum wire discussed in Sections 6.5 to 6.7, by (6.72)–(6.80) or similar equations, we can understand that for the electronic states with the same bulk energy band index n and with the same wave vector $\bar{\boldsymbol{k}}$ in the quantum wire, the following general relations exist:

The energy of the side-like state
> The energy of every surface-like state
> The energy of every relevant bulk-like state.

In an everywhere neutral semiconductor quantum wire, the side-like subbands should be as equally occupied as the bulk-like subbands. The side-like subbands are usually even higher in energy than the relevant surface-like subbands. Thus, in a quantum wire of a cubic semiconductor the side-like subbands originating from the valence bands might even be partly higher in energy than some bulk-like subbands originating from a conduction band. If such a case happens, the equivalence of the Fermi energy in the quantum wire must force some electrons to flow from those side-like subbands originating from the valence bands into the bulk-like subbands originating from that conduction band, to make the quantum wire of a semiconductor crystal have the electrical conductivity of a metal.

Based on similar reasoning, the sides of an alkali metal quantum wire could be even more positively charged than the surfaces.

There are also side-like subbands originating from bulk conduction bands in a semiconductor quantum wire. These side-like subbands will be even higher in energy than the surface-like subbands originating from the bulk conduction bands and, thus, will usually not be occupied. It seems unlikely that these side-like subbands will have a significant effect on the properties of a semiconductor quantum wire.

Although in a quantum wire there is only one side-like subband for each bulk energy band, it does not mean that all electronic states in that side-like subband have to be located on the same side of the wire. A clearer understanding of the properties of the electronic states in a side-like subband in a quantum wire requires a clearer understanding of the properties of the solutions of the partial differential equation (5.1), including the solutions in the band gap(s) and the non-Bloch state solutions in the ranges of permitted energy bands.

Although the electronic states in an ideal quantum wire discussed here are all one-dimensional Bloch waves in the $\boldsymbol{a}_1$ direction, they are solutions

of a *partial* differential equation (5.1) under the boundary conditions (6.2) and are fundamentally different from the case treated in Chapter 4, where all electronic states are solutions of an *ordinary* differential equation (4.1) under the boundary condition (4.4). Therefore, for the further quantum confinement of those one-dimensional Bloch waves in an ideal finite crystal or quantum dot, we should use the approach used in Chapter 5 and in this chapter rather than the results obtained in Chapter 4.

References

1. S. B. Zhang and A. Zunger: Appl. Phys. Lett. **63**, 1399 (1993)
2. S. B. Zhang, C-Y Yeh, and A. Zunger: Phys. Rev. **B48**, 11204 (1993)
3. A. Franceschetti and A. Zunger: Appl. Phys. Lett. **68**, 3455 (1996)

7 Electronic States in Ideal Finite Crystals or Quantum Dots

The electronic states in an ideal finite crystal or quantum dot can be considered as the electronic states in an ideal quantum wire further confined in one more direction. In this chapter, we are interested in the electronic states in an orthorhombic finite crystal or quantum dot that can be considered as the one-dimensional Bloch waves in a rectangular quantum wire discussed in Chapter 6 further confined by two boundary surfaces perpendicularly intersecting the $\boldsymbol{a}_1$ axis at $\tau_1\boldsymbol{a}_1$ and $(\tau_1 + N_1)\boldsymbol{a}_1$; here, N_1 is a positive integer. By using an approach similar to that used in the last two chapters, we can understand that the further quantum confinement of each set of one-dimensional Bloch waves in an ideal quantum wire will produce two different types of electronic states in the ideal finite crystal or quantum dot.

An orthorhombic finite crystal or quantum dot always has six boundary faces: two faces in the $(h_1k_1l_1)$ plane, two faces in the $(h_2k_2l_2)$ plane, and two faces in the $(h_3k_3l_3)$ plane. The electronic states in such a finite crystal or quantum dot can be considered as the electronic states in a quantum film with two faces in the $(h_3k_3l_3)$ plane further confined by two faces in the $(h_2k_2l_2)$ plane and, finally, further confined by two faces in the $(h_1k_1l_1)$ plane. They can also be considered as three-dimensional Bloch waves $\phi_n(\boldsymbol{k}, \boldsymbol{x})$ to be confined in the three directions in other confinement orders. There are all together six different orders. The results obtained in these six different confinement orders are equally valid and can be complementary to each other. By combining the results obtained from the six different confinement orders, we can obtain a more comprehensive understanding of the electronic states in the finite crystal or quantum dot.

The simplest cases where the results obtained in this chapter are applicable are the electronic states in an orthorhombic finite crystal or quantum dot with a sc, tetr, or ortho Bravais lattice in which (5.14), (6.10), and (6.20) are true. In those crystals, the three primitive lattice vectors $\boldsymbol{a}_1$, $\boldsymbol{a}_2$, and $\boldsymbol{a}_3$ are perpendicular to each other and are essentially equivalent. Properties of the electronic states in such an ideal finite crystal or quantum dot can be generally and analytically predicted.

Since many cubic semiconductors and metals have a fcc or bcc Bravais lattice, the electronic states in finite crystals or quantum dots with a fcc or bcc Bravais lattice often are practically more interesting. Based on the

general theory developed in this chapter, we can also give predictions on the electronic states in some ideal orthorhombic finite crystals or quantum dots of crystals with a fcc or a bcc Bravais lattice.

This chapter is organized as follows: In Sections 7.1–7.5, we investigate the consequences when the four sets of one-dimensional waves in an ideal quantum wire obtained in Sections 6.1–6.3 are further confined in one more direction, that is, the consequences of three-dimensional Bloch waves being confined in three directions in a specific confinement order. In Sections 7.6–7.8, we obtain predictions on the electronic states in several finite crystals or quantum dots from the understanding obtained in Sections 7.1–7.5 and by considering different quantum confinement orders. Section 7.9 is devoted to a summary and discussions.

7.1 Basic Considerations

In this chapter, we consider the further confinement of the one-dimensional Bloch waves $\bar{\psi}(\bar{\boldsymbol{k}}, \boldsymbol{x})$ obtained in Chapter 6 in the $\boldsymbol{a}_1$ direction. Such an orthorhombic finite crystal or quantum dot can be defined by a bottom face $x_3 = \tau_3$, a top face $x_3 = \tau_3 + N_3$, a front face perpendicularly intersecting the $\boldsymbol{a}_2$ axis at $\tau_2 \boldsymbol{a}_2$ and a rear face perpendicularly intersecting it at $(\tau_2 + N_2)\boldsymbol{a}_2$, and a left face perpendicularly intersecting the $\boldsymbol{a}_1$ axis at $\tau_1 \boldsymbol{a}_1$ and a right face perpendicularly intersecting it at $(\tau_1 + N_1)\boldsymbol{a}_1$; here, τ_1, τ_2, and τ_3 define the boundary face locations of the crystal or quantum dot and N_1, N_2, and N_3 are three positive integers indicating the size and/or shape of the crystal or quantum dot. We look for the eigenvalues Λ and eigenfunctions $\psi(\boldsymbol{x})$ of the following two equations:

$$-\nabla^2 \psi(\boldsymbol{x}) + [v(\boldsymbol{x}) - \Lambda]\psi(\boldsymbol{x}) = 0 \quad \text{if } \boldsymbol{x} \in \text{ the crystal} \tag{7.1}$$

and

$$\psi(\boldsymbol{x}) = 0 \quad \text{if } \boldsymbol{x} \notin \text{ the crystal.} \tag{7.2}$$

Corresponding to the further quantum confinement of each set of one-dimensional Bloch waves in the quantum wire, $\bar{\psi}_n(\bar{\boldsymbol{k}}, \boldsymbol{x}; \tau_2, \tau_3)$, $\bar{\psi}_{n,j_3}(\bar{\boldsymbol{k}}, \boldsymbol{x}; \tau_2, \tau_3)$, $\bar{\psi}_{n,j_2}(\bar{\boldsymbol{k}}, \boldsymbol{x}; \tau_2, \tau_3)$, and $\bar{\psi}_{n,j_2,j_3}(\bar{\boldsymbol{k}}, \boldsymbol{x}; \tau_2, \tau_3)$, we will have a new eigenvalue problem and a new theorem similar to Theorem 6.1 or 6.2 for the electronic states in a quantum wire; each one will produce two types of confined electronic states in the finite crystal or quantum dot.

7.2 Further Quantum Confinement of $\bar{\psi}_n(\bar{\boldsymbol{k}}, \boldsymbol{x}; \tau_2, \tau_3)$

For the quantum confinement of the side-like states $\bar{\psi}_n(\bar{\boldsymbol{k}}, \boldsymbol{x}; \tau_2, \tau_3)$, we consider an orthorhombic parallelogram C as shown in Fig. 7.1 with a bottom

face $x_3 = \tau_3$, a top face $x_3 = \tau_3 + 1$, a front face perpendicularly intersecting the $\boldsymbol{a}_2$ axis at $\tau_2 \boldsymbol{a}_2$ and a rear face perpendicularly intersecting it at $(\tau_2 + 1)\boldsymbol{a}_2$, a left face perpendicularly intersecting the $\boldsymbol{a}_1$ axis at $\tau_1 \boldsymbol{a}_1$ and a right face perpendicularly intersecting it at $(\tau_1 + 1)\boldsymbol{a}_1$. The function set

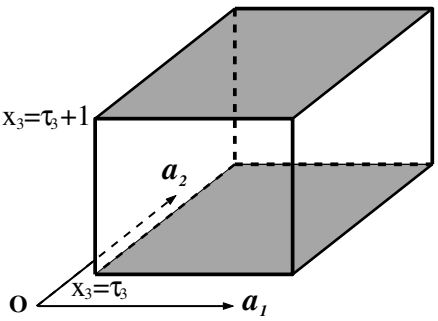

Fig. 7.1. The orthorhombic parallelogram C for the eigenvalue problem of (5.1) under the boundary condition (7.3). The two shadowed faces of ∂C_3 and the two thick-lined faces of ∂C_2 are the four faces on which each $\bar{\psi}_n(\bar{\boldsymbol{k}}, \boldsymbol{x}; \tau_2, \tau_3)$ is zero. The left face and the right face are the two faces on which each function $\phi(\boldsymbol{x}; \tau_1, \tau_2, \tau_3)$ is further required to be zero.

$\phi(\boldsymbol{x}; \tau_1, \tau_2, \tau_3)$ is defined by (5.1) and the boundary condition

$$\phi(\boldsymbol{x}; \tau_1, \tau_2, \tau_3) = 0 \quad \text{if } \boldsymbol{x} \in \partial C. \tag{7.3}$$

Here, ∂C is the boundary of C. The eigenvalues and eigenfunctions of (5.1) under the condition (7.3) are denoted by $\lambda_n(\tau_1, \tau_2, \tau_3)$ and $\phi_n(\boldsymbol{x}; \tau_1, \tau_2, \tau_3)$, respectively.

For each eigenvalue of the problem defined by (5.1) and (7.3) we have the following theorem between it and the eigenvalues $\bar{\Lambda}_n(\bar{\boldsymbol{k}}; \tau_2, \tau_3)$ in (6.9) of $\bar{\psi}_n(\bar{\boldsymbol{k}}, \boldsymbol{x}; \tau_2, \tau_3)$.

Theorem 7.1.

$$\lambda_n(\tau_1, \tau_2, \tau_3) \geq \bar{\Lambda}_n(\bar{\boldsymbol{k}}; \tau_2, \tau_3). \tag{7.4}$$

Since each $\bar{\psi}_n(\bar{\boldsymbol{k}}, \boldsymbol{x}; \tau_2, \tau_3)$ satisfies

$$\begin{aligned} \bar{\psi}(\bar{\boldsymbol{k}}, \boldsymbol{x} + \boldsymbol{a}_1; \tau_2, \tau_3) &= \mathrm{e}^{\mathrm{i}k_1} \bar{\psi}(\bar{\boldsymbol{k}}, \boldsymbol{x}; \tau_2, \tau_3), \quad -\pi < k_1 \leq \pi, \\ \bar{\psi}(\bar{\boldsymbol{k}}, \boldsymbol{x}; \tau_2, \tau_3) &= 0 \qquad \text{if } \boldsymbol{x} \in \partial C_2 \text{ or } \boldsymbol{x} \in \partial C_3. \end{aligned} \tag{7.5}$$

Theorem 7.1 can be proven similar to Theorem 5.1 given in Chapter 5. The major difference is in the Dirichlet integral

$$\begin{aligned} J(f, g) &= \int_C \{\nabla f(\boldsymbol{x}) \cdot \nabla g^*(\boldsymbol{x}) + v(\boldsymbol{x}) f(\boldsymbol{x}) g^*(\boldsymbol{x})\} \, \mathrm{d}\boldsymbol{x} \\ &= \int_C f(\boldsymbol{x}) \{-\nabla^2 g^*(\boldsymbol{x}) + v(\boldsymbol{x}) g^*(\boldsymbol{x})\} \, \mathrm{d}\boldsymbol{x} + \int_{\partial C} f \frac{\partial g^*}{\partial n} \, \mathrm{d}S; \end{aligned} \tag{7.6}$$

if both $f(\boldsymbol{x})$ and $g(\boldsymbol{x})$ satisfy the conditions (7.5), the integral over ∂C in (7.6) is zero since the integrals over the two opposite faces of ∂C_1 are cancelled out, $f(\boldsymbol{x}) = 0$ when $\boldsymbol{x} \in \partial C_2$ or $\boldsymbol{x} \in \partial C_3$. If $f(\boldsymbol{x}) = \phi_n(\boldsymbol{x}; \tau_1, \tau_2, \tau_3)$ and $g(\boldsymbol{x}) = \bar{\psi}(\bar{\boldsymbol{k}}, \boldsymbol{x}; \tau_2, \tau_3)$, the integral over ∂C in (7.6) is also zero since $f(\boldsymbol{x}) = 0$ when $\boldsymbol{x} \in \partial C$.

Theorem 7.1 is similar to Theorem 6.1 and the consequences of the quantum confinement of two-dimensional Bloch waves $\hat{\psi}_n(\hat{\boldsymbol{k}}, \boldsymbol{x}; \tau_3)$ in the $\boldsymbol{a}_2$ direction due to Theorem 6.1 can be similarly applied to the quantum confinement of $\bar{\psi}_n(\bar{\boldsymbol{k}}, \boldsymbol{x}; \tau_2, \tau_3)$ in the $\boldsymbol{a}_1$ direction.

For each bulk energy band n, there is one $\phi_n(\boldsymbol{x}; \tau_1, \tau_2, \tau_3)$.

Because $v(\boldsymbol{x} + \boldsymbol{a}_1) = v(\boldsymbol{x})$, the function $\phi_n(\boldsymbol{x}; \tau_1, \tau_2, \tau_3)$ has the form

$$\phi_n(\boldsymbol{x} + \boldsymbol{a}_1; \tau_1, \tau_2, \tau_3) = \mathrm{e}^{\mathrm{i}k_1} \phi_n(\boldsymbol{x}; \tau_1, \tau_2, \tau_3) \tag{7.7}$$

and, here, k_1 can be complex with a non-zero imaginary part or a real number.

If k_1 is real in (7.7), then $\phi_n(\boldsymbol{x}; \tau_1, \tau_2, \tau_3)$ is a $\bar{\psi}_{n'}(\bar{\boldsymbol{k}}, \boldsymbol{x}; \tau_2, \tau_3)$. According to Theorem 7.1, a $\bar{\psi}_{n'}(\bar{\boldsymbol{k}}, \boldsymbol{x}; \tau_2, \tau_3)$ cannot be a $\phi_n(\boldsymbol{x}; \tau_1, \tau_2, \tau_3)$ except in some special cases when $\bar{\psi}_{n'}(\bar{\boldsymbol{k}}, \boldsymbol{x}; \tau_2, \tau_3)$ has a nodal surface intersecting the $\boldsymbol{a}_1$ axis at $\tau_1 \boldsymbol{a}_1$. Thus, k_1 in (7.7) can be real only in such special cases; in most cases, k_1 in (7.7) is complex with a nonzero imaginary part.

The imaginary part of k_1 in (7.7) can be either positive or negative, corresponding to that $\phi_n(\boldsymbol{x}; \tau_1, \tau_2, \tau_3)$ decays in the either positive or negative direction of $\boldsymbol{a}_1$. Such states $\phi_n(\boldsymbol{x}; \tau_1, \tau_2, \tau_3)$ with a nonzero imaginary part of k_1 in (7.7) cannot exist in a quantum wire with translational invariance in the $\boldsymbol{a}_1$ direction since they are divergent in either the negative or the positive direction of $\boldsymbol{a}_1$. However, they can play a significant role in the electronic states in a finite crystal or quantum dot without translational invariance.

The further quantum confinement of the one-dimensional Bloch waves $\bar{\psi}_n(\bar{\boldsymbol{k}}, \boldsymbol{x}; \tau_2, \tau_3)$ in the $\boldsymbol{a}_1$ direction will produce two different types of electronic states in the finite crystal or quantum dot.

One type of nontrivial solutions of (7.1) and (7.2) can be obtained from (7.7) by assigning

$$\begin{array}{rll} \psi_n(\boldsymbol{x}; \tau_1, \tau_2, \tau_3) = & c_{N_1,N_2,N_3} \phi_n(\boldsymbol{x}; \tau_1, \tau_2, \tau_3) & \text{if } \boldsymbol{x} \in \text{ the crystal} \\ = & 0 & \text{if } \boldsymbol{x} \notin \text{ the crystal,} \end{array} \tag{7.8}$$

where c_{N_1,N_2,N_3} is a normalization constant. The corresponding eigenvalue

$$\Lambda_n(\tau_1, \tau_2, \tau_3) = \lambda_n(\tau_1, \tau_2, \tau_3) \tag{7.9}$$

is dependent on τ_1, τ_2, and τ_3 but not on N_1, N_2, and N_3. A consequence of Theorem 7.1 is that for each energy band index n, there is only one such solution (7.8) of (7.1) and (7.2). This is a corner-like state in the finite crystal or the quantum dot since, in most cases, $\phi_n(\boldsymbol{x}; \tau_1, \tau_2, \tau_3)$ decays in either the positive or the negative direction of $\boldsymbol{a}_1$, $\boldsymbol{a}_2$, and $\boldsymbol{a}_3$.

Now, we try to find other solutions of (7.1) and (7.2) from the further quantum confinement of $\bar{\psi}_n(\bar{\boldsymbol{k}}, \boldsymbol{x}; \tau_2, \tau_3)$. We can expect that there are stationary Bloch states in the $\boldsymbol{a}_1$ direction, formed due to multiple reflections of $\bar{\psi}_n(\bar{\boldsymbol{k}}, \boldsymbol{x}; \tau_2, \tau_3)$ between the two boundary surfaces intersecting the $\boldsymbol{a}_1$ axis at $\tau_1 \boldsymbol{a}_1$ and $(\tau_1 + N_1)\boldsymbol{a}_1$.

Since[1]

$$\bar{\Lambda}_n(\bar{\boldsymbol{k}}; \tau_2, \tau_3) = \bar{\Lambda}_n(-\bar{\boldsymbol{k}}; \tau_2, \tau_3),$$

in general

$$f_{n,k_1}(\boldsymbol{x}; \tau_2, \tau_3) = c_+ \bar{\psi}_n(k_1 \bar{\boldsymbol{b}}_1, \boldsymbol{x}; \tau_2, \tau_3) + c_- \bar{\psi}_n(-k_1 \bar{\boldsymbol{b}}_1, \boldsymbol{x}; \tau_2, \tau_3), \quad 0 < k_1 < \pi,$$

where $c_\pm$ are not zero, is a nontrivial solution of (7.1).

In order to be a solution of (7.1) and (7.2), the function $f_{n,k_1}(\boldsymbol{x}; \tau_2, \tau_3)$ is further required to be zero at the left and the right faces of the finite crystal or quantum dot. By writing the left face equation of the finite crystal as $x_1 = x_{1,l}(x_2, x_3)$ and the right face equation of the finite crystal as $x_1 = x_{1,r}(x_2, x_3)$, we have

$$\begin{aligned} c_+ \bar{\psi}_n[k_1 \bar{\boldsymbol{b}}_1, \boldsymbol{x} \in \ & x_{1,l}(x_2, x_3); \tau_2, \tau_3] \\ & + c_- \bar{\psi}_n[-k_1 \bar{\boldsymbol{b}}_1, \boldsymbol{x} \in x_{1,l}(x_2, x_3); \tau_2, \tau_3] = 0, \\ c_+ \bar{\psi}_n[k_1 \bar{\boldsymbol{b}}_1, \boldsymbol{x} \in \ & x_{1,r}(x_2, x_3); \tau_2, \tau_3] \\ & + c_- \bar{\psi}_n[-k_1 \bar{\boldsymbol{b}}_1, \boldsymbol{x} \in x_{1,r}(x_2, x_3); \tau_2, \tau_3] = 0. \end{aligned} \tag{7.10}$$

Since $x_{1,r}(x_2, x_3) = x_{1,l}(x_2, x_3) + N_1$, we have

$$\bar{\psi}_n[k_1 \bar{\boldsymbol{b}}_1, \boldsymbol{x} \in x_{1,r}(x_2, x_3); \tau_2, \tau_3] = \mathrm{e}^{\mathrm{i} k_1 N_1} \bar{\psi}_n[k_1 \bar{\boldsymbol{b}}_1, \boldsymbol{x} \in x_{1,l}(x_2, x_3); \tau_2, \tau_3]$$

and

$$\hat{\psi}_n[-k_1 \bar{\boldsymbol{b}}_1, \boldsymbol{x} \in x_{1,r}(x_2, x_3); \tau_2, \tau_3] = \mathrm{e}^{-\mathrm{i} k_1 N_1} \hat{\psi}_n[-k_1 \bar{\boldsymbol{b}}_1, \boldsymbol{x} \in x_{1,l}(x_2, x_3); \tau_2, \tau_3]$$

due to (7.5). Therefore, if $c_\pm$ in (7.10) are not both zero, $\mathrm{e}^{\mathrm{i} k_1 N_1} - \mathrm{e}^{-\mathrm{i} k_1 N_1} = 0$ has to be true for these stationary Bloch states, independent of τ_1.

Stationary Bloch state solutions of (7.1) and (7.2) from the further confinement of $\bar{\psi}_n(\bar{\boldsymbol{k}}, \boldsymbol{x}; \tau_2, \tau_3)$ should have the form

$$\begin{aligned} \psi_{n,j_1}(\boldsymbol{x}; \tau_1, \tau_2, \tau_3) &= f_{n,\kappa_1}(\boldsymbol{x}; \tau_1, \tau_2, \tau_3) \quad && \text{if } \boldsymbol{x} \in \text{ the crystal} \\ &= 0 && \text{if } \boldsymbol{x} \notin \text{ the crystal,} \end{aligned} \tag{7.11}$$

where

$$f_{n,k_1}(\boldsymbol{x}; \tau_1, \tau_2, \tau_3) = c_{n,k_1;\tau_1} \bar{\psi}_n(k_1 \bar{\boldsymbol{b}}_1, \boldsymbol{x}; \tau_2, \tau_3) + c_{n,-k_1;\tau_1} \bar{\psi}_n(-k_1 \bar{\boldsymbol{b}}_1, \boldsymbol{x}; \tau_2, \tau_3);$$

here, $c_{n,\pm k_1;\tau_1}$ are dependent on τ_1 and

[1] As solutions of (6.1) and (6.2), $\bar{\psi}(\bar{\boldsymbol{k}}, \boldsymbol{x})$ and $\bar{\psi}^*(\bar{\boldsymbol{k}}, \boldsymbol{x})$ have the same energy $\bar{\Lambda}$. $\bar{\psi}^*_n(\bar{\boldsymbol{k}}, \boldsymbol{x}; \tau_2, \tau_3) = \bar{\psi}_n(-\bar{\boldsymbol{k}}, \boldsymbol{x}; \tau_2, \tau_3)$ leads to $\bar{\Lambda}_n(-\bar{\boldsymbol{k}}; \tau_2, \tau_3) = \bar{\Lambda}_n(\bar{\boldsymbol{k}}; \tau_2, \tau_3)$.

$$\kappa_1 = j_1\ \pi/N_1, \quad j_1 = 1, 2, ..., N_1 - 1, \tag{7.12}$$

where j_1 is a stationary Bloch state index. These solutions $\psi_{n,j_1}(\boldsymbol{x}; \tau_1, \tau_2, \tau_3)$ satisfying (7.1) and (7.2) have energies Λ given by

$$\Lambda_{n,j_1}(\tau_2, \tau_3) = \bar{\Lambda}_n(\kappa_1 \bar{\boldsymbol{b}}_1; \tau_2, \tau_3). \tag{7.13}$$

Each energy given in (7.13) is dependent on N_1 and τ_2, τ_3 but not on τ_1 and N_2, N_3. For each bulk energy band n, there are $N_1 - 1$ such states. They are side-like states in the finite crystal or quantum dot since $\bar{\psi}_n(\bar{\boldsymbol{k}}, \boldsymbol{x}; \tau_2, \tau_3)$ are side-like states in the quantum wire.

Because of (7.4), (7.9), and (7.13), for the further quantum confinement of one-dimensional Bloch wave $\bar{\psi}_n(\bar{\boldsymbol{k}}, \boldsymbol{x}; \tau_2, \tau_3)$, in general the energy of the corner-like state is always above the energy of every relevant side-like state:

$$\Lambda_n(\tau_1, \tau_2, \tau_3) > \Lambda_{n,j_1}(\tau_2, \tau_3). \tag{7.14}$$

7.3 Further Quantum Confinement of $\bar{\psi}_{n,j_3}(\bar{\boldsymbol{k}}, \boldsymbol{x}; \tau_2, \tau_3)$

For the quantum confinement of surface-like states $\bar{\psi}_{n,j_3}(\bar{\boldsymbol{k}}, \boldsymbol{x}; \tau_2, \tau_3)$, we consider an orthorhombic parallelogram C' having a rectangular bottom face $x_3 = \tau_3$, a rectangular top face $x_3 = \tau_3 + N_3$, a front face perpendicularly intersecting the $\boldsymbol{a}_2$ axis at $\tau_2 \boldsymbol{a}_2$ and a rear face perpendicularly intersecting it at $(\tau_2 + 1)\boldsymbol{a}_2$, and a left face perpendicularly intersecting the $\boldsymbol{a}_1$ axis at $\tau_1 \boldsymbol{a}_1$ and a right face perpendicularly intersecting it at $(\tau_1 + 1)\boldsymbol{a}_1$, as shown in Fig. 7.2. We define a function set $\phi_{j_3}(\boldsymbol{x}; \tau_1, \tau_2, \tau_3)$ by the condition that each function is zero at the bottom and top faces of C' and behaves as a Bloch stationary state $\bar{\psi}_{j_3}(\bar{\boldsymbol{k}}, \boldsymbol{x}; \tau_2, \tau_3)$ [2] with a wave number $j_3/N_3\ \pi|\boldsymbol{b}_3|$ in the $\boldsymbol{b}_3$ direction and is zero at the other four faces of C'. The eigenvalues and eigenfunctions of (5.1) with this condition are denoted by $\lambda_{n,j_3}(\tau_1, \tau_2)$ and $\phi_{n,j_3}(\boldsymbol{x}; \tau_1, \tau_2, \tau_3)$, where $n\ = 0, 1, 2, ...$ For each eigenvalue $\lambda_{n,j_3}(\tau_1, \tau_2)$ of the problem defined by (5.1) and this condition, we have the following theorem between it and the eigenvalues $\bar{\Lambda}_{n,j_3}(\bar{\boldsymbol{k}}; \tau_2)$ in (6.19) of $\bar{\psi}_{n,j_3}(\bar{\boldsymbol{k}}, \boldsymbol{x}; \tau_2, \tau_3)$.

Theorem 7.2.

$$\lambda_{n,j_3}(\tau_1, \tau_2) \geq \bar{\Lambda}_{n,j_3}(\bar{\boldsymbol{k}}; \tau_2). \tag{7.15}$$

Theorem 7.2 can be proven similar to Theorem 7.1; we only need to note that $\bar{\psi}_{n,j_3}(\bar{\boldsymbol{k}}, \boldsymbol{x}; \tau_2, \tau_3)$ with different j_3 are orthogonal to each other; thus, each one of $\bar{\psi}_{n,j_3}(\bar{\boldsymbol{k}}, \boldsymbol{x}; \tau_2, \tau_3)$ with a different j_3 will be confined in the $\boldsymbol{a}_1$ direction independently.

[2] $\bar{\psi}_{j_3}(\bar{\boldsymbol{k}}, \boldsymbol{x}; \tau_2, \tau_3)$ generally can be a (any) linear combination of $\bar{\psi}_{n,j_3}(\bar{\boldsymbol{k}}, \boldsymbol{x}; \tau_2, \tau_3)$ with different n.

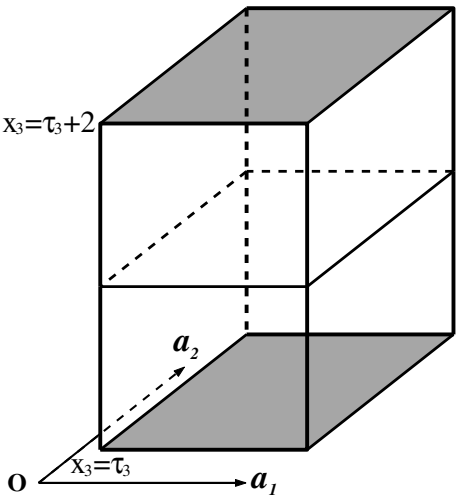

Fig. 7.2. The orthorhombic parallelogram C' for the further quantum confinement of $\bar{\psi}_{n,j_3}(\bar{\boldsymbol{k}}, \boldsymbol{x}; \tau_2, \tau_3)$. The two shadowed faces of $\partial C_3'$ determined by $x_3 = \tau_3$ and $x_3 = \tau_3 + N_3$ (in the figure is shown the case $N_3 = 2$) and the two thick-lined faces of $\partial C_2'$ are the four faces on which each function $\bar{\psi}_{n,j_3}(\bar{\boldsymbol{k}}, \boldsymbol{x}; \tau_2, \tau_3)$ is zero. The left face and the right face are the two faces on which each function $\phi_{j_3}(\boldsymbol{x}; \tau_1, \tau_2, \tau_3)$ is further required to be zero.

Theorem 7.2 is similar to Theorem 7.1; the consequences of the quantum confinement of one-dimensional Bloch waves $\bar{\psi}_n(\bar{\boldsymbol{k}}, \boldsymbol{x}; \tau_2, \tau_3)$ in the $\boldsymbol{a}_1$ direction due to Theorem 7.1 can be similarly applied to the quantum confinement of one-dimensional Bloch waves $\bar{\psi}_{n,j_3}(\bar{\boldsymbol{k}}, \boldsymbol{x}; \tau_2, \tau_3)$ in the $\boldsymbol{a}_1$ direction.

Because $v(\boldsymbol{x} + \boldsymbol{a}_1) = v(\boldsymbol{x})$, the function $\phi_{n,j_3}(\boldsymbol{x}; \tau_1, \tau_2, \tau_3)$ has the form

$$\phi_{n,j_3}(\boldsymbol{x} + \boldsymbol{a}_1; \tau_1, \tau_2, \tau_3) = \mathrm{e}^{\mathrm{i}k_1} \phi_{n,j_3}(\boldsymbol{x}; \tau_1, \tau_2, \tau_3). \tag{7.16}$$

k_1 in (7.16) can be complex with a nonzero imaginary part or a real number. If k_1 is real in (7.16), then $\phi_{n,j_3}(\boldsymbol{x}; \tau_1, \tau_2, \tau_3)$ is a $\bar{\psi}_{n',j_3}(\bar{\boldsymbol{k}}, \boldsymbol{x}; \tau_2, \tau_3)$. According to Theorem 7.2, a $\bar{\psi}_{n',j_3}(\bar{\boldsymbol{k}}, \boldsymbol{x}; \tau_2, \tau_3)$ cannot be a $\phi_{n,j_3}(\boldsymbol{x}; \tau_1, \tau_2, \tau_3)$ except in some special cases when $\bar{\psi}_{n',j_3}(\bar{\boldsymbol{k}}, \boldsymbol{x}; \tau_2, \tau_3)$ has a nodal surface intersecting the $\boldsymbol{a}_1$ axis at $\tau_1 \boldsymbol{a}_1$. Therefore, k_1 in (7.16) can be real only in such special cases; in most cases, k_1 in (7.16) is complex with a nonzero imaginary part.

The imaginary part of k_1 in (7.16) can be either positive or negative, corresponding to that $\phi_{n,j_3}(\boldsymbol{x}; \tau_1, \tau_2, \tau_3)$ decays in either the positive or the negative direction of $\boldsymbol{a}_1$. Such states $\phi_{n,j_3}(\boldsymbol{x}; \tau_1, \tau_2, \tau_3)$ with a nonzero imaginary part of k_1 in (7.16) cannot exist in a quantum wire with translational invariance in the $\boldsymbol{a}_1$ direction since they are divergent in either the negative or the positive direction of $\boldsymbol{a}_1$. However, they can play a significant role in the electronic states in a finite crystal or quantum dot without translational invariance.

The further quantum confinement in the $\boldsymbol{a}_1$ direction of one-dimensional Bloch waves $\bar{\psi}_{n,j_3}(\bar{\boldsymbol{k}}, \boldsymbol{x}; \tau_2, \tau_3)$ will produce two different types of electronic states in the finite crystal or quantum dot.

One type of nontrivial solutions of (7.1) and (7.2) can be obtained from (7.16) by assigning

$$\begin{aligned} \psi_{n,j_3}(\boldsymbol{x}; \tau_1, \tau_2, \tau_3) &= c_{N_1,N_2,N_3}\phi_{n,j_3}(\boldsymbol{x}; \tau_1, \tau_2, \tau_3) \quad \text{if } \boldsymbol{x} \in \text{ the crystal} \\ &= 0 \qquad\qquad\qquad\qquad\qquad\quad \text{if } \boldsymbol{x} \notin \text{ the crystal,} \end{aligned} \tag{7.17}$$

where c_{N_1,N_2,N_3} is a normalization constant. The corresponding eigenvalue

$$\Lambda_{n,j_3}(\tau_1, \tau_2) = \lambda_{n,j_3}(\tau_1, \tau_2) \tag{7.18}$$

is dependent on N_3, τ_1, and τ_2 but not on N_1, N_2 and τ_3. A consequence of Theorem 7.2 is that for each bulk energy band n and each j_3, there is only one such solution (7.17) of (7.1) and (7.2). For each bulk energy band, there are $N_3 - 1$ such states in the finite crystal or quantum dot. They are side-like states in the finite crystal or quantum dot since $\psi_{n,j_3}(\boldsymbol{x}; \tau_1, \tau_2, \tau_3)$ decays in either the positive or the negative direction of $\boldsymbol{a}_1$ and $\boldsymbol{a}_2$ in most cases.

Now, we try to find other solutions of (7.1) and (7.2) from the further quantum confinement of $\bar{\psi}_{n,j_3}(\bar{\boldsymbol{k}}, \boldsymbol{x}; \tau_2, \tau_3)$. We can expect that there are stationary Bloch states in the $\boldsymbol{a}_1$ direction, formed due to the multiple reflections of the one-dimensional Bloch waves $\bar{\psi}_{n,j_3}(\bar{\boldsymbol{k}}, \boldsymbol{x}; \tau_2, \tau_3)$ between two boundary surfaces intersecting the $\boldsymbol{a}_1$ axis at $\tau_1\boldsymbol{a}_1$ and $(\tau_1 + N_1)\boldsymbol{a}_1$.

Since the energies (6.19) of $\bar{\psi}_{n,j_3}(\bar{\boldsymbol{k}}, \boldsymbol{x}; \tau_2, \tau_3)$ satisfy[3]

$$\bar{\Lambda}_{n,j_3}(\bar{\boldsymbol{k}}; \tau_2) = \bar{\Lambda}_{n,j_3}(-\bar{\boldsymbol{k}}; \tau_2), \tag{7.19}$$

in general

$$\begin{aligned} f_{n,k_1,j_3}(\boldsymbol{x}; \tau_2, \tau_3) &= c_+\bar{\psi}_{n,j_3}(k_1\bar{\boldsymbol{b}}_1, \boldsymbol{x}; \tau_2, \tau_3) \\ &\quad + c_-\bar{\psi}_{n,j_3}(-k_1\bar{\boldsymbol{b}}_1, \boldsymbol{x}; \tau_2, \tau_3), \quad 0 < k_1 < \pi, \end{aligned}$$

where $c_\pm$ are not zero, is a nontrivial solution of (7.1) because of (7.19). Very similarly to what we did in Section 7.2, we can obtain that the stationary Bloch state solutions of (7.1) and (7.2) from the further confinement of $\bar{\psi}_{n,j_3}(\bar{\boldsymbol{k}}, \boldsymbol{x}; \tau_2, \tau_3)$ should have the form

$$\begin{aligned} \psi_{n,j_1,j_3}(\boldsymbol{x}; \tau_1, \tau_2, \tau_3) &= f_{n,\kappa_1,j_3}(\boldsymbol{x}; \tau_1, \tau_2, \tau_3) \quad \text{if } \boldsymbol{x} \in \text{ the crystal} \\ &= 0 \qquad\qquad\qquad\qquad\quad \text{if } \boldsymbol{x} \notin \text{ the crystal,} \end{aligned} \tag{7.20}$$

where

$$\begin{aligned} f_{n,k_1,j_3}(\boldsymbol{x}; \tau_1, \tau_2, \tau_3) &= c_{n,k_1,j_3;\tau_1}\bar{\psi}_{n,j_3}(k_1\bar{\boldsymbol{b}}_1, \boldsymbol{x}; \tau_2, \tau_3) \\ &\quad + c_{n,-k_1,j_3;\tau_1}\bar{\psi}_{n,j_3}(-k_1\bar{\boldsymbol{b}}_1, \boldsymbol{x}; \tau_2, \tau_3); \end{aligned}$$

[3] $\bar{\psi}^*_{n,j_3}(\bar{\boldsymbol{k}}, \boldsymbol{x}; \tau_2, \tau_3) = \bar{\psi}_{n,j_3}(-\bar{\boldsymbol{k}}, \boldsymbol{x}; \tau_2, \tau_3)$ leads to (7.19).

$c_{n,\pm k_1,j_3;\tau_1}$ are dependent on τ_1, $\kappa_1 = j_1\ \pi/N_1$, and $j_1 = 1, 2, ..., N_1 - 1$ as in (7.12). Stationary Bloch state solutions $\psi_{n,j_1,j_3}(\boldsymbol{x}; \tau_1, \tau_2, \tau_3)$ satisfying (7.1) and (7.2) have energies Λ given by

$$\Lambda_{n,j_1,j_3}(\tau_2) = \bar{\Lambda}_{n,j_3}(\kappa_1 \bar{\boldsymbol{b}}_1; \tau_2). \tag{7.21}$$

Each energy in (7.21) for this case is dependent on N_1, N_3, and τ_2, but independent of τ_1, τ_3, and N_2. Those are surface-like states in the finite crystal or quantum dot because $\bar{\psi}_{n,j_3}(\bar{\boldsymbol{k}}, \boldsymbol{x}; \tau_2, \tau_3)$ are surface-like states in the quantum wire. For each bulk energy band n, there are $(N_1 - 1)(N_3 - 1)$ such states in the finite crystal or quantum dot.

Similar to (7.14), because of (7.15), (7.18), and (7.21), for the further quantum confinement of $\bar{\psi}_{n,j_3}(\bar{\boldsymbol{k}}, \boldsymbol{x}; \tau_2, \tau_3)$, in general, the energy of a side-like state is above the energy of a relevant surface-like state:

$$\Lambda_{n,j_3}(\tau_1, \tau_2) > \Lambda_{n,j_1,j_3}(\tau_2). \tag{7.22}$$

7.4 Further Quantum Confinement of $\bar{\psi}_{n,j_2}(\bar{\boldsymbol{k}}, x; \tau_2, \tau_3)$

The further quantum confinement of the surface-like states $\bar{\psi}_{n,j_2}(\bar{\boldsymbol{k}}, \boldsymbol{x}; \tau_2, \tau_3)$ in the quantum wire $\boldsymbol{a}_1$ direction can be similarly discussed and for each energy band n it will give $N_2 - 1$ side-like states and $(N_1 - 1)(N_2 - 1)$ surface-like states in the finite crystal or quantum dot.

For the quantum confinement of $\bar{\psi}_{n,j_2}(\bar{\boldsymbol{k}}, \boldsymbol{x}; \tau_2, \tau_3)$, we consider an orthorhombic parallelogram C'' having a rectangular bottom face $x_3 = \tau_3$, a rectangular top face $x_3 = \tau_3 + 1$, a front face perpendicularly intersecting the $\boldsymbol{a}_2$ axis at $\tau_2 \boldsymbol{a}_2$ and a rear face perpendicularly intersecting it at $(\tau_2 + N_2)\boldsymbol{a}_2$, and a left face perpendicularly intersecting the $\boldsymbol{a}_1$ axis at $\tau_1 \boldsymbol{a}_1$ and a right face perpendicularly intersecting it at $(\tau_1 + 1)\boldsymbol{a}_1$, as shown in Fig. 7.3. We define a function set $\phi_{j_2}(\boldsymbol{x}; \tau_1, \tau_2, \tau_3)$ by the condition that each function is zero at the bottom and top faces of C'', is zero at the front face and the rear face of C'' and behaves as a Bloch stationary state $\bar{\psi}_{j_2}(\bar{\boldsymbol{k}}, \boldsymbol{x}; \tau_2, \tau_3)$ [4] with a wave number $j_2/N_2\ \pi|\hat{\boldsymbol{b}}_2|$ in the $\hat{\boldsymbol{b}}_2$ direction, and is zero at the two faces $\partial C_1''$ of C''. The eigenvalues and eigenfunctions of (5.1) with this condition are denoted by $\lambda_{n,j_2}(\tau_1, \tau_3)$ and $\phi_{n,j_2}(\boldsymbol{x}; \tau_1, \tau_2, \tau_3)$, where $n = 0, 1, 2, ...$ For each eigenvalue $\lambda_{n,j_2}(\tau_1, \tau_3)$ of the problem defined by (5.1) and this boundary condition, we have the following theorem between it and the eigenvalues $\bar{\Lambda}_{n,j_2}(\bar{\boldsymbol{k}}; \tau_3)$ in (6.14) of $\bar{\psi}_{n,j_2}(\bar{\boldsymbol{k}}, \boldsymbol{x}; \tau_2, \tau_3)$.

Theorem 7.3.

$$\lambda_{n,j_2}(\tau_1, \tau_3) \geq \bar{\Lambda}_{n,j_2}(\bar{\boldsymbol{k}}; \tau_3). \tag{7.23}$$

[4] $\bar{\psi}_{j_2}(\bar{\boldsymbol{k}}, \boldsymbol{x}; \tau_2, \tau_3)$ generally can be a (any) linear combination of $\bar{\psi}_{n,j_2}(\bar{\boldsymbol{k}}, \boldsymbol{x}; \tau_2, \tau_3)$ of different n.

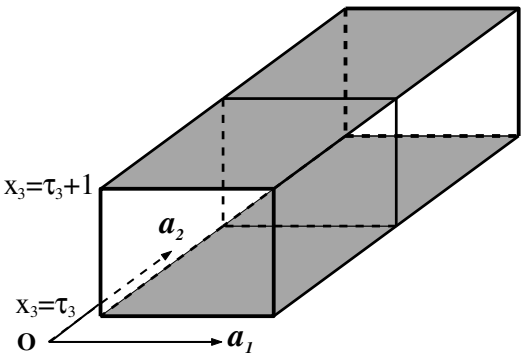

Fig. 7.3. The parallelogram C'' for the quantum confinement of $\bar{\psi}_{n,j_2}(\bar{\boldsymbol{k}}, \boldsymbol{x}; \tau_2, \tau_3)$. The two shadowed faces of $\partial C_3''$ determined by $x_3 = \tau_3$ and $x_3 = \tau_3 + 1$ and the two thick-lined faces of $\partial C_2''$ determined by $\tau_2 \boldsymbol{a}_2$ and $(\tau_2 + N_2)\boldsymbol{a}_2$ (in the figure is shown the case $N_2 = 2$) are the four faces on which each function $\bar{\psi}_{n,j_2}(\bar{\boldsymbol{k}}, \boldsymbol{x}; \tau_2, \tau_3)$ is zero. The left face and the right face of $\partial C_1''$ are the two faces on which each function $\phi_{j_2}(\boldsymbol{x}; \tau_1, \tau_2, \tau_3)$ is further required to be zero.

Theorem 7.3 can be proven similar to Theorem 7.1; we only need to note that $\bar{\psi}_{n,j_2}(\bar{\boldsymbol{k}}, \boldsymbol{x}; \tau_2, \tau_3)$ with different j_2 are orthogonal to each other, thus, each one of them will be confined in the $\boldsymbol{a}_1$ direction independently.

Theorem 7.3 is similar to Theorem 7.1; the consequences of the quantum confinement of one-dimensional Bloch waves $\bar{\psi}_n(\bar{\boldsymbol{k}}, \boldsymbol{x}; \tau_2, \tau_3)$ in the $\boldsymbol{a}_1$ direction due to Theorem 7.1 can be similarly applied to the quantum confinement of one-dimensional Bloch waves $\bar{\psi}_{n,j_2}(\bar{\boldsymbol{k}}, \boldsymbol{x}; \tau_2, \tau_3)$ in the $\boldsymbol{a}_1$ direction.

Because $v(\boldsymbol{x} + \boldsymbol{a}_1) = v(\boldsymbol{x})$, the function $\phi_{n,j_2}(\boldsymbol{x}; \tau_1, \tau_2, \tau_3)$ has the form

$$\phi_{n,j_2}(\boldsymbol{x} + \boldsymbol{a}_1; \tau_1, \tau_2, \tau_3) = \mathrm{e}^{\mathrm{i}k_1} \phi_{n,j_2}(\boldsymbol{x}; \tau_1, \tau_2, \tau_3). \tag{7.24}$$

k_1 in (7.24) can be complex with a nonzero imaginary part or a real number. If k_1 is real in (7.24), then $\phi_{n,j_2}(\boldsymbol{x}; \tau_1, \tau_2, \tau_3)$ is a $\bar{\psi}_{n',j_2}(\bar{\boldsymbol{k}}, \boldsymbol{x}; \tau_2, \tau_3)$. According to Theorem 7.3, a $\bar{\psi}_{n',j_2}(\bar{\boldsymbol{k}}, \boldsymbol{x}; \tau_2, \tau_3)$ cannot be a $\phi_{n,j_2}(\boldsymbol{x}; \tau_1, \tau_2, \tau_3)$ except in some special cases when $\bar{\psi}_{n',j_2}(\bar{\boldsymbol{k}}, \boldsymbol{x}; \tau_2, \tau_3)$ has a nodal surface intersecting the $\boldsymbol{a}_1$ axis at $\tau_1 \boldsymbol{a}_1$. Therefore, k_1 in (7.24) can be real only in such special cases; in most cases, k_1 in (7.24) is complex with a nonzero imaginary part.

The imaginary part of k_1 in (7.24) can be either positive or negative; this corresponds to that $\phi_{n,j_2}(\boldsymbol{x}; \tau_1, \tau_2, \tau_3)$ decays in either the positive or the negative direction of $\boldsymbol{a}_1$. Such states $\phi_{n,j_2}(\boldsymbol{x}; \tau_1, \tau_2, \tau_3)$ with a nonzero imaginary part of k_1 in (7.24) cannot exist in a quantum wire with translational invariance in the $\boldsymbol{a}_1$ direction because they are divergent in either the negative or the positive direction of $\boldsymbol{a}_1$. However, these states can play a significant role in the electronic states in a finite crystal or quantum dot without translational invariance.

The further quantum confinement in the $\boldsymbol{a}_1$ direction of one-dimensional Bloch waves $\bar{\psi}_{n,j_2}(\bar{\boldsymbol{k}}, \boldsymbol{x}; \tau_2, \tau_3)$ will produce two different types of electronic states in the finite crystal or quantum dot.

One type of nontrivial solutions of (7.1) and (7.2) can be obtained from (7.24) by assigning

$$\begin{aligned} \psi_{n,j_2}(\boldsymbol{x}; \tau_1, \tau_2, \tau_3) &= c_{N_1,N_2,N_3}\phi_{n,j_2}(\boldsymbol{x}; \tau_1, \tau_2, \tau_3) \quad \text{if } \boldsymbol{x} \in \text{ the crystal} \\ &= 0 \qquad\qquad\qquad\qquad\qquad\quad \text{if } \boldsymbol{x} \notin \text{ the crystal,} \end{aligned} \tag{7.25}$$

where c_{N_1,N_2,N_3} is a normalization constant. The corresponding eigenvalue is

$$\Lambda_{n,j_2}(\tau_1, \tau_3) = \lambda_{n,j_2}(\tau_1, \tau_3). \tag{7.26}$$

For each band n and each j_2, there is one electronic state $\psi_{n,j_2}(\boldsymbol{x}; \tau_1, \tau_2, \tau_3)$ which is $\phi_{n,j_2}(\boldsymbol{x}; \tau_1, \tau_2, \tau_3)$ inside the crystal or dot but zero otherwise, whose energy $\Lambda_{n,j_2}(\tau_1, \tau_3)$ depends on τ_1, τ_3, and N_2 but not on N_1, N_3, and τ_2. For each bulk energy band n, there are $N_2 - 1$ such states in the finite crystal or quantum dot. They are side-like states in the finite crystal or quantum dot since $\phi_{n,j_2}(\boldsymbol{x}; \tau_1, \tau_2, \tau_3)$ decays in either the positive or the negative direction of $\boldsymbol{a}_1$ and $\boldsymbol{a}_3$ in most cases.

Now, we try to find other solutions of (7.1) and (7.2) from the quantum confinement of $\bar{\psi}_{n,j_2}(\bar{\boldsymbol{k}}, \boldsymbol{x}; \tau_2, \tau_3)$. We can expect that there are stationary Bloch states in the $\boldsymbol{a}_1$ direction, formed due to the multiple reflections of $\bar{\psi}_{n,j_2}(\bar{\boldsymbol{k}}, \boldsymbol{x}; \tau_2, \tau_3)$ between two boundary surfaces perpendicularly intersecting the $\boldsymbol{a}_1$ axis at $\tau_1\boldsymbol{a}_1$ and $(\tau_1 + N_1)\boldsymbol{a}_1$.

Since for the energies of the electronic states $\bar{\psi}_{n,j_2}(\bar{\boldsymbol{k}}, \boldsymbol{x}; \tau_2, \tau_3)$ in the quantum wire we have[5]

$$\bar{\Lambda}_{n,j_2}(\bar{\boldsymbol{k}}; \tau_3) = \bar{\Lambda}_{n,j_2}(-\bar{\boldsymbol{k}}; \tau_3), \tag{7.27}$$

in general

$$\begin{aligned} f_{n,k_1,j_2}(\boldsymbol{x}; \tau_2, \tau_3) &= c_+\bar{\psi}_{n,j_2}(k_1\bar{\boldsymbol{b}}_1, \boldsymbol{x}; \tau_2, \tau_3) \\ &\quad + c_-\bar{\psi}_{n,j_2}(-k_1\bar{\boldsymbol{b}}_1, \boldsymbol{x}; \tau_2, \tau_3), \qquad 0 < k_1 < \pi, \end{aligned}$$

where $c_\pm$ are not zero, is a nontrivial solution of (7.1) due to (7.27). Similar to the cases in Sections 7.2 and 7.3, we can obtain that the stationary Bloch state solutions of (7.1) and (7.2) originating from the quantum confinement of $\bar{\psi}_{n,j_2}(\bar{\boldsymbol{k}}, \boldsymbol{x}; \tau_2, \tau_3)$ should have the form

$$\begin{aligned} \psi_{n,j_1,j_2}(\boldsymbol{x}; \tau_1, \tau_2, \tau_3) &= f_{n,\kappa_1,j_2}(\boldsymbol{x}; \tau_1, \tau_2, \tau_3) \quad \text{if } \boldsymbol{x} \in \text{ the crystal} \\ &= 0 \qquad\qquad\qquad\qquad\quad \text{if } \boldsymbol{x} \notin \text{ the crystal,} \end{aligned} \tag{7.28}$$

where

$$\begin{aligned} f_{n,k_1,j_2}(\boldsymbol{x}; \tau_1, \tau_2, \tau_3) &= c_{n,k_1,j_2;\tau_1}\bar{\psi}_{n,j_2}(k_1\bar{\boldsymbol{b}}_1, \boldsymbol{x}; \tau_2, \tau_3) \\ &\quad + c_{n,-k_1,j_2;\tau_1}\bar{\psi}_{n,j_2}(-k_1\bar{\boldsymbol{b}}_1, \boldsymbol{x}; \tau_2, \tau_3), \end{aligned}$$

[5] $\bar{\psi}^*_{n,j_2}(\bar{\boldsymbol{k}}, \boldsymbol{x}; \tau_2, \tau_3) = \bar{\psi}_{n,j_2}(-\bar{\boldsymbol{k}}, \boldsymbol{x}; \tau_2, \tau_3)$ leads to (7.27).

$c_{n,\pm k_1,j_2;\tau_1}$ are dependent on τ_1, $\kappa_1 = j_1\pi/N_1$, and $j_1 = 1, 2, ..., N_1 - 1$ as in (7.12). Stationary Bloch state solutions $\psi_{n,j_1,j_2}(\boldsymbol{x}; \tau_1, \tau_2, \tau_3)$ satisfying (7.1) and (7.2) have energies Λ given by

$$\Lambda_{n,j_1,j_2}(\tau_3) = \bar{\Lambda}_{n,j_2}(\kappa_1 \bar{\boldsymbol{b}}_1; \tau_3). \tag{7.29}$$

Each energy $\Lambda_{n,j_1,j_2}(\tau_3)$ for this case is dependent on N_1, N_2, and τ_3, but independent of τ_1, τ_2, and N_3. These are surface-like states in the finite crystal or quantum dot since $\bar{\psi}_{n,j_2}(\bar{\boldsymbol{k}}, \boldsymbol{x}; \tau_2, \tau_3)$ are surface-like states in the quantum wire. For each bulk energy band n, there are $(N_1 - 1)(N_2 - 1)$ such states in the finite crystal or quantum dot.

Similar to (7.22), because of (7.23), (7.26), and (7.29), for the further quantum confinement of $\bar{\psi}_{n,j_2}(\bar{\boldsymbol{k}}, \boldsymbol{x}; \tau_2, \tau_3)$ in general the energy of a side-like state is above the energy of a relevant surface-like state:

$$\Lambda_{n,j_2}(\tau_1, \tau_3) > \Lambda_{n,j_1,j_2}(\tau_3). \tag{7.30}$$

7.5 Further Quantum Confinement of $\bar{\psi}_{n,j_2,j_3}(\bar{\boldsymbol{k}}, \boldsymbol{x}; \tau_2, \tau_3)$

For the quantum confinement of bulk-like states $\bar{\psi}_{n,j_2,j_3}(\bar{\boldsymbol{k}}, \boldsymbol{x}; \tau_2, \tau_3)$, we consider an orthorhombic parallelogram C''' having a rectangular bottom face at $x_3 = \tau_3$, a rectangular top face at $x_3 = \tau_3 + N_3$, a front face perpendicularly intersecting the $\boldsymbol{a}_2$ axis at $\tau_2\boldsymbol{a}_2$ and a rear face perpendicularly intersecting it at $(\tau_2 + N_2)\boldsymbol{a}_2$, and a left face perpendicularly intersecting the $\boldsymbol{a}_1$ axis at $\tau_1\boldsymbol{a}_1$ and a right face perpendicularly intersecting it at $(\tau_1 + 1)\boldsymbol{a}_1$, as shown in Fig. 7.4. We define a function set $\phi_{j_2,j_3}(\boldsymbol{x}; \tau_1, \tau_2, \tau_3)$ by the condition that each function is zero at the two faces of $\partial C_2'''$ and behaves as a Bloch stationary state with a wave number $j_2/N_2\ \pi|\hat{\boldsymbol{b}}_2|$ in the $\hat{\boldsymbol{b}}_2$ direction, is zero at the two faces of $\partial C_3'''$ and behaves as a Bloch stationary state with a wave number $j_3/N_3\ \pi|\boldsymbol{b}_3|$ in the $\boldsymbol{b}_3$ direction as $\bar{\psi}_{j_2,j_3}(\bar{\boldsymbol{k}}, \boldsymbol{x}; \tau_2, \tau_3)$, [6] and is zero at the two faces $\partial C_1'''$. The eigenvalues and eigenfunctions of (5.1) under this condition are denoted by $\lambda_{n,j_2,j_3}(\tau_1)$ and $\phi_{n,j_2,j_3}(\boldsymbol{x}; \tau_1, \tau_2, \tau_3)$, where $n = 0, 1, 2, ...$ For each eigenvalue $\lambda_{n,j_2,j_3}(\tau_1)$ of the problem defined by (5.1) and this condition, we have the following theorem between it and the eigenvalues $\bar{\Lambda}_{n,j_2,j_3}(\bar{\boldsymbol{k}})$ in (6.22) of $\bar{\psi}_{n,j_2,j_3}(\bar{\boldsymbol{k}}, \boldsymbol{x}; \tau_2, \tau_3)$.

Theorem 7.4.

$$\lambda_{n,j_2,j_3}(\tau_1) \geq \bar{\Lambda}_{n,j_2,j_3}(\bar{\boldsymbol{k}}). \tag{7.31}$$

Theorem 7.4 can be proven similar to Theorems 7.1 to 7.3; we only need to note that $\bar{\psi}_{n,j_2,j_3}(\bar{\boldsymbol{k}}, \boldsymbol{x}; \tau_2, \tau_3)$ with different j_2 or j_3 are orthogonal to each other, thus, each one of $\bar{\psi}_{n,j_2,j_3}(\bar{\boldsymbol{k}}, \boldsymbol{x}; \tau_2, \tau_3)$ with a different j_2 or j_3 will be confined in the $\boldsymbol{a}_1$ direction independently.

[6] $\bar{\psi}_{j_2,j_3}(\bar{\boldsymbol{k}}, \boldsymbol{x}; \tau_2, \tau_3)$ can in general be a (any) linear combination of $\bar{\psi}_{n,j_2,j_3}(\bar{\boldsymbol{k}}, \boldsymbol{x}; \tau_2, \tau_3)$ with different n.

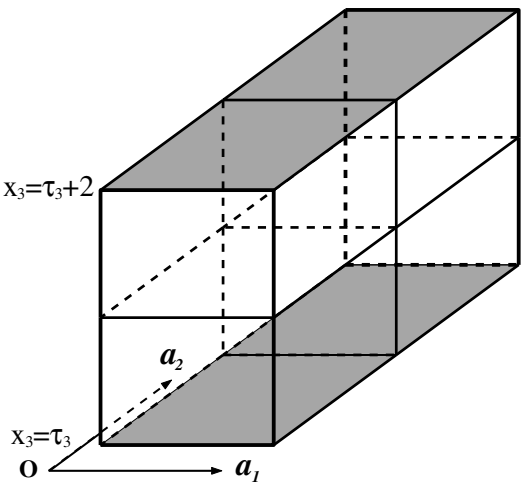

Fig. 7.4. The parallelogram C''' for the quantum confinement of $\bar{\psi}_{n,j_2,j_3}(\bar{\boldsymbol{k}},\boldsymbol{x};\tau_2,\tau_3)$. The two shadowed faces of $\partial C_3'''$ determined by $x_3 = \tau_3$ and $x_3 = (\tau_3 + N_3)$ (in the figure is shown the case $N_3 = 2$) and the two thick-lined faces of $\partial C_2'''$ determined by $\tau_2\boldsymbol{a}_2$ and $(\tau_2 + N_2)\boldsymbol{a}_2$ (in the figure is shown the case $N_2 = 2$) are the four faces on which each function $\bar{\psi}_{n,j_2,j_3}(\bar{\boldsymbol{k}},\boldsymbol{x};\tau_2,\tau_3)$ is zero. The left face and the right face of $\partial C_1'''$ are the two faces on which each function $\phi_{j_2,j_3}(\boldsymbol{x};\tau_1,\tau_2,\tau_3)$ is further required to be zero.

Theorem 7.4 is similar to Theorem 7.1; the consequences of the quantum confinement of one-dimensional Bloch waves $\bar{\psi}_n(\bar{\boldsymbol{k}},\boldsymbol{x};\tau_2,\tau_3)$ in the $\boldsymbol{a}_1$ direction due to Theorem 7.1 can be similarly applied to the quantum confinement of one-dimensional Bloch waves $\bar{\psi}_{n,j_2,j_3}(\bar{\boldsymbol{k}},\boldsymbol{x};\tau_2,\tau_3)$ in the $\boldsymbol{a}_1$ direction.

Because $v(\boldsymbol{x}+\boldsymbol{a}_1) = v(\boldsymbol{x})$, the function $\phi_{n,j_2,j_3}(\boldsymbol{x};\tau_1,\tau_2,\tau_3)$ has the form

$$\phi_{n,j_2,j_3}(\boldsymbol{x}+\boldsymbol{a}_1;\tau_1,\tau_2,\tau_3) = \mathrm{e}^{\mathrm{i}k_1}\phi_{n,j_2,j_3}(\boldsymbol{x};\tau_1,\tau_2,\tau_3). \tag{7.32}$$

k_1 in (7.32) can be complex with a nonzero imaginary part or a real number. If k_1 is real in (7.32), then $\phi_{n,j_2,j_3}(\boldsymbol{x};\tau_1,\tau_2,\tau_3)$ is a $\bar{\psi}_{n',j_2,j_3}(\bar{\boldsymbol{k}},\boldsymbol{x};\tau_2,\tau_3)$. According to Theorem 7.4, only in special cases when a $\bar{\psi}_{n',j_2,j_3}(\bar{\boldsymbol{k}},\boldsymbol{x};\tau_2,\tau_3)$ has a nodal surface intersecting the $\boldsymbol{a}_1$ axis at $\tau_1\boldsymbol{a}_1$, the $\bar{\psi}_{n',j_2,j_3}(\bar{\boldsymbol{k}},\boldsymbol{x};\tau_2,\tau_3)$ can be a $\phi_{n,j_2,j_3}(\boldsymbol{x};\tau_1,\tau_2,\tau_3)$. Therefore, k_1 in (7.32) can be real only in such special cases; in most cases, it is complex with a non-zero imaginary part.

The imaginary part of k_1 in (7.32) can be either positive or negative, corresponding to that $\phi_{n,j_2,j_3}(\boldsymbol{x};\tau_1,\tau_2,\tau_3)$ decays in either the positive or the negative direction of $\boldsymbol{a}_1$. Such states $\phi_{n,j_2,j_3}(\boldsymbol{x};\tau_1,\tau_2,\tau_3)$ with a nonzero imaginary part of k_1 in (7.32) cannot exist in a quantum wire with translational invariance in the $\boldsymbol{a}_1$ direction because they are divergent in either the negative or the positive direction of $\boldsymbol{a}_1$. However, they can play a significant role in the electronic states in a finite crystal or quantum dot without translational invariance.

The further quantum confinement in the $\boldsymbol{a}_1$ direction of one-dimensional Bloch waves $\bar{\psi}_{n,j_2,j_3}(\bar{\boldsymbol{k}}, \boldsymbol{x}; \tau_2, \tau_3)$ will produce two different types of electronic states in the finite crystal or quantum dot.

One type of nontrivial solutions of (7.1) and (7.2) can be obtained from (7.32) by assigning

$$\begin{aligned} \psi_{n,j_2,j_3}(\boldsymbol{x}; \tau_1, \tau_2, \tau_3) &= c_{N_1,N_2,N_3}\phi_{n,j_2,j_3}(\boldsymbol{x}; \tau_1, \tau_2, \tau_3) \quad \text{if } \boldsymbol{x} \in \text{ the crystal} \\ &= 0 \qquad\qquad\qquad\qquad\qquad\qquad\quad \text{if } \boldsymbol{x} \notin \text{ the crystal,} \end{aligned} \tag{7.33}$$

where c_{N_1,N_2,N_3} is a normalization constant. The corresponding eigenvalue is

$$\Lambda_{n,j_2,j_3}(\tau_1) = \lambda_{n,j_2,j_3}(\tau_1). \tag{7.34}$$

For each energy band and each j_2, j_3, there is one state $\psi_{n,j_2,j_3}(\boldsymbol{x}; \tau_1, \tau_2, \tau_3)$ which is $\phi_{n,j_2,j_3}(\boldsymbol{x}; \tau_1, \tau_2, \tau_3)$ inside the finite crystal or quantum dot but zero otherwise, whose energy $\Lambda_{n,j_2,j_3}(\tau_1)$ depends on τ_1, N_2, and N_3 but not on N_1, τ_2, and τ_3. For each bulk energy band n there are $(N_2 - 1)(N_3 - 1)$ such states in the finite crystal or quantum dot. They are surface-like states in the finite crystal or quantum dot since $\phi_{n,j_2,j_3}(\boldsymbol{x}; \tau_1, \tau_2, \tau_3)$ decays in either the positive or the negative direction of $\boldsymbol{a}_1$ in most cases.

Now, we try to find out other solutions of (7.1) and (7.2) from the quantum confinement of $\bar{\psi}_{n,j_2,j_3}(\bar{\boldsymbol{k}}, \boldsymbol{x}; \tau_2, \tau_3)$. We can expect that there are stationary Bloch states in the $\boldsymbol{a}_1$ direction, formed due to multiple reflections of $\bar{\psi}_{n,j_2,j_3}(\bar{\boldsymbol{k}}, \boldsymbol{x}; \tau_2, \tau_3)$ between two boundary surfaces perpendicularly intersecting the $\boldsymbol{a}_1$ axis at $\tau_1\boldsymbol{a}_1$ and $(\tau_1 + N_1)\boldsymbol{a}_1$.

Since we have[7]

$$\bar{\Lambda}_{n,j_2,j_3}(\bar{\boldsymbol{k}}) = \bar{\Lambda}_{n,j_2,j_3}(-\bar{\boldsymbol{k}}), \tag{7.35}$$

in general

$$\begin{aligned} f_{n,k_1,j_2,j_3}(\boldsymbol{x}; \tau_2, \tau_3) = {} & c_+\bar{\psi}_{n,j_2,j_3}(k_1\bar{\boldsymbol{b}}_1, \boldsymbol{x}; \tau_2, \tau_3) \\ & + c_-\bar{\psi}_{n,j_2,j_3}(-k_1\bar{\boldsymbol{b}}_1, \boldsymbol{x}; \tau_2, \tau_3), \quad 0 < k_1 < \pi, \end{aligned}$$

where $c_\pm$ are not zero, is a nontrivial solution of (7.1) due to (7.35). Similar to what was done in Sections 7.2–7.4, we can see that the stationary Bloch state solutions of (7.1) and (7.2) originating from the further quantum confinement of $\bar{\psi}_{n,j_2,j_3}(\bar{\boldsymbol{k}}, \boldsymbol{x}; \tau_2, \tau_3)$ should have the form

$$\begin{aligned} \psi_{n,j_1,j_2,j_3}(\boldsymbol{x}; \tau_1, \tau_2, \tau_3) &= f_{n,\kappa_1,j_2,j_3}(\boldsymbol{x}; \tau_1, \tau_2, \tau_3) \quad \text{if } \boldsymbol{x} \in \text{ the crystal} \\ &= 0 \qquad\qquad\qquad\qquad\qquad\quad \text{if } \boldsymbol{x} \notin \text{ the crystal,} \end{aligned} \tag{7.36}$$

where

$$\begin{aligned} f_{n,k_1,j_2,j_3}(\boldsymbol{x}; \tau_1, \tau_2, \tau_3) = {} & c_{n,k_1,j_2,j_3;\tau_1}\bar{\psi}_{n,j_2,j_3}(k_1\bar{\boldsymbol{b}}_1, \boldsymbol{x}; \tau_2, \tau_3) \\ & + c_{n,-k_1,j_2,j_3;\tau_1}\bar{\psi}_{n,j_2,j_3}(-k_1\bar{\boldsymbol{b}}_1, \boldsymbol{x}; \tau_2, \tau_3), \end{aligned}$$

[7] $\bar{\psi}^*_{n,j_2,j_3}(\bar{\boldsymbol{k}}, \boldsymbol{x}; \tau_2, \tau_3) = \bar{\psi}_{n,j_2,j_3}(-\bar{\boldsymbol{k}}, \boldsymbol{x}; \tau_2, \tau_3)$ leads to (7.35).

$c_{n,\pm k_1,j_2,j_3;\tau_1}$ are dependent on τ_1, $\kappa_1 = j_1\pi/N_1$, and $j_1 = 1,2,...,N_1-1$, as in (7.12). These stationary Bloch state solutions $\psi_{n,j_1,j_2,j_3}(\boldsymbol{x};\tau_1,\tau_2,\tau_3)$ satisfying (7.1) and (7.2) have energies Λ given by

$$\Lambda_{n,j_1,j_2,j_3} = \bar{\Lambda}_{n,j_2,j_3}(\kappa_1\bar{\boldsymbol{b}}_1). \tag{7.37}$$

Each energy Λ_{n,j_1,j_2,j_3} in (7.37) for this case is dependent on N_1, N_2, and N_3 but not on τ_1, τ_2, and τ_3. The energies Λ_{n,j_1,j_2,j_3} map the bulk energy band $\varepsilon_n(\boldsymbol{k})$ exactly: From (7.37), (6.22), and (5.32), one obtains that $\Lambda_{n,j_1,j_2,j_3} = \bar{\Lambda}_{n,j_2,j_3}(\kappa_1\bar{\boldsymbol{b}}_1) = \hat{\Lambda}_{n,j_3}(\kappa_1\bar{\boldsymbol{b}}_1+\kappa_2\hat{\boldsymbol{b}}_2) = \varepsilon_n(\kappa_1\bar{\boldsymbol{b}}_1+\kappa_2\hat{\boldsymbol{b}}_2+\kappa_3\boldsymbol{b}_3)$. These stationary states can be considered as bulk-like states in the finite crystal or quantum dot. For each band index n, there are $(N_1-1)(N_2-1)(N_3-1)$ such bulk-like states in the finite crystal or quantum dot.

Because of (7.31), (7.34), and (7.37), for the further quantum confinement of one-dimensional Bloch waves $\bar{\psi}_{n,j_2,j_3}(\bar{\boldsymbol{k}},\boldsymbol{x};\tau_2,\tau_3)$ in general the energy of a surface-like state is always above the energy of every relevant bulk-like state:

$$\Lambda_{n,j_2,j_3}(\tau_1) > \Lambda_{n,j_1,j_2,j_3}. \tag{7.38}$$

We have seen that the effects of the further quantum confinement of one-dimensional Bloch waves $\bar{\psi}_n(\bar{\boldsymbol{k}},\boldsymbol{x};\tau_2,\tau_3)$, $\bar{\psi}_{n,j_3}(\bar{\boldsymbol{k}},\boldsymbol{x};\tau_2,\tau_3)$, $\bar{\psi}_{n,j_2}(\bar{\boldsymbol{k}},\boldsymbol{x};\tau_2,\tau_3)$, and $\bar{\psi}_{n,j_2,j_3}(\bar{\boldsymbol{k}},\boldsymbol{x};\tau_2,\tau_3)$ are similar to what we have seen in Chapters 5 and 6: Each set will produce two different types of electronic states in an ideal finite crystal or quantum dot. They can be grouped into eight sets and have different behaviors. For each bulk energy band n, there are the following:

$(N_1-1)(N_2-1)(N_3-1)$ bulk-like states $\psi_{n,j_1,j_2,j_3}(\boldsymbol{x};\tau_1,\tau_2,\tau_3)$ in (7.36); the energy Λ_{n,j_1,j_2,j_3} in (7.37) of each state depends on N_1, N_2, and N_3 but not on τ_1, τ_2, and τ_3;

$(N_1-1)(N_2-1)$ surface-like states $\psi_{n,j_1,j_2}(\boldsymbol{x};\tau_1,\tau_2,\tau_3)$ in (7.28); the energy $\Lambda_{n,j_1,j_2}(\tau_3)$ in (7.29) of each state depends on N_1, N_2, and τ_3 but not on τ_1, τ_2, and N_3;

$(N_2-1)(N_3-1)$ surface-like states $\psi_{n,j_2,j_3}(\boldsymbol{x};\tau_1,\tau_2,\tau_3)$ in (7.33); the energy $\Lambda_{n,j_2,j_3}(\tau_1)$ in (7.34) of each state depends on N_2, N_3, and τ_1 but not on τ_2, τ_3, and N_1;

$(N_1-1)(N_3-1)$ surface-like states $\psi_{n,j_1,j_3}(\boldsymbol{x};\tau_1,\tau_2,\tau_3)$ in (7.20); the energy $\Lambda_{n,j_1,j_3}(\tau_2)$ in (7.21) of each state depends on N_1, N_3, and τ_2 but not on τ_1, τ_3, and N_2;

(N_1-1) side-like states $\psi_{n,j_1}(\boldsymbol{x};\tau_1,\tau_2,\tau_3)$ in (7.11); the energy $\Lambda_{n,j_1}(\tau_2,\tau_3)$ in (7.13) of each state depends on N_1, τ_2, and τ_3 but not on τ_1, N_2, and N_3;

(N_2-1) side-like states $\psi_{n,j_2}(\boldsymbol{x};\tau_1,\tau_2,\tau_3)$ in (7.25); the energy $\Lambda_{n,j_2}(\tau_1,\tau_3)$ in (7.26) of each state depends on N_2, τ_1, and τ_3 but not on τ_2, N_1, and N_3;

(N_3-1) side-like states $\psi_{n,j_3}(\boldsymbol{x};\tau_1,\tau_2,\tau_3)$ in (7.17); the energy $\Lambda_{n,j_3}(\tau_1,\tau_2)$ in (7.18) of each state depends on N_3, τ_1, and τ_2 but not on τ_3, N_1, and N_2;

one corner-like state $\psi_n(\boldsymbol{x};\tau_1,\tau_2,\tau_3)$ in (7.8); the energy $\Lambda_n(\tau_1,\tau_2,\tau_3)$ in (7.9) depends on τ_1, τ_2, and τ_3 but not on N_1, N_2, and N_3.

We have seen again that the effect of the quantum confinement in one more direction actually is to *always have one and only one* boundary-dependent state for each subband of the electronic states in the quantum wire investigated in Chapter 6. The other states are size-dependent states and their energies can be directly obtained from either the side-like subband structure $\bar{\Lambda}_n(\bar{\boldsymbol{k}};\tau_2,\tau_3)$ by (7.13), the surface-like subband structure $\bar{\Lambda}_{n,j_3}(\bar{\boldsymbol{k}};\tau_2)$ by (7.21), the surface-like subband structure $\bar{\Lambda}_{n,j_2}(\bar{\boldsymbol{k}};\tau_3)$ by (7.29), or the bulk-like subband structure $\bar{\Lambda}_{n,j_2,j_3}(\bar{\boldsymbol{k}})$ by (7.37) in the quantum wire. In general, the energy of the boundary-dependent state is always above the energy of every size-dependent state if they are obtained from the quantum confinement of the same subband of one-dimensional Bloch waves.

The electronic states in a finite crystal or quantum dot can be considered as the electronic states in a film defined by $\boldsymbol{a}_1$ and $\boldsymbol{a}_2$, then further confined in the $\boldsymbol{a}_2$ direction, and, finally, confined in the $\boldsymbol{a}_1$ direction, as we did in Sections 5.3–5.5, 6.1–6.3, and 7.1–7.5. This is a specific quantum confinement order. Equivalently, they can also be considered as the three-dimensional Bloch waves are confined in three directions in other different confinement orders. By considering the results obtained from all six different quantum confinement orders, we could obtain a more comprehensive understanding on the electronic states in an ideal finite crystal or quantum dot and a more specific expression for each set of electronic states and energies, such as (6.24) and (6.25) are more specific than (6.18) and (6.19).

7.6 Finite Crystals or Quantum Dots with a sc, tetr, or ortho Bravais Lattice

We expect that the simplest cases where the theory in this chapter can be applied are the orthorhombic finite crystals or quantum dots of crystals with a sc, tetr, or ortho Bravais lattice in which (5.14), (6.10), and (6.20) are true. In such a crystal, the three primitive lattice vectors $\boldsymbol{a}_1$, $\boldsymbol{a}_2$, and $\boldsymbol{a}_3$ are perpendicular to each other and equivalent; consequently, the three primitive lattice vectors in k space, $\boldsymbol{b}_1$, $\boldsymbol{b}_2$, and $\boldsymbol{b}_3$, are also perpendicular to each other and equivalent. By considering the quantum confinement in six different orders, similarly to what we did in Section 6.4, we can obtain that for such a finite crystal or quantum dot with a size N_1a_1 in the $\boldsymbol{a}_1$ direction, a size N_2a_2 in the $\boldsymbol{a}_2$ direction, and a size N_3a_3 in the $\boldsymbol{a}_3$ direction; for each bulk energy band, there are $(N_1-1)(N_2-1)(N_3-1)$ bulk-like states, $(N_1-1)(N_2-1)+(N_2-1)(N_3-1)+(N_3-1)(N_1-1)$ surface-like states, $(N_1-1)+(N_2-1)+(N_3-1)$ side-like states, and one corner-like state. They are as follows:
$(N_{001}-1)(N_{1\bar{1}0}-1)(N_{110}-1)$ bulk-like states with energies

$$\Lambda_{n,j_1,j_2,j_3}=\varepsilon_n\left[\frac{j_1\pi}{N_1}\boldsymbol{b}_1+\frac{j_2\pi}{N_2}\boldsymbol{b}_2+\frac{j_3\pi}{N_3}\boldsymbol{b}_3\right] \tag{7.39}$$

from (7.37), (6.22), and (5.32);
$(N_1-1)(N_2-1)$ surface-like states with energies

$$\Lambda_{n,j_1,j_2}(\tau_3) = \hat{\Lambda}_n\left[\frac{j_1\pi}{N_1}\boldsymbol{b}_1 + \frac{j_2\pi}{N_2}\boldsymbol{b}_2; \tau_3\right] \tag{7.40}$$

from (7.29) and (6.14);
$(N_2-1)(N_3-1)$ surface-like states with energies

$$\Lambda_{n,j_2,j_3}(\tau_1) = \hat{\Lambda}_n\left[\frac{j_2\pi}{N_2}\boldsymbol{b}_2 + \frac{j_3\pi}{N_3}\boldsymbol{b}_3; \tau_1\right] \tag{7.41}$$

from equations similar to (7.29) or (6.14) obtained by considering different confinement orders;
$(N_3-1)(N_1-1)$ surface-like states with energies

$$\Lambda_{n,j_3,j_1}(\tau_2) = \hat{\Lambda}_n\left[\frac{j_3\pi}{N_3}\boldsymbol{b}_3 + \frac{j_1\pi}{N_1}\boldsymbol{b}_1; \tau_2\right] \tag{7.42}$$

from (7.21) and (6.25);
(N_1-1) side-like states with energies

$$\Lambda_{n,j_1}(\tau_2,\tau_3) = \bar{\Lambda}_n\left[\frac{j_1\pi}{N_1}\boldsymbol{b}_1; \tau_2, \tau_3\right] \tag{7.43}$$

from (7.13);
(N_2-1) side-like states with energies

$$\Lambda_{n,j_2}(\tau_3,\tau_1) = \bar{\Lambda}_n\left[\frac{j_2\pi}{N_2}\boldsymbol{b}_2; \tau_3, \tau_1\right] \tag{7.44}$$

(N_3-1) side-states with energies

$$\Lambda_{n,j_3}(\tau_1,\tau_2) = \bar{\Lambda}_n\left[\frac{j_3\pi}{N_3}\boldsymbol{b}_3; \tau_1, \tau_2\right] \tag{7.45}$$

from equations similar to (7.13) obtained by considering different confinement orders;
one corner state with energy

$$\Lambda_n(\tau_1,\tau_2,\tau_3) = \lambda_n(\tau_1,\tau_2,\tau_3) \tag{7.46}$$

from (7.9).
Here, $j_1 = 1, 2, ..., N_1 - 1$, $j_2 = 1, 2, ..., N_2 - 1$, and $j_3 = 1, 2, ..., N_3 - 1$. τ_1, τ_2, and τ_3 define the boundary surface locations of the finite crystal or quantum dot in the $\boldsymbol{a}_1$, $\boldsymbol{a}_2$, and $\boldsymbol{a}_3$ directions. $\hat{\Lambda}_n[\hat{\boldsymbol{k}}; \tau_l]$ is the surface-like band structure of a quantum film with film plane oriented in the $\boldsymbol{a}_l$ direction with a wave vector $\hat{\boldsymbol{k}}$ in the film plane. $\bar{\Lambda}_n[\bar{\boldsymbol{k}}; \tau_l, \tau_m]$ is the side-like band

structure of a rectangular quantum wire with the wire faces oriented in the $\boldsymbol{a}_l$ or the $\boldsymbol{a}_m$ direction with a wave vector $\bar{\boldsymbol{k}}$ in the wire direction.

Furthermore, from (7.14), (7.22), (7.30), (7.38), and similar equations obtained from other confinement orders, we can obtain that in general

$$\Lambda_n(\tau_1, \tau_2, \tau_3) > \Lambda_{n,j_l}(\tau_m, \tau_n) > \Lambda_{n,j_l,j_m}(\tau_n) > \Lambda_{n,j_l,j_m,j_n}; \tag{7.47}$$

here, each one of l, m, and n can be any one of 1, 2, and 3, but no two of l, m, and n are equal (l, m, and n are combinations of 1, 2, and 3). Relation (7.47) indicates that in such an ideal finite crystal or quantum dot for the electronic states with the same bulk energy band index n, the corner-like state has the highest energy, above the energy of every side-like state. A side-like state has an energy above the energy of every relevant surface-like state. A surface-like state has an energy above the energy of every relevant bulk-like state.

Probably the practically more interesting cases are finite crystals or quantum dots of crystals with a fcc or bcc Bravais lattice in which (5.21), (6.10), and (6.20) are true. The choosing of the primitive lattice vectors in those crystals depends on the film direction. Based on the results obtained in Sections 5.1–5.5, 6.1–6.3, and 7.1–7.5, we can understand the consequences of the three-dimensional Bloch waves of such crystals being confined in such a finite crystal or quantum dot in a specific order. Similar to what was done in Chapter 6, by combining the results obtained from different confinement orders, a more comprehensive understanding on the electronic states in some finite crystals and quantum dots can be obtained.

7.7 fcc Finite Crystals with (001), (110), and $(1\bar{1}0)$ Surfaces

For a fcc finite crystal with (001), (110), and $(1\bar{1}0)$ surfaces and having an orthorhombic size $N_{001}a \times N_{110}a/\sqrt{2} \times N_{1\bar{1}0}a/\sqrt{2}$, for each bulk energy band n, there are $2N_{001}N_{110}N_{1\bar{1}0}$ electronic states. They can be obtained by combining the results of the further quantum confinement in the $[1\bar{1}0]$ direction of the one-dimensional Bloch waves obtained in Section 6.5, the results of the further quantum confinement in the [001] direction of the one-dimensional Bloch waves obtained in Section 6.6, and the similar results of the further quantum confinement of the one-dimensional Bloch waves in a quantum wire in the [110] direction with faces oriented in the $(1\bar{1}0)$ plane or in the (001) plane. Note the results obtained in either Section 6.5 or 6.6 are actually the results of two different confinement orders. Similar to the way that we obtained results in Section 6.5, we can obtain that the properties of the electronic states in such a finite crystal or quantum dot are as follows.

For each bulk energy band n, there are $2(N_{001}-1)(N_{1\bar{1}0}-1)(N_{110}-1)+(N_{001}-1)(N_{1\bar{1}0}-1)+(N_{110}-1)(N_{001}-1)+(N_{1\bar{1}0}-1)(N_{110}-1)+(N_{1\bar{1}0}-1)+(N_{110}-1)+(N_{001}-1)+1$ bulk-like states in the finite crystal or quantum

dot. They are as follows:
$(N_{001}-1)(N_{1\bar{1}0}-1)(N_{110}-1)$ states with energies

$$\Lambda^{bk,a}_{n,j_{001},j_{1\bar{1}0},j_{110}} = \varepsilon_n \left[\frac{j_{001}\pi}{N_{001}a}(0,0,1) + \frac{j_{1\bar{1}0}\pi}{N_{1\bar{1}0}a}(1,-1,0) + \frac{j_{110}\pi}{N_{110}a}(1,1,0) \right]; \tag{7.48}$$

$(N_{001}-1)(N_{1\bar{1}0}-1)(N_{110}-1)$ states with energies

$$\Lambda^{bk,c}_{n,j_{001},j_{1\bar{1}0},j_{110}} = \varepsilon_n \left[\frac{j_{001}\pi}{N_{001}a}(0,0,1) + \frac{j_{1\bar{1}0}\pi}{N_{1\bar{1}0}a}(1,-1,0) + \frac{j_{110}\pi}{N_{110}a}(1,1,0) + \frac{2\pi}{a}(1,1,0) \right]; \tag{7.49}$$

$(N_{001}-1)(N_{1\bar{1}0}-1)$ states with energies

$$\Lambda^{bk,b_1}_{n,j_{001},j_{1\bar{1}0}} = \varepsilon_n \left[\frac{j_{001}\pi}{N_{001}a}(0,0,1) + \frac{j_{1\bar{1}0}\pi}{N_{1\bar{1}0}a}(1,-1,0) + \frac{\pi}{a}(1,1,0) \right]; \tag{7.50}$$

$(N_{110}-1)(N_{001}-1)$ states with energies

$$\Lambda^{bk,b_2}_{n,j_{110},j_{001}} = \varepsilon_n \left[\frac{j_{110}\pi}{N_{110}a}(1,1,0) + \frac{j_{001}\pi}{N_{001}a}(0,0,1) + \frac{\pi}{a}(1,-1,0) \right]; \tag{7.51}$$

$(N_{1\bar{1}0}-1)(N_{110}-1)$ states with energies

$$\Lambda^{bk,b_3}_{n,j_{1\bar{1}0},j_{110}} = \varepsilon_n \left[\frac{j_{1\bar{1}0}\pi}{N_{1\bar{1}0}a}(1,-1,0) + \frac{j_{110}\pi}{N_{110}a}(1,1,0) + \frac{\pi}{a}(0,0,1) \right]; \tag{7.52}$$

$(N_{001}-1)$ states with energies

$$\Lambda^{bk,d_1}_{n,j_{001}} = \varepsilon_n \left[\frac{j_{001}\pi}{N_{001}a}(0,0,1) + \frac{\pi}{a}(1,-1,0) + \frac{\pi}{a}(1,1,0) \right]; \tag{7.53}$$

$(N_{110}-1)$ states with energies

$$\Lambda^{bk,d_2}_{n,j_{110}} = \varepsilon_n \left[\frac{j_{110}\pi}{N_{110}a}(1,1,0) + \frac{\pi}{a}(0,0,1) + \frac{\pi}{a}(1,-1,0) \right]; \tag{7.54}$$

$(N_{1\bar{1}0}-1)$ states with energies

$$\Lambda^{bk,d_3}_{n,j_{1\bar{1}0}} = \varepsilon_n \left[\frac{j_{1\bar{1}0}\pi}{N_{1\bar{1}0}a}(1,-1,0) + \frac{\pi}{a}(1,1,0) + \frac{\pi}{a}(0,0,1) \right]; \tag{7.55}$$

one state with energy

$$\Lambda^{bk,d_4}_{n} = \varepsilon_n \left[\frac{\pi}{a}(1,-1,0) + \frac{\pi}{a}(1,1,0) + \frac{\pi}{a}(0,0,1) \right]. \tag{7.56}$$

Here, $j_{001} = 1, 2, ..., N_{001} - 1$, $j_{1\bar{1}0} = 1, 2, ..., N_{1\bar{1}0} - 1$, $j_{110} = 1, 2, ..., N_{110} - 1$, and $\varepsilon(k_x, k_y, k_z)$ is the bulk energy band structure in the Cartesian system. Equation (7.48) comes from the size-dependent states of the further quantum confinement of the bulk-like subbands (6.46), (6.56), or a similar equation for a quantum wire in the [110] direction. Equation (7.49) comes from the size-dependent states of the further quantum confinement of the bulk-like subbands (6.47), (6.57), or a similar equation for a quantum wire in the [110] direction. Equations (7.50)–(7.52) come from the size-dependent states of further quantum confinement of the bulk-like subbands (6.48) and (6.49), and/or (6.58) and (6.59) or two similar equations for a quantum wire in the [110] direction. Equations (7.53)–(7.55) come from the size-dependent states of the further quantum confinement of the bulk-like subbands (6.50) and (6.60), and a similar equation for a quantum wire in the [110] direction. Equation (7.56) comes from the boundary-dependent state of the further quantum confinement of the bulk-like subbands (6.50), (6.60), and/or a similar equation for a quantum wire in the [110] direction. Similarly, as it was found that $\bar{\Lambda}_n^{bk,d}(\bar{\boldsymbol{k}})$ in (6.50) (and in (6.60) and in a similar equation for a quantum wire in the [110] direction) actually is a bulk-like subband in a quantum wire, such a state is in fact a bulk-like state in the finite crystal or quantum dot.

The energies of all these bulk-like states can be directly obtained from the energy band structure $\varepsilon_n(\boldsymbol{k})$ of the corresponding bulk crystal.

For each bulk energy band n, there are $(N_{001} - 1)(N_{1\bar{1}0} - 1) + (N_{110} - 1)(N_{001} - 1) + (N_{1\bar{1}0} - 1)(N_{110} - 1)$ surface-like states in the crystal. They are as follows:

$(N_{001} - 1)(N_{1\bar{1}0} - 1)$ states with energies

$$\Lambda^{sf,a_1}_{n,j_{001},j_{1\bar{1}0}}(\tau_{110}) = \hat{\Lambda}_n \left[\frac{j_{001}\pi}{N_{001}a}(0,0,1) + \frac{j_{1\bar{1}0}\pi}{N_{1\bar{1}0}a}(1,-1,0); \tau_{110} \right]; \qquad (7.57)$$

$(N_{110} - 1)(N_{001} - 1)$ states with energies

$$\Lambda^{sf,a_2}_{n,j_{110},j_{001}}(\tau_{1\bar{1}0}) = \hat{\Lambda}_n \left[\frac{j_{110}\pi}{N_{110}a}(1,1,0) + \frac{j_{001}\pi}{N_{001}a}(0,0,1); \tau_{1\bar{1}0} \right]; \qquad (7.58)$$

$(N_{1\bar{1}0} - 1)(N_{110} - 1)$ states with energies

$$\Lambda^{sf,a_3}_{n,j_{1\bar{1}0},j_{110}}(\tau_{001}) = \hat{\Lambda}_n \left[\frac{j_{1\bar{1}0}\pi}{N_{1\bar{1}0}a}(1,-1,0) + \frac{j_{110}\pi}{N_{110}a}(1,1,0); \tau_{001} \right]. \qquad (7.59)$$

Here, τ_{110}, $\tau_{1\bar{1}0}$, or τ_{001} define the boundary surface locations of the finite crystal or quantum dot in the [110], [1$\bar{1}$0], or [001] direction, $\hat{\Lambda}_n[\hat{\boldsymbol{k}}; \tau_l]$ is the surface-like band structure of a quantum film with the film plane oriented in the $[l]$ direction with a wave vector $\hat{\boldsymbol{k}}$ in the film plane. l can be either one of 001, 110, or 1$\bar{1}$0. Equations (7.57)–(7.59) come from the size-dependent states of the further quantum confinement of the surface-like subbands (6.51) and (6.52), or (6.61) and (6.62), and/or two similar equations for a quantum wire in the [110] direction.

For each bulk energy band n, there are $(N_{001}-1)+(N_{110}-1)+(N_{1\bar{1}0}-1)$ side-like states in the crystal. They are as follows:
$(N_{001}-1)$ states with energies

$$\Lambda^{sd,a_1}_{n,j_{001}}(\tau_{1\bar{1}0},\tau_{110}) = \bar{\Lambda}_n\left[\frac{j_{001}\pi}{N_{001}a}(0,0,1);\tau_{1\bar{1}0},\tau_{110}\right]; \tag{7.60}$$

$(N_{110}-1)$ states with energies

$$\Lambda^{sd,a_2}_{n,j_{110}}(\tau_{1\bar{1}0},\tau_{001}) = \bar{\Lambda}_n\left[\frac{j_{110}\pi}{N_{110}a}(1,1,0);\tau_{1\bar{1}0},\tau_{001}\right]; \tag{7.61}$$

$(N_{1\bar{1}0}-1)$ states with energies

$$\Lambda^{sd,a_3}_{n,j_{1\bar{1}0}}(\tau_{001},\tau_{110}) = \bar{\Lambda}_n\left[\frac{j_{1\bar{1}0}\pi}{N_{1\bar{1}0}a}(1,-1,0);\tau_{001},\tau_{110}\right]. \tag{7.62}$$

Here, $\bar{\Lambda}_n[\bar{\boldsymbol{k}};\tau_l,\tau_m]$ is the side-like band structure of a rectangular quantum wire with the wire faces oriented in the $[l]$ or the $[m]$ direction with a wave vector $\bar{\boldsymbol{k}}$ in the wire direction. l and m can be two of 001, 110, and $1\bar{1}0$.

For each bulk energy band n, there is one corner state in the finite crystal with energy

$$\Lambda^{cr}_n(\tau_{001},\tau_{1\bar{1}0},\tau_{110}) = \lambda_n(\tau_{001},\tau_{1\bar{1}0},\tau_{110}). \tag{7.63}$$

Equations (7.60)–(7.62) come from the size-dependent states of the further quantum confinement of the side-like subband (6.38) or (6.45), (6.63), and a similar equation for a quantum wire in the [110] direction. Equation (7.63) comes from the boundary-dependent state of the further quantum confinement of the side-like subband (6.38) or (6.45), or (6.63), or a similar equation for a quantum wire in the [110] direction.

Since one VBM state in a cubic semiconductor can never have *three* nodal surfaces in the three planes, (001), (110), and $(1\bar{1}0)$, simultaneously, consequently, there is not an electronic state in such a quantum dot whose energy is the energy of the VBM and does not change as the dot size changes. This is a fact observed in the numerical calculations of Franceschetti and Zunger [1] on free-standing GaAs quantum dots, as shown in Fig. 5.4(c).

7.8 bcc Finite Crystals with (100), (010), and (001) Surfaces

For a bcc finite crystal or quantum dot with (100), (010), and (001) surfaces and having an orthorhombic size $N_{100}a\times N_{010}a\times N_{001}a$, for each bulk energy band n, there are $2N_{100}N_{010}N_{001}$ electronic states. They can be obtained by combining the results of the further quantum confinement in the [100] direction of the one-dimensional Bloch waves in the quantum wire with the

(001) and (010) surfaces discussed in Section 6.7, the results of the further quantum confinement of the electronic states in a quantum wire with the (100) and (010) surfaces, and the results of the further quantum confinement of the electronic states in a quantum wire with the (100) and (001) surfaces.

For each bulk energy band n, there are $2(N_{100}-1)(N_{010}-1)(N_{001}-1)+(N_{001}-1)(N_{010}-1)+(N_{100}-1)(N_{001}-1)+(N_{010}-1)(N_{100}-1)+(N_{100}-1)+(N_{010}-1)+(N_{001}-1)+1$ bulk-like states in the finite crystal or quantum dot. They are as follows:

$(N_{100}-1)(N_{010}-1)(N_{001}-1)$ states with energies

$$\Lambda^{bk,a}_{n,j_{100},j_{010},j_{001}} = \varepsilon_n \left[\frac{j_{100}\pi}{N_{100}a}(1,0,0) + \frac{j_{010}\pi}{N_{010}a}(0,1,0) + \frac{j_{001}\pi}{N_{001}a}(0,0,1) \right]; \quad (7.64)$$

$(N_{100}-1)(N_{010}-1)(N_{001}-1)$ states with energies

$$\begin{aligned} \Lambda^{bk,c}_{n,j_{100},j_{010},j_{001}} = \varepsilon_n \, [\, & \frac{j_{100}\pi}{N_{100}a}(1,0,0) + \frac{j_{010}\pi}{N_{010}a}(0,1,0) \\ & + \frac{j_{001}\pi}{N_{001}a}(0,0,1) + \frac{2\pi}{a}(1,0,0) \,]; \end{aligned} \quad (7.65)$$

$(N_{010}-1)(N_{001}-1)$ states with energies

$$\Lambda^{bk,b_1}_{n,j_{010},j_{001}} = \varepsilon_n \left[\frac{j_{010}\pi}{N_{010}a}(0,1,0) + \frac{j_{001}\pi}{N_{001}a}(0,0,1) + \frac{\pi}{a}(1,0,0) \right]; \quad (7.66)$$

$(N_{001}-1)(N_{100}-1)$ states with energies

$$\Lambda^{bk,b_2}_{n,j_{001},j_{100}} = \varepsilon_n \left[\frac{j_{001}\pi}{N_{001}a}(0,0,1) + \frac{j_{100}\pi}{N_{100}a}(1,0,0) + \frac{\pi}{a}(0,1,0) \right]; \quad (7.67)$$

$(N_{100}-1)(N_{010}-1)$ states with energies

$$\Lambda^{bk,b_3}_{n,j_{100},j_{010}} = \varepsilon_n \left[\frac{j_{100}\pi}{N_{100}a}(1,0,0) + \frac{j_{010}\pi}{N_{010}a}(0,1,0) + \frac{\pi}{a}(0,0,1) \right]; \quad (7.68)$$

$(N_{100}-1)$ states with energies

$$\Lambda^{bk,d_1}_{n,j_{100}} = \varepsilon_n \left[\frac{j_{100}\pi}{N_{100}a}(1,0,0) + \frac{\pi}{a}(0,1,0) + \frac{\pi}{a}(0,0,1) \right]; \quad (7.69)$$

$(N_{010}-1)$ states with energies

$$\Lambda^{bk,d_2}_{n,j_{010}} = \varepsilon_n \left[\frac{j_{010}\pi}{N_{010}a}(0,1,0) + \frac{\pi}{a}(0,0,1) + \frac{\pi}{a}(1,0,0) \right]; \quad (7.70)$$

$(N_{001}-1)$ states with energies

$$\Lambda^{bk,d_3}_{n,j_{001}} = \varepsilon_n \left[\frac{j_{001}\pi}{N_{001}a}(0,0,1) + \frac{\pi}{a}(1,0,0) + \frac{\pi}{a}(0,1,0) \right]; \quad (7.71)$$

one state with energy

$$\Lambda_n^{bk,d_4} = \varepsilon_n \left[\frac{\pi}{a}(1,0,0) + \frac{\pi}{a}(0,1,0) + \frac{\pi}{a}(0,0,1) \right]. \tag{7.72}$$

Here, $j_{100} = 1, 2, ..., N_{100} - 1$, $j_{010} = 1, 2, ..., N_{010} - 1$, $j_{001} = 1, 2, ..., N_{001} - 1$, and $\varepsilon(k_x, k_y, k_z)$ is the bulk energy band structure in the Cartesian system. Equation (7.64) comes from the size-dependent states of the further quantum confinement of the bulk-like subbands (6.64) or two similar equations for quantum wires in the [010] or [001] directions. Equation (7.65) comes from the size-dependent states of the further quantum confinement of the bulk-like subbands (6.65) or two similar equations for quantum wires in the [010] or [001] directions. Equations (7.66)–(7.68) come from the size-dependent states of the further quantum confinement of the bulk-like subbands (6.66), (6.67), and/or four similar equations for quantum wires in the [010] or [001] directions. Equations (7.69)–(7.71) come from the size-dependent states of the further quantum confinement of the bulk-like subband (6.68) and two similar equations for quantum wires in the [010] or [001] directions. Equation (7.72) come from the boundary-dependent state of the further quantum confinement of the bulk-like subband (6.68) and two similar equations for quantum wires in the [010] or the [001] directions. Similar to the bulk-like state Λ_n^{bk,d_4} in (7.56), Λ_n^{bk,d_4} in (7.72) is also a bulk-like state. The energies of all these bulk-like states can be directly obtained from the energy band structure $\varepsilon_n(\boldsymbol{k})$ of the corresponding bulk crystal.

For each bulk energy band n, there are $(N_{010} - 1)(N_{001} - 1) + (N_{001} - 1)(N_{100} - 1) + (N_{100} - 1)(N_{010} - 1)$ surface-like states in the finite crystal or quantum dot. They are as follows:
$(N_{010} - 1)(N_{001} - 1)$ states with energies

$$\Lambda_{n,j_{010},j_{001}}^{sf,a_1}(\tau_{100}) = \hat{\Lambda}_n \left[\frac{j_{010}\pi}{N_{010}a}(0,1,0) + \frac{j_{001}\pi}{N_{001}a}(0,0,1); \tau_{100} \right]; \tag{7.73}$$

$(N_{001} - 1)(N_{100} - 1)$ states with energies

$$\Lambda_{n,j_{001},j_{100}}^{sf,a_2}(\tau_{010}) = \hat{\Lambda}_n \left[\frac{j_{001}\pi}{N_{001}a}(0,0,1) + \frac{j_{100}\pi}{N_{100}a}(1,0,0); \tau_{010} \right]; \tag{7.74}$$

$(N_{100} - 1)(N_{010} - 1)$ states with energies

$$\Lambda_{n,j_{100},j_{010}}^{sf,a_3}(\tau_{001}) = \hat{\Lambda}_n \left[\frac{j_{100}\pi}{N_{100}a}(1,0,0) + \frac{j_{010}\pi}{N_{010}a}(0,1,0); \tau_{001} \right]. \tag{7.75}$$

Here, τ_{100}, τ_{010}, or τ_{001} defines the boundary surface locations of the finite crystal or quantum dot in the [100], [010], or [001] direction, respectively; $\hat{\Lambda}_n[\hat{\boldsymbol{k}}; \tau_l]$ is the surface-like band structure of a quantum film with the film plane oriented in the $[l]$ direction with a wave vector $\hat{\boldsymbol{k}}$ in the film plane. l can be either one of 100, 010, or 001. Equations (7.73)–(7.75) come from the

size-dependent states of the further quantum confinement of the surface-like subbands (6.69), (6.70), and/or four similar equations for the quantum wires in the [010] or the [001] direction.

For each bulk energy band n, there are $(N_{100}-1)+(N_{010}-1)+(N_{001}-1)$ side-like states in the finite crystal or quantum dot. They are as follows: $(N_{100}-1)$ side-like states with energies

$$\Lambda^{sd,a_1}_{n,j_{100}}(\tau_{010},\tau_{001}) = \bar{\Lambda}_n\left[\frac{j_{100}\pi}{N_{100}a}(1,0,0);\tau_{010},\tau_{001}\right]; \tag{7.76}$$

$(N_{010}-1)$ side-like states with energies

$$\Lambda^{sd,a_2}_{n,j_{010}}(\tau_{001},\tau_{100}) = \bar{\Lambda}_n\left[\frac{j_{010}\pi}{N_{010}a}(0,1,0);\tau_{001},\tau_{100}\right]; \tag{7.77}$$

$(N_{001}-1)$ side-like states with energies

$$\Lambda^{sd,a_3}_{n,j_{001}}(\tau_{100},\tau_{010}) = \bar{\Lambda}_n\left[\frac{j_{001}\pi}{N_{001}a}(0,0,1);\tau_{100},\tau_{010}\right]. \tag{7.78}$$

Here, $\bar{\Lambda}_n[\bar{\boldsymbol{k}};\tau_l,\tau_m]$ is the side-like band structure of a rectangular quantum wire with the wire faces oriented in the $[l]$ or the $[m]$ direction with a wave vector $\bar{\boldsymbol{k}}$ in the wire direction. l and m can be two of 100, 010, and 001.

For each bulk energy band n, there is one corner state in the finite crystal or quantum dot with energy

$$\Lambda^{cr}_{n}(\tau_{100},\tau_{010},\tau_{001}) = \lambda_n(\tau_{100},\tau_{010},\tau_{001}). \tag{7.79}$$

Equations (7.76)–(7.78) come from the size-dependent states of the further quantum confinement of the side-like subband (6.71) and two similar equations for the quantum wires in the [001] or the [010] direction. Equation (7.79) comes from the boundary-dependent state of the further quantum confinement of the side-like subband (6.71) or two similar equations for the quantum wires in the [010] or the [001] direction.

7.9 Summary and Discussions

We have seen that in an ideal rectangular finite crystal or quantum dot discussed in Sections 7.6–7.8, there are four different types of electronic states: bulk-like states, surface-like states, side-like states, and corner-like states. The crystal structure has an effect on how the numbers of each type of electronic states in a finite crystal or quantum dot depend on the sizes in the three dimensions: The simplest cases discussed in Section 7.6 are somewhat different from the cases of crystals with a fcc or a bcc Bravais lattice discussed in Sections 7.7 and 7.8.

However, since the results in Sections 7.7 and 7.8 were also essentially obtained from an understanding of the further quantum confinement of one-dimensional Bloch waves discussed in Sections 7.1 to 7.5, there are similar relationships among the four different types of electronic states. For example, for an ideal fcc finite crystal or quantum dot with $(1\bar{1}0)$, (110), and (001) surfaces, we should have

$$\Lambda_n^{cr}(\tau_{1\bar{1}0}, \tau_{110}, \tau_{001}) > \Lambda_{n,j_{001}}^{sd,a_1}(\tau_{1\bar{1}0}, \tau_{110}), \tag{7.80}$$

$$\Lambda_n^{cr}(\tau_{1\bar{1}0}, \tau_{110}, \tau_{001}) > \Lambda_{n,j_{110}}^{sd,a_2}(\tau_{1\bar{1}0}, \tau_{001}), \tag{7.81}$$

and

$$\Lambda_n^{cr}(\tau_{1\bar{1}0}, \tau_{110}, \tau_{001}) > \Lambda_{n,j_{1\bar{1}0}}^{sd,a_3}(\tau_{110}, \tau_{001}) \tag{7.82}$$

between the energy of a corner-like state in (7.63) and the energies of side-like states in (7.60), (7.61), and (7.62), and

$$\Lambda_n^{cr}(\tau_{1\bar{1}0}, \tau_{110}, \tau_{001}) > \Lambda_n^{bk,d_4} \tag{7.83}$$

between the energy of a corner-like state in (7.63) and the energies of a bulk-like state in (7.56).

We have

$$\Lambda_{n,j_{001}}^{sd,a_1}(\tau_{1\bar{1}0}, \tau_{110}) > \Lambda_{n,j_{001},j_{1\bar{1}0}}^{sf,a_1}(\tau_{110}) \tag{7.84}$$

and

$$\Lambda_{n,j_{001}}^{sd,a_1}(\tau_{1\bar{1}0}, \tau_{110}) > \Lambda_{n,j_{110},j_{001}}^{sf,a_2}(\tau_{1\bar{1}0}) \tag{7.85}$$

between the energy of a side-like state in (7.60) and the energies of relevant surface-like states in (7.57) and (7.58), and

$$\Lambda_{n,j_{001}}^{sd,a_1}(\tau_{1\bar{1}0}, \tau_{110}) > \Lambda_{n,j_{001}}^{bk,d_1} \tag{7.86}$$

between the energy of a side-like state in (7.60) and the energy of a relevant bulk-like state in (7.53).

We have

$$\Lambda_{n,j_{110}}^{sd,a_2}(\tau_{1\bar{1}0}, \tau_{001}) > \Lambda_{n,j_{110},j_{001}}^{sf,a_2}(\tau_{1\bar{1}0}) \tag{7.87}$$

and

$$\Lambda_{n,j_{110}}^{sd,a_2}(\tau_{1\bar{1}0}, \tau_{001}) > \Lambda_{n,j_{1\bar{1}0},j_{110}}^{sf,a_3}(\tau_{001}) \tag{7.88}$$

between the energy of a side-like state in (7.61) and the energies of relevant surface-like states in (7.58) and (7.59), and

$$\Lambda_{n,j_{110}}^{sd,a_2}(\tau_{1\bar{1}0}, \tau_{001}) > \Lambda_{n,j_{110}}^{bk,d_2} \tag{7.89}$$

between the energy of a side-like state in (7.61) and the energy of relevant bulk-like state in (7.54).

We have

$$\Lambda_{n,j_{1\bar{1}0}}^{sd,a_3}(\tau_{001}, \tau_{110}) > \Lambda_{n,j_{001},j_{1\bar{1}0}}^{sf,a_1}(\tau_{110}) \tag{7.90}$$

and

$$\Lambda^{sd,a_3}_{n,j_{1\bar{1}0}}(\tau_{001},\tau_{110}) > \Lambda^{sf,a_3}_{n,j_{1\bar{1}0},j_{110}}(\tau_{001}) \tag{7.91}$$

between the energy of a side-like state in (7.62) and the energies of relevant surface-like states in (7.57) and (7.59), and

$$\Lambda^{sd,a_3}_{n,j_{1\bar{1}0}}(\tau_{001},\tau_{110}) > \Lambda^{bk,d_3}_{n,j_{1\bar{1}0}} \tag{7.92}$$

between the energy of a side-like state in (7.62) and the energy of a relevant bulk-like state in (7.55).

We have

$$\Lambda^{sf,a_1}_{n,j_{001},j_{1\bar{1}0}}(\tau_{110}) > \Lambda^{bk,a}_{n,j_{001},j_{1\bar{1}0},j_{110}} \tag{7.93}$$

and

$$\Lambda^{sf,a_1}_{n,j_{001},j_{1\bar{1}0}}(\tau_{110}) > \Lambda^{bk,c}_{n,j_{001},j_{1\bar{1}0},j_{110}} \tag{7.94}$$

between the energy of a surface-like state in (7.57) and the energies of relevant bulk-like states in (7.48) and in (7.49), and

$$\Lambda^{sf,a_1}_{n,j_{001},j_{1\bar{1}0}}(\tau_{110}) > \Lambda^{bk,b_1}_{n,j_{001},j_{1\bar{1}0}} \tag{7.95}$$

between the energy of a surface-like state in (7.57) and the energy of a relevant bulk-like state in (7.50).

We have

$$\Lambda^{sf,a_2}_{n,j_{110},j_{001}}(\tau_{1\bar{1}0}) > \Lambda^{bk,a}_{n,j_{001},j_{1\bar{1}0},j_{110}} \tag{7.96}$$

and

$$\Lambda^{sf,a_2}_{n,j_{110},j_{001}}(\tau_{1\bar{1}0}) > \Lambda^{bk,c}_{n,j_{001},j_{1\bar{1}0},j_{110}} \tag{7.97}$$

between the energy of a surface-like state in (7.58) and the energies of relevant bulk-like states in (7.48) and in (7.49), and

$$\Lambda^{sf,a_2}_{n,j_{110},j_{001}}(\tau_{1\bar{1}0}) > \Lambda^{bk,b_2}_{n,j_{110},j_{001}} \tag{7.98}$$

between the energy of a surface-like state in (7.58) and the energy of a relevant bulk-like state in (7.51).

We have

$$\Lambda^{sf,a_3}_{n,j_{1\bar{1}0},j_{110}}(\tau_{001}) > \Lambda^{bk,a}_{n,j_{001},j_{1\bar{1}0},j_{110}} \tag{7.99}$$

and

$$\Lambda^{sf,a_3}_{n,j_{1\bar{1}0},j_{110}}(\tau_{001}) > \Lambda^{bk,c}_{n,j_{001},j_{1\bar{1}0},j_{110}} \tag{7.100}$$

between the energy of a surface-like state in (7.59) and the energies of relevant bulk-like states in (7.48) and in (7.49), and

$$\Lambda^{sf,a_3}_{n,j_{1\bar{1}0},j_{110}}(\tau_{001}) > \Lambda^{bk,b_3}_{n,j_{1\bar{1}0},j_{110}} \tag{7.101}$$

between the energy of a surface-like state in (7.59) and the energy of a relevant bulk-like state in (7.52). These relationships can be obtained just as

the relationships in Section 6.8 were obtained, using reasoning based on the relationships (7.14), (7.22), (7.30), or (7.38) obtained in Sections 7.2 to 7.5.

Corresponding relationships for the four different types of electronic states in an ideal bcc finite crystal or quantum dot with (100), (010), and (001) surfaces can be similarly obtained.

As a surface-like electronic state is better understood as an electronic state whose properties and energy are determined by the surface location and a side-like electronic state is better understood as an electronic state whose properties and energy are determined by the side location, a corner-like electronic state is better understood as an electronic state whose properties and energy are determined by the corner location, rather than a state located near a specific corner. To better understand the properties of corner states, it is necessary to have a better understanding of the properties of the solutions of (5.1), including the solutions in the band gap(s) and the non-Bloch state solutions in the permitted energy ranges.

Similar to surface-like states and side-like states, the physics origin of a corner state is also related to a bulk energy band. The energy of a corner state is above the energies of relevant side-like states and surface-like states; thus, the corners of an ideal orthorhombic alkali metal finite crystal or quantum dot could be even more positively charged than the sides and the surfaces.

Only when a Bloch function has three different nodal surfaces that are the surfaces of the quantum dot might the corner state be a Bloch state. It seems that this kind of cases rarely happens in most finite crystals or quantum dots of general interest.

For the electronic states in an ideal orthorhombic finite crystal or quantum dot with the same bulk energy band index n, summarizing (7.47), (7.80)–(7.101), and similar equations for a bcc finite crystal or quantum dot discussed in Section 7.8, the following general relations exist:

The energy of the corner-like state
> The energy of every side-like state
> The energy of every relevant surface-like state
> The energy of every relevant bulk-like state.

Therefore, we have seen that in many simple and interesting cases, the properties of electronic states in an ideal orthorhombic finite crystal or quantum dot such as shown in Fig. 1.3 can be understood, how the energies of those electronic states depend on the size and/or shape can be analytically predicted, and the energies of many electronic states can be obtained from the energy band structures of the bulk crystal. Again, the major obstacle due to the lack of translational invariance actually can be circumvented.

The results obtained here provided a more concrete and comprehensive understanding of the boundary effects than the discussions in [2].

References

1. A. Franceschetti and A. Zunger: Appl. Phys. Lett. **68**, 3455 (1996)
2. M. Born and K. Huang: *Dynamical Theory of Crystal Lattices* (Clarendon Press, Oxford 1954), Appendix IV

8 Concluding Remarks

We have presented a single-electron nonspin analytical theory on the electronic states in some simple ideal low-dimensional systems and finite crystals, based on a theory of differential equations approach. By ideal, it is assumed that (i) the potential $v(\boldsymbol{x})$ inside the low-dimensional system or the finite crystal is the same as in a crystal with translational invariance and (ii) the electronic states are completely confined in the limited size of the low-dimensional system or the finite crystal.

8.1 Summary and Brief Discussions

The most essential results obtained in this book can be summarized as follows:

1. In *a unified theoretical frame*, we have understood that in some simple low-dimensional systems and finite crystals, due to the existence of boundaries and a finite size in one, two, or three directions, the electronic states in low-dimensional systems or finite crystals are not progressive Bloch waves as required by the Bloch theorem in traditional solid state physics. Instead, they are either (i) stationary Bloch states in the one, two, or three directions due to the finite size or (ii) other type(s) of electronic states closely related to the very existence of the boundary. Therefore, the two fundamental difficulties mentioned in Section 1.3 are overcome in a unified theoretical frame for those simple ideal low-dimensional systems and finite crystals.
2. It is found that due to the very existence of the boundary-dependent electronic states, the properties of electronic states in simple low-dimensional systems and finite crystals may be substantially different from the properties of electronic states in crystals with translational invariance as understood in traditional solid state physics; they may also be substantially different from what is traditionally believed in the solid state physics community regarding the properties of the electronic states in low-dimensional systems and finite crystals.

These results were obtained by trying to understand the quantum confinement effects of Bloch waves.

We have seen that there are similarities and differences between the quantum confinement of Bloch waves and the well-known quantum confinement of plane waves: The most significant feature in the quantum confinement of Bloch waves is the existence of boundary(τ in this book)-dependent states. We have also seen that there are similarities and differences between the quantum confinement effects of Bloch waves in one-dimensional space and the quantum confinement effects of Bloch waves in three-dimensional space: The most distinct feature in the quantum confinement of Bloch waves in one-dimensional space is that each of the boundary-dependent states is always in a band gap or at a band edge.

In the well-known quantum confinement of plane waves, all permitted states are stationary waves. This is closely related to the fact that in the cases of the quantum confinement of plane waves, the unconfined potential is everywhere equal – the potential has a *continuous* translational invariance; there is not a minimum translation unit of the potential. On the other hand, in the cases of the quantum confinement of Bloch waves, the unconfined potential is not everywhere equal – the potential has a *discrete* translational invariance; there is a nonzero minimum translation unit of the potential. Consequently, the confinement effects of the plane waves and the confinement effects of Bloch waves will have some differences: The former will not depend on the boundary locations since everywhere the potential is equal and the latter will depend on the boundary locations since the potential is not everywhere equal.

Therefore, naturally, in general the quantum confinement effects of the Bloch waves should depend on the boundary locations. Suppose that a specific branch of Bloch waves is completely confined in a specific direction and in a specific length Na – where a is the minimum translational unit in that direction and N is a positive integer, then if for this branch of Bloch waves a specific condition such as (5.21), (6.10), or (6.20) is satisfied, $N-1$ stationary Bloch states could be formed.[1] Each stationary Bloch state consists of two Bloch waves from this branch with wave vector components k and $-k$ in the specific direction, as a result of the multiple reflections of the Bloch waves at the two boundary locations. Independent of the boundary location, each stationary Bloch state can only have an integer number of half-wave lengths of the Bloch wave in the confined region. Under such a requirement, the wave vectors and the energies of these $N-1$ stationary Bloch states will be determined by the confinement length, but will not depend on the boundary locations. We can expect that there are a total of N confined electronic states from the quantum confinement of this specific branch of Bloch waves. Hence,

[1] This is closely related to the fact that for such a specific branch of Bloch waves, the Bloch wave with a wave vector at the Brillouin zone boundary is different from most other Bloch waves with a wave vector inside the Brillouin zone: Only one Bloch wave with a wave vector at the Brillouin zone boundary exists for this specific branch; thus, it cannot form a stationary Bloch state.

the energy of the one remaining $[N - (N - 1)]$ confined state should be dependent on the confinement boundary locations.

We have also seen that the surface states originating from the termination of the periodic potential are merely special cases of the boundary-dependent confined electronic states in low-dimensional systems or finite crystals.

Theoretically, the results obtained can be an interesting and substantial supplement to the well-known quantum confinement of plane waves and thus could improve our understanding on the fundamental quantum confinement effects. Practically, the results may also find valuable applications in relevant problems in modern solid state physics and related fields. If the well-known quantum confinement of plane waves has provided many interesting and valuable insights on the physics in low-dimensional systems and finite crystals, we have reason to expect that a clearer understanding of the quantum confinement of Bloch waves could be a substantial step toward a more comprehensive and in-depth understanding of the physics in low-dimensional systems and finite crystals.

The Schrödinger differential equation in a one-dimensional crystal is an ordinary differential equation. The properties of solutions of the relevant ordinary differential equations – including the solutions of ordinary differential equations with periodic coefficients – have been well understood mathematically. It is on the basis of those mathematical understandings – in particular those obtained in Eastham's book [1] – as summarized in Chapter 2 that the results presented in Chapter 4 can be rigorously proven.

However, the properties of solutions of the Schrödinger differential equation in a three-dimensional crystal – the second-order elliptic partial differential equation, especially the elliptic partial differential equation with periodic coefficients – are mathematically much less understood.[2] Although the basis of the treatment in Part III is rigorous according to the author's understanding – such as Theorem 5.1 and other relevant theorems are rigorous – much of the reasoning used in obtaining results on the electronic states in ideal quantum films, wires, dots, and finite crystals had to be based, to a large extent, on physical intuition rather than on rigorous mathematical arguments. Consequently, many results for low-dimensional systems and finite crystals presented in Part III were not as rigorously proven as in the one-dimensional cases in Part II. A mathematically more rigorous treatment and comprehensive understanding on the problems treated in Chapters 5–7 will probably have to wait for further progress in the relevant mathematical fields.

We have seen that the analytical theory in Chapter 5 is consistent with many previously published numerical results and, therefore, it might provide a more in-depth understanding of those numerical results. However, the

[2]It may be noticed that no general theory on the properties of the energy band structure of three-dimensional crystals – a theory corresponding to the Kramers's theory on the energy band structure of one-dimensional crystals [2] – was published, even for a simplest crystal structure.

author has not found numerical results that can be directly compared with the general predictions in Chapters. 6 and 7. We have also seen that there are cases where there are differences between the general theory in Chapter 5 and published numerical results in [3,4]. The author hopes that the analytical theory presented in this book will stimulate further numerical calculations to check the general analytical predictions obtained here. Either those analytical general predictions obtained by reasoning based on the relevant mathematical theorems plus physical intuition will be confirmed or be negated somewhere, it could significantly improve our current understandings on this very interesting and fundamental problem on the electronic states in low-dimensional systems and finite crystals and the quantum confinement of Bloch waves, including the clarification of those previously mentioned differences. If the general predictions presented are incorrect in places, the defects in the reasoning in this book should be relatively easily and straightforwardly traced and hopefully a corrected theory can be established.

Our analytical and general predictions on the electronic states in low-dimensional systems and finite crystals were obtained based on a very simple model; real crystals are certainly more complicated. Nevertheless, by using such a simple model, we have clearly understood some of the most fundamental differences between the electronic states in low-dimensional systems and finite crystals and the electronic states in crystals with translational invariance. The effects of those differences on the properties of a low-dimensional system become more significant as the size of the system decreases. We have also seen that the properties of electronic states in low-dimensional systems and finite crystals may also be substantially different from what is traditionally believed in the solid state physics community, such as the ideas derived from the well-known effective mass approximation.

Probably some of the practically most interesting and straightforward predications in this book are as follows:

1. Ideal low-dimensional systems of a cubic semiconductor actually may have a band gap smaller than the band gap of the bulk semiconductor. This is a consequence of relevant theorems such as Theorem 5.1 and the properties of the valence band maximum (VBM) of cubic semiconductors.[3] Because in a semiconductor the most important physical processes always happen near the band gap, an improved understanding of the band gap in low-dimensional semiconductors may have some effect on the physics of low-dimensional semiconductors and possible applications.
2. Ideal low-dimensional systems of a cubic semiconductor actually may even have the electrical conductivity of a metal, since the boundary-dependent states originating from the bulk valence bands may even become energet-

[3]Even in cases of one-dimensional crystals, (2.72) and the analysis in Section 4.3 actually indicate the same consequence: A finite crystal of a one-dimensional semiconductor has a band gap smaller than the band gap of the corresponding infinite crystal, if the boundary τ is not a zero of the VBM wave function.

ically above the size-dependent states originating from a bulk conduction band. It is well known that one of the greatest successes of the theory of electronic states in traditional solid state physics is that it clearly explains the basic difference between the electrical conductivities of metals and semiconductors (and insulators) of macroscopic size. This new prediction indicates that such a basic difference of macroscopic solids may become obscure when the size of the solid becomes much smaller and, thus, the effects of the existence of the boundary of the low-dimensional system or the finite crystal has to be considered.[4]

We may also look at these results from an even more general point of view. If different matters are arranged according to the number of atoms in each matter, the two ends of each spectrum of matters are usually understood much better than the wide range of matters in between: At one end is the matter consisting of a few atoms and at the other end is the crystal of infinite size, both of which are easier to understand: A problem of a few atoms can be relatively easily treated in quantum mechanics and a problem on a crystal of infinite size – with translational invariance – can be essentially reduced to a problem of a few atoms in a unit cell and can also be relatively easily treated. However, the wide range of matters in between is usually more difficult to understand due to the mathematical difficulties in treating large systems of many atoms. In this book, it was demonstrated that in some simple cases, the electronic structure of ideal truncated periodic systems of various size – which were difficult to understand earlier due to the large number of atoms and the lack of translational invariance – can be better understood now. Therefore, in some sense, a route for understanding is opened, from one end with matter of a few atoms to the other end with crystal of infinite size and in between containing a whole range of ideal truncated periodic systems of various size.

Despite of all these new understandings, however, what we have understood is really only the very beginning. The model used in this book is the simplest model. The low-dimensional systems and finite crystals treated in this book are also some of the simplest cases. For the little we have just understood, there is so much more we do not understand.

For example, we even have not understood the properties of electronic states in a (111) ideal quantum film of crystals with a simple cubic Bravais lattice in our simplest model yet, not to mention many others. There are many ways to improve the model or to investigate different cases. Each new

[4] A very recent work by Rurali and Lorenti [5] seems to support such a prediction. They studied nano Si quantum wires in the $< 100 >$ direction with density-functional calculations and found that such Si nano wires may become strong metallic. Our treatment is more general, but for ideal low-dimensional systems. For quantum wires, we treated only those with rectangular cross sections. Their results might be an indication that the nonrectangular cross section of the wire and the surface reconstructions do not eliminate the metallic conductivity of Si $< 100 >$ nanowires.

progress obtained from an improved model or from more investigations on different cases could improve our understanding of the electronic states, the physical properties, and the physical processes in low-dimensional systems and finite crystals.

In this book is presented only an investigation on the electronic states in low-dimensional systems and finite crystals. Although it is found that the existence of the boundary-dependent electronic states in low-dimensional systems or finite crystals is a fundamental distinction of the quantum confinement of Bloch waves, in order to have a better understanding of the physical properties of the low-dimensional systems or finite crystals, there is much more we need to learn. Even if we keep working only with the simplified model of ideal low-dimensional systems or finite crystals, we need to understand issues such as how are the specific boundary surface locations determined for a low-dimensional system or finite crystal? What are the specific forms of those boundary-dependent electronic states in the low-dimensional system or finite crystal with such boundary surface locations? Does the existence of and the properties of boundary-dependent electronic states in ideal quantum films have any thing to do with surface reconstructions in semiconductors? If the answer is yes, then how? Further, how does the existence of boundary-dependent electronic states affect physical processes in low-dimensional systems or finite crystals, such as optical transitions, scattering, transport processes, and many others? We may have reason to expect that the physical processes between the stationary Bloch states can be understood – to a large extent – on the basis of the physical processes between the progressive Bloch states, as treated in traditional solid state physics; however, for physical processes in which the boundary-dependent states are involved, we understand very little or basically nothing. If we go beyond the simplified model, there is even much more we do not understand. There is still a long long way to go before we have a more comprehensive understanding on the physical properties of and the physical processes in low-dimensional systems or finite crystals.

8.2 Some Relevant Systems

The results obtained for the electronic states in ideal low-dimensional systems or finite crystals naturally may also provide inspiration on some relevant problems.

8.2.1 Electronic States in Ideal Cavity Structures

A cavity structure is a structure formed when a low-dimensional system is removed from an infinite crystal. The electronic states in such a cavity structure usually were not easy to investigate theoretically: The structure does not have a translational invariance and the theoretical approaches previously

used in the investigations of electronic states in low-dimensional systems – such as the effective-mass-approximation-based approaches or numerical calculations – are not easily and/or effectively used here to obtain a meaningful understanding. However, the approach we used to understand the electronic states in ideal low-dimensional systems of some simple crystals in the main parts of this book can be used to obtain understanding of the electronic states in ideal cavity structures of simple crystals. Such a theory is presented in Appendix B.

8.2.2 Other Finite Periodic Systems, such as Finite Photonic Crystals

Naturally, an interesting question is, do the eigenmodes in other truncated periodic systems have similar interesting properties, similar to the electronic states in low-dimensional systems or finite crystals?

An interesting problem is the properties of classical waves in periodic media, such as elastic waves in periodic structures of alternative elastic mediums, electromagnetic waves in photonic crystals and so forth. In such systems, the periodic structure can be flexibly designed and shaped to a large extent, including that the surface plane may be located anywhere in the unit cell. Therefore, the parameter τ in this book can be a really controllable quantity. The boundary-dependent states might thus be tailored by suitable choice of the surface location.

In particular, an area of much current interest is the properties of electromagnetic waves in photonic crystals. It will be interesting to see whether the results obtained in the major part of this book can be extended to photonic crystals.

However, such an extension, at least, will not be straightforward. To show this point, we consider the simplest photonic crystals. We assume that the magnetic permeability of the photonic crystal is equal to that in free space μ_0 and that the dielectric constant $\epsilon(\boldsymbol{x})$ is isotropic, real, and periodic with $\boldsymbol{x}$, and does not depend on frequency. The Maxwell equations for the propagation of light in such a photonic crystal composed of a mixed homogeneous dielectric medium with no free charges or currents lead to four equations [6,7]:

$$\begin{aligned} \tfrac{1}{\epsilon(\boldsymbol{x})}\nabla\times\nabla\times\boldsymbol{E}(\boldsymbol{x},t) &= -\tfrac{1}{c^2}\tfrac{\partial^2}{\partial t^2}\boldsymbol{E}(\boldsymbol{x},t), \\ \nabla\times\left[\tfrac{1}{\epsilon(\boldsymbol{x})}\nabla\times\boldsymbol{H}(\boldsymbol{x},t)\right] &= -\tfrac{1}{c^2}\tfrac{\partial^2}{\partial t^2}\boldsymbol{H}(\boldsymbol{x},t), \\ \nabla\cdot\epsilon(\boldsymbol{x})\boldsymbol{E}(\boldsymbol{x},t) &= 0, \\ \nabla\cdot\boldsymbol{H}(\boldsymbol{x},t) &= 0. \end{aligned} \tag{8.1}$$

Here, $\boldsymbol{E}(\boldsymbol{x},t)$ and $\boldsymbol{H}(\boldsymbol{x},t)$ are the electric field and the magnetic field, respectively, c is the speed of light in free space, and $\epsilon(\boldsymbol{x})$ is the relative dielectric constant of the photonic crystal.

We are interested in the solutions of (8.1) with the form

$$\boldsymbol{E}(\boldsymbol{x},t) = \boldsymbol{E}(\boldsymbol{x})\mathrm{e}^{-\mathrm{i}\omega t},$$
$$\boldsymbol{H}(\boldsymbol{x},t) = \boldsymbol{H}(\boldsymbol{x})\mathrm{e}^{-\mathrm{i}\omega t},$$

where ω is the eigen-angular frequency and $\boldsymbol{E}(\boldsymbol{x})$ and $\boldsymbol{H}(\boldsymbol{x})$ are the eigenfunctions of the equations:

$$\frac{1}{\epsilon(\boldsymbol{x})}\nabla\times\nabla\times\boldsymbol{E}(\boldsymbol{x}) - (\frac{\omega}{c})^2\boldsymbol{E}(\boldsymbol{x}) = 0 \tag{8.2}$$

and

$$\nabla\times\left[\frac{1}{\epsilon(\boldsymbol{x})}\nabla\times\boldsymbol{H}(\boldsymbol{x})\right] - (\frac{\omega}{c})^2\boldsymbol{H}(\boldsymbol{x}) = 0. \tag{8.3}$$

Since $\boldsymbol{\Xi}$ in

$$\boldsymbol{\Xi}\ \boldsymbol{E}(\boldsymbol{x}) \equiv \frac{1}{\epsilon(\boldsymbol{x})}\nabla\times\nabla\times\boldsymbol{E}(\boldsymbol{x})$$

is not a Hermitian operator and $\boldsymbol{\Theta}$ in

$$\boldsymbol{\Theta}\ \boldsymbol{H}(\boldsymbol{x}) \equiv \nabla\times\left[\frac{1}{\epsilon(\boldsymbol{x})}\nabla\times\boldsymbol{H}(\boldsymbol{x})\right]$$

is a Hermitian operator [6], the electromagnetic wave modes in a photonic crystal are usually solved by using (8.3) and

$$\nabla\cdot\boldsymbol{H}(\boldsymbol{x}) = 0.$$

$\boldsymbol{E}(\boldsymbol{x})$ can be obtained from $\boldsymbol{H}(\boldsymbol{x})$ using

$$\nabla\times\boldsymbol{H}(\boldsymbol{x}) - \frac{\mathrm{i}\omega}{c}\epsilon(\boldsymbol{x})\boldsymbol{E}(\boldsymbol{x}) = 0.$$

In the simple cases where $\epsilon(\boldsymbol{x})$ is a function of x only and is a periodic function of $x : \epsilon(x+a) = \epsilon(x)$ and the light propagates in the x direction, the master equation (8.3) can be rewritten as

$$\frac{d}{dx}\left[\frac{1}{\epsilon(x)}\frac{d}{dx}\boldsymbol{H}(x)\right] + (\frac{\omega}{c})^2\boldsymbol{H}(x) = 0. \tag{8.4}$$

In the simplest model, $\epsilon(x)$ is a piecewise continuous step function rather than a continuous function; thus, (8.4) is not a Hill's equation as in (2.12) or in (2.37) in a rigorous sense: $[\frac{1}{\epsilon(x)}]$ is not a continuous function and $[\frac{1}{\epsilon(x)}]'$ is not piecewise continuous. The theory on the Hill's equation in Chapter 2 cannot be straightforwardly applied.

Furthermore, even for an ideally regular finite photonic crystal, the electric-magnetic waves cannot be completely confined in the finite photonic crystal with vacuum outside it.

Therefore, a corresponding theory on finite photonic crystals might not be a simple extension of the major parts of this book.

8.3 Could a More General Theory Be Possible?

In many cases, it is the general symmetry of a system rather than the details of the specific dynamic equation of a physical problem that determines the general properties of the solutions. For systems with translational invariance, even though the relevant dynamic equations can be quite different, such as the Schrödinger differential equation with a periodic potential for the electronic states, the atomic vibrational equation for phonons in crystals, Maxwell's equations for photonic crystals, and so forth are all different, it is the symmetry of the systems – the translational invariance – that determines the general properties of the solutions. The states or modes have the common property

$$\psi(\boldsymbol{x} + \boldsymbol{a}_i) = e^{i\boldsymbol{k}\cdot\boldsymbol{a}_i}\psi(\boldsymbol{x}), \tag{8.5}$$

where $\boldsymbol{a}_i$ are the minimum translational units and the wave vector $\boldsymbol{k}$ can be limited in a Brillouin zone, determined by the system's symmetry. The eigenvalues of the problem are the functions of wave vector $\boldsymbol{k}$:

$$\lambda = \lambda_n(\boldsymbol{k}). \tag{8.6}$$

Although (8.5) and (8.6) can be obtained from investigations on the solutions of each individual dynamic equation, it is now understood that (8.5) and (8.6) are consequences of the symmetry of the concerned system – the translational invariance (and other relevant symmetries) of the system – independent of the specific dynamic equation(s) involved. The group theory is a powerful mathematical theory that can be used to investigate the general properties of symmetrical systems. It is application of the group theory in different physical problems that leads to such general consequences.

Now the question is, do those similarities found in different systems exist in their truncated structures as well? That is, in systems which have translational invariance in common but their specific dynamic equations might be quite different, are there general similar correspondences between the eigenmodes of a truncated finite structure and a nontruncated infinite structure? This question seems interesting.

The author was quite surprised when he first obtained the result that the size effect and the boundary effect on the energies of electronic states in simple low-dimensional systems and finite crystals can be separated. He does not know of any other problem that also has such an interesting behavior: Usually when one solves an eigenvalue boundary problem of a differential equation, both the region and the boundary have an effect on all eigenvalues of the problem. He has also talked to mathematicians and has not met anyone who knew of a similar behavior in other problems.

Is this a particular behavior of the specific Schrödinger differential equations on the electronic states in low-dimensional systems and finite crystals, or might it be one of the consequences of *a whole class* of more general relevant problems? The results presented in this book were obtained by using

a theory of differential equations approach; however, are they really mere properties of the particular differential equations or might they actually be consequences of a more general class of problems concerning the truncated translational invariance?

If the existence of two different types of states or modes (boundary-dependent or size-dependent) is a general behavior of ideal truncated periodic systems – despite of the fact that the corresponding dynamic equations might be quite different – then it must be the common symmetric properties of truncated periodic structures in different systems with translational invariance (such as electronic crystals, lattice vibrations, photonic crystals, etc.) that determine the very existence of such general correspondences. The most significant common feature of the truncated periodic structures is that the translational symmetry of the periodic structure is broken, in a specific way. Can such a general correspondence be a consequence of a more general theory of *the translational symmetry breaking* – without the explicit forms of the specific dynamic equations involved?

To further explore such a prospect should be very interesting.

References

1. M. S. P. Eastham: *The Spectral Theory of Periodic Differential Equations* (Scottish Academic Press, Edinburgh 1973) and references therein
2. H. A. Kramers: Physica **2**, 483 (1935)
3. S. B. Zhang and A. Zunger: Appl. Phys. Lett. **63**, 1399 (1993)
4. S. B. Zhang, C-Y Yeh, and A. Zunger: Phys. Rev. **B48**, 11204 (1993)
5. R. Rurali and N. Lorenti: Phys. Rev. Lett. **94**, 026805 (2005)
6. J. D. Joannopoulos, R. D. Meade, and J. N. Winn: *Photonic crystals* (Princeton University Press, Princeton 1995)
7. K. Sakoda: *Optical Properties of Photonic Crystals* (Springer, Berlin Heidelberg 2001)

Part V

Appendices

A Electronic States in One-Dimensional Symmetric Finite Crystals with a Finite V_{out}

The Schrödinger differential equation for a one-dimensional crystal can be written as

$$-y''(x) + [v(x) - \lambda]y(x) = 0. \tag{A.1}$$

Here, $v(x) = v(x + a)$ is the periodic potential of the crystal.

For a one-dimensional crystal of finite length $L = Na$, the eigenvalues Λ and eigenfunctions $\psi(x)$ are solutions of the equation

$$-\psi''(x) + [v(x) - \Lambda]\psi(x) = 0, \quad \tau < x < \tau + L, \tag{A.2}$$

inside the crystal with certain boundary conditions at the two boundaries τ and $\tau + L$. If the potential outside the crystal $V_{out} = +\infty$, we have the boundary conditions

$$\psi(x) = 0 \quad x = \tau \text{ or } x = \tau + L. \tag{A.3}$$

This is the case treated in Chapter 4. It is found that for each band gap, there is always one and only one state whose energy is boundary dependent but independent on the crystal length. A surface state is one of the two possibilities of such a boundary-dependent state. Therefore, there is *at most* one surface state in each band gap in an *ideal* one-dimensional finite crystal.

Many years ago, Shockley published a classic paper [1] indicating that in a one-dimensional symmetric finite crystal when the potential period a is so small that the boundary curves for allowed energy bands have crossed and the number of atoms N in the crystal is *very large*, the surface states appear *in pairs* in band gap. To clearly understand the relationship between the results of [1] and Chapter 4, in this Appendix we investigate the cases where the electrons are not completely confined in the crystal as in [1] and the crystal length may not be very long.

Now, we need to consider the cases where V_{out} is finite. Qualitatively, the effect of a finite V_{out} can be directly obtained from a theorem in [2]: A finite V_{out} moves all energy levels lower. Quantitatively, a finite V_{out} will allow a small part of the electronic state spills out of the finite crystal and thus make the boundary conditions be

$$\begin{aligned} (\psi'/\psi)_{x=\tau} &= \sigma_1, \\ (\psi'/\psi)_{x=\tau+L} &= -\sigma_2 \end{aligned} \tag{A.4}$$

instead of (A.3). Here, σ_1 and σ_2 are positive numbers depending on V_{out}. Note that (A.3) corresponds to $\sigma_1 = \sigma_2 = +\infty$, and σ_1 and σ_2 will decrease monotonically as V_{out} decreases. Although V_{out} may have different forms, the effect of different V_{out} to the problem treated here can be simplified to be the effect of σ_1 and σ_2. Shockley treated one-dimensional symmetric finite crystals with finite V_{out}, where $\sigma_1 = \sigma_2 = \sigma$. His treatment provided a way to investigate how much the results obtained in Chapter 4 are dependent on V_{out} for symmetric one-dimensional finite crystals. For the convenience of comparison with the results in his original paper, we use his approach and assume that inside the crystal, the cell potential is symmetric and use same notations as in [1], except the energy is λ rather than E and the number of atoms in the crystal is N. As in Shockley's paper, we also consider the two lowest band gaps: one at $k = \pi/a$ and one at $k = 0$.

Assuming $g(x)$ and $u(x)$ are two independent solutions of the Schrödinger differential equation (A.1) in an unit cell, symmetric or antisymmetric to the cell center $x = 0$, Shockley obtained $g(a/2)u'(a/2)(1 - e^{-ika}) = g'(a/2)u(a/2)(1+e^{ika})$ and further obtained that $\sigma = \mu \tan(ka/2) \tan(Nka/2)$ and $\sigma = -\mu \tan(ka/2) \cot(Nka/2)$ (Eqs. (11) and (12) in [1]) give the energies of electronic states in the one-dimensional finite crystal; here, $\mu = u'(a/2)/u(a/2)$. Therefore, the effect of finite V_{out} can be found from the σ dependence of energy levels. In Fig. A.1 is shown a numerical calculation for the electronic states near the upper bandedge $\varepsilon_2(0)$ of the band gap at $k = 0$ in crystals of two different lengths, $N = 14$ and $N = 15$, with a model cell potential

$$\begin{aligned} v(x) &= -30 \quad \text{if } |x| \le 0.38 \\ &= 0 \qquad \text{if } 0.38 < |x| \le 0.5 \end{aligned}$$

and $a = 1$. It can be seen that lowering V_{out} (thus lowering σ) moves all energy levels downward. However, the energy of the state in the bandgap depends on the crystal length much less than the states in the energy band: The major difference between the state corresponding to a band gap and the states corresponding to an energy band obtained in Section 4.2 remains.

For many physical situations, σ can be considered as sufficiently large [3]. It can be shown that for those states in Fig. A.1, in the limit of large σ (i.e., large V_{out}), the energies of the states in the energy band can approximately be given by

$$\Lambda_{2,j} = \varepsilon_2(k_j)$$

and

$$k_j = \frac{j\pi}{Na} - \frac{2}{Na}\,\frac{\mu}{\sigma}\,\tan\left(\frac{j\pi}{2N}\right), \quad j = 1, 2, ..., N-1, \tag{A.5}$$

where $\mu > 0$. On the other hand, the energy of the state in the gap is given approximately by ($\varepsilon_2''(0) > 0$)

$$\Lambda_{1,gap} = \varepsilon_2(0) - \varepsilon_2''(0)\frac{6(c-1)}{(cN^2-1)a^2};$$

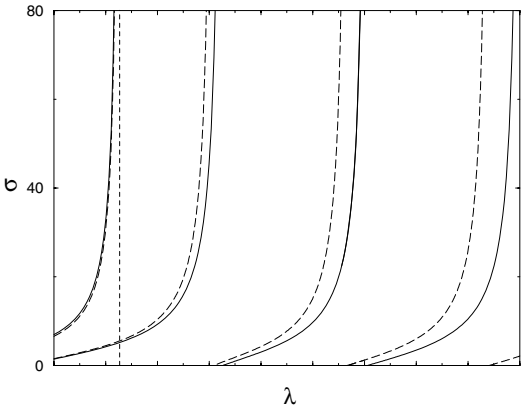

Fig. A.1. $\sigma = \mu \tan(ka/2) \tan(Nka/2)$ and $\sigma = -\mu \tan(ka/2) \cot(Nka/2)$ calculated for $N = 14$ (solid lines) and $N = 15$ (long dashed lines) near the upper band edge $\varepsilon_2(0)$ of the band gap at $k = 0$. The short-dashed vertical line is the band edge $\varepsilon_2(0)$. Note the energy of the state in the band gap almost does not depend on the crystal length, even for a finite σ.

here, $c = -\sigma N/\mu > 1$, $\mu < 0$, and $c \to 1$ when $\sigma \to +\infty$. Again, it can be clearly seen that lowering σ (lowering V_{out}) moves all energy levels downward and the energy of the state in the bandgap depends on the crystal length much less than the energies of the states in the energy band.

Shockley found that when (i) the potential period a is so small that the boundary curves for allowed energy bands have crossed and (ii) the number of atoms in the crystal N is *very large*, the surface states appear *in pairs* in the bandgap. Now, we try to give this problem a more careful investigation and try to understand whether and how "two surface states" in a bandgap could happen in a one-dimensional symmetric finite crystal. We also consider the cases of N is even, as in [1].

In general, inside a bandgap, an electronic state as a nontrivial solution of (A.1) always has the form

$$y(x) = A\mathrm{e}^{\beta x} f_1(x) + B\mathrm{e}^{-\beta x} f_2(x) \tag{A.6}$$

from (2.60) or (2.63); here, A and B are not both zero, $\beta > 0$, and $f_i(x)$ is either a periodic function ($f_i(x + a) = f_i(x)$) if the band gap is at $k = 0$ or a semi-periodic function ($f_i(x + a) = -f_i(x)$) if the band gap is at $k = \pi/a$. Equation (A.6) is more general than the simple surface states in which either A or B is zero and, thus, the state is localized near *one* end of the crystal. Actually, such a state (A.6) in a symmetric one-dimensional finite crystal must be either symmetric ($A = B$) or antisymmetric ($A = -B$) and, thus, is equally localized near the *both* ends of the finite crystal and can be considered as a generalized surface state. We are trying to investigate how many states

of type (A.6), as solutions of (A.2) with the boundary conditions (A.4), are in a specific band gap.

For the gap at $k = \pi/a$, two bandedge states are given by either $g(a/2) = 0$ or $u'(a/2) = 0$, as in [1]. Both bandedge wavefunctions have one node in an unit cell $[-a/2, a/2)$ (Theorem 2.7). One (given by $g(a/2) = 0$) is symmetric to the cell center and has its most electron density at the cell center and zero density at the cell boundaries; the other one (given by $u'(a/2) = 0$) is antisymmetric to the cell center and has its most electronic density at the cell boundaries $x = \pm a/2$ and zero density at the cell center.

No matter how small a is, if the cell potential at the cell boundaries is higher than the potential at the cell center as shown in Fig. 1(a) in [1] and the form of the cell potential is reasonable and not very irregular, we expect that $g(a/2) = 0$ gives the lower bandedge state and $u'(a/2) = 0$ gives the higher bandedge state: *A state with most of its electronic density in the potential valley should have lower energy than a state with most of its electronic density around the potential peak.* In fact, Levine [3] did not observe a band-crossing either. Shockley has shown that the two surface states in the gap can happen only when $g(a/2) = 0$ gives the higher bandedge state. Thus, the existence of two surface states in the lowest gap at $k = \pi/a$, as shown in Fig. 2 in [1], seems unlikely for a reasonably regular one-dimensional finite crystal. Consistent with the analysis here, many other authors did not obtain a "Shockley" surface state in the lowest gap at $k = \pi/a$ either [3,4].

Then we consider the next band gap at k=0. The two bandedge states are given by either $g'(a/2) = 0$ or $u(a/2) = 0$; which one is higher depends on the form of the cell potential. If $V_{out} = +\infty$, equations (11) and (12) in [1] for $\sigma = +\infty$ give $N - 1$ states ($k_j = j\pi/Na,\ j = 1, 2, ..., N - 1$) for each energy band and one confined band-edge state for each bandgap. The confined bandedge state for this bandgap is the bandedge state given by $u(a/2) = 0$ since its wavefunction is zero at the crystal boundaries. This is the same as obtained in Section 4.4.

If the confined bandedge state is at the *lower* bandedge $\varepsilon_1(0)$ when $V_{out} = +\infty$, a (any) finite V_{out} will move it downward into the energy band $\varepsilon_1(k)$ below and, thus, will not make a surface state. Only if the confined bandedge state is at the *upper* bandedge $\varepsilon_2(0)$ when $V_{out} = +\infty$, a (any) finite V_{out} will move it downward into the bandgap and thus make a surface state. That corresponds to the case that $u(a/2) = 0$ gives the higher bandedge state.

In Fig. A.2 is shown a numerical calculation of such a case, using the same model cell potential as in Fig. A.1, in comparison with Fig. 4 in [1]. When $V_{out} = +\infty(\sigma = +\infty)$, $u(a/2) = 0$ gives an antisymmetric confined bandedge state at the upper bandedge $\varepsilon_2(0)$. Any finite σ due to a finite V_{out} can move this state (long-dashed line) into the bandgap and thus make one antisymmetric gap state. However, moving a symmetric state (solid line) crossing the higher bandedge $\varepsilon_2(0)$ into the bandgap and making another surface state requires

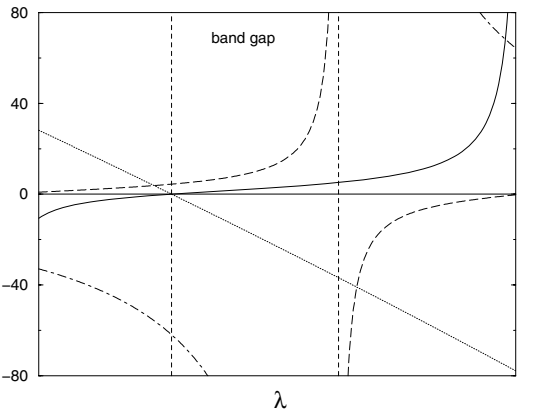

Fig. A.2. $\gamma \times 100$ (dotted line), μ (chained line), $\mu \tan(ka/2) \tan(Nka/2)$ (solid line) and $-\mu \tan(ka/2) \cot(Nka/2)$ (long-dashed line) for $N = 14$ near the band gap at $k = 0$ where the surface state(s) may exist. The left short-dashed vertical line corresponds to the lower band edge $\varepsilon_1(0)$ and the right short-dashed vertical line corresponds to the upper band edge $\varepsilon_2(0)$.

$$\sigma < -N\gamma_u; \tag{A.7}$$

here, γ_u is γ $(= g'(a/2)/g(a/2))$ at the upper band-edge, a negative number. Therefore, in principle, if there are two surface states (one antisymmetric and one symmetric) in the gap, σ (or V_{out}) needs to be small and N needs to be large. However, a too small σ (or V_{out}) may even move the antisymmetric surface state crossing the lower band edge $\varepsilon_1(0)$ out of the bandgap and into the lower energy band $\varepsilon_1(k)$. This happens when $\sigma < -\mu_l/N$; here, μ_l is μ at the lower bandedge $\varepsilon_1(0)$, also a negative number. Note that μ_l and γ_u are determined by the cell potential and σ is dependent on V_{out}. Figure A.2 shows the case for $N = 14$: When a small enough σ (or V_{out}) moves the symmetric state (solid line) from the upper band $\varepsilon_2(k)$ into the bandgap, the antisymmetric surface state (long-dashed line) almost enters the lower band $\varepsilon_1(k)$. In fact, σ usually is quite large [3].[1] Depending on σ or V_{out}, usually a much larger N is needed to satisfy $\sigma < -N\gamma_u$. An even larger N is needed if the two surface states are almost degenerate. Two degenerate gap states of (A.6) type - one symmetric and one antisymmetric in a symmetric one-dimensional finite crystal - can be linearly combined and transformed to two surface states, one at each end.

The calculations here, as in Shockley's paper [1], are for symmetric one-dimensional finite crystals. Nevertheless, we can also obtain some understanding of the surface states in general one-dimensional finite crystals: Since there

[1] In almost all previously published numerical calcuations, the deviations from $k_j = j\pi/(Na)$ is small; for example, see [5,6]. Thus, from (A.5), one can obtain that usually $(2\mu/\sigma) \tan(j\pi/2N) << 1$.

is only one state corresponding to each gap for general one-dimensional finite crystals when $V_{out} = +\infty$ and a finite V_{out} always moves all energy levels downward, in any case if there are two states in a band gap, one of them must come from the energy band above that bandgap and it must have the energy $\varepsilon_{2m+2}(\pi/Na)$ (for the gaps at $k = 0$) or $\varepsilon_{2m+1}[(N-1)\pi/Na]$ (for the gaps at $k = \pi/a$) when $V_{out} = +\infty$ (independent of whether the crystal is symmetric or not) and only a small enough V_{out} (depending on N) can move it crossing the bandedge into the bandgap. The smaller N is, the further the state is to the upper bandedge $\varepsilon_{2m+2}(0)$ or $\varepsilon_{2m+1}(\pi/a)$ and the more difficult is the state to be moved into the band gap by a finite V_{out}. Therefore, we can expect that a not very long one-dimensional finite crystal has at most one gap state in each bandgap. However, the localization of this gap state might be somewhat different for a nonsymmetric finite crystal: Because when $V_{out} = +\infty$, a gap state in a nonsymmetric finite crystal may have either $A = 0$ or $B = 0$ in (A.6) (i.e., the state could be localized near one end of the crystal), as V_{out} decreases there seems no understandable reason for that the localization behavior of the gap state will have a dramatic change. Thus, we can expect that a such gap state might be mainly localized near *one* end of the nonsymmetric finite crystal.

References

1. W. Shockley: Phys. Rev. **56**, 317 (1939)
2. R. Courant and D. Hilbert: *Methods of Mathematical Physics* (Interscience, New York 1953), Vol. 1, p. 409, Theorem 3 and the relevant footnote
3. J. D. Levine: Phys. Rev. **171**, 701 (1968)
4. S. G. Davison and M. Stęślicka: *Basic Theory of Surface States* (Clarendon Press, Oxford 1992)
5. S. B. Zhang and A. Zunger: Appl. Phys. Lett. **63**, 1399 (1993)
6. S. B. Zhang, C-Y Yeh, and A. Zunger: Phys. Rev. **B48**, 11204 (1993)

B Electronic States in Ideal Cavity Structures

In this appendix, we investigate the electronic states in cavity structures where a low-dimensional system such as investigated in Chapters 4–7 is removed from an infinite crystal.

For the electronic states in ideal cavity structures treated in this appendix, we assume that (i) the potential $v(x)$ or $v(\boldsymbol{x})$ *outside* the cavity is the same as in (4.1) or (5.1) and (ii) the electronic states are completely confined outside the cavity.

B.1 Electronic States in Ideal Cavity Structures of One-Dimensional Crystals

An ideal cavity structure of a one-dimensional crystal is a structure formed when a one-dimensional finite crystal bounded at τ and $\tau+L$ is removed from an infinite one-dimensional crystal with a potential period a. Here, $L = Na$ and N is a positive integer.

The eigenvalues Λ and eigenfunctions $\psi(x)$ of the electronic states in such an ideal cavity structure are solutions of the Schrödinger differential equation

$$-\psi''(x) + [v(x) - \Lambda]\psi(x) = 0, \quad x \leq \tau \text{ or } x \geq \tau + L, \tag{B.1}$$

inside the crystal with the condition

$$\psi(x) = 0, \quad \tau < x < \tau + L. \tag{B.2}$$

Actually, (B.1) and (B.2) can be considered as the equations of electronic states in two ideal semi-infinite one-dimensional crystals: one left semi-infinite crystal in the range of $(-\infty, \tau)$ and one right semi-infinite crystal in the range of $(\tau + L, +\infty)$. The two ideal semi-infinite crystals are not independent of each other, since $L = Na$ and N is a positive integer. For those two semi-infinity crystals, as in Section 3.1 we are interested only in the electronic states whose energies are dependent on the boundary τ or $\tau+L$. The properties and energies of those boundary-dependent electronic states in the cavity structure can be easily obtained as long as the τ-dependent electronic states in the ideal finite crystal are obtained.

We have presented an analysis on the τ-dependent states in ideal one-dimensional finite crystals in Section 4.3. Actually, the boundary-dependent electronic states in an ideal cavity structure of a one-dimensional crystal can be easily obtained from that analysis.

We also take a band gap at $k = 0$ as an example. For a specific band gap index n, the boundary τ could be in one of three cases.

1. If τ is in the set $L(n)$, in the finite crystal bounded at τ and $\tau + L$, a surface state with a form of $e^{-\beta x}p(x, \Lambda)$ in which $\beta > 0$ exists in the band gap, indicating a surface state with an energy Λ located near the left boundary τ of the finite crystal. Correspondingly, $\tau + L$ is also in the set $L(n)$; therefore, a surface state with the same form of $e^{-\beta x}p(x, \Lambda)$ and the same energy Λ exists near the left boundary $\tau + L$ of the right semi-finite crystal, whereas no τ-dependent state exists in the left semi-finite crystal.
2. If τ is in the set $R(n)$, in the finite crystal bounded at τ and $\tau + L$, a surface state with a form of $e^{\beta x}p(x, \Lambda)$ in which $\beta > 0$ exists in the band gap, indicating a surface state with an energy Λ located near the right boundary $\tau + L$ of the finite crystal. Correspondingly, a surface state with the same form of $e^{\beta x}p(x, \Lambda)$ and the same energy Λ exists near the right boundary τ of the left semi-finite crystal, whereas no τ-dependent state exists in the right semi-finite crystal.
3. If τ is in the set $M(n)$, a band edge state with a form of $p(x, \Lambda)$ and the band edge energy exists in the finite crystal bounded at τ and $\tau + L$, indicating a confined band edge state periodically distributed in the finite crystal. Correspondingly, a band edge state with the same form of $p(x, \Lambda)$ and the same energy Λ exists in both the right semi-infinite crystal $(\tau + L, +\infty)$ and the left semi-finite crystal $(-\infty, \tau)$.

Band gaps at $k = \pi/a$ can be similarly analyzed; only the semi-periodic functions $s(x, \Lambda)$ should be used instead of periodic functions $p(x, \Lambda)$.

Therefore, the τ-dependent states in such a cavity structure can be obtained similar to the τ-dependent states in the finite crystal removed. The major difference is that in case 1 and case 2; the corresponding surface state wave function in the cavity structure should be normalized in the semi-infinite crystal rather than in the finite crystal; In case 3, the corresponding band edge state wave functions should be normalized as in an infinite crystal.

B.2 Electronic States in Ideal Two-Dimensional Cavity Structures of Three-Dimensional Crystals

A two-dimensional cavity structure in a three-dimensional infinite crystal is a structure formed when a film of a specific orientation and a specific thickness is removed from an infinite crystal. In this section, we are only interested in such cavity structures where an ideal quantum film as investigated in

Chapter 5 is removed from an infinite crystal. As in Chapter 5, we assume that the film plane is defined by two primitive lattice vectors $\boldsymbol{a}_1$ and $\boldsymbol{a}_2$, $x_3 = \tau_3$ defines the bottom of the removed film, and N_3 is a positive integer indicating the thickness of the removed film. Such a cavity structure has two separated parts: an upper semi-infinite crystal part and a lower semi-infinite crystal part.

The electronic states $\hat{\psi}(\hat{\boldsymbol{k}}, \boldsymbol{x})$ in a two-dimensional cavity are solutions of the following two equations:

$$-\nabla^2 \hat{\psi}(\hat{\boldsymbol{k}}, \boldsymbol{x}) + [v(\boldsymbol{x}) - \hat{\Lambda}]\hat{\psi}(\hat{\boldsymbol{k}}, \boldsymbol{x}) = 0 \quad \text{if } x_3 \le \tau_3 \text{ or } x_3 \ge \tau_3 + N_3 \tag{B.3}$$

and

$$\hat{\psi}(\hat{\boldsymbol{k}}, \boldsymbol{x}) = 0 \quad \text{if } \tau_3 < x_3 < \tau_3 + N_3. \tag{B.4}$$

The electronic states $\hat{\psi}(\hat{\boldsymbol{k}}, \boldsymbol{x})$ in such a cavity structure are two-dimensional Bloch waves with a wave vector $\hat{\boldsymbol{k}}$ in the film plane.

As in Section B.1, we are only interested in the boundary-dependent electronic states in such a cavity structure. Very similar to what we have seen in Section B.1, the boundary-dependent states in such a cavity structure can be similarly obtained as the boundary-dependent states in the removed film treated in Chapter 5: For each bulk energy band n and each wave vector $\hat{\boldsymbol{k}}$ in the film plane, there is one such electronic state in the cavity structure, which can be obtained from (5.11) by assigning a nondivergent $\hat{\phi}_n(\hat{\boldsymbol{k}}, \boldsymbol{x}; \tau_3)$ in the cavity structure:

$$\begin{aligned} \hat{\psi}_n(\hat{\boldsymbol{k}}, \boldsymbol{x}; \tau_3) &= c\, \hat{\phi}_n(\hat{\boldsymbol{k}}, \boldsymbol{x}; \tau_3) \quad \text{if } x_3 \le \tau_3 \text{ or } x_3 \ge \tau_3 + N_3 \\ &= 0 \qquad\qquad\qquad\quad \text{if } \tau_3 < x_3 < \tau_3 + N_3, \end{aligned} \tag{B.5}$$

where c is a normalization constant. Unlike in (5.33), c in (B.5) does not depend on the thickness N_3 of the removed film. The divergent part of $\hat{\phi}_n(\hat{\boldsymbol{k}}, \boldsymbol{x}; \tau_3)$ in (B.5) should be abandoned. Correspondingly, the energy of such a state is given by

$$\hat{\Lambda}_n(\hat{\boldsymbol{k}}; \tau_3) = \hat{\lambda}_n(\hat{\boldsymbol{k}}; \tau_3), \tag{B.6}$$

as in (5.34). There is one solution (B.5) of (B.3) and (B.4) for each energy band n and each $\hat{\boldsymbol{k}}$. Each $\hat{\psi}_n(\hat{\boldsymbol{k}}, \boldsymbol{x}; \tau_3)$ defined in (B.5) is an electronic state in the cavity structure whose energy $\hat{\Lambda}_n(\hat{\boldsymbol{k}}; \tau_3)$ in (B.6) depends on the cavity boundary τ_3 but not on the cavity thickness N_3. By Theorem 5.1, $\hat{\Lambda}_n(\hat{\boldsymbol{k}}; \tau_3)$ is either above or at the energy maximum of $\varepsilon_n(\boldsymbol{k})$ with that n and that $\hat{\boldsymbol{k}}$.

In the special cases where $\hat{\phi}_n(\hat{\boldsymbol{k}}, \boldsymbol{x}; \tau_3)$ in (B.5) is a Bloch function,

$$\hat{\phi}_n(\hat{\boldsymbol{k}}, \boldsymbol{x}; \tau_3) = \phi_{n'}(\boldsymbol{k}, \boldsymbol{x}), \quad n \le n', \tag{B.7}$$

the corresponding Bloch function $\phi_{n'}(\boldsymbol{k}, \boldsymbol{x})$ has a nodal surface at $x_3 = \tau_3$ and thus has nodal surfaces at $x_3 = \tau_3 + \ell$, where $\ell = 1, 2, ..., N_3$. The wave

function $\hat{\phi}_n(\hat{\boldsymbol{k}}, \boldsymbol{x}; \tau_3)$ in (B.5) exists in both the upper semi-infinite crystal part and the lower semi-infinite crystal part of the cavity structure.

In most cases, $\hat{\phi}_n(\hat{\boldsymbol{k}}, \boldsymbol{x}; \tau_3)$ in (B.5) is not a Bloch function. Consequently, in such a case, there is a nonzero imaginary part of k_3 in (5.11), indicating that $\hat{\psi}_n(\hat{\boldsymbol{k}}, \boldsymbol{x}; \tau_3)$ in (B.5) is a surface state located near either the top surface of the lower semi-infinite crystal part (if the imaginary part of k_3 in (5.11) is negative) or the bottom surface of the upper semi-infinite crystal part (if the imaginary part of k_3 in (5.11) is positive) of the cavity structure: It exists in one of the two semi-infinite crystal parts of the cavity structure. Correspondingly, the energy of such a state

$$\hat{\Lambda}_n(\hat{\boldsymbol{k}}; \tau_3) > \varepsilon_n(\boldsymbol{k}) \quad \text{for } (\boldsymbol{k} - \hat{\boldsymbol{k}}) \cdot \boldsymbol{a}_i = 0, \quad i = 1, 2, \tag{B.8}$$

is true by Theorem 5.1. However, there is no reason to expect that $\hat{\Lambda}_n(\hat{\boldsymbol{k}}; \tau_3)$ has to be in a band gap.

Therefore, for each bulk energy band n, there is one surface-like subband $\hat{\Lambda}_n(\hat{\boldsymbol{k}}; \tau_3)$ in (B.6) in such an ideal cavity structure.

Those results should be correct for cavity structures of crystals with a sc, tetr, or an ortho Bravais lattice for which an ideal (001) film is removed. More generally, they should also be correct for ideal cavity structures of crystals with a fcc or a bcc Bravais lattice for which an ideal (001) or (110) film is removed.

We have seen in Sections B.1–B.2 that the boundary-dependent electronic states in a cavity structure actually can be obtained similar to the boundary-dependent electronic states in the removed low-dimensional systems. This is due to the simple fact that the ideal cavity structure and the ideal low-dimensional system removed have the same boundary. The same idea can be applied to obtain the boundary-dependent electronic states in ideal one-dimensional or zero-dimensional cavity structures in three-dimensional crystals.

B.3 Electronic States in Ideal One-Dimensional Cavity Structures of Three-Dimensional Crystals

A one-dimensional cavity structure in a three-dimensional infinite crystal is a structure formed when a quantum wire is removed from the infinite crystal. In this section, we are only interested in such cavity structures where an ideal rectangular quantum wire as investigated in Chapter 6 is removed from an infinite crystal.

As in Chapter 6, we choose the primitive vector $\boldsymbol{a}_1$ in the wire cavity direction. Such a rectangular wire cavity can be defined by a bottom face $x_3 = \tau_3$, a top face $x_3 = \tau_3 + N_3$, a front face perpendicularly intersecting the $\boldsymbol{a}_2$ axis at $\tau_2 \boldsymbol{a}_2$, and a rear face perpendicularly intersecting it at $(\tau_2 + N_2)\boldsymbol{a}_2$;

here, τ_2 and τ_3 define the boundary faces of the wire cavity and N_2 and N_3 are two positive integers indicating the size and/or shape of the wire cavity.

For the electronic states in such an ideal cavity structure, we look for the eigenvalues $\bar{\Lambda}$ and eigenfunctions $\bar{\psi}(\bar{\boldsymbol{k}}, \boldsymbol{x})$ of the following two equations:

$$-\nabla^2\bar{\psi}(\bar{\boldsymbol{k}}, \boldsymbol{x}) + [v(\boldsymbol{x}) - \bar{\Lambda}]\bar{\psi}(\bar{\boldsymbol{k}}, \boldsymbol{x}) = 0 \quad \text{if } \boldsymbol{x} \notin \text{ the cavity} \tag{B.9}$$

and

$$\bar{\psi}(\bar{\boldsymbol{k}}, \boldsymbol{x}) = 0 \quad \text{if } \boldsymbol{x} \in \text{ the cavity.} \tag{B.10}$$

The solutions $\bar{\psi}(\bar{\boldsymbol{k}}, \boldsymbol{x})$ of (B.9) and (B.10) are one-dimensional Bloch waves with a wave vector $\bar{\boldsymbol{k}}$ in the wire direction $\boldsymbol{a}_1$.

There are different types of electronic state solutions of these two equations. As in Sections B.1 and B.2, in this section we are only interested in the solutions of (B.9) and (B.10) whose energies are dependent on the cavity boundary locations τ_2 and/or τ_3. Based on similar arguments to that we had in Chapters 5–6 and in Sections B.1 and B.2, we can easily understand that the electronic states whose energies are dependent on the cavity boundary location τ_2 *or* τ_3 are surface-like states in the cavity structure; they are located near the opposite surface of the cavity structure in comparison with the corresponding surface-like states in the removed quantum wire: If there is a surface-like state located near the top surface of the removed quantum wire, then there is a corresponding surface-like state located near the bottom surface of the cavity and vice versa. If there is a surface-like state located near the front surface of the removed quantum wire, then there is a corresponding surface-like state located near the rear surface of the cavity and vice versa. Similarly, the electronic states whose energies are dependent on the cavity boundary locations τ_2 *and* τ_3 are side-like states in the cavity structure; they are located near the opposite side of the cavity in comparison with the corresponding side-like states in the removed quantum wire.

B.3.1 Wire Cavities in Crystals with a sc, tetr, or ortho Bravais Lattice

For an ideal one-dimensional cavity structure of crystals with a sc, tetr, or ortho Bravais lattice, if the rectangular quantum wire removed has its two boundary faces in the $\boldsymbol{a}_2$ direction which are defined by τ_2 and are $N_2\boldsymbol{a}_2$ apart from each other and has the two other boundary faces in the $\boldsymbol{a}_3$ direction which are defined by τ_3 and are $N_3\boldsymbol{a}_3$ apart from each other, for each bulk energy band n in the cavity structure there are the following:
$(N_3 - 1)$ surface-like subbands with energies

$$\bar{\Lambda}_{n,j_3}(\bar{\boldsymbol{k}}; \tau_2) = \hat{\Lambda}_n\left(\bar{\boldsymbol{k}} + \frac{j_3\pi}{N_3}\boldsymbol{b}_3; \tau_2\right); \tag{B.11}$$

$(N_2 - 1)$ surface-like subbands with energies

$$\bar{\Lambda}_{n,j_2}(\bar{\boldsymbol{k}};\tau_3) = \hat{\Lambda}_n\left(\bar{\boldsymbol{k}} + \frac{j_2\pi}{N_2}\boldsymbol{b}_2;\tau_3\right); \tag{B.12}$$

one side-like subbands with energy $\bar{\Lambda}_n(\bar{\boldsymbol{k}};\tau_2,\tau_3)$ depending on both τ_2 and τ_3, similar to (6.29), (6.30), and (6.31) in Section 6.4.
Here, $j_2 = 1, 2, ..., N_2 - 1$ and $j_3 = 1, 2, ..., N_3 - 1$. $\hat{\Lambda}_n(\hat{\boldsymbol{k}};\tau_3)$ is the surface-like band structure in a quantum film with the film plane oriented in the $\boldsymbol{a}_3$ direction. $\hat{\Lambda}_n(\hat{\boldsymbol{k}};\tau_2)$ is the surface-like band structure in a quantum film with the film plane oriented in the $\boldsymbol{a}_2$ direction.

However, probably the practically more interesting cases are cavity structures of crystals with a fcc or bcc Bravais lattice. In the following, we give predictions on the electronic states in several such one-dimensional cavity structures.

B.3.2 Wire Cavities with (001) and (110) Surfaces in fcc Crystals

A cavity structure with (001) and (110) surfaces in fcc crystals is a structure formed when a $[1\bar{1}0]$ quantum wire is removed from an infinite crystal with a fcc Bravais lattice. The removed quantum wire has (001) and (110) surfaces and has a rectangular cross section $N_{110}a/\sqrt{2} \times N_{001}a$, where N_{110} and N_{001} are two positive integers.

For each bulk energy band n, there are $(N_{001} - 1) + (N_{110} - 1)$ surface-like subbands in such a cavity structure. They are $(N_{001} - 1)$ subbands with energies

$$\bar{\Lambda}^{sf,a_1}_{n,j_{001}}(\bar{\boldsymbol{k}};\tau_{110}) = \hat{\Lambda}_n\left[\bar{\boldsymbol{k}} + \frac{j_{001}\pi}{N_{001}a}(0,0,1);\tau_{110}\right] \tag{B.13}$$

and $(N_{110} - 1)$ subbands with energies

$$\bar{\Lambda}^{sf,a_2}_{n,j_{110}}(\bar{\boldsymbol{k}};\tau_{001}) = \hat{\Lambda}_n\left[\bar{\boldsymbol{k}} + \frac{j_{110}\pi}{N_{110}a}(1,1,0);\tau_{001}\right], \tag{B.14}$$

similar to (6.51) and (6.52). Here, τ_{001} or τ_{110} define the boundary faces of the cavity in the [001] or [110] direction, $j_{001} = 1, 2, ..., N_{001} - 1$, and $j_{110} = 1, 2, ..., N_{110} - 1$. $\hat{\Lambda}_n(\hat{\boldsymbol{k}};\tau_{001})$ is the surface-like band structure in a quantum film with the film plane oriented in the [001] direction. $\hat{\Lambda}_n(\hat{\boldsymbol{k}};\tau_{110})$ is the surface-like band structure in a quantum film with the film plane oriented in the [110] direction.

For each bulk energy band n, there is one side-like subband in the cavity structure with energy $\bar{\Lambda}^{sd}_n(\bar{\boldsymbol{k}};\tau_{001},\tau_{110})$ depending on both τ_{001} and τ_{110}, similar to (6.38) or (6.45).

B.3.3 Wire Cavities with (110) and (1$\bar{1}$0) Surfaces in fcc Crystals

A cavity structure with (110) and (1$\bar{1}$0) surfaces in fcc crystals is a structure formed when a [001] quantum wire is removed from an infinite crystal with a fcc Bravais lattice. The removed quantum wire has (110) and (1$\bar{1}$0) surfaces and has a rectangular cross section $N_{110}a/\sqrt{2} \times N_{1\bar{1}0}a/\sqrt{2}$, where N_{110} and $N_{1\bar{1}0}$ are two positive integers.

For each bulk energy band n, there are $(N_{1\bar{1}0}-1)+(N_{110}-1)$ surface-like subbands in the cavity structure. They are $(N_{1\bar{1}0}-1)$ subbands with energies

$$\bar{\Lambda}^{sf,a_1}_{n,j_{1\bar{1}0}}(\bar{\boldsymbol{k}};\tau_{110}) = \hat{\Lambda}_n\left[\bar{\boldsymbol{k}} + \frac{j_{1\bar{1}0}\pi}{N_{1\bar{1}0}a}(1,-1,0);\tau_{110}\right] \tag{B.15}$$

and $(N_{110}-1)$ subbands with energies

$$\bar{\Lambda}^{sf,a_2}_{n,j_{110}}(\bar{\boldsymbol{k}};\tau_{1\bar{1}0}) = \hat{\Lambda}_n\left[\bar{\boldsymbol{k}} + \frac{j_{110}\pi}{N_{110}a}(1,1,0);\tau_{1\bar{1}0}\right], \tag{B.16}$$

similar to (6.61) and (6.62). Here, τ_{110} or $\tau_{1\bar{1}0}$ define the boundary faces of the cavity in the [110] or [1$\bar{1}$0] direction, $j_{110} = 1,2,...,N_{110}-1$, and $j_{1\bar{1}0} = 1,2,...,N_{1\bar{1}0}-1$. $\hat{\Lambda}_n(\hat{\boldsymbol{k}};\tau_{110})$ is the surface-like band structure in a quantum film with the film plane oriented in the [110] direction. $\hat{\Lambda}_n(\hat{\boldsymbol{k}};\tau_{1\bar{1}0})$ is the surface-like band structure in a quantum film with the film plane oriented in the [1$\bar{1}$0] direction.

For each bulk energy band n, there is one side-like subband in the cavity structure with energy $\bar{\Lambda}^{sd}_n(\bar{\boldsymbol{k}};\tau_{110},\tau_{1\bar{1}0})$ depending on both τ_{110} and $\tau_{1\bar{1}0}$, similar to (6.63).

B.3.4 Wire Cavities with (010) and (001) Surfaces in bcc Crystals

A cavity structure with (010) and (001) surfaces in bcc crystals is a structure formed when a [100] quantum wire is removed from an infinite crystal with a bcc Bravais lattice. The removed quantum wire has (010) and (001) surfaces and has a rectangular cross section $N_{010}a \times N_{001}a$, where N_{010} and N_{001} are two positive integers.

For each bulk energy band n, there are $(N_{001}-1)+(N_{010}-1)$ surface-like subbands in the cavity structure. They are $(N_{001}-1)$ subbands with energies

$$\bar{\Lambda}^{sf,a_1}_{n,j_{001}}(\bar{\boldsymbol{k}};\tau_{010}) = \hat{\Lambda}_n\left[\bar{\boldsymbol{k}} + \frac{j_{001}\pi}{N_{001}a}(0,0,1);\tau_{010}\right] \tag{B.17}$$

and $(N_{010}-1)$ subbands with energies

$$\bar{\Lambda}^{sf,a_2}_{n,j_{010}}(\bar{\boldsymbol{k}};\tau_{001}) = \hat{\Lambda}_n\left[\bar{\boldsymbol{k}} + \frac{j_{010}\pi}{N_{010}a}(0,1,0);\tau_{001}\right], \tag{B.18}$$

similar to (6.69) and (6.70). Here, τ_{010} or τ_{001} define the boundary faces of the cavity in the [010] or [001] direction, $j_{001} = 1, 2, ..., N_{001} - 1$, and $j_{010} = 1, 2, ..., N_{010} - 1$. $\hat{\Lambda}_n(\hat{\boldsymbol{k}}; \tau_{001})$ is the surface-like band structure in a quantum film with the film plane oriented in the [001] direction. $\hat{\Lambda}_n(\hat{\boldsymbol{k}}; \tau_{010})$ is the surface-like band structure in a quantum film with the film plane oriented in the [010] direction.

For each bulk energy band n, there is one side-like subband in the cavity structure with energy $\bar{\Lambda}_n^{sd}(\bar{\boldsymbol{k}}; \tau_{001}, \tau_{010})$ depending on both τ_{001} and τ_{010}, similar to (6.71).

B.4 Electronic States in Ideal Zero-Dimensional Cavity Structures of Three-Dimensional Crystals

A zero-dimensional cavity structure in a three-dimensional infinite crystal is a structure formed when a quantum dot is removed from the infinite crystal. In this section, we are only interested in ideal cavity structures where an orthorhombic quantum dot investigated in Chapter 7 is removed from an infinite crystal.

Such an orthorhombic cavity can be defined by a bottom face $x_3 = \tau_3$, a top face $x_3 = \tau_3 + N_3$, a front face perpendicularly intersecting the $\boldsymbol{a}_2$ axis at $\tau_2 \boldsymbol{a}_2$ and a rear face perpendicularly intersecting it at $(\tau_2 + N_2)\boldsymbol{a}_2$, and a left face perpendicularly intersecting the $\boldsymbol{a}_1$ axis at $\tau_1 \boldsymbol{a}_1$ and a right face perpendicularly intersecting it at $(\tau_1 + N_1)\boldsymbol{a}_1$; here, τ_1, τ_2, and τ_3 define the boundary faces of the cavity and N_1, N_2, and N_3 are three positive integers indicating the cavity size and/or shape. We look for the eigenvalues Λ and eigenfunctions $\psi(\boldsymbol{x})$ of the following two equations:

$$-\nabla^2 \psi(\boldsymbol{x}) + [v(\boldsymbol{x}) - \Lambda]\psi(\boldsymbol{x}) = 0 \quad \text{if } \boldsymbol{x} \notin \text{ the cavity} \tag{B.19}$$

and

$$\psi(\boldsymbol{x}) = 0 \quad \text{if } \boldsymbol{x} \in \text{ the cavity.} \tag{B.20}$$

There are different types of electronic state solutions of (B.19) and (B.20). As in Sections B.1–B.3, in this section we are only interested in the solutions of (B.19) and (B.20) whose energies are dependent on the cavity boundary τ_1, τ_2, and/or τ_3. Based on similar arguments we had in Chapters 5–7 and in Sections B.1–B.3, we can easily understand that the electronic states whose energies are dependent on *one* of the cavity boundary locations τ_1, τ_2, or τ_3 are surface-like states in the cavity structure; they are located near the opposite surface of the cavity structure in comparison with the corresponding surface-like states in the removed quantum dot: If there is a surface-like state located near one specific surface in the removed quantum dot, then there is a corresponding surface-like state located near the opposite surface of the

cavity. The electronic states whose energies are dependent on *two* of the cavity boundary locations τ_1, τ_2, or τ_3 are side-like states in the cavity structure; they are located near the opposite side of the cavity in comparison with the corresponding side-like states in the removed quantum dot. The electronic states whose energies are dependent on all *three* cavity boundary locations τ_1, τ_2, and τ_3 are corner-like states in the cavity structure; they are located near the opposite corner of the cavity in comparison with the corresponding corner-like states in the removed quantum dot.

B.4.1 Dot Cavities in Crystals with a sc, tetr, or ortho Bravais Lattice

For such a cavity structure with a size $N_1 a_1$ in the $\boldsymbol{a}_1$ direction, a size $N_2 a_2$ in the $\boldsymbol{a}_2$ direction, and a size $N_3 a_3$ in the $\boldsymbol{a}_3$ direction in a crystal with a sc, tetr, or ortho Bravais lattice, for each bulk energy band there are $(N_1 - 1)(N_2 - 1) + (N_2 - 1)(N_3 - 1) + (N_3 - 1)(N_1 - 1)$ surface-like states, $(N_1 - 1) + (N_2 - 1) + (N_3 - 1)$ side-like states, and one corner-like state in the cavity structure. They are as follows:
$(N_1 - 1)(N_2 - 1)$ surface-like states with energies

$$\Lambda_{n,j_1,j_2}(\tau_3) = \hat{\Lambda}_n \left[\frac{j_1 \pi}{N_1} \boldsymbol{b}_1 + \frac{j_2 \pi}{N_2} \boldsymbol{b}_2; \tau_3 \right]; \tag{B.21}$$

$(N_2 - 1)(N_3 - 1)$ surface-like states with energies

$$\Lambda_{n,j_2,j_3}(\tau_1) = \hat{\Lambda}_n \left[\frac{j_2 \pi}{N_2} \boldsymbol{b}_2 + \frac{j_3 \pi}{N_3} \boldsymbol{b}_3; \tau_1 \right]; \tag{B.22}$$

$(N_3 - 1)(N_1 - 1)$ surface-like states with energies

$$\Lambda_{n,j_3,j_1}(\tau_2) = \hat{\Lambda}_n \left[\frac{j_3 \pi}{N_3} \boldsymbol{b}_3 + \frac{j_1 \pi}{N_1} \boldsymbol{b}_1; \tau_2 \right]; \tag{B.23}$$

$(N_1 - 1)$ side-like states with energies

$$\Lambda_{n,j_1}(\tau_2, \tau_3) = \bar{\Lambda}_n \left[\frac{j_1 \pi}{N_1} \boldsymbol{b}_1; \tau_2, \tau_3 \right]; \tag{B.24}$$

$(N_2 - 1)$ side-like states with energies

$$\Lambda_{n,j_2}(\tau_3, \tau_1) = \bar{\Lambda}_n \left[\frac{j_2 \pi}{N_2} \boldsymbol{b}_2; \tau_3, \tau_1 \right]; \tag{B.25}$$

$(N_3 - 1)$ side-states with energies

$$\Lambda_{n,j_3}(\tau_1, \tau_2) = \bar{\Lambda}_n \left[\frac{j_3 \pi}{N_3} \boldsymbol{b}_3; \tau_1, \tau_2 \right]; \tag{B.26}$$

one corner state with energy $\Lambda_n(\tau_1, \tau_2, \tau_3)$ depending all three τ_1, τ_2, and τ_3, similar to (7.40)–(7.46).
Here $j_1 = 1, 2, ..., N_1 - 1$, $j_2 = 1, 2, ..., N_2 - 1$, and $j_3 = 1, 2, ..., N_3 - 1$. τ_1, τ_2, and τ_3 define the boundary faces of the cavity in the $\boldsymbol{a}_1$, $\boldsymbol{a}_2$, and $\boldsymbol{a}_3$ directions. $\hat{\Lambda}_n[\hat{\boldsymbol{k}}; \tau_l]$ is the surface-like band structure of a quantum film with the film plane oriented in the $\boldsymbol{a}_l$ direction. $\bar{\Lambda}_n[\bar{\boldsymbol{k}}; \tau_l, \tau_m]$ is the side-like band structure of a rectangular quantum wire with the wire faces oriented in the $\boldsymbol{a}_l$ or the $\boldsymbol{a}_m$ direction.

Probably the practically more interesting cases are the cavity structures in crystals with a fcc or bcc Bravais lattice. Similar to what was done in Sections B.1–B.3, electronic states in those cavity structures can be obtained.

B.4.2 Dot Cavities with $(1\bar{1}0)$, (110), and (001) Surfaces in fcc Crystals

For a cavity structure in crystals with a fcc Bravais lattice, if the cavity has (001), (110), and $(1\bar{1}0)$ surfaces and has an orthorhombic size $N_{001}a \times N_{110}a/\sqrt{2} \times N_{1\bar{1}0}a/\sqrt{2}$, the boundary-dependent electronic states in such a cavity structure can be obtained similar to the boundary-dependent electronic states in an ideal quantum dot obtained in Section 7.7.

For each bulk energy band n, there are $(N_{001} - 1)(N_{1\bar{1}0} - 1) + (N_{110} - 1)(N_{001} - 1) + (N_{1\bar{1}0} - 1)(N_{110} - 1)$ surface-like states in the cavity structure. They are as follows:
$(N_{001} - 1)(N_{1\bar{1}0} - 1)$ states with energies

$$\Lambda^{sf,a_1}_{n,j_{001},j_{1\bar{1}0}}(\tau_{110}) = \hat{\Lambda}_n \left[\frac{j_{001}\pi}{N_{001}a}(0,0,1) + \frac{j_{1\bar{1}0}\pi}{N_{1\bar{1}0}a}(1,-1,0); \tau_{110} \right]; \qquad \text{(B.27)}$$

$(N_{110} - 1)(N_{001} - 1)$ states with energies

$$\Lambda^{sf,a_2}_{n,j_{110},j_{001}}(\tau_{1\bar{1}0}) = \hat{\Lambda}_n \left[\frac{j_{110}\pi}{N_{110}a}(1,1,0) + \frac{j_{001}\pi}{N_{001}a}(0,0,1); \tau_{1\bar{1}0} \right]; \qquad \text{(B.28)}$$

$(N_{1\bar{1}0} - 1)(N_{110} - 1)$ states with energies

$$\Lambda^{sf,a_3}_{n,j_{1\bar{1}0},j_{110}}(\tau_{001}) = \hat{\Lambda}_n \left[\frac{j_{1\bar{1}0}\pi}{N_{1\bar{1}0}a}(1,-1,0) + \frac{j_{110}\pi}{N_{110}a}(1,1,0); \tau_{001} \right], \qquad \text{(B.29)}$$

similar to (7.57)–(7.59).
Here, $j_{001} = 1, 2, ..., N_{001}-1$, $j_{1\bar{1}0} = 1, 2, ..., N_{1\bar{1}0}-1$, and $j_{110} = 1, 2, ..., N_{110}-1$. τ_{110}, $\tau_{1\bar{1}0}$, or τ_{001} define the boundary faces of the cavity in the [110], $[1\bar{1}0]$, or [001] direction, $\hat{\Lambda}_n[\hat{\boldsymbol{k}}; \tau_l]$ is the surface-like band structure of a quantum film with the film plane oriented in the $[l]$ direction. l can be either one of 110, $1\bar{1}0$, or 001, .

For each energy band n, there are $(N_{001} - 1) + (N_{110} - 1) + (N_{1\bar{1}0} - 1)$ side-like states in the cavity structure. They are as follows:
$(N_{001} - 1)$ states with energies

$$\Lambda^{sd,a_1}_{n,j_{001}}(\tau_{1\bar{1}0},\tau_{110}) = \bar{\Lambda}_n\left[\frac{j_{001}\pi}{N_{001}a}(0,0,1);\tau_{1\bar{1}0},\tau_{110}\right]; \tag{B.30}$$

$(N_{110}-1)$ states with energies

$$\Lambda^{sd,a_2}_{n,j_{110}}(\tau_{1\bar{1}0},\tau_{001}) = \bar{\Lambda}_n\left[\frac{j_{110}\pi}{N_{110}a}(1,1,0);\tau_{1\bar{1}0},\tau_{001}\right]; \tag{B.31}$$

$(N_{1\bar{1}0}-1)$ states with energies

$$\Lambda^{sd,a_3}_{n,j_{1\bar{1}0}}(\tau_{001},\tau_{110}) = \bar{\Lambda}_n\left[\frac{j_{1\bar{1}0}\pi}{N_{1\bar{1}0}a}(1,-1,0);\tau_{001},\tau_{110}\right], \tag{B.32}$$

similar to (7.60)–(7.62).
Here, $\bar{\Lambda}_n[\bar{\boldsymbol{k}};\tau_l,\tau_m]$ is the side-like band structure of a rectangular quantum wire with the wire faces oriented in the $[l]$ or the $[m]$ direction. l and m can be two of 001, 110, and $1\bar{1}0$.

For each bulk energy band n, there is one corner state in the cavity structure with energy $\Lambda^{cr}_n(\tau_{001},\tau_{1\bar{1}0},\tau_{110})$ depending all three τ_{001}, $\tau_{1\bar{1}0}$, and τ_{110}, similar to (7.63).

B.4.3 Dot Cavities with (100), (010), and (001) Surfaces in bcc Crystals

For a cavity structure in crystals with a bcc Bravais lattice, if the cavity has (100), (010), and (001) surfaces and has an orthorhombic size $N_{100}a\times N_{010}a\times N_{001}a$, the boundary-dependent electronic states in the cavity structure can be obtained similar to the boundary-dependent electronic states in an ideal quantum dot obtained in Section 7.8.

For each bulk energy band n, there are $(N_{100}-1)(N_{010}-1)+(N_{010}-1)(N_{001}-1)+(N_{001}-1)(N_{100}-1)$ surface-like states in the cavity structure. They are as follows:
$(N_{010}-1)(N_{001}-1)$ states with energies

$$\Lambda^{sf,a_1}_{n,j_{010},j_{001}}(\tau_{100}) = \hat{\Lambda}_n\left[\frac{j_{010}\pi}{N_{010}a}(0,1,0)+\frac{j_{001}\pi}{N_{001}a}(0,0,1);\tau_{100}\right]; \tag{B.33}$$

$(N_{001}-1)(N_{100}-1)$ states with energies

$$\Lambda^{sf,a_2}_{n,j_{001},j_{100}}(\tau_{010}) = \hat{\Lambda}_n\left[\frac{j_{001}\pi}{N_{001}a}(0,0,1)+\frac{j_{100}\pi}{N_{100}a}(1,0,0);\tau_{010}\right]; \tag{B.34}$$

$(N_{100}-1)(N_{010}-1)$ states with energies

$$\Lambda^{sf,a_3}_{n,j_{100},j_{010}}(\tau_{001}) = \hat{\Lambda}_n\left[\frac{j_{100}\pi}{N_{100}a}(1,0,0)+\frac{j_{010}\pi}{N_{010}a}(0,1,0);\tau_{001}\right], \tag{B.35}$$

similar to (7.73)–(7.75).
Here, $j_{100} = 1, 2, ..., N_{100}-1$, $j_{010} = 1, 2, ..., N_{010}-1$, and $j_{001} = 1, 2, ..., N_{001}-1$. τ_{100}, τ_{010}, or τ_{001} define the boundary faces of the cavity in the [100], [010], or [001] direction, $\hat{\Lambda}_n[\hat{\boldsymbol{k}}; \tau_l]$ is the surface-like band structure of a quantum film with the film plane oriented in the $[l]$ direction. l can be either one of 100, 010, or 001.

For each bulk energy band n, there are $(N_{100}-1)+(N_{010}-1)+(N_{001}-1)$ side-like states in the cavity structure. They are as follows:
$(N_{100}-1)$ side-like states with energies

$$\Lambda^{sd,a_1}_{n,j_{100}}(\tau_{010}, \tau_{001}) = \bar{\Lambda}_n \left[\frac{j_{100}\pi}{N_{100}a}(1,0,0); \tau_{010}, \tau_{001} \right]; \tag{B.36}$$

$(N_{010}-1)$ side-like states with energies

$$\Lambda^{sd,a_2}_{n,j_{010}}(\tau_{001}, \tau_{100}) = \bar{\Lambda}_n \left[\frac{j_{010}\pi}{N_{010}a}(0,1,0); \tau_{001}, \tau_{100} \right]; \tag{B.37}$$

$(N_{001}-1)$ side-like states with energies

$$\Lambda^{sd,a_3}_{n,j_{001}}(\tau_{100}, \tau_{010}) = \bar{\Lambda}_n \left[\frac{j_{001}\pi}{N_{001}a}(0,0,1); \tau_{100}, \tau_{010} \right], \tag{B.38}$$

similar to (7.76)–(7.78).
Here, $\bar{\Lambda}_n[\bar{\boldsymbol{k}}; \tau_l, \tau_m]$ is the side-like band structure of a rectangular quantum wire with the wire faces oriented in the $[l]$ or the $[m]$ direction. l and m can be two of 100, 010, and 001.

For each bulk energy band n, there is one corner state in the cavity structure with energy $\Lambda^{cr}_n(\tau_{100}, \tau_{010}, \tau_{001})$ depending all three τ_{100}, τ_{010}, and τ_{001}, similar to (7.79).

Index